

University of Bath



**PHD**

**Biopharmaceutical considerations and in vitro-in vivo correlations (IVIVCs) for orally administered amorphous formulations**

Long, Chiau Ming

*Award date:*  
2014

*Awarding institution:*  
University of Bath

[Link to publication](#)

**General rights**

Copyright and moral rights for the publications made accessible in the public portal are retained by the authors and/or other copyright owners and it is a condition of accessing publications that users recognise and abide by the legal requirements associated with these rights.

- Users may download and print one copy of any publication from the public portal for the purpose of private study or research.
- You may not further distribute the material or use it for any profit-making activity or commercial gain
- You may freely distribute the URL identifying the publication in the public portal ?

**Take down policy**

If you believe that this document breaches copyright please contact us providing details, and we will remove access to the work immediately and investigate your claim.

**Biopharmaceutical considerations and  
*in vitro-in vivo* correlations (IVIVCs) for  
orally administered amorphous formulations**

Chiau Ming Long

A thesis submitted for the degree of Doctor of Philosophy  
University of Bath  
Department of Pharmacy and Pharmacology  
June 2014

COPYRIGHT

Attention is drawn to the fact that copyright of this thesis rests with the author. A copy of this thesis has been supplied on condition that anyone who consults it is understood to recognise that its copyright rests with the author and that they must not copy it or use material from it except as permitted by law or with the consent of the author.

This thesis may not be consulted, photocopied or lent to other libraries without the permission of the author and Dr Nikoletta Fotaki for one year from the date of acceptance of the thesis.

## Table of Contents

Acknowledgement .....	x
Dissemination (Oral and poster presentation) .....	xii
List of Figures .....	xiii
List of Tables .....	xix
List of Abbreviations .....	xxi
Table of Units .....	xxiv
Abstract .....	1
1. Introduction .....	2
1.1 Amorphous state .....	2
1.1.1 Preparation of amorphous solids .....	2
1.1.1.1 Solid dispersion .....	3
1.1.2 Solubility of amorphous compound .....	3
1.1.3 Saturation, supersaturation and precipitation .....	5
1.2 <i>In vitro</i> dissolution testing .....	8
1.2.1 Applications of <i>in vitro</i> dissolution testing .....	8
1.2.2 Biorelevant dissolution method .....	9
1.3 The dissolution medium .....	11
1.3.1 Compendial media .....	11
1.3.2 Media containing artificial surfactant .....	12
1.3.3 Biorelevant dissolution media .....	13
1.3.3.1 Media to simulate the contents of the stomach .....	14
1.4 Types of hydrodynamics .....	21
1.4.1 USP apparatus 1 and USP apparatus 2 .....	22
1.4.2 USP apparatus 4 .....	22
1.5 Surface UV dissolution imaging .....	24
1.5.1 Operational and intrinsic dissolution rate (IDR) of ActiPix™ .....	24
1.5.2 Applications and advantages of surface UV dissolution using ActiPix™ technology .....	26
1.6 Oral Drug Absorption and PBPK modeling .....	27
1.6.1 Parameters to be considered in drug absorption modeling .....	27
1.6.1.1 Physiological parameters .....	27
1.6.1.2 Biochemical parameters .....	28
1.6.1.3 Drug physicochemical parameters .....	30
1.6.1.4 Dosage form and formulation parameters .....	32

1.6.2 PBPK modeling .....	32
1.6.2.1 Physiologically-based pharmacokinetic (PBPK) models for the prediction of oral absorption.....	32
1.6.2.2 Advanced Compartmental Absorption and Transit (ACAT) model.....	33
1.7 <i>In vitro-in vivo</i> correlations/relationships (IVIVC/Rs).....	35
1.7.1 The Levels of Correlation .....	35
1.7.2 Application of an IVIVC .....	37
1.7.3 Development of IVIVCs.....	38
1.7.4 Establish IVIVC using <i>in vivo</i> and <i>in vitro</i> dissolution data.....	39
1.7.5 IVIVCs of amorphous formulations .....	40
1.8 Compounds selected (Amorphous state) .....	42
1.8.1 Cefuroxime axetil (CA) .....	42
1.8.2 Itraconazole (ITR) .....	44
1.8.3 Compound X (CX).....	45
1.9 Aim of study .....	48
2. Experimental Methods .....	49
2.1 Materials .....	49
2.2 Apparatus .....	50
2.3 Amorphous formulation of compounds selected .....	52
2.3.1 CA.....	52
2.3.2 ITR .....	52
2.3.3 CX.....	53
2.4 Methods of Part 1: <i>In vitro</i> solubility and dissolution testing .....	55
2.4.1 Chromatographic conditions.....	55
2.4.2 Limit of detection and limit of quantification and linearity .....	56
2.4.3 Drug adsorption test.....	57
2.4.4 Preparation of media .....	57
2.4.5 Equilibrium solubility studies (Itraconazole) .....	60
2.4.6 <i>In vitro</i> dissolution testing with USP apparatus 1 and 2 .....	60
2.4.7 Standard curves analysis using HPLC.....	62
2.4.8 Drug degradation studies (Cefuroxime axetil).....	65
2.4.9 <i>In vitro</i> dissolution with USP apparatus 4 .....	66
2.4.10 Drug precipitation study.....	68
2.4.11 Statistical analysis: Dissolution profile comparison .....	69
2.4.12 Dissolution kinetics modeling .....	70
2.5 Methods of Part 2: Surface UV dissolution imaging .....	72
2.5.1 Experiment setup and protocol.....	72
2.5.2 Preparation of compacts .....	72

2.5.3 Design of experiment .....	73
2.6 Methods of Part 3: Physiologically Based Pharmacokinetics (PBPK) Modeling ....	78
2.6.1 Computer hardware and software .....	78
2.6.2 Advanced Compartmental Absorption and Transit (ACAT) model description	78
2.6.3 Effective permeability ( $P_{eff}$ ) .....	85
2.6.4 The pharmacokinetic model .....	87
2.6.5 Enzyme and transporter metabolism .....	92
2.6.6 Physiology tab .....	98
2.6.7 Intestinal first-pass effect and chemical degradation (CA) .....	100
2.6.8 Approach and design of simulation.....	101
2.6.9 Prediction of <i>in vivo</i> performance based on PBPK models .....	104
2.6.10 Parameter sensitivity analysis .....	105
2.6.11 Analysis and comparison of plasma concentration vs time data .....	107
2.7 Methods of Part 4: Deconvolution and development of <i>In vitro-in vivo</i> correlation	108
2.7.1 Deconvolution analysis.....	108
2.7.2 Development of IVIVC .....	109
3. Results and discussion .....	110
3.1 Results and discussion of Part 1: <i>In vitro</i> solubility and dissolution testing .....	110
3.1.1 Validation of chromatographic methods.....	110
3.1.2 Development of modified media .....	113
3.2 Results and Discussion of Part 1: <i>In vitro</i> dissolution testing (Cefuroxime axetil)	117
3.2.1 Degradation study of cefuroxime axetil.....	117
3.2.2 Dissolution testing in USP apparatus 2.....	118
3.2.3 2 stage dissolution studies .....	122
3.2.4 Dissolution testing in USP apparatus 4.....	123
3.3 Results and Discussion of Part 1: <i>In vitro</i> solubility and dissolution testing (ITR)	127
3.3.1 Equilibrium solubility studies.....	127
3.3.2 Dissolution testing in USP apparatus 1.....	128
3.3.3 2 stage dissolution studies .....	131
3.3.4 Dissolution testing in USP apparatus 4.....	135
3.3.5 Simulation of physiological relevant <i>in vivo</i> precipitation.....	144
3.4 Results and Discussion of Part 1: <i>In vitro</i> dissolution testing (CX).....	147
3.4.1 Dissolution testing in USP apparatus 2.....	147
3.4.2 2 stage dissolution studies .....	148
3.4.3 Dissolution testing in USP apparatus 4.....	149
3.4.4 Simulation of physiological relevant <i>in vivo</i> precipitation.....	156
3.5 Results and Discussion of Part 2: Surface UV dissolution imaging .....	158
3.5.1 Calibration curves .....	158

3.5.2 <i>In vitro</i> surface UV dissolution imaging studies.....	159
3.6 Results and Discussion of Part 3: PBPK modeling (CA).....	173
3.6.1 Prediction of <i>in vivo</i> performance based on PBPK models.....	173
3.6.2 Parameter sensitivity analysis .....	177
3.7 Results and Discussion of Part 3: PBPK modeling (ITR).....	180
3.7.1 Prediction of <i>in vivo</i> performance based on PBPK models .....	180
3.7.2 Parameter sensitivity analysis .....	187
3.8 Results and Discussion of Part 3: PBPK modeling (CX) .....	190
3.8.1 Prediction of <i>in vivo</i> performance based on PBPK models .....	190
3.8.2 Parameter sensitivity analysis .....	198
3.9 Results and Discussion of Part 4: Deconvolution analysis .....	200
3.9.1 CA.....	200
3.9.2 ITR.....	201
3.9.3 CX.....	202
3.10 Results and Discussion of Part 4: Development of IVIVR/IVIVC models.....	205
3.10.1 Qualitative IVIVRs .....	205
3.10.2 Mathematical IVIVC.....	208
4 Conclusions and future work.....	220
Appendix 1 .....	252
Appendix 2 .....	254
Appendix 3 .....	255
Appendix 4 .....	257
Appendix 5 .....	258
Appendix 6 .....	259
Appendix 7 .....	260
Appendix 8 .....	263

## Acknowledgement

I would like to express my deepest and heartfelt gratitude to my supervisor Dr Nikoletta Fotaki who has given me the opportunity to pursue this project under her supervision. I thank her for her time, support and constant encouragement.

I would like to express my appreciation to Dr M. Begona Delgado-Charro (University of Bath) and Prof Dr Clive G. Wilson (Strathclyde Institute of Pharmacy and Biomedical Sciences, University of Strathclyde, Glasgow) for kind acceptance to be the examiner of my thesis. Dr Karen Edler is also acknowledged for allowing the use of the surface tension meter in her lab.

*“Terima kasih banyak banyak”* Malaysian language for *thank you very much* to the following great people:

Especially to Dr Irena Tomaszewska, Dr Liz O’Donovan, Dr Amit Nathubhai, Mr Kai Hui Leong, Mr Wei Chern Ang for their time and kind assistance.

Mr Luis Rodrigo Contreras-Rojas, Dr Luis Nogueiras Nieto, Dr Quan Yang, Dr Premrutai Thitilertdecha, Dr Natalie Belsey, Nour Alhusein, Jin Zhang, Wing Sin Chiu and Dr Fengbin Ye for their kind advice and caring towards me.

Dedicated staffs of Department of Pharmacy and Pharmacology University of Bath: Ms Sarah Cordery, Mr Pascal Loizeau, Mr Kevin Smith, Mr Rod Murray, Mr Stephen Phillips, Ms Jo Carter, Mr Donald Perry, Ms Patricia Higgins, Ms Joanne Arlett, Mr Sam *etc...*

My friends in Universiti Teknologi MARA and USM (Malaysia): Prof Abu Bakar Abdul Majeed, Dr Wong Tin Wui, Dr Yvonne Tan, Dr Tham Sook Yin, Dr Muhammad Abdul Hadi, Dr Zoe Lim, Dr Lee Wee Leng, Ms Yap Yen Ling, Dr Dr Yaman Kassab, Mr Muhammad Abdul Hameed, Dr Sarmed Nabhan Yaseen, Dr Neoh Chin Fen, Dr Chan Siok Yee, Dr Wong Yuen Fei, Dr Irna Elina Ridzwan and Dr Baharudin Ibrahim.

Special thanks go to my best team-mate Dr Irena Tomaszewska who is always there for me regardless of happy and sorrow times. I wouldn’t be able to do it without her. Likewise to me, your friendship is priceless.

Hoffmann La-Roche (US) and Universiti Teknologi MARA (Malaysia) are sincerely acknowledged for providing the financial support and studentship for this PhD project.

## **Dedication**

My mother .... She is always a constant source of inspiration and motivation in my life.

My late father ...He sacrificed so much for the family and yet I took him for granted.

To my beloved sisters and brother...Thanks for your unconditional love and support especially when I was away from home.

To both my eyes ....relentlessly providing me visual even after suffering from glaucoma.

To Buddha... for the wisdom and teaching and tranquil inner peace bestows on me



## Dissemination (Oral and poster presentation)

1. C.Long, K. Tang, H. Chokshi, N. Fotaki, *Surface dissolution UV imaging for studying properties of a poorly soluble weak basic compound*. AAPS Annual Meeting and Exposition, St Antonio, 2013.
2. C.Long, K. Tang, H. Chokshi, N. Fotaki, *Development of a PBPK model for a poorly soluble drug: prediction of in vivo performance from amorphous formulation: importance of in vitro solubility and dissolution data*. AAPS Annual Meeting and Exposition, Chicago, 2012.
3. C.Long, K. Tang, H. Chokshi, N. Fotaki, *In vitro dissolution characterization of an amorphous formulation of a BCS Class II compound*. PharmSci UK 2012, Nottingham 2012.
4. C.Long, K. Tang, H. Chokshi, N. Fotaki, *Investigation on the physiological relevant amount of surfactant in simulated gastric fluids for in vitro solubility and dissolution studies*. International conference and exhibition on pharmaceutical, nutraceutical and cosmeceutical technology, Kuala Lumpur, Malaysia 2012.
5. C.Long, K. Tang, H. Chokshi, N. Fotaki, *In vitro-in vivo correlations for an amorphous formulation of a poorly soluble compound*. FIP Centennial Congress, Amsterdam, the Netherlands; 3 - 8 October, 2012.
6. C.Long, K. Tang, H. Chokshi, N. Fotaki, *Dissolution testing for amorphous formulation: effect of media and hydrodynamics* AAPS Conference, Washington DC, 2011.

## List of Figures

Figure 1. Schematic structure of crystalline and amorphous states.....	2
Figure 2. Concentrations in the solution and the solid compositions as a function of time during the solution-mediated phase transformation.....	4
Figure 3. Chemical structure of SLS .....	13
Figure 4. Chemical structure of HTAB .....	13
Figure 5. Schematic diagram of the USP apparatus 1 and 2.....	22
Figure 6. Schematic diagram of the USP apparatus 4, the inset shows the components of the flow-through cell.....	23
Figure 7. Photograph of ActiPix™ SDI 300 dissolution imaging system and the experimental UV imaging apparatus setup schematic.....	25
Figure 8. Schematic illustration of intestinal drug absorption processes.....	28
Figure 9. Schematic of ACAT model interpretation of <i>in vivo</i> drug behaviour.....	34
Figure 10. Level A IVIVCs of DCMT-1. ....	40
Figure 11. Multiple level C IVIVCs between $C_{max}$ (or AUC) and $Q_{5min}$ or $Q_{60min}$ of ritonavir amorphous dispersions.. ....	41
Figure 12. Schematic diagram of cell setup for the USP apparatus .....	66
Figure 13. Examples of Sporanox pellet (A), ITR API (B) and CA API (C) compact used for the surface dissolution imaging studies. ....	73
Figure 14. Particle size distribution of amorphous CA.....	84
Figure 15. <i>In vitro</i> $V_{max}$ ( $\times 10^{-2}$ pmol/min/mg protein) as a function of <i>in vivo</i> intrinsic clearance (L/h).....	95
Figure 16. <i>In vivo</i> $V_{max}$ (mg/s) as a function of <i>in vivo</i> intrinsic clearance ( $\times 10^3$ L/h). ...	97
Figure 17. Mean ( $\pm$ SD) plasma concentration vs time profiles of CX in beagle dogs (n=4) after a single administration of F1, F2, F3, F4, F5, F6 and F7 of CX.....	105
Figure 18. Surface tension vs log SLS concentration (mM) (CMC determination of SLS) in SGF at 25°C. ....	113
Figure 19. Mean $\pm$ SD surface tension vs HTAB concentration (%) in SGF and potassium phosphate buffer .....	115
Figure 20. The relationship between the pH of the dissolution medium and the mean $\pm$ SD degradation rate constant, K.....	117
Figure 21. Mean $\pm$ SD % cumulative CA dissolved from Zinnat® tablets in various media using the USP apparatus 2. ....	118
Figure 22. Mean $\pm$ SD % CA dissolved from 250mg Zinnat® tablet in FeSSGF and FeSSIF-V2 with USP apparatus 2.....	119
Figure 23. Mean $\pm$ SD % CA dissolved from 2 stage dissolution, 250 mL FaSSGF for 30min/500 mL FaSSIF-V1 or -V2 with USP apparatus 2.....	122
Figure 24. Mean $\pm$ SD % cumulative CA dissolved from Zinnat® tablet.....	123
Figure 25. Mean $\pm$ SD % CA dissolved from Zinnat® tablet in fed state.....	125
Figure 26. Equilibrium solubility ( $\mu$ g/mL, Mean $\pm$ SD) of ITR.....	127
Figure 27. Mean $\pm$ SD % ITR dissolved from Sporanox® capsule with USP apparatus 1. ....	128
Figure 28. Mean $\pm$ SD ITR concentration yielded from 100mg Sporanox® capsule with USP apparatus 1 .....	129
Figure 29. Mean $\pm$ SD % ITR dissolved from 100mg Sporanox® capsule with FeSSIF-V2, FeSSGF, early FeSSGF and digested early FeSSGF with USP apparatus 1. ....	130
Figure 30. Mean $\pm$ SD % ITR dissolved from 100mg Sporanox® capsule from 2 stage dissolution with USP apparatus 1. ....	131
Figure 31. Mean $\pm$ SD % ITR dissolved from Sporanox® capsules. ....	135

Figure 32. Proposed dissolution and precipitation mechanisms of ITR dissolved from Sporanox <sup>®</sup> .....	137
Figure 33. Mean± SD % ITR dissolved from Sporanox <sup>®</sup> capsule in fed state media FeSSGF/ FeSSIF-V2 and FeSSGF/FeSSIF-V2 (6mLmin <sup>-1</sup> ; 2h/ 6mLmin <sup>-1</sup> ; 4h) using the USP apparatus 4 .....	138
Figure 34. Mean± SD % dose precipitation of ITR from Sporanox <sup>®</sup> with various media with USP apparatus 4 .....	145
Figure 35. Mean± SD % CX dissolved from CX formulation (F8) with various media with USP apparatus 2 .....	147
Figure 36. Mean± SD % CX dissolved from CX formulation (F8) using 2 stage dissolution, 250 mL FaSSGF for 30min/500 mL FaSSIF-V1 or -V2 with USP apparatus 2. ....	148
Figure 37. Mean± SD % CX dissolved from CX formulations.....	149
Figure 38. Mean± SD % CX concentration yielded from CX formulation in post media change .....	151
Figure 39. Mean± SD % of CX dissolved from CX tablet in fed state media FeSSGF (6 mL/min; 2 h)/ FeSSIF-V1 or -V2 (6 mL/min; 4 h) using the USP apparatus 4 .....	151
Figure 40. Mean± SD % precipitation (A: sample precipitated; B: dose precipitated) of CX from its formulations in various media with USP apparatus 4.....	156
Figure 41. Mean absorbance values as a function of concentration for pixel subselection obtained by flowing ITR and CA standard solutions through the laminar flow cell.....	158
Figure 42. Linear velocity of ActiPix™'s flow cell vs flow rate.....	159
Figure 43. Dense layer formed immediately after Zinnat <sup>®</sup> compact exposure to dissolution medium. ....	160
Figure 44. Mean± SD IDR of CA from its API compact in compendial and biorelevant media. ....	161
Figure 45. Mean± SD IDR and amount of CA dissolved at 5 min from its API compact with compendial and biorelevant media. ....	162
Figure 46. UV concentration maps of CA dissolved from API compacts with SGF (0.8 mL/min;6 min)/ SIF (0.4 mL/min;18 min) using surface UV imaging apparatus .....	163
Figure 47. Mean± SD IDR of CA dissolved from its API compact with SGF. ....	164
Figure 48. Mean± SD IDR of ITR from its API compact and Sporanox <sup>®</sup> compact in compendial and biorelevant media. ....	165
Figure 49. Mean± SD IDR and amount of ITR dissolved at 5 min from its API compact and Sporanox <sup>®</sup> compact with compendial and biorelevant media. ....	166
Figure 50. Mean± SD IDR and amount of ITR dissolved from its API and Sporanox <sup>®</sup> compact with SGF(0.8 mL/min;6 min)/ SIF (0.4 mL/min;18 min) and FaSSGF(0.8 mL/min;6 min)/ FaSSIF-V1(0.4 mL/min;18 min) .....	168
Figure 51. UV concentration maps of ITR dissolved from API and Sporanox <sup>®</sup> pellet compacts with SGF (0.8 mL/min;6 min)/ SIF (0.4 mL/min;18 min) and FaSSGF (0.8 mL/min;6 min)/ FaSSIF-V1 (0.4 mL/min;18 min) using surface UV imaging apparatus. ....	171
Figure 52. Simulation (line) of oral Zinnat <sup>®</sup> profiles in humans with various media with USP apparatus 2 and reference solubility in FaSSIF-V2.....	173
Figure 53. Simulation (line) of oral Zinnat <sup>®</sup> profiles in humans with various media with USP apparatus 2 and reference solubility in FaSSIF-V2.....	174
Figure 54. Simulation (line) of oral Zinnat <sup>®</sup> profiles in humans with various media with USP apparatus 4 and reference solubility in FaSSIF-V2.....	174

Figure 55. Simulation (line) of oral Zinnat <sup>®</sup> profiles in humans using reference solubility in FeSSIF-V2 and dissolution profiles measured in FeSSGF and FeSSIF-V2 with USP apparatus 2. ....	175
Figure 56. Simulation (line) of oral Zinnat <sup>®</sup> profiles in humans using reference solubility in FeSSIF-V2 and dissolution profiles measured in FeSSGF/FeSSIF-V1 and FeSSGF/FeSSIF-V2 with USP apparatus 4.....	176
Figure 57. PSA of absorption and pharmacokinetic parameters of CA (fasted state)	177
Figure 58. PSA of absorption and pharmacokinetic parameters of CA (fed state). ....	179
Figure 59. Simulation (line) of oral Sporanox <sup>®</sup> profiles in humans using dissolution profiles measured in FaSSIF-V2, SGF and FaSSGF with USP apparatus 1. ....	181
Figure 60. Simulation (line) of oral Sporanox <sup>®</sup> profiles in humans using dissolution profiles measured in 2 stage media experiments with USP apparatus 1. ....	182
Figure 61. Simulation (line) of oral Sporanox <sup>®</sup> profiles in humans using scaled FaSSIF-V1 solubility and dissolution profiles obtained with USP apparatus 4.....	183
Figure 62. Simulation (line) of oral Sporanox <sup>®</sup> profiles in humans using reference solubility in scaled FeSSIF-V1 and dissolution profiles measured in digested early FeSSGF and early FeSSGF with USP apparatus 1 .....	184
Figure 63. Simulation (line) of oral Sporanox <sup>®</sup> profiles in humans using reference solubility-pH in scaled FeSSIF-V1 and dissolution profiles measured in FeSSGF and FeSSIF-V2 with USP apparatus 1.....	184
Figure 64. Simulation (line) of oral Sporanox <sup>®</sup> profiles in humans using dissolution profiles with FeSSGF/FeSSIF-V1 and FeSSGF/FeSSIF-V2 (reference solubility: scaled FeSSIF-V1) with USP apparatus 4. ....	185
Figure 65. PSA of absorption and pharmacokinetic parameters of ITR (fasted state). ....	187
Figure 66. PSA of absorption and pharmacokinetic parameters of ITR (fed state). ...	189
Figure 67. Simulation (line) of oral CX profiles in dogs using reference solubility measured in FaSSIF-V1, FeSSIF-V1, scaled FaSSIF-V1 and scaled FeSSIF-V1.....	190
Figure 68. Simulation (line) of oral CX profiles in dogs using reference solubility-pH range in aqueous buffer pH 3/FeSSIF-V1 and aqueous buffers at pH 1.1, 3, 4.5, 6.8, 7.5 and 8.5 .....	191
Figure 69. Simulation (line) of oral CX profiles in dogs using reference solubility in FeSSIF-V1 and dissolution profiles measured in SIF-M4 and SIF-M5 with USP apparatus 2. ....	192
Figure 70. Simulation (line) of oral CX profiles in dogs using reference solubility in FeSSIF-V1 and dissolution profiles measured in 2 stage-V1 (FaSSGF/FaSSIF-V1) and 2 stage-V2 (FaSSGF/FaSSIF-V2) dissolution models with USP apparatus 2.....	193
Figure 71. Simulation (line) of oral CX profiles in dogs using reference solubility in FeSSIF-V1 and dissolution profiles measured in FaSSGF/FaSSIF-V1 and FaSSGF/FaSSIF-V2 with USP apparatus 4.....	194
Figure 72. Simulation (line) of oral CX profiles of F4, F5, F6 and F7 in dogs using reference solubility in FeSSIF-V1 and dissolution profiles measured with FaSSGF/FaSSIF-V2 with USP apparatus 4. ....	194
Figure 73. Simulation (line) of oral CX profiles in dogs using reference solubility in FeSSIF-V1 and dissolution profiles measured in SGF-M1/SIF-M1, SGF-M1/SIF-M2, SGF-M2/SIF-M3 with USP apparatus 4 .....	195
Figure 74. Simulation (line) of oral CX profiles in dogs using reference solubility in FeSSIF-V1 and dissolution profiles measured in FeSSGF/FeSSIF-V2 with USP apparatus 4 with F4, F5, F6 and F7.....	195

Figure 75. Simulation (line) of oral CX profiles in dogs using reference solubility in FeSSIF-V1 and dissolution profiles measured in FeSSGF/FeSSIF-V1 and FeSSGF/FeSSIF-V2 with USP apparatus 4 with F8.....	196
Figure 76. PSA of absorption and pharmacokinetic parameters of CX (fed state).....	198
Figure 77. Mean cumulative CA absorbed (A) and absorption rate (B) in fasted and fed state (Deconvolution data).....	200
Figure 78. Mean cumulative ITR absorbed (A) and absorption rate (B) in fasted and fed state (Deconvolution data).....	201
Figure 79. Summary of mean (n=4) cumulative amount absorbed (mg) CX Formulation 1,2,3,4,5,6 and 7 in beagle dogs.....	203
Figure 80. Summary of mean (n=4) absorption rate (mg/h) CX Formulation 1,2,3,4,5,6 and 7 in beagle dogs. ....	203
Figure 81. Mean± SD cumulative amount absorbed (deconvolution using PCDCON). ....	204
Figure 82. % CA absorbed.....	205
Figure 83. % ITR absorbed.....	206
Figure 84. % CX absorbed (fed state).....	207
Figure 85. Mean % CA absorbed in humans vs mean % CA dissolved <i>in vitro</i> with USP apparatus 4. ....	208
Figure 86. Mean % CA absorbed in humans vs mean % CA dissolved <i>in vitro</i> with USP apparatus 4 (fed state models) ....	210
Figure 87. Mean % ITR absorbed in humans vs mean % ITR dissolved with SGF with USP apparatus 1. ....	212
Figure 88. Mean % ITR absorbed in fasted state humans vs mean % ITR dissolved with USP apparatus 4. ....	212
Figure 89. Mean % ITR absorbed in humans (fed state) vs mean % ITR dissolved <i>in vitro</i> with USP apparatus 1. ....	214
Figure 90. Mean % CX absorbed in dogs vs mean % CX dissolved <i>in vitro</i> with FeSSGF with USP apparatus 2. ....	215
Figure 91. Mean % CX Formulation 4, 5, 6 and 7 absorbed in dogs (fed state) vs mean % CX dissolved <i>in vitro</i> with FeSSGF/FeSSIF-V2 with USP apparatus 4.....	216
Figure 92. Mean % CX absorbed in dogs vs mean % CX dissolved <i>in vitro</i> with SGF-M2/SIF-M3 with USP apparatus 4. Inset: Intestinal phase ( <i>in vitro</i> 2- 6 h).....	217
Figure 93. Mean % CX absorbed in dogs vs mean % CX dissolved <i>in vitro</i> with USP apparatus 4 (F8). ....	217

## List of Tables

Table 1. Composition of SGF and SIF .....	12
Table 2. Composition of the media to simulate gastric contents in the fed state.....	16
Table 3. Composition of the media to simulate the contents of the small intestine in the fasted state.....	18
Table 4. Composition of the media to simulate the contents of the small intestine in the fed state.....	21
Table 5. IVIVC expectations for immediate release products based on BCS .....	38
Table 6. Physicochemical properties summary of CA .....	42
Table 7. Physicochemical properties summary of ITR .....	44
Table 8. Physicochemical properties summary of CX .....	46
Table 9. Critical manufacturing variables for 8 formulations of CX .....	54
Table 10. Parameters for the HPLC analysis .....	56
Table 11. Type and name of modified media used in this project.....	60
Table 12. Parameters for standard curves of aqueous media .....	63
Table 13. Parameters for standard curves of milk-based media .....	64
Table 14. The periods during which formulations were exposed to the various dissolution media and flow rates.....	67
Table 15. The types of experiments performed for CX formulations.....	68
Table 16. Dissolution kinetics model applied .....	71
Table 17. Linear velocity of ActiPix™'s flow through cell from various flow rates.....	74
Table 18. The periods the compact was exposed to the dissolution media and the flow rate of each medium pumped through the cell .....	75
Table 19. Physicochemical characteristics and <i>in vivo</i> study parameters of CA.....	80
Table 20. Physicochemical characteristics and <i>in vivo</i> study parameters of ITR .....	81
Table 21. Physicochemical characteristics and <i>in vivo</i> study parameters of CX.....	83
Table 22. Compartmental analysis (1, 2 and 3 compartmental models) of cefuroxime in humans after administration of 500mg cefuroxime IV bolus .....	88
Table 23. Compartmental analysis (1, 2 and 3 compartmental models) of ITR in humans after administration of 100mg ITR IV infusion (1 h).....	89
Table 24. Reported IV pharmacokinetic parameters of ITR applied in ITR model .....	90
Table 25. Mean± SD IV pharmacokinetics parameters of CX 240mg tablet orally in dogs using linear pharmacokinetic compartmental analysis.....	91
Table 26. Mean± SD IV pharmacokinetic parameters of CX 240mg tablet orally in dogs using non-linear pharmacokinetic compartmental analysis .....	91
Table 27. Reported IV pharmacokinetic parameters of CX applied in CX model.....	92
Table 28. ACAT physiological model parameters for simulation of CA and ITR (fasted state humans).....	99
Table 29. ACAT physiological model parameters for simulation of CA and ITR (fed state humans).....	99
Table 30. Physiological parameters for CX model (fed state).....	100
Table 31. Chemical degradation rate vs pH data .....	101
Table 32. Simulations using solubility-based model.....	102
Table 33. Simulation design using solubility combined with dissolution-based models .....	103
Table 34. The range of parameters used for the PSA of CA .....	106
Table 35. The range of parameters used for the PSA of ITR. ....	106
Table 36. The range of parameters used for the PSA of CX .....	106
Table 37. The solubility value and dissolution profiles used for PSA.....	107

Table 38. Input response used in the deconvolution .....	108
Table 39. Analytical parameters of calibration curve in aqueous media. ....	110
Table 40. Analytical parameters of calibration curve in milk-based media.....	110
Table 41. LOQ and LOD ( $\mu\text{g/mL}$ ) for the investigated drugs in aqueous media .....	111
Table 42. LOQ and LOD ( $\mu\text{g/mL}$ ) for the investigated drugs in milk-based media.....	111
Table 43. Mean $\pm$ SD of % recovery of the three investigated drugs.....	111
Table 44. Mean $\pm$ SD of % fat partition of the three investigated drugs.....	112
Table 45. % recovery $\pm$ SD from filtrate for filter adsorption studies .....	112
Table 46. Comparison of physicochemical properties between modified compendial medium for the fasted stomach and fasted state human gastric fluid. ....	114
Table 47. Mean $\pm$ SD dissolution kinetic parameters of CA dissolved from Zinnat <sup>®</sup> tablet in simulated fasted and fed states media with USP apparatus 2 .....	120
Table 48. Mean $\pm$ SD dissolution kinetic parameters of CA dissolved from Zinnat <sup>®</sup> tablet in simulated fasted and fed states media using the USP apparatus 4. ....	126
Table 49. Mean $\pm$ SD dissolution kinetic parameters of ITR dissolved from Sporanox <sup>®</sup> 100mg capsule .....	133
Table 50. Mean $\pm$ SD dissolution kinetic parameters of ITR dissolved from Sporanox <sup>®</sup> 100mg capsule in simulating fasted state media using the USP apparatus 4.....	140
Table 51. Mean $\pm$ SD dissolution kinetic parameters (first order and Power law with gastric and intestinal phase) of ITR from Sporanox <sup>®</sup> .....	142
Table 52. Mean $\pm$ SD dissolution kinetic parameters (single Weibull with whole curve) of ITR dissolved from Sporanox.....	143
Table 53. Mean $\pm$ SD dissolution kinetic parameters (first order with intestinal phase and single Weibull function) of CX from CX formulations with biorelevant media .....	153
Table 54. Mean $\pm$ SD dissolution kinetic parameters (first order with intestinal phase and single Weibull function) of CX from CX formulations with modified media .....	153
Table 55. Mean $\pm$ SD dissolution kinetic parameters (first order with gastric and intestinal phase and single Weibull function) of CX from CX formulations.....	155
Table 56. Obtained regression parameters from relations between <i>in vivo</i> absorption and <i>in vitro</i> dissolution data (USP apparatus 4) .....	209
Table 57. Obtained regression parameters from relations between <i>in vivo</i> absorption and <i>in vitro</i> dissolution data (simulating fed state condition).....	210
Table 58. Obtained regression parameters from relations between <i>in vivo</i> absorption and <i>in vitro</i> dissolution data (fasted state).....	213
Table 59. Obtained regression parameters from relations between <i>in vivo</i> absorption and <i>in vitro</i> dissolution data in the fed state .....	214
Table 60. (A) Obtained regression parameters from relations between <i>in vivo</i> absorption* and <i>in vitro</i> dissolution data (Formulation 8) (B) <i>in vivo</i> absorption <sup>#</sup> and <i>in</i> <i>vitro</i> dissolution data with FeSSGF/ FeSSIF-V2 with USP apparatus 4 of Formulation 4, 5, 6 and 7. ....	218

## List of Abbreviations

Abbreviation	Full description
$\delta$	Unit impulse
2D	Two - dimensional
3D	Three - dimensional
®	Registered trademark
a	Time scale parameter
ACAT	Advanced Compartmental Absorption and Transit
ADAM	Advanced drug absorption and metabolism
ADME	Absorption, Distribution, Metabolism and Excretion
AIC	Akaike Information Criterion
Amt	Amount
<b>active compound</b>	Active pharmaceutical ingredient
ASD	Amorphous solid dispersion
AUC	Area under the curve
b	Shape parameter
BC	Buffer capacity
BCS	Biopharmaceutics classification system
BDM	Biorelevant dissolution media
c	First order rate constant
$C_{(t)}$	Input response
$C_{12}E_8$	Polyoxyethylene lauryl ether
ca	Approximately
CA	Cefuroxime axetil
CAT	Compartmental Absorption and Transit
$c_i$	Molar concentration of the ion
$C_{max}$	Maximum plasma concentration
CMC	Critical micelle concentration
CR	Controlled- release
$C_s$	Saturation solubility
CV	Coefficient of variation
CX	Compound X
D	Diffusion coefficient constant
DLM	Diffusion layer model
DTAB	Dodecyltrimethylammonium bromide
ESF	enzyme distribution factor
<i>et al.</i>	And others
F	Formulation
FaSSGF	Fasted state simulated gastric fluid
FaSSIF-V1	Fasted state simulated intestinal fluid, version 1
FaSSIF-V2	Fasted state simulated intestinal fluid, version 2
FDA	Food and Drug Administration
FeSSGF	Fed state simulated gastric fluid
FeSSIF-V1	Fed state simulated intestinal fluid, version 1
FeSSIF-V2	Fed state simulated intestinal fluid, version 2
$f_t$	Percentage of drug dissolved at time t
GE	Gastric Emptying
GI	Gastrointestinal
GIT	Gastrointestinal tract
GMO	Glyceryl monooleate
h	Diffusion layer thickness
HCl	Hydrochloric acid



<b>HIF</b>	Humans intestinal fluid
<b>HPLC</b>	High Performance Liquid Chromatography
<b>HPMCAS</b>	Hydroxypropyl methylcellulose acetate succinate
<b>HTAB</b>	Hexadecyltrimethylammonium bromide
<b>I</b>	Ionic strength
<b>IDR</b>	Intrinsic dissolution rate
<b>IR</b>	Immediate release
<b>ITR</b>	Itraconazole
<b>IVIVC</b>	<i>In vitro – in vivo</i> correlation
<b>IVIVR</b>	<i>In vitro-in vivo</i> relationship
<b>k</b>	Rate constant
<b>k<sub>0</sub></b>	Zero – order release/dissolution constant
<b>k<sub>1</sub></b>	First – order release/dissolution constant
<b>k<sub>a</sub></b>	Absorption rate constant
<b>K<sub>a</sub></b>	Dissociation constant
<b>k<sub>e</sub></b>	Elimination rate constant
<b>K<sub>m</sub></b>	Michaelis-Menten constant
<b>LOD</b>	Limit of detection
<b>LOQ</b>	Limit of quantification
<b>M<sub>∞</sub></b>	Cumulative percentage of drug dissolved at infinite time
<b>Max</b>	Maximum percentage dissolved
<b>MDCK</b>	Madin-Darby Canine Kidney
<b>MDR-1</b>	multidrug resistance-1
<b>MM</b>	Michaelis-Menten
<b>MMC</b>	Migrating motor complex
<b>M<sub>t</sub></b>	Cumulative percentage of drug dissolved at time t
<b>n</b>	Number of replicates
<b>NA</b>	Not applicable
<b>NaOH</b>	sodium hydroxide
<b>Na-SIF</b>	Sodium based SIF
<b>NaTC</b>	Sodium taurocholate
<b>PAMPA</b>	Parallel artificial membrane permeability assay
<b>PBPK</b>	Physiologically Based Pharmacokinetic
<b>P<sub>eff</sub></b>	Humans effective permeability
<b>PK</b>	Pharmacokinetics
<b>pK<sub>a</sub></b>	Dissociation constant
<b>Prec</b>	Precipitation
<b>PSD</b>	Particle size distribution
<b>QC</b>	Quality control
<b>R</b>	Segment radius
<b>R<sup>2</sup></b>	Goodness of fit
<b>Re</b>	Reynolds number
<b>Ref</b>	Reference
<b>RH</b>	Relative humidity
<b>Rpm</b>	Rotation per min
<b>S</b>	Surface area
<b>S/N</b>	Serial number
<b>SD</b>	Standard deviation
<b>SDI</b>	Surface dissolution imager
<b>SF</b>	scale factor
<b>SGF</b>	Simulated gastric fluid
<b>SGF-M1</b>	SGF+0.01% SLS
<b>SGF-M2</b>	SGF+0.015% HTAB
<b>SIF</b>	Simulated intestinal fluid

<b>SIF-M1</b>	Simulated intestinal fluid-modified 1 (SIF+0.2% SLS)
<b>SIF-M2</b>	Simulated intestinal fluid-modified 2 (blank FaSSiF-V2+0.1% SLS)
<b>SIF-M3</b>	Simulated intestinal fluid-modified 3 (SIF+0.1% HTAB)
<b>SIF-M4</b>	Simulated intestinal fluid-modified 4 (SIF+1% HTAB)
<b>SIF-M5</b>	Simulated intestinal fluid-modified 5 (sodium-based SIF+1% SLS)
<b>SLS</b>	Sodium lauryl sulphate
<b>ST</b>	Surface tension
<b>ST</b>	Surface tension
<b>SUPAC</b>	Scale-up post approval changes
<b>t</b>	Time
<b>T<sub>50%</sub></b>	gastric half-emptying time
<b>TFA</b>	Trifluoroacetic acid
<b>T<sub>g</sub></b>	Glass transition temperature
<b>T<sub>i</sub></b>	The percentage dissolved of the test profile at the i time
<b>T<sub>lag</sub></b>	Lag time
<b>™</b>	Trademarked
<b>T<sub>max</sub></b>	Time to reach maximum plasma concentration
<b>UHT</b>	Ultra-heat-treated
<b>UK</b>	United Kingdom
<b>US</b>	United States
<b>USP</b>	United States Pharmacopoeia
<b>V</b>	Volume
<b>V<sub>max</sub></b>	maximum velocity
<b>vs.</b>	Versus
<b>WF</b>	Weighting function
<b>WF</b>	Wang Flanagan
<b>W<sub>max</sub></b>	Maximal amount of drug dissolved
<b>W<sub>t</sub></b>	Amount of the drug dissolved in time t
<b>z<sub>i</sub></b>	Charge number of ion

## Table of Units

<b>%</b> Percent
<b>°C</b> Degrees Celsius
<b>cm</b> Centimetre
<b>cm<sup>3</sup></b> Centimetre cube
<b>g</b> Grams
<b>h</b> Hour
<b>kg</b> Kilograms
<b>L</b> Liters
<b>mg</b> Milligrams
<b>min</b> Minutes
<b>mL</b> Milliliters
<b>mM (mmoL)</b> Millimolar
<b>mm</b> Millimetre
<b>mN/m</b> MilliNewton/metre
<b>N</b> Newton
<b>mOsmo</b> MilliOsmoles
<b>rpm</b> Rotation per minute
<b>w/v</b> weight by volume

## **Abstract**

Dissolution testing and physiological based pharmacokinetic modeling are the essential methods during drug development. However, there is a lack of a sound approach and understanding of the parameter that controls dissolution and absorption of amorphous formulations. Robust dissolution conditions and setup and PBPK models that have a predictability of *in vivo* results will expedite and facilitate the drug development process. In this project, cefuroxime axetil, CA (Zinnat<sup>®</sup> as the amorphous formulations); itraconazole, ITR (Sporanox<sup>®</sup> as the amorphous formulation) and a compound undergoing clinical trial, Compound X, CX (CX tablet as the amorphous formulation) were chosen. The design of experiments for the *in vitro* dissolution studies using different apparatus, media and setup which closely simulate the physiological condition of humans (CA and ITR) and dogs (CX) were implemented. The dissolution of CA, ITR and CX formulations was successfully characterised using different dissolution apparatus, setting and media (compendial, biorelevant and modified media) to simulate the changes of pH, contents, hydrodynamic conditions (flow rate and rotation speed) in human gastrointestinal tract (fasted and fed state). The change of hydrodynamics combined with media change that corresponded to the physiological conditions created with USP apparatus 4 and biorelevant dissolution media were able to mimic the *in vivo* performance of the tested formulations. Furthermore, surface UV dissolution imaging methodology that could be used to understand the mechanism of CA and ITR (Active compounds and their amorphous formulations) dissolution were developed in this project. The UV images developed using surface UV imaging apparatus provided a visual representation and a means for the qualitative as well as quantitative assessment of the differences in dissolution rates and concentration for the model compounds used. In this project, validated PBPK models for fasted state (CA, ITR) and fed state (CA, ITR and CX) were developed. These models incorporated *in vitro* degradation, particle size distribution, *in vitro* solubility and dissolution data as well as *in vivo* human/ dog pharmacokinetics data. Similarly, the results showed that level A IVIVCs for all three model compounds were successfully established. Dissolution profiles with USP apparatus 4 combined with biorelevant media showed close correlation with the *in vivo* absorption profiles. Overall, this project successfully provides a comprehensive biorelevant methodology to develop PBPK models and IVIVCs for orally administered amorphous formulations.

## 1. Introduction

### 1.1 Amorphous state

Solid forms are classified into crystalline and amorphous states based on the order of molecular packing (1-3). Molecules aggregate together with long-range order in the crystalline state. The term “long range order” refers to molecular units in a crystal lattice that are repeated according to a three-dimensional pattern in crystallographic directions. The relative location and orientation between neighbouring components of a solid that has long range order can be accurately described at the molecular level (4). But, this is not the case for the amorphous state (1, 5). The amorphous state is characterised by random distribution in the relative orientation of neighbouring molecular units. Furthermore, the translational and rotational orders are present in the crystalline solids but they are absent in the amorphous solids (Figure 1).


	
<b>Crystalline state</b> Solid with orientational and positional long-range order in three dimensions.	<b>Amorphous state</b> Solid with no orientational or positional long-range order

Figure 1. Schematic structure of crystalline and amorphous states.

The crystalline state and the liquid state above the melting temperature ( $T_m$ ) are thermodynamically stable. On the other hand, amorphous materials are thermodynamically unstable. The kinetic stability of amorphous material depends on the physical state of the material. Two physical states can be defined for amorphous material: the amorphous state and the super-cooled liquid state. The amorphous state is the preferred type of drug formulation because it is kinetically stable. This implies that the equilibrium state, *i.e.* crystalline, is not reached within the timeframe of the experiment or the shelf life of the product. It should be noted that in some definitions the terms “glass/glassy”, “amorphous” and “non-crystalline” are synonymous and interchangeable (6).

#### 1.1.1 Preparation of amorphous solids

In the pharmaceutical industry, some drug candidates during the pre-formulation phase are first prepared as partially or totally amorphous forms unintentionally due to isolation

methods (e.g., lyophilisation) or a higher impurity level (7). As a solid state of increasing importance, the amorphous state of a compound can be formed by various methods such as lyophilisation, spray drying, melt extrusion, melt quench cooling, solution evaporation and solid dispersion (8).

#### **1.1.1.1 Solid dispersion**

Solid dispersion can be defined as one type of method to produce an amorphous compound by incorporating a hydrophobic drug into a hydrophilic carrier (9). It also can be referred to as a product formed by converting a fluid drug-carrier combination to the solid state (10). Essentially, it is a group of solid products consisting of at least two different components, generally a hydrophilic matrix and a hydrophobic drug. The matrix can be either in crystalline or amorphous form. Alternatively, the drug can be dispersed or dissolved molecularly throughout the carrier matrix (termed as a solid solution) (9).

It is one of the most studied methods to solubilise and to enhance dissolution rates of Biopharmaceutical Classification System (BCS) class 2 compounds (11). For instance, a solid dispersion of ritonavir (12) and ER-3421 (a dual 5-lipoxygenase/cyclooxygenase inhibitor) (13) were found to have a much higher dissolution rate than the crystalline counterpart and resulted in higher AUC and  $C_{max}$  in *in vivo* study. Another example is solid dispersion of piroxicam in polyvinylpyrrolidone K-30 at ratio 1:4 generating the amorphous state of the drug. An approximate 38-fold increase in dissolution rate compared with that of the pure drug was also observed (14).

#### **1.1.2 Solubility of amorphous compound**

The amorphous form has attracted increasing interest within the pharmaceutical field because its higher solubility could achieve better dissolution rate, absorption rate and increase the bioavailability of poorly water-soluble compounds (15). The solubility increment of amorphous forms over crystalline states depends on the potential energy difference between these physical states (16, 17). It was estimated that 10-1600 folds of solubility increment can be achieved by applying the amorphous form (18-22).

From the physical stability point of view, the drug which is formulated in an amorphous state should be preserved and stabilised to exert its solubility advantage even during

the dissolution process. There are only a handful of oral pharmaceutical products containing amorphous compound that have been successfully marketed despite several decades of effort in research and development. These products are Zinnat<sup>®</sup> (CA), Sporanox<sup>®</sup> (ITR), Rezulin<sup>®</sup> (troglitazone), Intelence<sup>®</sup> (etravirine), Rezulin<sup>®</sup> (everolimus) and Crestor<sup>®</sup> (rosuvastatin). The limited commercial success indicates the challenges with the stability of the amorphous formulations (8, 23). One of the issues relating to the stability of the amorphous state is its solution-mediated transformation characteristic. Solution-mediated transformation of amorphous to crystalline state is the conversion of metastable solids such as amorphous solids to the crystalline state when the solids are exposed to a solvent. The transformation to the more thermodynamically stable crystalline state occurs at a higher rate because of the higher mobility in the solution state than in the solid (8, 23).

In drug process development, characterisation of solution mediated transformations in the amorphous state is important because it describes information on amorphous crystallisation (24). The schematic representation of concentrations in the solution, as well as the solid compositions as a function of time, is shown in Figure 2 for a typical solution-mediated transformation process (24).

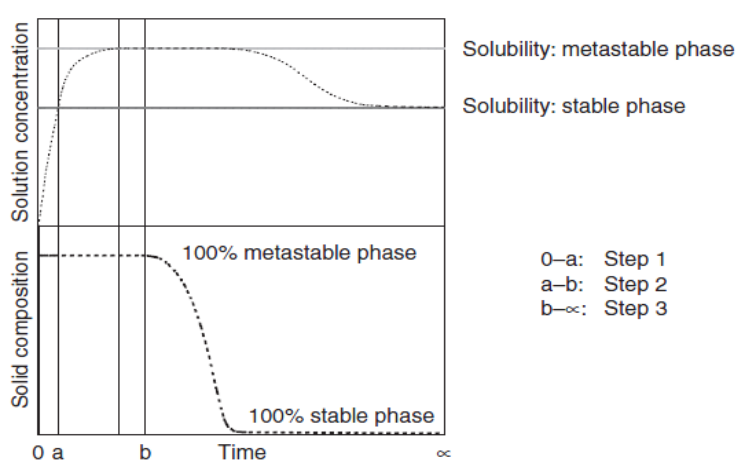


Figure 2. Concentrations in the solution and the solid compositions as a function of time during the solution-mediated phase transformation. Reproduced with permission from (24).

As depicted in Figure 2, three consecutive steps are involved in a solution-mediated transformation (25-27): (1) Initial dissolution of the metastable phase into the solution to reach and exceed the solubility of the stable phase; (2) Nucleation of the stable phase. (3) Crystal growth of the stable phase coupled with the continuous dissolution of the metastable phase. For the overall solution-mediated transformation process, step (2) is usually the slowest. Therefore, this is the rate-determining step as nucleation is involved. When step (2) is the rate-determinant, factors such as the

solubility and the solubility difference between the phases, processing temperature, contact surfaces, agitation, and soluble excipients/impurities that affect nucleation will influence the overall transformation.

### 1.1.3 Saturation, supersaturation and precipitation

Amorphous compounds are high energy solid systems that are capable of reaching higher kinetic solubility values (supersaturation) than would be expected from the equilibrium solubility of a crystalline material (28). Amorphous solid dispersions aim at generating high and possibly supersaturated intraluminal concentrations of poorly water soluble compounds. The dissolution characteristics of solid dispersions depend to a large extent on the physical state (ideally: amorphous), drug dispersivity (ideally: molecular dispersion) and particle size (29). Research has shown supersaturation of a compound can be achieved using several methods:

1. The *in vivo* gastrointestinal conditions: effect of pH and content changes from stomach to intestine

Due to the pH gradient in the GI lumen (pH 1.5–2 in the stomach compared with pH 5–8 in the intestine), the solubility of weak bases in gastric fluid (ionised form) typically exceeds their solubility in the intestinal fluid (unionised form). Therefore, higher dissolution of poorly water-soluble weak bases in the stomach before transfer to the intestine may result in supersaturation (29, 30).

2. Solubilised formulations

The hydrophobic drug is formulated as a solution which is in dissolved form. For example, drugs are solubilised in the formulation in a mixture of hydrophilic cosolvents, water-soluble and water-insoluble surfactants, complexing agents (*e.g.*, cyclodextrins) and oils (29).

3. High-energy and rapidly dissolving solid forms

As mentioned earlier, amorphous state requires less energy to dissolve, resulting in higher apparent solubility and increased dissolution rates (22). Methods such as particle size reduction through milling and co-grinding that can form an amorphous state may increase dissolution rates by enhancing the surface area available for dissolution (29, 31). Co-crystals and crystalline salt forms may provide improved solubility and dissolution properties without being thermodynamically unstable (32).

In recent pharmaceutical literature, the terms “equilibrium (thermodynamic) solubility” and “kinetic or apparent solubility” are often used for the systems with stable and metastable equilibria, respectively (33, 34). Essentially, solubility can be defined as the



analytical composition of a mixture or solution that is saturated with one of the components of the mixture or solution, expressed in terms of the proportion of the specific component in the mixture or solution (35).

A solid phase is crystallised from solution if the chemical potential of the solid phase is less than that of the dissolved component. A solution in which the chemical potential of the solute is the same as that of the corresponding solid phase and is in equilibrium with the solid phase under the given conditions (temperature, pH, and concentration) is called a saturated solution (35). In order for crystallisation from solution to occur, however, this equilibrium concentration or solubility must be exceeded. This excess concentration or chemical potential, called the supersaturation, is the driving force for nucleation and crystal growth (36).

For poorly water-soluble drugs, the maximum achievable intraluminal drug concentration may limit absorption. However, the intraluminal concentration of a drug is not necessarily limited by its solubility in gastrointestinal fluids (29). Drugs may be in solution at a concentration above their saturation solubility, that is, in a state of supersaturation. The degree of supersaturation can be expressed by the supersaturation ratio,  $S$  (Equation 1) (29):

$$S = C/C_{eq} \quad \text{Equation 1}$$

where  $C$  and  $C_{eq}$  represent the solubility and equilibrium solubility (saturation) respectively. Theoretically, supersaturated states may be created by increasing the solute concentration or decreasing the solute (36).

A solution is defined as unsaturated, saturated or supersaturated based on the following relationships:  $S < 1$ ,  $S = 1$  or  $S > 1$ , respectively (29).

A supersaturated drug solution is thermodynamically unstable compared to the equilibrium condition (saturation). Thus, it has the tendency to return to the equilibrium state (lowest chemical potential) by drug precipitation. The higher the supersaturation the more precipitation will take place as the former is the driving force for the latter (37).

A thermodynamically unstable, supersaturated solution of a drug can only be generated from a higher energy form of the drug (as compared to the crystalline powder) such as an amorphous form. The delivery of high-energy solid forms that provides an accelerated dissolution and a higher apparent solubility could induce the

generation of supersaturated solutions in the gastrointestinal lumen that can result in increased flux across the intestinal wall (29).

This higher initial solubility may be sufficient to ensure increased and more rapid absorption for a drug with good permeability such as BCS class 1 and 2 compound. But a more thermodynamically stable form may crystallise at any time inside the GIT and the crystallisation would have a major impact on the product performance *in vivo* (31, 36). The higher dissolution rate and apparent solubility of an amorphous compound usually causes supersaturation during *in vivo* dissolution. Therefore, this may lead to precipitation in the GI tract (as the supersaturation is the driving force for the precipitation) and compromise oral bioavailability (29). If a crystallisation-inhibitory polymer is incorporated into the amorphous solid dispersion, the *in vivo* precipitation may be delayed or completely eliminated, resulting in much improved oral absorption. It is ideal if the polymeric carrier can function as a precipitation (crystallisation) inhibitor during *in vivo* dissolution (24).

In the stomach and intestine, drug solubility can be enhanced by food and bile components such as bile salts, lecithin, and fatty acids. Supersaturation in the intestinal fluid is an important property that can play a significant role in drug absorption. For compounds with poor intrinsic solubility in the intestinal fluid, solubility is often a limiting factor for absorption. For many of these compounds, it may not be possible to enhance the saturation solubility to the extent required such that the whole dose is dissolved in the GI fluid. In this case, creating or maintaining supersaturation in the intestinal fluid can be an effective way to enhance the absorption of these compounds (28).

## **1.2 *In vitro* dissolution testing**

In this section, the application of *in vitro* dissolution testing in industry and research is presented. Then, the characteristics of a surfactant and some commonly used surfactants are discussed. This is followed by a detailed description of the dissolution media (compendial, biorelevant and modified media) and three major dissolution apparatus namely basket (USP apparatus 1), paddle (USP apparatus 2) and flow-through cell (USP apparatus 4). The biorelevant dissolution media, apparatus and test conditions will be discussed with emphasis on their relevance to the physiological factors, including the pH, composition of the GI fluids, volume, GI hydrodynamics/motility and food effect. A brief review of statistical approaches of comparing *in vitro* dissolution profiles is presented as well.

### **1.2.1 Applications of *in vitro* dissolution testing**

Dissolution testing is an essential test in the development and production of solid dosage forms. For example, at the early stage of drug research and development, dissolution testing is used for active compound characterisation and formulation screening. It is also used to develop and evaluate the performance of new formulations by examining drug dissolution from dosage forms, evaluating the stability of these formulations, and monitoring and assessing the formulation consistency and changes (38, 39). Dissolution testing is also used in process development and scale up. For example, it is used to determine the critical process variables for formulations. It is used to show the effect of different polymer or excipients on manufacture variables and to determine changes in the formulation or manufacturing process (40, 41). Meanwhile, dissolution testing serves as an important quality control (QC) tool to verify manufacturing and product consistency (42). It is also employed to evaluate the stability of the product during its shelf life.

Moreover, appropriate dissolution methods can be developed to obtain an *in vitro-in vivo* correlation (IVIVC) and dissolution specifications (43) and other biorelevant information that will guide bioavailability and bioequivalent assessment of drug products (44, 45). For example, dissolution testing was used to understand and improve the prediction of *in vivo* dissolution and absorption of lipophilic compounds (46), poorly soluble weak bases (47) and several BCS Class 2 compounds (48). Similarly, the dosage-form related food effects for marketed nifedipine tablets that were previously observed in human bioequivalence studies could be predicted with dissolution testing (49). It is noteworthy that the stomach to intestine pH-shift can be

simulated in dissolution testing (such as with USP apparatus 4 with media change setup). A dissolution study at a single pH is not able to predict the performance of formulations of weak bases *in vivo* (50). For instance, a study demonstrated that the results of *in vitro* dissolution tests in an acidic medium and *in vivo* absorption for four solid dispersions of a poorly soluble weak base compound did not correlate well as faster release and increased supersaturation in an acidic medium correlated with lower bioavailability (51). Presumably, this effect can be explained by differences in the recrystallisation rate upon transfer to the small intestine (increased driving force for precipitation in case of higher supersaturation).

As mentioned earlier, dissolution serves as an *in vitro* surrogate for *in vivo* bioequivalence studies by development of *in vivo* – *in vitro* correlation (IVIVC) which can be used to support a biowaiver, especially for BCS (Biopharmaceutics Classification System) Class I compounds. A biowaiver allows the use of dissolution results as a surrogate to bioequivalent results to prove bio-equivalence of formulation or effect of change in the manufacturing process. This approach minimises the cost and time of the drug approval process because dissolution testing is used instead of human study (41).

### **1.2.2 Biorelevant dissolution method**

Biorelevant dissolution testing refers to the *in vitro* dissolution study utilising the dissolution media that mimic the conditions in the GI tract and the apparatus that can simulate the dynamic environments that the dosage form experiences in the GIT as well as evaluate the fate of the dosage form and active compound in the GI lumen (52). Thus, in comparison to dissolution methods used for quality control (QC) (compendial dissolution method), which at best simulate pH effects and/or osmolality on the drug release under *in vivo* conditions, biorelevant dissolution media are generally more complex and more predictive of *in vivo* dissolution (53).

Under the current industry setting, the design of dissolution testing used for QC is primarily based upon the selection of discriminatory media, apparatus, and conditions that can be used routinely for QC purposes (53). Nevertheless, there is an increasing demand for the development of biorelevant dissolution methods that can provide some predictive estimates of the drug release with respect to the *in vivo* drug product performance (54, 55).

In biorelevant dissolution testing, the experimental conditions represent and simulate the GI tract environment, thus this type of testing is predictive of complex *in vivo* dissolution behavior of poorly-soluble compounds (46, 54-56). Currently, a large number of different media are used, from water to various buffer solutions having different pH values as described in the USP monographs (42), biorelevant dissolution media (52, 57) and modified media which contain artificial surfactants such as SLS and Triton-X (58, 59).

### 1.3 The dissolution medium

Literature has reported a wide range of dissolution media for simulating gastric and intestinal contents (60). Compendial media are simple aqueous preparations used to simulate mainly the pH and ionic strength of the fasted human GI compartments (54). The compendial media do not include surfactants and therefore are less likely to simulate the solubilisation and the wetting effect that occur *in vivo* because compounds which are sparingly water-soluble are solubilised in the body by endogenous surfactants such as bile acids, bile salts, lecithin, *etc* before the drug molecules are absorbed. Media containing artificial surfactant and biorelevant media (prepared using bio-surfactant, bile salt and lecithin) with more complex composition aimed to mimic osmolality, buffer capacity and surface tension of different GI segments were introduced at a later stage (60).

#### 1.3.1 Compendial media

In the 1970's two main compendial media were introduced in pharmacopeia (61). Such media mainly simulate the pH and ionic environment of gastric and intestinal environments (54).

The first medium is used to simulate the fasted human stomach (simulated gastric fluid, SGF). SGF consists of an unbuffered aqueous sodium chloride solution with the pH adjusted to 1.2 with hydrochloric acid (Table 1). According to the United States Pharmacopeia, SGF could be prepared with or without the addition of pepsin (3.2 mg/mL), an enzyme that exists in the human stomach (42).

The second medium is formulated to represent the human fasted buffered intestine fluid (simulated intestinal fluid, SIF). SIF is a mixture of phosphate buffer and sodium hydroxide solution at pH 6.8 (Table 1). This medium can also be prepared with or without pancreatin (62). Pepsin and pancreatin play a minimum role in drug dissolution; nevertheless these enzymes could enhance dissolution of a cross-linked hard gelatin capsule (57, 62). It is noteworthy that the concentration of pepsin indicated in the SGF described in the USP (3.2 mg/mL) (42) is too high compared with that in the basal gastric pepsin output *in vivo* (the upper limit of pepsin concentration is 0.8 mg/mL in an empty stomach) (63).

Table 1. Composition of SGF and SIF

	SGF (42).	SIF (42).
NaCl (mM)	34.2	-
Hydrochloric acid (mM)	70.96	-
Potassium dihydrogen orthophosphate (mM)	-	49.96
Sodium hydroxide (mM)		15.4
pH	1.2	6.8
Surface tension (mN/m)	70	70
Buffer capacity (mmol/l/ΔpH)	Not buffered	18.4±0.2
Osmolality (mOsm/kg)	Not reported	113

### 1.3.2 Media containing artificial surfactant

Bile salt used in biorelevant media presents some practical problems in terms of assay requirements and cost. Thus, for routine quality assurance, it would be favourable to exchange with synthetic surfactant systems that match the surface tension lowering and solubilisation properties of the natural surfactants (64). It is likely that the wettability of pharmaceutical materials may be different for bile salt compared to other surfactants, and currently there is no consensus as to which surfactants, and amount, should be used to accurately simulate *in vivo* behaviour (65). The use of synthetic surfactants such as SLS and HTAB in dissolution of poorly soluble compounds is expected to be more biorelevant to the *in vivo* situations than the addition of co-solvents or hydroalcoholic media (38, 64).

#### Sodium Lauryl Sulfate

Sodium Lauryl Sulfate (SLS), also known as sodium dodecyl sulfate (SDS) ( $\text{CH}_3(\text{CH}_2)_{11}\text{OSO}_3\text{Na}$  (MW 288.38), is an ionic surfactant. The molecule has a tail of 12 carbon atoms (Figure 3), attached to a sulfate group, giving the molecule the amphiphilic properties required for solubilisation (66).

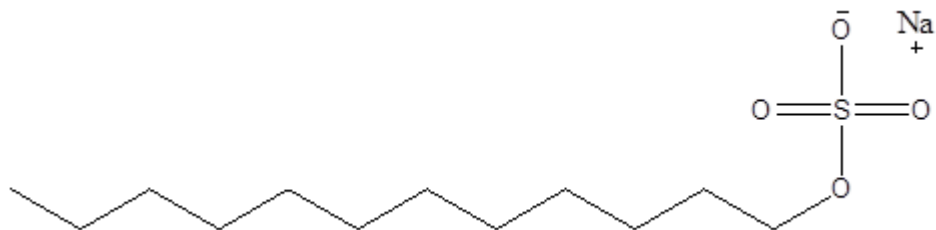


Figure 3. Chemical structure of SLS

### Hexadecyltrimethylammonium bromide

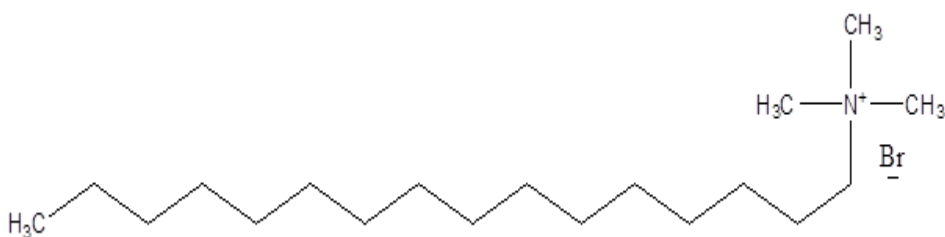


Figure 4. Chemical structure of HTAB

Hexadecyltrimethylammonium bromide or HTAB ( $C_{19}H_{42}BrN$ , Figure 4) has a molecular weight of 364.5 (67). It is a cationic surfactant and its activity is neutralised by soaps and anionic detergents, such as SLS. It is freely soluble in water (solubility 100 mg/mL) and is stable in acidic solution (67).

### 1.3.3 Biorelevant dissolution media

The biorelevant dissolution media (BDM) are designed with the aim of simulating the human physiological fluids for drug compound dissolution and solubility assessment (68).

It is a well-known fact that better understanding of the intraluminal factors that affect dissolution in both fasted and fed state would allow a definition of more appropriate biorelevant media (29). For example, the biopharmaceutic scientists still need to know more about the influence of endo and exogeneous components such as bile salts, phospholipids and food digestion products on the rate and extent of intraluminal dissolution (29, 69).



### 1.3.3.1 Media to simulate the contents of the stomach

#### Fasted state

Physiologically the volume of gastric fluid in the fasted state is in the range of 15–50 mL (70, 71). It was reported that average gastric pH ranges from 1.5 to 2.9 and its values vary among individuals (72, 73). Gastric fluid is hypo-osmotic ( $\leq 200$  mOsm/kg) (72, 74, 75) and the main cation and anion is  $\text{Na}^+$  and  $\text{Cl}^-$  respectively. Literature suggests that the surface tension in fasted gastric fluids is in the range of 41.9–45.7 mN/m, lower than water (approximately 70 Nm/m) (73). It was reported that pepsin can only partly be responsible for this reduced surface tension because it is not able to reduce the surface tension to less than 55 Nm/m (46). Thus the presence of low amounts of bile salts, refluxed from the duodenum, or lyso-phospholipids, from breakdown of gastric mucosal cells might explain the low surface tension in the preprandial state (76).

Furthermore the pH of the SGF medium is only 1.2, an acidity level that is rarely observed even in young healthy volunteers (especially after the ingestion of a glass of water). Values between 1.5 and 2.5 are more the norm in such subjects. In order to tackle this issue, fasted-state simulated gastric fluid (FaSSGF) as a dissolution medium simulating the preprandial stomach was developed. This medium has a pH of 1.6 with 34.2 mM NaCl, 0.1 mg/mL pepsin, 80  $\mu\text{M}$  bile salts and 20  $\mu\text{M}$  lecithin. The medium has a surface tension of 42.6 mN/m and osmolality of  $120.7 \pm 2.5$  mOsmol/kg which are close to human physiological values (46).

#### Fed State

It is a challenge to establish appropriate but easy to work dissolution media for simulating the fed-state stomach. Firstly, conditions in the stomach after meal intake can vary largely, depending on meal type. Initially, the composition of the gastric fluids will be close to the composition of the meal with regard to pH, osmolality and surface tension. Over time, with secretion of gastric juices and following gastric emptying, values will return to those of the fasted state (73). A study has suggested that the capacity of the human stomach is 1–1.6 L (77). The time to return to fasted state values has been reported to be between 1 and 4 h, depending on the composition and volume of the ingested meal (78, 79).

Milk (3.5% fat) has been used to simulate fed conditions in the stomach because it contains nutrients comparable to a typical western diet (80, 81). The surface tension of milk decreases with increasing fat content (up to 4% fat); for example the surface tension of skimmed milk and whole milk are 52.5 and 47.5 mNm<sup>-1</sup> respectively (82). These values are much higher than the surface tension of the fed stomach of a human (30-31 mNm<sup>-1</sup>(83)). Furthermore, milk has much lower osmolality and buffer capacity values than a homogenised meal, making it less suitable as a fed state simulated gastric fluid (84). Milk has a pH of about 6.5 and research has shown that it might be too high for the later stages of gastric digestion, even for the initial post-prandial state (76). Generally, milk and/or nutritional liquid products can be used only for simulation of initial gastric conditions in the fed state because the composition of the stomach contents in the fed state changes with time as secretions, digestion and gastric emptying proceed. Under *in vivo* conditions, lipids and casein micelles in the milk are partly digested during gastric residence, so the addition of enzymes might simulate the physiological conditions even closer (76).

Later on, researchers proposed to change intragastric composition through a gradually digesting milk technique (63, 85) and to use “snapshot” milk-based media to represent the changing composition of gastric content (57) (Table 2). Both techniques use homogenized long-life milk (3.5% fat) as the initial liquid medium. The lower nutrient content of milk compared to nutritional liquid products provides closer simulation of the intra-gastric conditions, where significant secretions (dilution of meal) take place. In addition, the ratio of carbohydrate/protein/fat in milk is close to that observed in the stomach of healthy volunteers after the administration of meals typically administered in BA/BE studies in the fed state (73).

The first technique establishes the concept of gradual digestion of the meal during the dissolution experiment (63). The initial medium is homogenized long-life milk (3.5% fat) which is gradually digested by integrating physiologically relevant amounts of a hydrochloric solution (1.83 M) containing 1.1 mg of protein (pepsin) per mL into the vessel every 15 min from 0 to 90 min. This concept of digestion of milk was modified in this current project with the aim of testing the effect of digested protein (as observed in the fed human stomach) to the dissolution of one of the model compounds, ITR. The study was modified by changing the milk (pH 7.5) with early FeSSGF (a milk solution with the ionic strength adjusted using sodium chloride and pH adjusted to pH 6.4) (Table 2).

Table 2. Composition of the media to simulate gastric contents in the fed state

	Early FeSSGF (57)	Digested early FeSSGF (57)	FeSSGF (Middle) (57)	Late FeSSGF (57)
Sodium chloride (mM)	148	148	237.02	122.6
Acetic acid (mM)	-	-	17.12	-
Sodium acetate (mM)	-	-	29.75	-
Ortho-phosphoric acid (mM)	-	-	-	5.5
Sodium dihydrogen phosphate (mM)	-	-	-	32
Milk : buffer	1: 0	1: 0	1: 1	1:3
1.83 M HCl aq solution containing 1.1mg/ mL pepsin	-	Addition of 1 mL/15min	-	-
Diluted HCl	qs pH 6.4	-	-	-
pH	6.4	Gradual reducing to pH 1.5	5	3
Osmolality (mOsmol/kg)	559 ± 10	No data	400 ± 10	300 ± 10
Buffer capacity (mmol/l/ΔpH)	21.33	No data	25	25
Surface tension (mN/m)	49.7±0.3	No data	52.3±0.3	58.1±0.2

In the second technique, three “snapshot” media were composed, each one corresponding to a certain post prandial timeframe (57). Medium composition was designed in order to reflect the pH value, buffer capacity and osmolality of the gastric contents during the first 75 min (early), from 75-165 min (middle) and after 165 min (late) following meal ingestion. Table 2 summarizes the composition of these media. The “middle” medium Fed State Simulated Gastric Fluid (FeSSGF) is considered as a representative of after food conditions for comparing formulations and/or predicting food effects compared with FaSSGF (57).

Therefore fed-state simulated gastric fluid (FeSSGF) can be used to observe food effects in the stomach (86). It contains UHT-milk and acetate buffer mixed in equal volumes and has a pH of 5.0 (53) (Table 2). This medium nearly represents the gastric conditions observed in the 75 to 165 min time frame, postprandially. For example, a recent study has shown that the percentage dissolved of a lipid-based formulation of RZ-50 (a weakly acidic BCS class 2 drug with a pKa of 4.31) in FeSSGF with USP apparatus 3 correlates best with the *in vivo* percentage absorbed data (87).

### 1.3.3.2 Media to simulate contents of the small intestine

#### Fasted state

The pH of the GI fluids changes from acidic to neutral within a distance of a few centimetres when shifting from the stomach to the duodenum. Average pH values between 6 and 7.1 have been observed for the fasted duodenum and upper jejunum, bicarbonates being the principal species responsible for the buffer capacity (72, 73, 79, 88). Osmolality is increased compared to the gastric fluids (270 mOsm/kg), with Na<sup>+</sup> and Cl<sup>-</sup> still the dominant ions (72).

Bile is supposedly only secreted as a response to food intake, but the fasted small intestine also contains low amounts of bile, which are partly responsible for the low surface tension (between 30 and 34mN/m) (73, 75). In human small intestinal fluids, mean values between 1.5 and 3mM bile salt have been reported under fasted conditions (89-91). Bile salts are secreted together with phospholipids, primarily phosphatidylcholine. In the fasted state, the ratio between bile salts and phospholipids have been reported to be between 2:1 and 10:1 in the intestinal fluids (90, 92).

Subsequently, Dressmann and co-workers (54, 59) suggested a biorelevant medium, simulating the fluids in the fasted small intestine (FaSSIF-V1, Table 3). Since then, FaSSIF-V1 has been widely used in dissolution studies and to determinate the biorelevant solubility, both in industry and academia. The composition of FaSSIF-V1 was developed by taking into consideration pH, osmolarity, buffer capacity and solubilizing capacity of the fluids in the fasted upper small intestine. Phospholipids such as lecithin are added in a 1:4 molar ratio to taurocholate, which is within the physiological relevant range. However, it must be noted that even with the addition of bile salt and lecithin the surface tension of both FaSSIF-V1 is much higher than the surface tension of human intestinal fluids (HIF) (54 vs 33.6 mN/m) (64).

As research progressed, Jantratid *et al.* improved the composition of FaSSIF-V1 with some modifications and proposed FaSSIF-V2 (57). The amount of lecithin was decreased from 0.75 mM in FaSSIF-V1 to 0.2 mM in FaSSIF-V2, osmolality was lowered and a maleate buffer was used instead of a phosphate buffer (Table 3). Physiologically, the principal buffer compound in the fasted small intestine is the bicarbonates but it is problematic to use in a medium due to the constant need of sprinkling with carbon dioxide to maintain the desired pH, buffer capacity, ionic strength

and osmolality (93). Thus buffers are selected mainly according to their ability to achieve the desired combination of pH, osmolality and buffer capacity (57, 94).

Table 3. Composition of the media to simulate the contents of the small intestine in the fasted state.

	FaSSIF-V1 (62)	FaSSIF-V2 (57)
Sodium taurocholate (mM)	3	3
Lecithin (mM)	0.75	0.2
Dibasic sodium phosphate (mM)	28.65	-
Maleic acid (mM)	-	19.12
Sodium hydroxide (mM)	8.7	34.8
Sodium chloride (mM)	105.85	68.62
Potassium dihydrogen Phosphate (mM)		
pH	6.5	6.5
Osmolality (mOsmol/kg)	270 ± 10	180 ± 10
Buffer capacity (mmol/L/ΔpH)	12	10
Surface tension (mN/m)	53	54

## Fed state

Similar to the fasted state in the stomach, the compositions of the fluids in the upper small intestine during the fed state will also be dependent on the type of food ingested but to a lower extent than in the stomach. Upon arrival in the duodenum, the chyme is mixed with bile and pancreatic secretions, both being slightly alkaline, which results in a pH in the duodenum to be in the range of 5.5 to 6.5; this is slightly lower than in the fasted state (73, 88, 90).

Large fluctuations in the pH are observed in the proximal duodenum, but the fluctuations diminish when the chyme moves along the small intestine. In addition, there is a pH gradient which increases between the duodenum and the ileum (79). As a consequence of chyme and intestinal secretions, both buffer capacity and osmolality in the intestinal fluids have been reported to increase after meal intake. Values of approximately 18-30 mmol/L/pH and 300–400 mOsm/kg during the first 2 h after a meal have been reported for the buffer capacity and the osmolality, respectively (73). In contrast, surface tension does not change significantly between fasted and fed state (73, 90).

Further studies have confirmed that food-induced bile secretions result in bile salt levels in the small intestine between 8 and 20mM with single measurements up to 40Mm (95-97). The molar ratio between bile salts and phospholipids in the fed state will be dependent on the phospholipid level in the food and has been reported to be in the range of 2:1 to 5:1 (98).

Together with FaSSIF-V1 mentioned above, a fed state simulated intestinal media (FeSSIF-V1) was developed (62). FeSSIF-V1 simulates the fluids in the fed upper small intestine in terms of bile salt and phospholipids levels, pH, osmolality and buffer capacity. The pH was set at 5.0, which is in the lower end of what has lately been reported in the literature (83). By the addition of sodium chloride, the osmolality is adjusted to  $635 \pm 10$  mOsm/kg, and acetic acid is added to maintain a higher buffer capacity of 76 mmol/L/pH, both values aiming at simulating the fed state. *In vivo*, the main buffer capacity probably originates from the food components, like generated peptides and amino acids (76).

Like FaSSIF-V1, taurocholate is used as bile salt in FeSSIF-V1. The ratio between the bile salt and phospholipids is kept at 4:1, even though ingested food often contains phospholipids that will decrease this ratio (76). FeSSIF-V1 was found to be suitable for a qualitative prediction of formulation and food effects for a series of compounds tested by Nicolaidis *et al.* (99) and Löbenberg *et al.* (100).

As a comparison to FaSSIF-V1, FeSSIF-V1 has lower pH (pH 5) and higher ionic strength. Both these factors can also impact drug solubility and dissolution. Mefenamic acid, an analgesic agent with a log P of 5.3 and a pKa of 4.2, has a better dissolution in FaSSIF-V1 compared to FeSSIF-V1 since the drug is more soluble at pH 6.5 than 5.0 (62). On the other hand, troglitazone, an antidiabetic drug, which is also a weak acid with pKa values of 6.1 and 12.0, shows a significantly improved dissolution in FeSSIF-V1 compared to FaSSIF-V1 (99). Whether the bioavailability of troglitazone is dependent on food intake has not yet been published, but bioavailability of mefenamic acid has been shown to be independent of food intake (101) indicating that a comparison between dissolution curves in FaSSIF-V1 and FeSSIF-V1 might be predictive for *in vivo* behaviour. Charman *et al.* observed a three-fold increase in danazol bioavailability upon food intake (102) and it was closely simulated by using FaSSIF-V1 and FeSSIF-V1 as dissolution media; whereas compendial media incorrectly suggested the absence of a food effect (62). FeSSIF-V1 is considered a reasonable starting point for assessment of food effects on drug dissolution in the small intestine. However, it does not account for the presence of lipolytic products (free fatty acids and monoglycerides) from dietary or formulation triglycerides in the intestine and may underestimate dissolution of lipophilic compounds (99).

As discussed in the fasted state, Jantratid *et al.* (57) modified the composition of FeSSIF-V1 based on recent studies related to the characterization of the fed intestinal contents under conditions simulating BA/BE (73), indicating that the pH in the upper small intestine decreases slowly after meal intake (57). In the updated media (FeSSIF-V2), the presence of lipolysis products (glyceryl monooleate and sodium oleate) were taken into account in the fed intestinal contents which also contributes to the surface tension of 40.45 mN/m, a value close to the aspirates (32.2-36.7 mN/m (103)). On the other hand FeSSIF-V1, which does not contain a lipolysis product, has a surface tension of  $46.3 \pm 0.1$  mN/m (104).

As with the biorelevant media simulating the contents of the stomach, FeSSIF-V2 (Table 4) is suggested as a representative of postprandial conditions in the small intestine for comparing formulations and/or predicting food effects compared with FaSSIF-V2 (57).

Table 4. Composition of the media to simulate the contents of the small intestine in the fed state

	FeSSIF-V1 (62)	FeSSIF-V2 (57)
Sodium taurocholate (mM)	15	10
Lecithin (mM)	3.75	2
Glyceryl monooleate (mM)	-	5
Sodium oleate (mM)	-	0.8
Acetic Acid	144	-
Maleic acid (mM)	--	55.02
Sodium hydroxide (mM)	101	81.65
Sodium chloride (mM)	173	125.5
pH	5.0	5.8
Osmolality (mOsmol/kg)	635±10	390 ± 10
Buffer capacity (mmol/l/ΔpH)	76	25
Surface tension (mN/m)	47.4	40.45

#### 1.4 Types of hydrodynamics

Dissolution testing plays such an important role in the pharmaceutical industry that an individual chapter describing the types and detailed specifications of dissolution apparatus has been included in United States Pharmacopoeia (42), European Pharmacopoeia (105) and Japanese Pharmacopoeia (106).

Wide variations in the hydrodynamic conditions can be obtained through the use of the four different USP test methods: the rotating basket (USP apparatus 1), the rotating paddle (USP apparatus 2), the reciprocating cylinder (USP apparatus 3) and the flow-through cell (USP apparatus 4) (42). In addition, different conditions can be obtained within one apparatus by changing the stirring rate, reciprocating frequency, or flow rate. The USP apparatus 2 is the most widely used dissolution method. Despite the simple design of the USP paddle dissolution apparatus, the hydrodynamics are complex and likely to be variable at different sites in the vessel (107) as different fluid velocities exist at various points in the dissolution vessel (108).



### 1.4.1 USP apparatus 1 (Basket apparatus) and USP apparatus 2 (Paddle apparatus)

In the 1970's United States Pharmacopoeia first introduced USP apparatus 1 and 2 as official testing apparatuses and a number of monographs were used to determine compliance with dissolution requirement for a formulation. Since then the USP apparatus 1 and 2 have become the most commonly used in the modern pharmaceutical laboratory (61). The basic components of the USP apparatus 1 and 2 are shown in Figure 5 and the set-up of the systems are standardised to the major references such as USP (42), British Pharmacopoeia (109) and the European Pharmacopoeia (105).

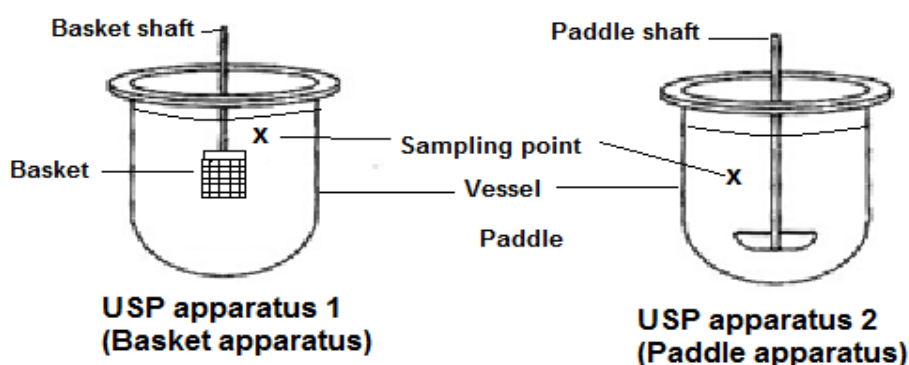


Figure 5. Schematic diagram of the USP apparatus 1 and 2.

USP apparatus 1 is used for dosage forms that tend to float or disintegrate slowly, for example capsules and powders; these dosage forms can be held inside the basket, whereas USP apparatus 2 is normally used for tablets which are placed on the bottom of the vessel. The dissolution vessel is cylindrical with a spherical bottom which is used to hold the dissolution medium. The vessel is filled with a fixed volume of media to which the formulation is exposed throughout the experiment (42).

### 1.4.2 USP apparatus 4 (Flow through cell apparatus)

Chapter <724> USP 29 (42) describes the dimensions and test method of flow through the cell apparatus which is also called USP apparatus 4 (Figure 6).

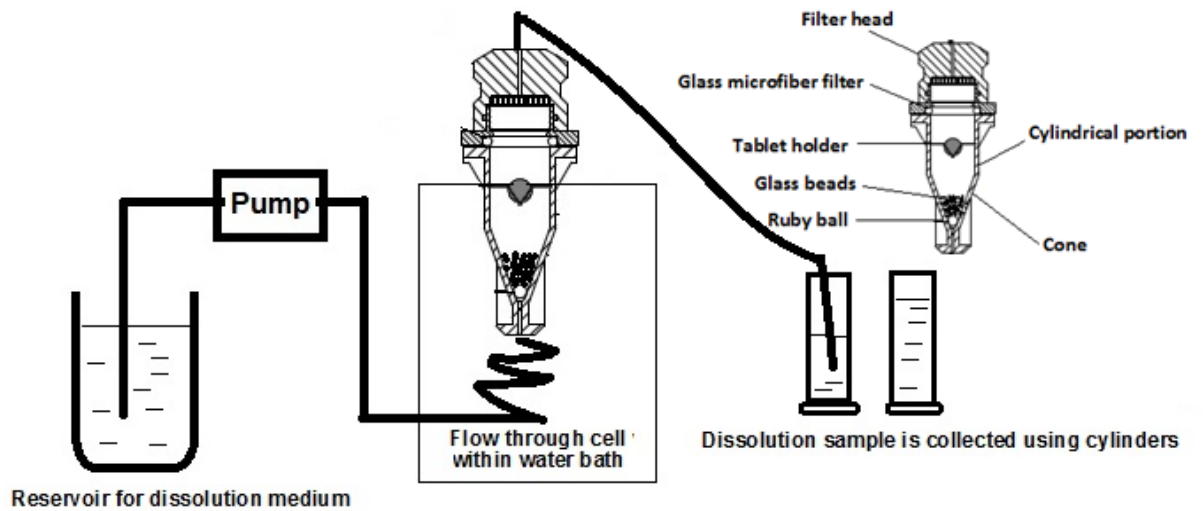


Figure 6. Schematic diagram of the USP apparatus 4, the inset shows the components of the flow-through cell

The apparatus consists of a reservoir containing a dissolution medium, a pump that forces the medium upwards through the vertically positioned flow-through cell, and a water bath. Generally the bottom cone of the cell is filled with small glass beads of about 1 mm diameter and a ruby ball of about 5 mm diameter is placed at the bottom of the cell acting as a check valve and prevents glass beads from blocking the cell channel. A filter (often a glass fibre filter) is positioned at the inner top of the cell (Figure 6). The filter only allows the dissolved particles to pass through and keeps the undissolved particles within the cell. Normally single or combination filters of different pore sizes are used to optimise the filtration.

The USP requirement for the pump is to deliver 4.0 mL, 8.0 mL and 16.0 mL per minute at 120 strokes with an accuracy of  $\pm 5\%$ . In order to achieve this requirement constant calibration of the flow rate is highly recommended to ensure optimum pump performance.

## 1.5 Surface UV dissolution imaging

Literature has shown that surface ultraviolet (UV) dissolution imaging is very useful in characterising active compounds and their formulations because the captured images illustrate the concentration distribution of drug compounds, which can be translated into the amount and rate of drug dissolution (110-115). The surface UV dissolution imaging is possible because most pharmaceutical drug substances contain a UV chromophore. The intensity of the measured light is converted to absorbance, creating a high-resolution, real-time 2D absorbance and concentration map of dissolution events within the flow cell which presents a detailed view of the dissolution process occurring on the surface of the drug compact (116). The data can then be processed for measurement of the intrinsic dissolution rate (IDR) of the active compound, with the whole process typically taking around 20 min (117). Using surface UV imaging mechanistic information such as swelling of the formulation, particle release and dissolution can be obtained. The ActiPix™ Surface Dissolution Imager system (SDI) and the operational and mathematical principles are discussed in this section.

### 1.5.1 Operational and intrinsic dissolution rate (IDR) of ActiPix™

The ActiPix™ SDI 300 (Paraytec Ltd., York, UK) comprises a sample flow cell, syringe pump, UV lamp and detector, and control and data analysis system. A single wavelength of light enters the flow cell while the dissolution medium is pumped into the cell at pre-set rates. The sample surface is parallel to the buffer flow but perpendicular to the light and camera creating a 4 dimensional array ( X,Y, intensity, time) which is used to extract data in and around the solid-liquid interface. The UV light transmission through the flow through cell is recorded by the camera chip behind the flow cell. The effluent will then leave the flow cell downstream from the sample surface via the waste outlet (Figure 7).

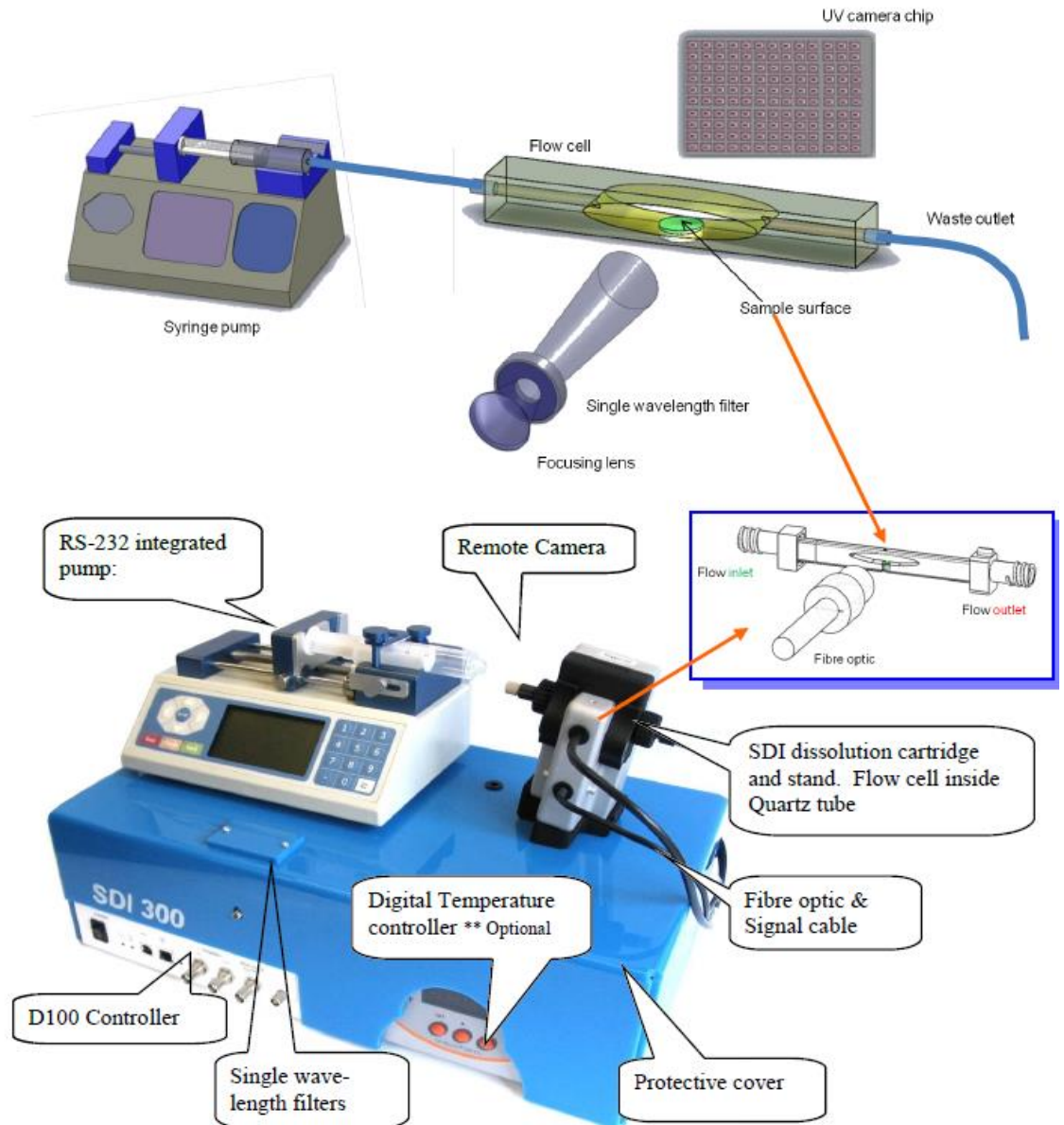


Figure 7. Photograph of ActiPix™ SDI 300 dissolution imaging system and the experimental UV imaging apparatus setup schematic (Reproduced with permission from (116)).

Meanwhile, ActiPix™ software uses validated equation reported in literature to calculate the intrinsic dissolution rate (IDR; mass/time/area: unit in mg/min/cm<sup>2</sup>) (116, 117). IDR values are calculated from the velocity at z (z, distance perpendicular to the surface horizon) and the drug concentration in the measurement zone (shown in Figure 7) using Equation 2.

$$IDR = \frac{\sum_{z=0}^{H/2} v_z M c_z W \Delta z}{S} \quad \text{Equation 2}$$

Where  $v_z$  = velocity at z, M = molecular weight,  $c_z$  = concentration at z, W = width of flow cell,  $\Delta z$  = effective pixel height, S = surface area of sample, H = height of flow cell in observation region.

### 1.5.2 Applications and advantages of surface UV dissolution using ActiPix™ technology

The ActiPix™ SDI300 is a multipurpose UV area imaging system which enables quantitative imaging of surface dissolution for various dosage forms such as active compound (110, 112, 114), transdermal patch (111), crystal (113), gels (118), polymer (119), cocrystal (120, 121) and oily liquid (122, 123). Using this system, temporal and high resolution spatial data from the solid-liquid interface can be observed. Measurement of this dissolution process offers insight into surface events such as boundary layer thickness, static diffusion rate, boundary layer gradient, surface concentration, contour distribution, concentration gradient profiles, and surface changes from swelling or gelling (124).

The ActiPix™ SDI300 also supplies special insights into processes occurring in microns to millimetres from the surface, the crucial distance range for recognizing dissolution. It enables both disintegration and dissolution to be visualised simultaneously (117). For example, before the dissolved material is diluted when transported to the bulk solution, the highest concentration achievable from a drug compound is directly at the surface. By selecting the corresponding chromophore wavelength, the concentration of the tested compound can be determined in the immediate vicinity of the sample.

Moreover, the dissolution medium can be changed easily (for example from simulated gastric medium to simulated intestinal medium) that will reveal the effect of medium (pH and buffer) and hydrodynamics (flow rate) to the precipitation and dissolution of the tested compound. The resulting images with media change setup may increase the understanding of the *in vivo* dissolution process, which may also increase the predictive ability of this dissolution test method. Owing to the fact that the flow cell volume is small, flow rate changes can be rapidly achieved. For example, the flow rate can go from high velocity (4 mL/min) down to no velocity (static, 0 mL/min) instantly. Similarly, the low volume also means that less dissolution medium is required. For example, for an experiment running at 1 mL/min for 20 min, a mere 20 mL of medium would be used. It is cost-effective when expensive media such as biorelevant media are used. The dissolution setup is very useful for screening potential drug compounds during the pre-formulation stages because the intrinsic dissolution rates can be obtained in less than 20 min compared to 24 h equilibrium IDR using the traditional dissolution system (Wood apparatus).

## 1.6 Oral Drug Absorption and PBPK modeling

### 1.6.1 Parameters to be considered in drug absorption modeling

Drug absorption from the human GIT is a very complex process (53). Parameters to be considered in drug absorption modeling can be divided into four categories: (1) Physiological (2) Biochemical (3) Physicochemical and (4) Dosage form and formulation parameters. The first and second categories consist of physiological parameters of the GIT such as gastrointestinal pH, gastric emptying, small intestinal transit time, active transport and efflux as well as gut metabolism (125-127). The third category represents physicochemical parameters of the drug such as pKa, solubility, stability, diffusivity and lipophilicity. The last category comprises formulation related parameters such as drug particle size, crystal form, surface area and type of dosage form such as tablet, capsule, solution, suspension (125, 126).

#### 1.6.1.1 Physiological parameters

The human GIT physiology allows maximum drug absorption in the small intestine, mainly due to the vast presence of villi and microvilli in the small intestine cell lining that provide large surface area and blood flow. For example, the surface area of the small intestine is approximately 200 m<sup>2</sup> and an estimated 1 L of blood is pumped through the intestinal capillaries each minute. To contrast, the corresponding estimates for the stomach are 1 m<sup>2</sup> and 0.15 L/min (128). Once the drug compound is emptied by the stomach to the small intestine, then the fate of the drug compound depends on the motility pattern (*in vivo* hydrodynamics) and small intestine transit time which determine the exposure of the drug to the absorption site.

Meanwhile, in order to reach the blood circulation, dissolved compounds have to pass a physical barrier, consisting of a mucous layer and the intestinal monolayer of enterocytes (Figure 8). Molecules (both nutrients and xenobiotics) can cross this monolayer via the paracellular (intercellular) or transepithelial (transcellular) route (Figure 8). As the intercellular space is very limited (*e.g.* 0.8 nm in human jejunum, 0.3 nm in human colon) due to the presence of tight junctions between the enterocytes, only small, highly hydrophilic molecules can use the paracellular route (129). However,

most drug molecules cross the monolayer through transepithelial transport following simple passive diffusion (130).

The absorbed drugs will be transported via the blood circulation to the liver where certain drugs will be metabolised during the hepatic first pass metabolism. Some drugs will undergo degradation and precipitation inside the lumen. Subsequently, the drug compound will go to the colon where minimum drug absorption takes place. The processes involved are illustrated in Figure 8.

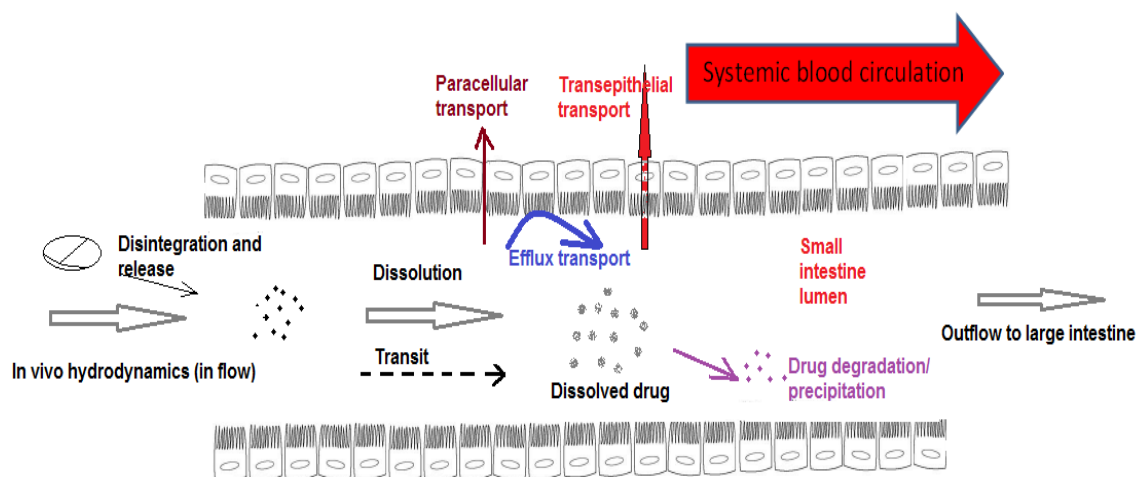


Figure 8. Schematic illustration of intestinal drug absorption processes.

The various physiological parameters that could affect the intestinal drug absorption can be classified as organic (related to GI organ system) parameters (e.g., gastric emptying, intestinal motility patterns, GI transit time, GI fluids characteristics (volume, osmolality, pH, buffer capacity) and biochemical parameters (e.g., GI and liver enzyme metabolism, efflux transporters and active uptake transporters) (126, 131-133).

### 1.6.1.2 Biochemical parameters

Apart from serving as a physical barrier, the intestinal epithelium also behaves as a biochemical (metabolism and efflux) barrier for the permeated drug molecules. Both the GI lumen and the intestinal enterocytes behave as a site of drug metabolism as they contains numerous enzymes, including esterases, phosphatase and cytochrome P450 (CYP450) isoenzymes. They may play an important role in the absorption of prodrugs and may limit oral absorption of substrate compounds of CYP3A isoenzymes and efflux transporters (P-gp, BCRP, and MRP-2).

## **Transporter-mediated uptake and elimination**

Intestinal efflux may affect the absorption of various compounds by the active secretion of molecules from epithelial cells into the luminal or serosal side of intestine. These transporters have broad substrate specificity and can be found in other organs as well, resulting in various effects on drug disposition. Thus, approximately 400 membrane transporters had been identified in human genomic study.

Examples of efflux transporters in the apical membrane of epithelial cells include P-gp, multi drug resistance-associated protein 2 (MRP2) and breast cancer resistance protein (BCRP) and ATP-binding cassette (ABC) proteins (134, 135). P-gp is an efflux transporter belongs to the ABC family. P-gp is considered to be a main contributor of non-linear absorption kinetics of many compounds (136). In the intestine, P-gp mediated efflux can reduce the bioavailability of drugs that are administered orally (137). Due to its very broad substrate specificity, P-gp mediated transport processes have been reported for a variety of drugs including: vincristine, vinblastine, doxorubicin, daunorubicin, etoposide, paclitaxel, cyclosporine A, ketoconazole, verapamil, and digoxin (138). Many newly marketed drugs had been tested to be substract of P-gp, for example UK-343,664 (Pfizer Inc.) (136) and PLX4032 (Roche Inc.) (139).

## **Cytochrome P450 metabolism**

Cytochrome P450 is a haem-containing superfamily of enzymes which includes isoenzymes that metabolise exogenous substrates including absorbed drug molecules. The CYP3A subfamily constitutes about 20% of CYP content in the liver and 50-70% of CYP content in the intestine. In humans, it has been shown that CYP3A4 is the most important Phase I enzyme involved in drug metabolism in the sense that approximately 50% of marketed drugs are CYP3A4 substrates (140). Thus, if a drug is strong CYP3A isoenzymes enzymes substrates, significant first-pass metabolism by the intestinal wall and hepatocytes could have a significant impact for its bioavailability (141).

Although the liver has long been thought to play the major role in drug biotransformation, the metabolic capacity of the intestine is increasingly recognised. Several *in vivo* studies have demonstrated that significant first-pass metabolism by the intestinal wall has implications for the bioavailability of many drugs (142, 143). Furthermore, the relevance of drug transporters in this process has been proven (143). Similarly, intestinal metabolism can result in a non-linear absorption kinetic behaviour that is mainly attributed to saturation of the intestinal metabolism, which will be



associated with a non-linear appearance in the mesenteric blood, rather than a saturable intestinal absorption from the lumen (144).

### **CYP3A4 and P-gp interplay of drug metabolism and efflux in the intestine**

CYP3A and P-gp overlap in substrate specificity and both are commonly localised near the apical membrane of enterocytes (145, 146). It has been hypothesised that for many drugs, the combined activity of CYP3A and P-gp increases efficiency of intestinal first-pass metabolism of orally administered drugs as a result of a potentially synergistic collaboration (147, 148).

Two mechanistic arguments have been brought forward to support a possible synergistic action of intestinal P-gp and CYP3A. First, the function of P-gp would lower the enterocyte intracellular concentration of a substrate drug and might thus prevent saturation of the CYP3A enzymes by keeping the concentration more within the linear range of the enzyme metabolising capacity. Consequently, a larger fraction of the intracellular drug can be metabolised, without increasing the speed of metabolism. P-gp activity would simply afford CYP3A more time to metabolise its substrates extensively. Thus, P-gp would allow CYP3A to efficiently metabolise drugs over a far higher dose range (145). Second, it has been suggested that the efflux function of P-gp combined with subsequent drug re-uptake may allow drug substrates to have repeated and therefore prolonged access to enterocyte CYP3A, thereby increasing the possibility that a drug will be metabolised. This repeated cycling of drugs would increase the total metabolism, even without considering saturating or non-saturating conditions for CYP3A4 (149, 150).

Successful prediction of the interplay between P-gp and CYP3A for their substrate compounds (*e.g.*, CX and ITR) on intestinal absorption could be one of the critical factors in PBPK modeling. Thus, in this project it was intended to elucidate the contribution of interplay between P-gp and CYP3A in the non-linear absorption kinetics of ITR and CX (model compounds used in this project) using PBPK modeling.

#### **1.6.1.3 Drug physicochemical parameters**

Solubility and intestinal permeation are important physicochemical parameters that affect the rate and extent of absorption of an oral drug product. However, drug solubility and permeability are not intrinsic properties of drug compounds and will be

influenced by formulation parameters and gastrointestinal variables. They are of course related to more fundamental physicochemical drug properties, including crystalline or amorphous form, lipophilicity, pKa, hydrogen-bonding capacity, molecular surface area and its functional groups (83, 126).

## **Solubility**

The pH dependent solubility and stability of a drug plays an important role in its absorption. In order to permeate across the biological membrane, drug molecule (especially BCS Class 1 and 2 compounds) must be in a solubilised, stable and unionised form (135). Differences in regional pH can affect solubilisation or provide an environment for degradation of the drug (83). This is why understanding the ionisation properties of a drug candidate are essential for the absorption potential. Most of drugs are weakly acidic or weakly basic compounds that cannot be ionised completely in aqueous media. Dissolution of ionised drugs is greatly dependent on the pH of the medium which is generally described by Henderson-Hasselbach equation which correlates pH and drug ionisation for weak acids and weak bases. For example, poorly soluble weak bases dissolve more readily in the stomach fluid (pH 1.6-3) than in the intestinal fluid (pH 6-7) (83). This can result in supersaturation as the drug moves from acidic to basic conditions. Upon the movement to basic pH, the degree of ionisation and equilibrium solubility are reduced causing supersaturation of the drug (29).

## **Permeability**

Permeability is a parameter that reveals the degree of a solute penetration into a membrane over a specific time span. It is expressed in velocity units length per time (133, 151). The permeability is the main parameter used for the quantification of a drug compound's penetration capacity across the biological membrane layers. Effective permeability ( $P_{\text{eff}}$ ) quantifies permeability across the intestinal membrane.  $P_{\text{eff}}$  depends on properties of the drug and the membrane. It is referred to as "effective" because it characterises absorption whether by passive diffusion, active transport, facilitated diffusion, paracellular diffusion or any other mechanism.

#### **1.6.1.4 Dosage form and formulation parameters**

The type of dosage form such as immediate release, enteric coated, modified release and formulation such as amorphous, micronised and lipid based delivery system would determine the scale and extent of drug release and dissolution (152). For example immediate release formulations are designed to be absorbed quickly, whereas modified release formulations are produced with controlled release profiles in different compartment of GIT (153). Furthermore various excipients can be used in order to produce desired dissolution profiles. For instance, disintegrants such as lactose helps to break the tablet apart. Wetting agents such as SLS can be added to the formulation to aid the penetration of water into the tablets.

With the advancement of drug delivery system, poorly soluble compounds can be formulated as a nanosuspension, cocrystal complexes, salt form and amorphous formulation in order to improve bioavailability (154). In this project, the main focus is on amorphous formulations which the details on the amorphous formulation characteristics is discussed in Section 2.3.

#### **1.6.2 PBPK modeling**

##### **1.6.2.1 Physiologically-based pharmacokinetic (PBPK) models for the prediction of oral absorption**

The advent of computer science catalysed the advancement of theoretical models capable of predicting oral drug absorption in humans (155-157). Once the drug is absorbed, its metabolism and excretion out of body compartments is an important factor for drug bioavailability. The Absorption-Distribution-Metabolism-Excretion (ADME) of a drug is a complex process. Advanced PBPK (physiological based pharmacokinetics) tools have the ability to generate plasma-concentration time profiles for the drugs, with detailed information about fraction absorbed across the apical membrane of the enterocytes ( $f_a$ ), fraction of the absorbed dose that is not metabolised in the gut wall ( $f_g$ ) and drug availability in the central compartment.

There are a few commercially available programmes based on the physiologically-based pharmacokinetic models such as Simcyp™ by Certara Inc. (158), PK-Sim™ by Bayer Inc. and GastroPlus™ by Simulations Plus Inc. (159). These software packages use physiologically based models, which try to account for all known factors influencing

the oral drug absorption and to predict the behaviour of a drug molecule interaction with the body system using mathematical approaches (160, 161).

#### **1.6.2.2 Advanced Compartmental Absorption and Transit (ACAT) model**

Dissolution and permeation are the major factors governing the rate and extent of drug absorption. Developing reliable PBPK models for the prediction of *in vivo* dissolution and absorption of orally administered compounds will significantly improve and expedite the drug discovery and development process (126, 162).

In the ACAT model, the GIT is divided into nine compartments and the drug release, dissolution, precipitation, absorption and transit across the compartments are all described by specific integrated or differential mathematical equations. The estimation of fraction of drug absorbed through the gastrointestinal mucosa in GastroPlus™ is based on the ACAT (advanced compartmental absorption and transit) model (126, 163). The mathematical models/equations take into account the physicochemical properties of the drug under study, e.g. pKa, solubility, diffusion coefficient and effective permeability; and the physiological variables e.g. pH, transit times, volume, length, enzymes and transporter proteins (influx/efflux) affecting drug absorption (161, 164, 165).

The model also includes linear transfer kinetics and non-linear metabolism transport kinetics, six states of drug component (unreleased, undissolved, dissolved, degraded, metabolised, and absorbed) and three states of excreted material (unreleased, undissolved, and dissolved). The unreleased row of sub-compartments is used only for controlled release dosage forms. For controlled release, the drug can be released into solution (dissolved) or as solid particles (undissolved). Undissolved material transits and dissolves to give dissolved material. Dissolved material undergoes transit, luminal degradation, absorption and may potentially precipitate back to undissolved material if its concentration exceeds the local solubility within a particular compartment. The undissolved (solid particles) and dissolved (drug in solution) drug undergoes linear kinetics transit through the GIT (126, 162). For tablet dosage forms, if a tablet was not absorbed before the end of the transit process, the drug would eventually be excreted from the colon (133) (Figure 9).

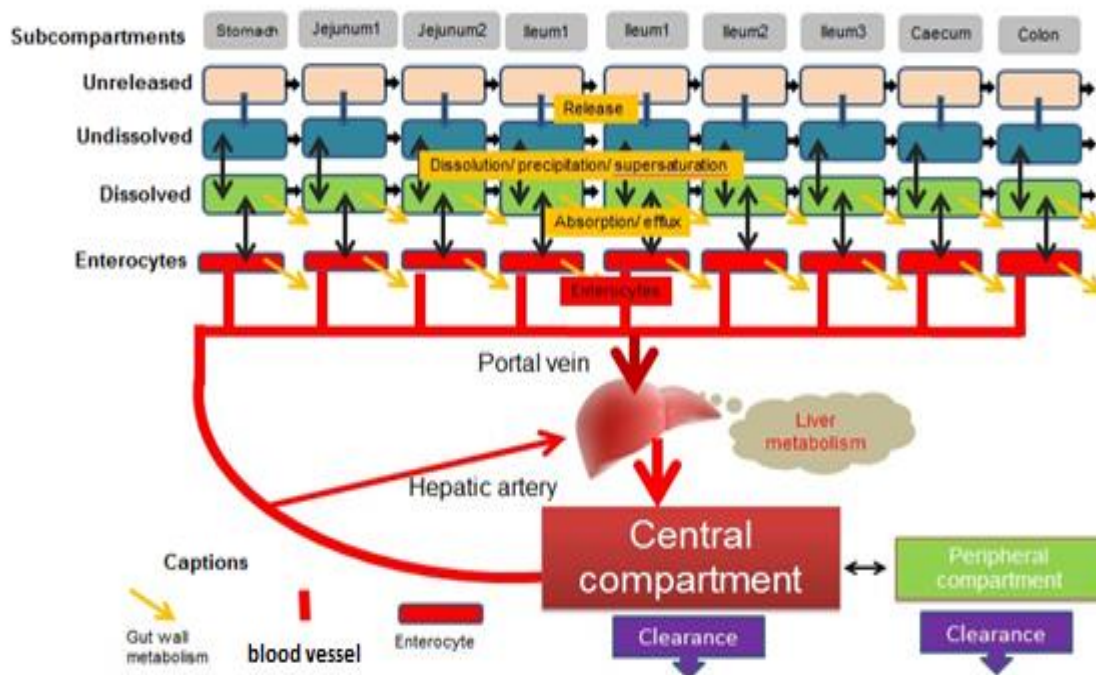


Figure 9. Schematic of ACAT model interpretation of *in vivo* drug behaviour. This diagram illustrates a total of nine compartments, each of which is divided into four sub-compartments: unreleased, undissolved, dissolved, and enterocyte.

In Figure 9, each arrow represents a process, hence a differential equation. Besides the dissolution process, all other processes (carrier-mediated transport in the gut, gut metabolism and liver metabolism) are taken into account as being linear processes. The transit of any form of material (unreleased, undissolved or dissolved) is permitted only to the same sub-compartment of the next compartment: undissolved material can only transit into the next compartment's undissolved sub-compartment. Modifications in form (unreleased to undissolved or dissolved, undissolved to dissolved, and dissolved to absorbed, undissolved, or degraded) are exclusively permitted to take place within a compartment (162, 164). Drug absorption can be passive and driven by the concentration gradient across the apical barrier or mediated by influx and efflux transporters in the enterocytes. The absorbed drug can also be subject to metabolism in the enterocytes. In GastroPlus™, the enterocytes act as well-mixed tanks where efflux, basolateral transport and gut metabolism compete for the drug (126, 164). Once the drug crosses the basolateral intestinal barrier, it reaches the portal vein and then the liver. First pass extraction and systemic extraction of the drug both take place in the liver. The drug escaping metabolism reaches the systemic circulation from where it will be distributed to peripheral compartments following the compartmental pharmacokinetics model. Meanwhile, renal and other forms of elimination can occur from the central and peripheral compartments (126).

## **1.7 *In vitro-in vivo* correlations/relationships (IVIVC/Rs)**

Dissolution is the rate limiting step in absorption for Biopharmaceutics Classification System (BCS) class 2 and class 4 compounds which exhibit low solubility (48). Appropriate selection of *in vitro* conditions (media and hydrodynamics) that simulate the *in vivo* conditions can lead to the development of successful *in vitro-in vivo* correlations (IVIVC) (54, 166). An established IVIVC can be further used to set meaningful dissolution specifications that take clinical consequences into account in the hope of facilitating regulatory approvals of post approval changes (167) and Quality by Design (168).

For the last three decades, there has been considerable interest within the pharmaceutical industry, academia, and regulatory sectors in *in vitro-in vivo* correlations (IVIVCs) of oral dosage forms (169); in particular, since the publication from the FDA Guidance of dissolution testing of immediate- release (IR) (43) and IVIVC of extended-release (ER) dosage forms in 1997 (170) and subsequent notes for guidance issued by the European regulatory authorities, EMA (171). The guidelines increase confidence and success in using *in vitro* tests to evaluate or predict *in vivo* performance of solid drug products based on IVIVC, especially ER dosage forms (172-179).

FDA defines IVIVC as a predictive mathematical model to describe the relationship between an *in vitro* property (usually the extent or rate of drug release), and a relevant *in vivo* response (e.g., plasma concentration or amount of drug absorbed) (170). *In vitro-in vivo* relationship (IVIVR) is defined as a qualitative or semi-quantitative association between the *in vitro* dissolution/ release and *in vivo* absorption data (180).

### **1.7.1 The Levels of Correlation**

The levels of correlation are categorised as:

#### **1.7.1.1 Level A correlation**

Level A correlation is defined as a hypothetical model which describes the relationship between the fraction of drug absorbed and the fraction of drug dissolved (170). It is considered as a predictive model for the relationship between the entire *in vitro* release time courses (181). Among all levels of correlation, Level A is the most meaningful for predicting purpose because it provides a relationship that directly links *in vivo* drug

absorption to *in vitro* dissolution. This level of correlation should be valid for a reasonably wide range of values of formulation and manufacturing parameters that are essential for the drug release characteristics. This level can be used as a surrogate for *in vivo* performance of a drug product (170). Therefore, *in vitro* dissolution data, without any additional *in vivo* data, can be employed to justify a change made in manufacturing sites, raw material supplies, minor formulation modifications, strength of dosage form (170). For Level A IVIVC, when *in vitro* curve and *in vivo* curve are superimposable, it is said to be a 1:1 relationship. On the contrary, if scaling factor is required to make the curve superimposable, the relationship is called a point-to-point relationship (182).

#### **1.7.1.2 Level B correlation**

It means *in vitro* dissolution time (MDT) is compared with either the mean *in vivo* residence time (MRT) or mean *in vivo* dissolution time derived by using the principle of statistical moment analysis (170). Therefore, it does not reflect the actual *in vivo* plasma concentration curve. Although it utilises all *in vitro* and *in vivo* data, it is not considered a point-to-point correlation because the numbers of *in vivo* curves can produce similar residence time value (170). Hence, it is the least useful for regulatory purposes.

#### **1.7.1.3 Level C Correlation**

A level C correlation represents a single-point relationship between a dissolution parameter (e.g.,  $t_{50\%}$ ) and a pharmacokinetic parameter (e.g., AUC,  $T_{max}$ ,  $C_{max}$ ). This correlation does not reflect the entire plasma-concentration–time curve or dissolution profile (170); therefore, it is considered the lowest correlation level. However, Level C correlation can provide useful information in early formulation development (183).

#### **1.7.1.4 Multiple Level C correlation**

A multiple level C correlation compares one or more pharmacokinetic parameters of interest (e.g.,  $C_{max}$ , AUC) to the amount of drug dissolved at several time points of the dissolution profile (170). This level of correlation may support a biowaiver if the correlation has been established over the entire dissolution profile with one or more pharmacokinetic parameters of interest. If a multiple level C correlation is possible, then it is likely that a level A correlation is possible as well. The latter is the preferred correlation.

### 1.7.2 Application of an IVIVC

Occasionally during the formulation development process, some changes to the formulation composition, manufacturing process or equipments are introduced. These changes normally require human clinical trials to demonstrate bioequivalence of new product with the biobatch. However, if IVIVC is successfully developed then it could be utilised to replace human studies (173, 179). Alternatively, IVIVC could serve as surrogate for *in vivo* bioavailability and biowaiver consideration (43). Other purpose of IVIVC is to assist in validating or setting dissolution specifications. The dissolution specifications are needed to ensure batch to- batch consistency within a range that guarantees acceptable biopharmaceutical performance *in vivo* and to distinguish between good and bad batches (182). An IVIVC includes *in vivo* relevance to *in vitro* dissolution specification which means that the dissolution specifications are set based on the *in vivo* performance of the biobatch (170).

It is important to note that in 1995, Biopharmaceutics Classification System (BCS), a theoretical framework that was based on the underlying processes controlling oral drug absorption was proposed (48). The BCS classifies drug compounds based on solubility and permeability of the compound (Table 5). Normally for rapidly dissolving BCS Class 1 compounds, IVIVC may not be possible because of their high solubility and high permeability characteristics; the *in vivo* dissolution is not the rate-limiting step (48, 184). For BCS Class 2 compounds, on the other hand, dissolution is the limiting step of the drug absorption. Therefore, an IVIVC may be expected (43, 54). More research is needed to develop and validate *in vitro* dissolution methods for class 2 compounds so that they can be used to predict *in vivo* dissolution (185). For BCS Class 3 compounds, permeability is the limiting step of the absorption, and a limited IVIVC may be expected. Finally, for BCS Class IV compounds, IVIVC is difficult. The compound will have both limited dissolution and permeability. So, it will be difficult to develop a dissolution model unless the permeability is borderline low (170).



Table 5. IVIVC expectations for immediate release products based on BCS

Class	Solubility	Permeability	Absorption rate control	IVIVC expectations for Immediate release product
I	High	High	Gastric emptying	IVIVC expected, if dissolution rate is slower than gastric emptying rate, otherwise limited or no correlations
II	Low	High	Dissolution	IVIVC expected, if <i>in vitro</i> dissolution rate is similar to <i>in vivo</i> dissolution rate, unless dose is very high.
III	High	Low	Permeability	Absorption (permeability) is rate determining and limited or no IVIVC with dissolution.
IV	Low	Low	Case by case	Limited or no IVIVC is expected.

### 1.7.3 Development of IVIVCs

A full-time course *in vivo* absorption-time profile is generally the most informative way of evaluating formulation performance from the plasma concentration-time data (186). The method of choice for determination of *in vivo* absorption-time profiles is deconvolution. In this section, the different methods of deconvolution (in order to obtain *in vivo* absorption profile) and the equation of IVIVC are discussed.

#### 1.7.3.1 Deconvolution

In deconvolution, three components are defined: input, weighting and response functions. The input function corresponds to the entry of the drug into the body, *i.e.* the *in vivo* dissolution- or absorption-time profiles for the oral test formulation. The weighting function corresponds to the time course of the drug within the body, as described by the plasma concentration-time profiles after administration of an oral or IV reference solution. Lastly, the response function is described by the plasma concentration-time curve for the test formulation (187).

One of the commonly used methods of deconvolution of plasma profiles is the numerical method which is a model independent method. This method uses a simpler algorithm and does not require any modeling of the plasma concentration-time data in the assessment of the absorption profile (187). However, intravenous or oral solution

plasma profile of the drug (weighting function) is required for the calculation of absorption. Some examples of the software available for numerical deconvolution are PCDCON (Austin, Texas) (188) and Phoenix<sup>®</sup> Winonlin<sup>®</sup> (Phoenix, US). Numerical deconvolution is considered the most reliable deconvolution method (189, 190) thus it is implemented in this project (IV profiles for the model compounds used in this project were available).

The integral for deconvolution is presented in Equation 3 (191):

$$c(t) = \int_0^t c_{\delta}(t-u)r_{abs}(u)du \quad \text{Equation 3}$$

Where the function  $C_{\delta}$  represents the concentration–time course that would result from the instantaneous absorption of a unit amount of drug. Typically, it is estimated from intravenous injection bolus data or reference oral solution data. In addition,  $c(t)$  is the plasma concentration vs time level of the tested oral formulation,  $r_{abs}$  is drug input rate of the oral solid dosage form, and  $u$  is variable of integration. In simple terms, the relationship between these terms can be represented as Equation 4 (191):

$$Y(t) = G(t) \cdot X(t) \quad \text{Equation 4}$$

Where  $Y(t)$  is the function which describes the plasma concentration–time curve following extravascular administration,  $G(t)$  is the function describing the concentration–time curve following bolus intravenous (or weighting function) administration, and  $X(t)$  is the function describing input, *i.e.*, dissolution from the dosage form.

#### 1.7.4 Establish IVIVC using *in vivo* and *in vitro* dissolution data

Good prediction of the dissolution properties of orally administered compounds is of great importance (57). A good correlation is a tool for predicting *in vivo* results based on *in vitro* data; if the absorption is dissolution rate limited, the optimum dissolution method for IVIVC is the method that best correlates with what happens *in vivo* (99).

A linear mathematical equation with intercept ( $a$ ) and gradient ( $b$ ) can be applied to define IVIVC (Equation 5) (192):

$$\% \text{ absorption } in \text{ vivo} = b \cdot \% \text{ dissolution } in \text{ vitro} + a \quad \text{Equation 5}$$

where % absorption *in vivo* and % dissolution *in vitro* are the mean percentages *in vivo* absorption and *in vitro* dissolution respectively;  $a$  is a constant additive term that

accounts for a percentage delay *in vivo* as compared with *in vitro* and the gradient  $b$  is a transformation factor for the mean percentages. This gradient,  $b$ , compares the rate and extent of the *in vivo* absorption and *in vitro* dissolution. For example, if  $a$  is zero and  $b$  is 2, this indicates that the mean % *in vivo* absorption is twice as high as the mean % *in vitro* dissolution.

### 1.7.5 IVIVCs of amorphous formulations

A few successful examples of IVIVC for amorphous formulation have been reported in literature, for example Level A IVIVC for oxidized mesoporous silicon (pSi-ox) amorphous indomethacin formulations and crystalline indomethacin powder. *In vitro* dissolution profile of pSi-ox amorphous indomethacin formulation was obtained with USP apparatus 2 (100 rpm) in a 500 mL phosphate buffer (0.05 M, pH 7.2). The *in vitro* dissolution data was compared directly with *in vivo* absorption data of a fasted rat (Sprague-Dawley). *In vivo* absorption profile of pSi-ox amorphous indomethacin formulation was generated from deconvolution of the corresponding plasma concentration profiles using the Wagner-Nelson method.

Another example is the Level A IVIVC development for disintegration-controlled matrix tablet (DCMT) amorphous nilvadipine formulation (193) (Figure 10). Two DCMT amorphous nilvadipine formulations, DCMT-1 and DCMT-2 with different compositions of disintegrant were prepared and tested *in vitro* and *in vivo*.

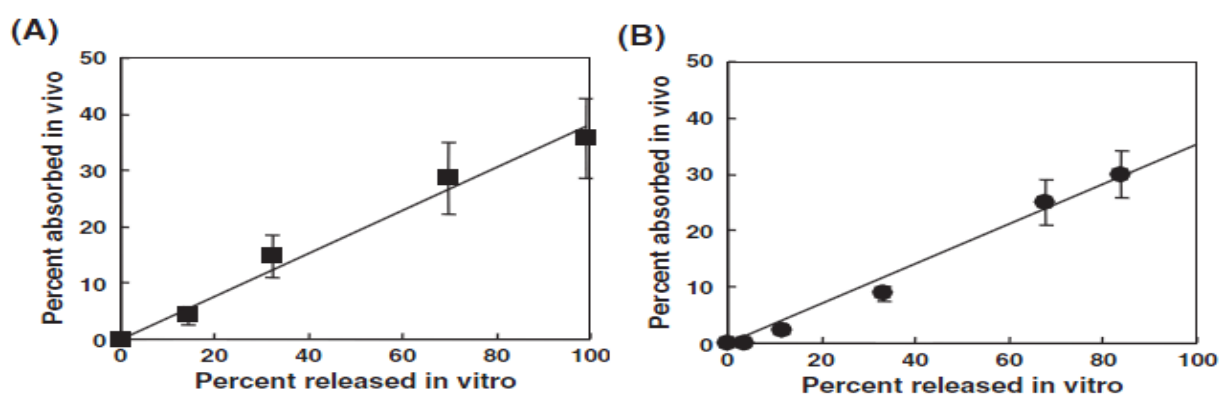


Figure 10. Level A IVIVCs of DCMT-1 (A) and DCMT-2 (B) amorphous nilvadipine formulation. The reported linear regressions were  $y=0.995x$  (A) and  $y=0.9512x$  (B) ( $R^2$  value was not reported). Reproduced with permission from (193).

*In vitro* dissolution profile was obtained by using USP apparatus 2 (100 rpm) in simulated gastric fluid (pH 1.2,  $37\pm 0.5^\circ\text{C}$ ). The *in vitro* dissolution data was directly

compared with *in vivo* absorption data of the fasted beagle dogs' model. *In vivo* absorption profiles were calculated by means of a numerical deconvolution method (193).

A multiple level C IVIVC correlation has been developed for poly(ethylene glycol) (PEG)–ritonavir amorphous solid dispersions formulations (194). In this study, *In vitro* dissolution was conducted with a USP apparatus 1 (50 rpm,  $37\pm 0.5^{\circ}\text{C}$ ) in 900 mL of 0.1N hydrochloric acid. The *in vivo* data was obtained from sequential blood samples of eight beagle dogs. The multiple level C IVIVCs correlating  $C_{\text{max}}$  (or AUC) and percentage released at 5 min ( $Q_{5\text{min}}$ ) or at 60 min ( $Q_{60\text{min}}$ ) are shown (Figure 11).

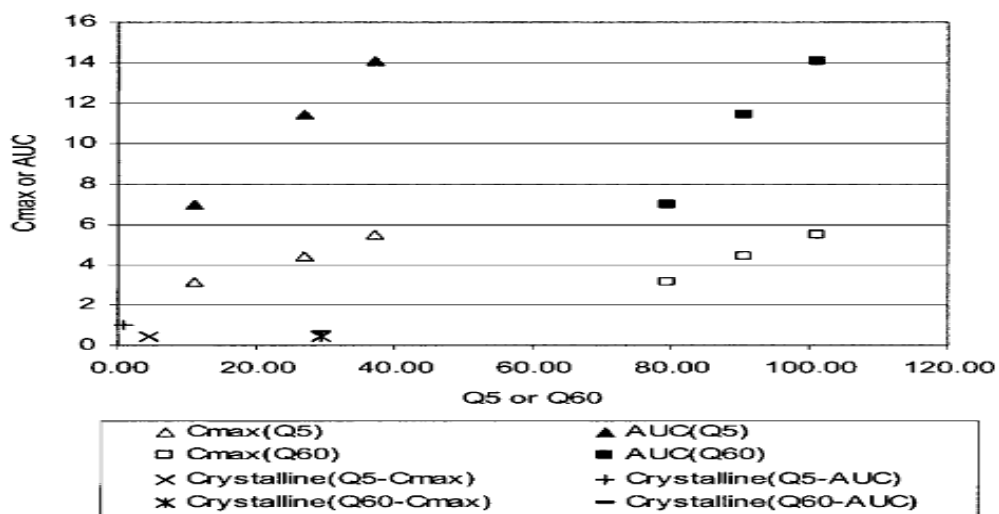


Figure 11. Multiple level C IVIVCs between  $C_{\text{max}}$  (or AUC) and  $Q_{5\text{min}}$  or  $Q_{60\text{min}}$  of ritonavir amorphous dispersions. Reproduced with permission from (194).

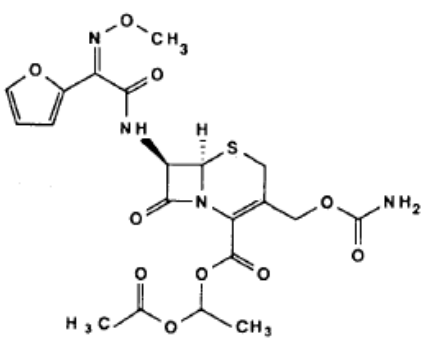
## 1.8 Compounds selected (Amorphous state)

This section describes physicochemical and pharmacokinetic properties of CA, ITR and CX (compounds selected for this study).

### 1.8.1 Cefuroxime axetil (CA)

Zinnat<sup>®</sup> was designed to be an oral dosage form of cefuroxime (Zinacef<sup>®</sup>), a second-generation cephalosporin antibiotic previously available via IV and IM injection (195, 196). Cefuroxime is not orally absorbed because it contains a highly polar carboxyl group that is ionized at intestinal pH, making transport across intestinal mucosa unlikely (197, 198). By masking the carboxylic acid side chains through esterification (199), the drug's lipophilicity and enteral absorption were successfully increased. It can penetrate through the intestinal mucosa and be rapidly hydrolysed by the enzyme esterase in the intestinal mucosa and the portal circulation *in vivo* to form an active cefuroxime molecule. A study has shown that it is not possible to detect CA itself in the systemic circulation (200). The equilibrium water solubility CA is low  $0.4 \pm 0.13 \mu\text{g/mL}$  (201). While limited by poor aqueous solubility, the lipophilicity of the compound renders high permeation of intestinal membranes. Therefore it is classified as a BCS (48) Class 2 compound. Some physicochemical properties of CA are presented in Table 6.

Table 6. Physicochemical properties summary of CA

Properties	Description
Molecular structure	
Pharmacological category	A cephalosporins group antibiotic (202)
Molecular Weight	510.48 (202)
pKa	Neutral drug
log P	0.25 (203)
Solubility	SGF: $10.4 \pm 0.13 \mu\text{g/mL}$ (201)

### 1.8.1.1 Bioconversion and hydrolysis of CA

It was initially discovered that the bioconversion of CA to cefuroxime requires hydrolysis by intestinal mucosa (enterocyte) esterases (197). Esterase hydrolysis leads to the formation of acetic acid and the unstable hydroxyethyl ester, which rapidly dissociates to acetaldehyde and the active cefuroxime (the microbiologically active form of the drug). An *in vitro* study indicates that the half-life of the CA is 3.5 min in fresh human blood, but the *in vivo* hydrolysis is so rapid that the intact CA cannot be detected in the serum, even when a 1 g dosage was administered orally to healthy adults (200). Furthermore, hydrolysis of CA may proceed *via* a reversible base-catalysed isomerisation. Both hydrolysis processes will remove some of the CA available for absorption. The result is incomplete bioavailability of the oral prodrug ester (204, 205). Later studies also showed that the hydrolysis of CA could take place at different rates under various pH, temperature and buffers (206).

### 1.8.1.2 Pharmacokinetics

Protein binding of cefuroxime is approximately 30%. Its volume of distribution value is 0.13 to 1.8 L/kg (207) and a Vd of 50 L was reported in healthy subjects administered a single oral Zinnat<sup>®</sup> 500 mg dose (208). Mean drug: creatinine clearance ratios were in the 1.1-1.3 range (197) which suggests that about half the drug is filtered and half is actively secreted by the kidney tubules. It is worth noting that a pharmacokinetic study has also demonstrated that cefuroxime follows linear pharmacokinetics (209).

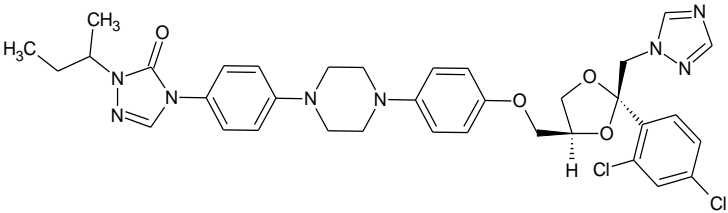
The bioavailability of cefuroxime administered as a Zinnat<sup>®</sup> 250 mg tablet was 52% when taken after food and 37% when taken on an empty stomach (209). The stability of CA is pH dependent. The rate of hydrolysis is faster in the fasted state (acidic gastric medium of pH 1.8) compared to the fed state (pH 4.5-5.6) (206). The inactive isomer of CA can also be formed under the acidic conditions and increased temperature (210). The optimal conditions for absorption of CA are found in the duodenum and the upper part of the small intestine, where pH is in the range of 4 to 6 (205). From this observation, it is suspected that the higher bioavailability of CA in the fed state is associated with the higher concentration of intact CA reaching the intestine, the main site of CA absorption. Many pharmacology and kinetic studies have failed to identify this issue and have proposed reasons such as saturable and selective absorption activity in the intestine (211-213). Another suggested reason for the lower

bioavailability in the fasted state is the rapid gastric emptying in this state. It results in an excessive amount of CA presented to the upper small intestine which saturates the absorption process leading presumably to zero-order absorption kinetics (205).

### 1.8.2 Itraconazole (ITR)

ITR is a triazole antifungal compound with a piperazine structure (214, 215). ITR has an extremely low solubility in water. ITR (pKa 3.7) has a strongly pH dependent solubility and it remains largely un-ionized in intestine secretions (pH 6.5) (216). The equilibrium solubility of ITR is very low (practically insoluble in water and thus is classified as a poorly water soluble drug (216)). The low aqueous solubility results in variable absorption and plasma concentration (217). While limited by poor aqueous solubility, the highly lipophilic nature of the compound (Table 7) allows for high permeation of intestinal membranes; therefore, it is classified as a BCS (48) Class 2 compound. Some physicochemical properties of ITR are presented in Table 7.

Table 7. Physicochemical properties summary of ITR

Properties	Description
Molecular structure	
Pharmacological category	A triazoles antifungal drug (218)
Molecular weight	705.65 (218)
pKa	3.7 (218)
log P	4.3 (218)
Solubility (µg/mL)	Water: 0.001 (216) SGF: 3.9±0.7 (219) SIF:0.003 (219)

### 1.8.2.1 Pharmacokinetics

ITR has a long elimination half-life, ranging from 35 to 64 h (220) and it takes 15 days to reach a steady state in the human body. Volume of distribution of ITR is approximately 11 L/kg (215) and protein binding is 99% (ITR, hydroxyl-ITR) (221-223).

A study of healthy volunteers evaluated the pharmacokinetics of ITR after a single 200 mg dose and 200 mg every 12 h for 15 days (steady state). The metabolism of ITR occurred by non-linear processes (224) as demonstrated by a fivefold greater  $AUC_{0-12h}$  at steady state ( $22.6\mu\text{g} \times \text{h/mL}$ ) compared to the AUC after a single dose ( $3.42\mu\text{g} \times \text{h/mL}$ ) (224). Similarly in another clinical pharmacokinetic study, ITR dosage was increased from 100 mg and 200 mg to 400 mg daily and a non-linear increase in the AUC was observed (225). Other studies also have shown that administration of a single oral dose of ITR of 100 or 200 mg to a healthy volunteer have resulted in bi-exponential reduction of the ITR plasma concentration with a terminal half-life of approximately 20 h (222). Strong evidence has shown that ITR is metabolised extensively in the liver, predominately by the cytochrome P450 3A4 isoenzyme system (222). Furthermore, ITR is both the substrate and inhibitor of the CYP3A4 enzyme (226, 227) and P-glycoprotein (137, 227).

A bioavailability study has shown that milk or a meal taken together with milk could substantially reduce the absorption of ITR (228). It was found that milk increased and prolonged the duration of gastric pH (at pH 5.6 for more than 4 h) and also acted as an antacid that could reduce the acidity of the stomach (229, 230). The acidity of the stomach is important for fast dissolution of ITR that allows a high supersaturated solution when entering the intestinal fluid (pH 6-pH 6.8) (231). Thus, the pH 5.6 medium greatly reduces the ITR dissolution compared to the high and fast dissolution in the acidic medium (30).

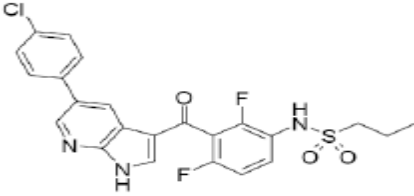
### 1.8.3 Compound X (CX)

Compound X is a newly marketed compound manufactured by Hoffmann-La Roche (232). CX is a kinase inhibitor available as a 240 mg/tablet for oral use. CX exists in several polymorphic forms, with polymorphic form II being the most stable. Polymorph I has higher solubility and bioavailability; however, it is unstable so formulation efforts have been made to increase the solubility of CX (233). CX is practically insoluble in aqueous media across the physiological pH range (concentration less than LOQ) (233). While limited by poor aqueous solubility, the highly lipophilic nature of the



compound (log P=3.84 allows for high permeability of intestinal membranes) means it is classified as a BCS (48) class 2 compound (234, 235). Some physicochemical properties of CX are presented in Table 8.

Table 8. Physicochemical properties summary of CX

Properties	Description
Molecular structure	
Pharmacological category	A novel small molecule selective inhibitor of the activated form of the BRAF serine-threonine kinase enzyme for the treatment of skin melanoma
Molecular Weight	489.93
pKa	7.9 and 11.1
log P	3.84 (pH 7.4)
Solubility	Practically insoluble in aqueous media across the physiological pH range H <sub>2</sub> O and SGF < 5µg/mL, FaSSIF-V1: 40µg/mL, FeSSIF-V1: 370µg/mL

### 1.8.3.1 Pharmacokinetics

CX is more than 99% bound to human albumin and alpha-1 acid glycoprotein plasma proteins (232). The apparent volume of distribution of CX is estimated to be 106 L in patients with metastatic melanoma (healthy volunteer study is not available as this drug can increase the risk of skin cancer) (232). The population apparent clearance is estimated to be 31 L/day in patients with metastatic melanoma (232). The median elimination half-life of CX is estimated to be 57h (232). Following oral administration of <sup>14</sup>C-CX 960 mg in the tablet formulation, plasma samples were analysed over 48 hours for CX and its metabolites. Mean data showed that CX and its metabolites represented 95% and 5% of the components in plasma, respectively. The majority of the CX in the body is excreted through faeces (94%) and approximately 1% is excreted through renal elimination (232). So far there is no bioavailability data of CX. Following oral administration of CX at 960 mg twice daily for 15 days to patients with metastatic

melanoma, the median  $T_{\max}$  was approximately 3h. A study has shown that a high-fat meal can increase the absorption of CX (236).

### **1.9 Aim of study**

The aim of the project was to provide a comprehensive methodology for the development of PBPK models and IVIVCs simulating fasted and fed states for orally administered amorphous formulations. *In vitro* dissolution of three model compounds, CA, ITR and CX was characterised using different dissolution apparatus (USP apparatus 1, 2, 4 and surface dissolution imager), setting (single stage, 2 stage, media and flow rate change) as well as media (compendial, biorelevant and modified media) to simulate the changes of pH, contents, and hydrodynamic conditions (flow rate and rotation speed) in the human gastrointestinal tract (fasted and fed state). The hypothesis of this study was that biorelevant dissolution media combined with USP apparatus 4 could mimic the *in vivo* performance of the tested formulations and achieve a good PBPK model and IVIVC.

## 2. Experimental Methods

### 2.1 Materials

Sporanox<sup>®</sup> capsules (Janssen-Cilag Ltd, Bucks, UK, batch no. 9EL5800, 100mg itraconazole <ITR> per capsule), Zinnat<sup>®</sup> tablets (GlaxoSmithKline, Middlesex, UK, Lot C420326, 250mg cefuroxime axetil <CA> per tablet) were purchased commercially. Compound X <CX> Formulation 4 -8 (Hoffmann-La Roche, Nutley, US, 240mg of CX per tablet, composition described later in Section 2.3.3), CX standard (99.6%) [Lot 80320404R, Nutley, USA, ITR standard (98% w/w) [batch no. 097K1156, St. Louis, MO] and CA standard [USP Reference Standard, Lot 09822G, Rockille, MD) were provided by Hoffmann-La Roche, Nutley USA.

Glyceryl monooleate (GMO, Rylo M19 Pharma<sup>®</sup>, 99.5% monoglyceride, batch number 4011742134) was a gift from Danisco A/S, Grindsted, Denmark. Egg phosphatidylcholine (Lipoid E PC<sup>®</sup>, 99.1% pure) was generously donated by Lipoid GmbH, Ludwigshafen, Germany. Sodium oleate (lot number SZBB0110V), pepsin (lot number 030M1571V) and sodium chloride (NaCl) were purchased from Sigma-Aldrich (Dorset, UK). Sodium taurocholate (NaTC, 97% pure, batch number 2011040152) was purchased from Prodotti Chimici e Alimentari SpA, Basaluzzo, Italy.

37% hydrochloric acid, maleic acid, potassium dihydrogen phosphate, sodium acetate trihydrate, sodium dihydrogen phosphate monohydrate and sodium hydroxide pellets were all of analytical grade and purchased from Fisher Scientific (Loughborough, UK).

Ultra-heat-treated (UHT) and homogenized milk containing 3.5% fat was purchased from a local supermarket (Tesco, UK).

A cellulose nitrate membrane filter 0.45 $\mu$ m  $\varnothing$  13mm (Whatman, Dassel, Germany) and glass microfiber filters GFD<sup>®</sup> 2.70 $\mu$ m  $\varnothing$  24mm (Batch no. K11670637, Whatman, Maidstone, England) were purchased from Fisher Scientific (UK). GF/F<sup>®</sup> 0.70 $\mu$ m  $\varnothing$  24mm (Whatman, Maidstone, England), glasswool (Sigma, UK) and acetic acid (>99.7%, Batch no 09214CJ, Sigma, UK) and Parafilm (4x125ft, Sigma UK) were purchased from Sigma-Aldrich (Dorset, UK).

Nylon membrane disc filters  $\varnothing$  13mm 0.45 $\mu$ m (Cronus, Gloucestershire, UK) and 10 $\mu$ m direct fit UHMW polyethylene cannula filters (Labhut Ltd, Gloucestershire UK) were purchased from SMI-Labhut Ltd (Gloucestershire, UK).

Dichloromethane, acetonitrile and methanol (HPLC grade) were from Fisher Scientific (Loughborough, UK). The Milli-Q water was obtained from a Nanopure<sup>®</sup> Diamond UF and UV/UF Water Barnstead System [Thermo Scientific, Dubuque, USA].

## 2.2 Apparatus

A VanKel<sup>®</sup> rotating basket (USP apparatus 1) and paddle (USP apparatus 2) dissolution system (model 10-1200, Edison, NJ, USA) and an Erweka<sup>®</sup> flow-through dissolution tester (USP apparatus 4, model DFZ720, Erweka GmbH, Heusenstamm, Germany) equipped with Ø 22.6mm cells and connected to an Erweka<sup>®</sup> Piston Pump (model HKP720) were used.

Sirius SDI (Surface Dissolution Imager, Sirius Analytical Instruments, East Sussex, UK) was used for *in vitro* surface UV imaging experiments. Sirius SDI consists of a pulsed Xenon lamp (Perkin Elmer, Waltham, MA) with PC interface control box, a remote UV camera sensor with fibre optic cable, band pass filter (wavelength 214,254, or 280 nm), Chemyx Fusion 200 syringe pump and a CADISS-2 dissolution cartridge. The CADISS-2 comprises a 62 mm rectangular Quartz tube, Luer lock connector flow cell inlet and outlet and a cartridge body. 20 mL and 50 mL BD plastic buffer delivery syringes were used to hold the dissolution medium.

A Quickset Minor<sup>®</sup> torque screwdriver (Torqueleader, M.H.H. Engineering Co. Ltd., England) and sample cup (316 stain steel, 2.0 mm ID 2.6 mm OD X 2.4 mm H, Paraytec, York) were used to prepare the drug compact for the surface UV dissolution experiment. The compacts were arranged on a manual press (Actipress, Paraytec, York).

The HPLC system consisted of an Agilent 1100 Quat pump, an Agilent 1100 DAD spectrophotometer, an Agilent 1100 ALS autosampler and ChemStation software (Agilent Technologies, Santa Clara, USA).

For the detection of drug compounds the following HPLC columns were used: Agilent Zorbax<sup>®</sup> SB-C18 (150mm× 4.6 mm, 3.5µm particle size) for CA, Water XTerra<sup>®</sup> RP18 (250mm× 4.6 mm, 5µm particle size) for ITR and Water Sunfire<sup>®</sup> C18 (150mm× 4.6mm, 3.5µm particle size) for CX.

Centrifuge tubes (Corning Inc. New York, US) were used in the analysis process of milk-based media. Glass syringe 5 mL with Luer –lock Fortuna<sup>®</sup> Optima<sup>®</sup> (Poulten & Graf Ltd, Essex, UK) and Swinny stainless steel 13 mm filter holders (Millipore, Billerica, US) were used for filtration during solubility. Bent SS<sup>™</sup> sampling cannula with a Luer adapter for 500 mL sampling (length: 195mm, inner diameter: 2.1mm, VanKel compatible, Varian, CA, US) was used for USP apparatus 1 and 2 dissolution studies

### **Other equipments used**

Shaking water bath (model Grant SS40-2, Grant Instruments, Cambridge, UK) was used for solubility studies. Rotary evaporator (Buchi R-114, Buchi, Switzerland) equipped with a water bath (Buchi B-480, Buchi, Switzerland) and vacuum pump (Vacuubrand CVC 2II, Vacuubrand GMBH, Germany) was used for the preparation of biorelevant media. Hydrus pH meter (model 300, Fisher Scientific, UK) was used for adjustment of the pH of the media used for solubility and dissolution studies. Sigma 701 tensionmeter (Attension, Biolin Scientific, Sweden) equipped with Titronic Universal Burette was used to measure surface tension of modified media. Sartorius balance (AG Gottingen, Germany) was used for all weighing. Vortex rotamixer (Hook & Tucker Instruments, England) was used for mixing samples. Ultrasound bath XB2 (Grant, Cambridgeshire, England) was used for degassing of the mobile phase for HPLC. Finnpiettes (Fisherbrand, UK) (Volume size 1-5 mL: S/N 9066708; 100-1000  $\mu$ L: S/N 9097462; 20-200  $\mu$ L: S/N 9113779) were used for standard preparations and treatment of precipitated samples. Ultrapure water was obtained from a NANOpure<sup>®</sup> Diamond UF and UV/UF Water Barnstead System (Thermo Scientific, Dubuque, US). Heating Magnetic Stirrer (Fisher Scientific, UK) was used for stirring the dissolution media. A timer (Fisherbrand) was used for timing the experiment in solubility and dissolution studies.

### **Software**

Excel 2007 (Microsoft, US) was used to process all data solubility, dissolution and IVIVC data. GastroPlus<sup>™</sup> v.8 (Simulation Plus, California, US) was used for the development of PBPK models. ActiPix<sup>™</sup> SDI300 application software (Paraytec and Sirius Analytical Instruments, East Sussex, UK) was used for the real time data capture and imaging, setting the integrated pump control and visualisation and dissolution analysis.

PCDCON<sup>®</sup> 1.1 Deconvolution Utility (by Dr. Gillespie, University of Texas, Austin, TX) was used for numerical deconvolution of plasma concentration data after oral administration of CA, ITR and CX.

Getdata Graph Digitizer (Moscow, Russia, freely available online) was used for extracting data from 2D graphs.

### **2.3 Amorphous formulation of compounds selected**

The marketed innovator amorphous formulation of CA, Zinnat<sup>®</sup> tablet, ITR, Sporanox<sup>®</sup> capsule and preclinical formulations of CX were studied in this project. These formulations were selected because good *in vivo*, IV and oral plasma concentration profiles are available. Studies confirmed that CA (237, 238), ITR (239) and CX formulations (234, 235) are of an amorphous state. The formulation characteristics of CA, ITR and CX are presented in the following section.

#### **2.3.1 CA**

Zinnat<sup>®</sup> (GlaxoSmithKline) amorphous formulation of CA is formulated based on US Patent No 4,562,181 "Amorphous Form of Cefuroxime Ester" (238). Clinical trials of CA were started in 1981 with large, uncoated tablets (T). Later on, the formulation was improved with film coating and a reduction in size (RS). A second version, RS2 was released for clinical trial in 1983. In RS2, the CA tends to form a gelatinous mass when in contact with the aqueous media. The gelling effect is temperature dependent and occurs at 37°C (240). Such gelling would lead to poor dissolution of CA and hence poor absorption from the gastrointestinal tract. Subsequently, a revised formulation (RS3 tablet version) was marketed in 1987 (198). Modification was done to improve the film coating to ensure its immediate disintegration following rupture of the film coat (241, 242). This was achieved using croscarmellose sodium, a type of disintegrant in the core to enhance the disintegration of the tablet (approximately 4 to 10% by weight) (241).

#### **2.3.2 ITR**

The innovator product of ITR is the Sporanox<sup>®</sup> capsule marketed by Janssen-Cilag Ltd (243). During the manufacturing process hydroxypropyl methylcellulose (HPMC) which is a hydrophilic carrier, is added to crystalline ITR. Dichloromethane and ethanol are used as solvents in order to form a uniform ITR/HPMC solution with weight ratios of 1:1.5:17.25:11.5 (ITR: HPMC:dichloromethane:ethanol) (244, 245). This solution is

coated on sugar beads using a fluidized bed and dried at temperatures up to 80 °C for 2–3 days to remove any remaining dichloromethane. A thin layer of polyethylene glycol (PEG) 20000 is used as a non-sticking agent in order to prevent sticking of the beads. PEG is first dissolved in dichloromethane and ethanol (1:5.4:3.6), and the solution is then sprayed on the previously coated sugar beads using a fluidized-bed granulator which are then dried (244, 245). After drying and capsule filling of the beads, ITR presents in a molecularly dispersed solid solution that dissolves to give a supersaturated solution of the drug in the GIT (15). Dissolution of HPMC in media simulating the gastric environment releases supersaturated concentrations which are maintained before eventually undergoing precipitation. HPMC is believed to prevent ITR from precipitation in the stomach and in the intestine, resulting in significant absorption (246).

### **2.3.3 CX**

CX is a compound with a low melting point and low organic solubility therefore traditional amorphous solid dispersion processing methods are not feasible. The formulation scientists invented is a novel amorphous solid dispersion method called micro-precipitated bulk powder (MBP) technology (247). The application of the MBP technology to CX is directly responsible for enhanced absorption of CX that allows a viable cancer chemotherapy that retards the further metastasis of skin cancer (233, 248).

This CX MBP formulation contains the active compound, CX and an ionic polymer type, hydroxypropylmethylcellulose acetate succinate (HPMCAS). The MBP technology involves a solvent and anti-solvent precipitation method (249, 250). The process utilises N,N-dimethylacetamide to dissolve CX and HPMCAS and then the solution is precipitated into acidified aqueous media. The precipitates are then filtered, repeatedly washed to remove residual acid and solvent content, dried, and milled to form the amorphous powder intermediate, MBP. Apart from increasing CX bioavailability, the CX MBP technology provides substantial physical stability. The stability of the amorphous dispersion is attributed to the high composite T<sub>g</sub>, intermolecular interactions between the drug and polymer as well as the moisture protective effect provided by the polymer. CX may be molecularly dispersed within a matrix formed by the polymer in its solid state such that the drug molecules are immobilised in its amorphous form (234, 235). The immobilization could prevent drug nucleation due to lack of molecule mobility within the polymer matrix (235). Furthermore, HPMCAS contains many substituents that are quite hydrophobic. As a result, even when HPMCAS becomes ionized, as it does at the pH



in the small intestine, the polymer is still only sparingly soluble and exists as colloidal polymer aggregates in aqueous solutions (251). This colloidal polymer helps to sustain a high free-drug concentration by replacing the free drug as it is absorbed over a biological membrane *in vivo*. Furthermore, HPMCAS is an enteric polymer that does not dissolve in an acidic medium but dissolves in buffers of pH greater than 4.5 and the exact pH value at which the polymer dissolves depends on the buffer type and ionic strength of the buffer (251).

In this project, plasma concentration data (post IV and oral administration) of 7 formulations (F1-F7) of CX were provided by the Hoffmann-La Roche, NJ USA (252). All tablets contain 240 mg of CX. The manufacturing process and parameter of these formulations were quite similar and only slight differ in the CX MBP particle size distribution (252) (Table 9).

Table 9. Critical manufacturing variables for 8 formulations of CX

Phase	Coating	MBP PSD ( $\mu\text{m}$ )	Coating (pink)	Tableting strength (N)
F1	Coated	-	Y	-
F2	Coated	37.2	Y	295
F3	Coated	93.8	Y	-
F4	Coated	48	Y	-
F5	Uncoated	37.2	N	341
F6	MBP film coated	64.9,60.9,61.8 (A mixture of 3 MBP lots)	-	-
F7	MBP film coated	62.8	-	-
F8	MBP film coated	-	-	-

## **2.4 Methods of Part 1: *In vitro* solubility and dissolution testing**

One of the objectives of this project is to develop *in vitro* dissolution methods simulating fast and fed states that are able to predict the *in vivo* performance of amorphous formulation. CA (Zinnat<sup>®</sup> as the amorphous formulations) and ITR (Sporanox<sup>®</sup> as the amorphous formulation) were chosen following an extensive literature search and CX (CX amorphous formulation) were provided by Roche, New Jersey, United States (252). *In vitro* dissolution using different apparatus, media and setup were performed. *In vitro* dissolution studies that stress biorelevant dissolution testing and which closely simulate the physiological conditions of humans (CA and ITR) and dogs (CX) were implemented.

New dissolution media simulating fasted state human stomach and intestine (simulated gastric fluid-modified: SGF-M1, SGF-M2 and simulated intestinal fluid-modified: SIF-M1, SIF-M2, SIF-M3, SIF-M4, SIF-M5) were developed. These modified media contain artificial surfactants such as SLS or HTAB at appropriate concentrations that could represent the more complex bile salt and lecithin surfactant system in biorelevant media.

Meanwhile, the simulation of a fed state model required more complex media that mimic pH, viscosity, surfactants and lipolytic products. Hence milk based media such as FeSSGF, early FeSSGF and digested early FeSSGF as well as biorelevant fed state media were used.

### **2.4.1 Chromatographic conditions**

The HPLC methods used for the analysis of ITR and CA are modifications of literature methods (253, 254). The HPLC method used for the analysis of CX is provided by Hoffmann-La Roche. The conditions are shown in Table 10.

Table 10. Parameters for the HPLC analysis

Compound	CA	ITR	CX
Mobile phase	Methanol and water 45:55 (v/v)	Methanol, water and diethylamine 74:26:0.1 (v/v/v)	Water, methanol, trifluoroacetic acid 150:850:1
Flow rate (mL/min)	1	1	1
Injection volume ( $\mu$ L)	20	20	20
Retention time (min)	4.9	10.6	3.3
Detection UV (nm)	280	260	254
Column	Agilent Zorbax <sup>®</sup> SB- C18 (150mm $\times$ 4.6 mm, 3.5 $\mu$ m particle size)	Water XTerra <sup>®</sup> RP18 (250mm $\times$ 4.6 mm, 5 $\mu$ m particle size)	Water Sunfire <sup>®</sup> C18 (150mm $\times$ 4.6mm, 3.5 $\mu$ m particle size)
Column temperature ( $^{\circ}$ C)	40	35	45
Autosampler temperature ( $^{\circ}$ C)	15	20	40

#### 2.4.2 Limit of detection and limit of quantification and linearity

LOD and LOQ were calculated based on Equations 6 and 7:

$$S_{y/x} = \sqrt{\frac{\sum (y_1 - \hat{y})^2}{(n - 2)}} \quad \text{Equation 6}$$

$$\text{LOD} = \frac{3.3S_{y/x}}{b} \quad \text{and} \quad \text{LOQ} = \frac{10S_{y/x}}{b} \quad \text{Equation 7}$$

Where

b is the gradient of the regression line.

$S_{y/x}$  is the standard error of estimate

For the establishment of the linearity range, calculation of the limit of detection (LOD) and the limit of quantification (LOQ) of the proposed method, calibration curves were prepared in the following range: CA: 0.4- 50.0, ITR: 0.1- 6.0, CX: 0.2- 8.0 (unit:  $\mu$ g/mL).

### 2.4.3 Drug adsorption test

To analyse the amount of each individual drug (CA, ITR and CX) adsorbed to the nylon filter (0.45 µm) the recovery of the drug in the filtered solution was determined. For each drug/medium combination, a sample of standard solution was withdrawn with a glass syringe and filtered through the nylon filter kept inside the swinny filter head twice. The first 1 mL of the filtrate was discarded and the concentration of the aliquot of the remaining filtrate was measured using HPLC. The values obtained with and without filtration were then compared and results reported as % recovery according to Equation 8 (255):

$$\% \text{ recovery} = \frac{A_{n+1 \text{ filtered}}}{A_n \text{ filtered}} \quad \text{Equation 8}$$

$A_{n+1 \text{ filtered}}$  = Area of filtered aliquot at n+1 time

$A_n \text{ filtered}$  = Area of filtered aliquot at n time

All results are reported as mean ± standard deviation, with recovery of > 95% as the criterion for acceptable adsorption of solute on the filter paper.

### 2.4.4 Preparation of media

The composition of each media was presented in Section 1.3, and the media used were:

#### 2.4.4.1 Compendial media

A fasted state simulating gastric fluid without pepsin (SGF) (42), and fasted state simulating intestinal fluid without pancreatin (SIF) (42) were used to simulate the fasting GI gastric and intestinal composition, respectively (Composition of the compendial media presented in Table 1).

#### 2.4.4.2 Biorelevant media

##### Simulated fasted state conditions

FaSSGF and FaSSIF-V1 and -V2 were prepared according to the procedures of Vertzoni *et al.* (46, 94) and Jantratid *et al.* (57) respectively (Composition of the biorelevant media presented in Table 3).

### **Simulated fed state conditions**

The fed state simulating gastric fluid, FeSSGF and early FeSSGF as well as the simulated intestinal fluids in the fed state FeSSIF-V2 were prepared according to Jantravid *et al.* (57). The digested early FeSSGF was prepared according to Fotaki *et al.* with the replacement of milk with early FeSSGF; (63) (Composition of the media presented in Table 2).

#### **2.4.4.3 Development of modified media**

Surface tension of the medium is an important factor, which affects the solubility and dissolution of drugs (256). Literature reports the surface tension values in the fasted state humans stomach range between 41.90-45.70 mN/m (83) with the levels of bio-surfactants *in vivo* was confirmed to be below critical micelle concentration (CMC) (257). On the other hand, the surface tension value of humans intestinal fluids (HIF) was reported to be 33.6 mN/m (73) which is much lower than the currently established biorelevant media, FaSSIF-V1 (surface tension 53 mN/m (62) and FaSSIF-V2 54 mN/m (57). Similarly the compendial media (SGF and SIF) do not include surfactants and therefore are less likely to simulate the solubilisation and the wetting effect that occur *in vivo*.

### **1. SLS (anionic surfactant) based modified media**

#### **Surface tension (ST) measurement**

The Du Nouy ring method was used to determine the critical micelle concentration (CMC) and ST of SLS (99% pure) with SGF as the dissolution medium. The temperature of the dissolution medium was controlled at 25 °C. Meanwhile, the measurement in simulated intestinal media SIF and blank FaSSIF-V2 were performed by Tomaszewska and Fotaki (258). Due to the precipitation of potassium from the phosphate salt (potassium based SIF) with lauryl sulphate from SLS, potassium salts were replaced with sodium phosphate salts (sodium-based SIF, Na-SIF) (259). An accurate amount of SLS was titrated dropwise using a built-in automatic titrator (up to a total concentration of 3% SLS) into the dissolution medium, which was constantly stirred using a built-in magnetic stirring system. Surface tension was automatically measured after each addition of surfactant into the glass beaker containing medium. 99% pure SLS was used as previous reports have shown that SLS purity could affect the CMC and dissolution of drugs used in the study (259, 260).

### **Ionic strength calculation**

Ionic strength of SGF and modified medium (with SLS) were calculated using Equation 9 (261):

$$I = \frac{1}{2} \sum_{i=1}^n c_i z_i^2 \quad \text{Equation 9}$$

Where I is ionic strength,  $c_i$  is the molar concentration of the ion and  $z_i$  is the charge number of that ion.

## **2. HTAB (cationic surfactant) based modified media**

One of the model drugs used in this project, CX, is practically insoluble in aqueous media (249). FDA clinical pharmacology and biopharmaceutics review states that solubility and surfactant screening studies of CX formulation have been performed in media with pH 6.8 (as HPMCAS, a main component of the CX formulation, is insoluble in acidic media). SLS (anionic type surfactant) and HTAB (cationic type surfactant) were added to the phosphate buffer at pH 6.8 and the kinetic solubility of CX was measured and results showed that HTAB is a better surfactant for the dissolution testing due to the precipitation of CX in the presence of SLS (233). Similar to the SLS based modified media, the development of HTAB based modified media is orientated on a dissolution medium that could mimic the physiological surfactant system and its *in vivo* surface tension value.

### **Surface tension (ST) measurement**

Complete ST and CMC dataset of HTAB in SGF and SIF had been presented in Stippler's PhD thesis (262), therefore the reported critical micelle concentration plot of HTAB in SGF and SIF (262) were used in the current study. In her study, the surface tension measurements were performed according to the maximum bubble pressure method using a SitaT10 device at a 0.5 Hz bubble rate and  $21^\circ\text{C} \pm 1^\circ\text{C}$ . The surfactant solutions were prepared in a concentration range from 0% to 1% surfactant immediately prior to the measurements.

Thus the modified media developed are listed in Table 11 (The full results and discussion are presented in Section 3.1.2)

Table 11. Type and name of modified media used in this project

Name	Composition
SGF-M1	Simulated gastric fluid-modified 1 (SGF+0.01%SLS)
SGF-M2	Simulated gastric fluid-modified 2 (SGF+0.015%HTAB)
SIF-M1	Simulated intestinal fluid-modified 1(Na-SIF+0.2%SLS)
SIF-M2	Simulated intestinal fluid-modified 2 (blank FaSSIF-V2+0.1%SLS)
SIF-M3	Simulated intestinal fluid-modified 3 (SIF+0.1% HTAB)
SIF-M4	Simulated intestinal fluid-modified 4 (SIF+1% HTAB)
SIF-M5	Simulated intestinal fluid-modified 5 (Na-SIF+1% SLS)

#### 2.4.5 Equilibrium solubility studies (Itraconazole)

Saturation solubility was determined using the following method (192): Screw cap vials containing 20 mL of medium (FaSSGF and FaSSIF-V2) are preheated to 37°C before adding 2 mg (excess amount) ITR powder (n= 3). The samples were gently agitated in a shaking bath (100 rpm) with the temperature maintained at 37 °C. 3 mL aliquots were removed after 1, 4, 8 and 24 h and filtered through a 0.45µm membrane filter. The first 1 mL of the filtrate was discarded. The filtrates were diluted with the medium (where appropriate) and then analysed using HPLC to determine the concentration of the drug in solution.

#### 2.4.6 *In vitro* dissolution testing with USP apparatus 1 and 2

Apart from the single stage dissolution method, an alternative method to simulate the physiological conditions using a 2 stage dissolution experiment was performed. In this model, the formulation is first dissolved in simulated gastric media (FaSSGF) and the medium was changed to intestinal media (FaSSIF-V1 or FaSSIF-V2), under near-physiological conditions with respect to the composition of the fluids and the gastric emptying time. The dissolution setup with USP apparatus 1 (for capsule) and 2 (for tablet) are presented below:

Dissolution medium volume	Single stage: 500 mL 2 stage: 250 mL (0-30 min, gastric stage) then 500 mL (30-180 min, intestinal stage)
---------------------------	---

Temperature	37±0.5°C
-------------	----------

Sample volume	3 mL
Sampling location	From a zone midway between the surface of the dissolution medium and the top of the rotating basket or blade, not less than 1cm from the vessel wall (42)
Sampling times	Single stage: 5, 10, 15, 20, 30, 45, 60, 75, 90, 120, 150, 180 2 stage: 5, 10, 15, 20, 30, 35, 40, 45, 60, 75, 90, 120, 150, 180
Number of experiments	n = 3 (triplicate)
Dissolution media	CA: Compendial media (SGF, SIF) Biorelevant media (FaSSIF-V1, FaSSIF-V2, FaSSGF, FeSSGF, FeSSIF-V2, digested early FeSSGF, early FeSSGF), 2 stage (FaSSGF/FaSSIF-V1 and FaSSGF/FaSSIF-V2) ITR: Compendial media (SGF, SIF) Biorelevant media (FaSSIF-V2, FaSSGF, FeSSGF, FeSSIF-V2), 2 stage (FaSSGF/FaSSIF-V1 and FaSSGF/FaSSIF-V2) CX: Biorelevant media (FeSSGF), Modified media (SIF-M4 and SIF-M5), 2 stage (FaSSGF/FaSSIF-V1 and FaSSGF/FaSSIF-V2)
Formulation tested:	CA: Zinnat <sup>®</sup> ITR: Sporanox <sup>®</sup> CX: CX formulation 8

Sampling procedure (USP apparatus 1 and 2):

### 1. Aqueous media

3 mL samples were removed using a 5 mL Fortuna<sup>®</sup> Optima<sup>®</sup> syringe fitted with a stainless cannula. The drawn volume was replaced with the same volume of fresh dissolution medium, which was kept in a separate vessel at a temperature of 37±0.5°C. Each sample (apart from the milk-based media) was filtered through a Whatman<sup>®</sup>



cellulose nitrate membrane filter 0.45µm (Whatman<sup>®</sup>, Maidstone, UK) equipped in a stainless steel filter holder swinny style (Millipore, Billerica, USA); after discarding the first 1 mL, an appropriate volume of the filtrate was diluted with the dissolution medium and injected into the HPLC system.

## **2. Milk-based media**

For the milk-based medium (FeSSGF, early FeSSGF and digested early FeSSGF) 3 mL samples were withdrawn through a 10 µm inline polyethylene cannula filter connected to the end of the cannula. Since simple filtration was not applicable for these media, samples were subjected to a preparation step consisting of protein precipitation using acetonitrile and subsequent centrifugation, prior to the filtration step. The filtered samples were added with 1:1 (for CA) or 1:2 (for ITR and CX) of acetonitrile. The mixture was vortexed for 1 min and centrifuged (at 8000 rpm for 10min and at 10 °C). The supernatant was filtered (0.45 µm nylon filter) before injecting into the HPLC.

### **2.4.7 Standard curves analysis using HPLC**

The stock solution of CA was prepared in methanol whereas the stock solutions of ITR and CX were prepared in acetonitrile. A calibration curve in dissolution media was prepared each time prior to each experiment to ensure consistency with the dissolution media, mobile phase and HPLC system. Appropriate amounts of stock solution were transferred into volumetric flasks and were diluted with tested media in order to achieve the desired standard concentration. Then an adequate volume of these solutions was injected into the HPLC system.

#### **2.4.7.1 Aqueous media**

Aqueous media refer to dissolution media (used in this project) that do not contain milk or digested milk. The concentrations used in the calibration curve in each dissolution media are presented in Table 12.

Table 12. Parameters for standard curves of aqueous media

Drug	Stock solution conc. (µg/mL)	Standards conc. range (µg/mL)	Standard conc. (µg/mL)
CA	1000	10-200	10, 15, 20, 30,50, 80, 100, 120, 140, 200
ITR	1000 and working stock solution 100	0.1-5	0.1, 0.2, 0.5, 1, 2, 3, 4, 5
CX	1000 and working stock solution 100	0.1-4	0.1, 0.2, 0.3, 0.4, 0.5, 0.6,1,1.5,2,3,4

The typical chromatograms of CA, ITR and CX are presented in Appendix 1.

#### 2.4.7.2 Milk-based media

Milk-based media refer to dissolution media (that were used in this project) that contain milk (FeSSGF, early FeSSGF and digested early FeSSGF, refer to Table 2 for composition of media). The protein precipitation and centrifugation analysis method for milk-based medium, as proposed by Fotaki *et al.* (63) were used. In this method the appropriate type and volume of organic solvent were added into the milk-based medium and then the mixture was vortexed before centrifuging to separate the milk protein and aqueous phase. Furthermore, drugs can distribute into several phases of milk: they can bind to the milk proteins or dissolve in the oily or the aqueous phase of the emulsion (57). Likewise, the standard solutions in milk-based media (Table 13) were prepared using the following steps: in a centrifuge tube containing 2 mL of milk-based medium, an appropriate amount of stock solution (reference standard dissolved in acetonitrile) was added. After vortexing for one minute, an appropriate amount of acetonitrile was added in order to achieve a ratio of 1:2 (Stock solution: Acetonitrile) for ITR and CX and a ratio of 1:1 (Stock solution: Acetonitrile) for CA (The use of higher ratio in ITR and CX is important to ensure no precipitation occurs in the mixture during analysis). After vortexing for one minute, the samples were centrifuged for 10 min at 8000 rpm and 10 °C. The clear supernatant was then filtered using a 0.45µm nylon filter before injecting into the HPLC system.

Table 13. Parameters for standard curves of milk-based media

Drug	Stock solution conc. (µg/mL)	Standards conc. range (µg/mL)	Standard conc. (µg/mL)
CA	1000	10-200	10, 15, 20, 30,50, 80, 100, 120, 140, 200
ITR	1000 and working stock solution 100	0.1-5	0.1, 0.2, 0.5, 1, 2, 3, 4, 5
CX	1000 and working stock solution 100	0.1-4	0.1, 0.2, 0.3, 0.4, 0.5, 0.6,1,1.5,2,3,4

In order to study and characterise the dissolution profile of Sporanox<sup>®</sup> in the fed stomach, digested early FeSSIF was used to simulate the gradual digestion of the meal. Digested early FeSSGF was prepared by adding a pepsin solution (1.11mg/mL of pepsin in HCl (1.83 N, 1 mL) into solutions at 0, 15, 30, 45, 60, 75 and 90 min time points) into flasks pre-filled with early FeSSGF. The solutions were mixed in a shaking water bath (37°C) for 60 min and a sample of 2 mL from each flask was then transferred into a centrifuge tube containing 4 mL of acetonitrile. After vortexing for 1 min, the sample was centrifuged for 10 min at 8000 rpm and 10 °C. The clear supernatant was then filtered using a 0.45 µm nylon filter before injecting into the HPLC system.

In order to ensure the analytical procedure to reproducibly and accurately quantify the amounts of drug released in the milk-based medium the following method validation studies were performed.

#### **Drug recovery study (milk-based media)**

Drug recovery studies (performed in milk-based media) were also performed. Similar calibration curves as presented in Section 2.4.7.1 were constructed but replacing milk-based medium with its blank media (media with the milk component replaced with water). The precision and accuracy occurring in spiked media with milk standards within this range (CA: 0.4-50, ITR: 0.1-6, CX: 0.2-8) using a standard addition method were evaluated (in triplicates). The recovery of tested drugs added to samples to determine the procedure's accuracy was calculated as follows (Equation 10) (263):

$$\% \text{Recovery} = \frac{\text{Calculated amt of drug in spiked sample (from std curve)} \times 100\%}{(\text{Amt drug added} + \text{Amt of drug in neat sample})} \quad \text{Equation 10}$$

### **Fat binding test (milk-based media)**

In the analysis process the milk was centrifuged to separate the precipitated protein with the aqueous phase. The aim of the fat binding test is to investigate the extent of drug (CA, ITR and CX) partition into the milk fat layer during centrifugation. Firstly, the control standard solutions were prepared by centrifuging the standard solutions, syringing out the supernatant component and then protein precipitation of the supernatant (through the addition of organic solvent). Thus a large amount of highly lipid soluble compound will be partitioned into the fat layer leaving a smaller amount of drug in the supernatant solution. Secondly, the tested standard solutions were prepared by following the normal steps of protein precipitation and then centrifugation whereby the standard solutions were added to organic solvent and then centrifuged. Percentages of drug partition into the milk fat layer are calculated using Equation 11.

$$\% \text{fat partition} = \frac{\text{Concentration of control sample} - \text{Concentration of test sample}}{\text{Concentration of control sample}} \times 100\% \quad \text{Equation 11}$$

### **2.4.8 Drug degradation studies (Cefuroxime axetil)**

CA could undergo hydrolysis to other isomers at different rates under various conditions as discussed in Section 1.8.1.1. Characterization of the rate and extent of CA hydrolysis during the dissolution test was carried out as part of the dissolution experiments carried out in SGF, FaSSGF, FaSSIF-V2 and SIF with USP apparatus 2. The dissolution testing conditions were stated in Section 2.4.8. For a more complete consideration of the degradation process the experiments were carried out up to at least 9 h (extra samples were collected at 240, 300, 360, 420, 480, 540 min). The concentration of CA after 120 min determined from USP apparatus 2 were plotted over time using Microsoft Excel™ (the CA concentration after 120 min showed a steep negative curve which was evidence of drug degradation). Since the CA degradation is a first order process (206, 264) the CA degradation rate constant was determined using Equation 12 (206):

Where  $k$  is the degradation rate constant,  $C$  is the concentration at a time " $t$ ",  $C_i$  is the initial concentration and  $t$  is time

#### 2.4.9 *In vitro* dissolution with USP apparatus 4

According to the United States Pharmacopeia (USP, edition 32) specifications a 5 mm–size glass was positioned in the tip of the cell (22.6 mm-size) (42), 1.7 g of 1 mm–size glass beads were added, while on the top of the cell a Whatman® GF/F and GF/D glass fibre filter were used. Additionally, 0.3 g of glasswool was used for CX formulation and Sporanox® dissolution study to enhance the filtration capacity. The Zinnat® and CX formulation were placed on the tablet holder whereas Sporanox® capsules were laid on the glass beads with inverted tablet holder to prevent the capsule from floating on the top of the cells (Figure 12).

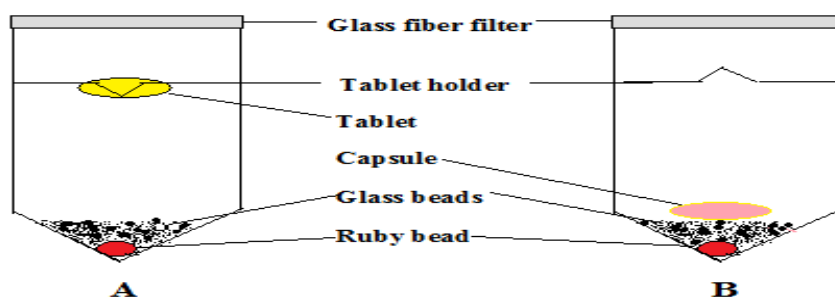


Figure 12. Schematic diagram of cell setup for the USP apparatus

(a) Zinnat® and CX formulation and (b) Sporanox® capsule.

The experiments were performed with sequential changes of the media and flow rates based on the method proposed by Fotaki *et al.* (265) (Table 14). Experiments were run in triplicate.

Table 14. The periods during which formulations were exposed to the various dissolution media and flow rates

Type of medium	Medium	Period (min)	Flow rate (mL/min)*
Compendial media (CA and ITR only)	SGF	0-60	8
	SIF	60-240 (CA) 60-600 (ITR)	4
Modified media (SGF-M1/ SIF-M1)	SGF+0.01%SLS	0-60	8
	Na-SIF+ 0.2% SLS	60-240 (CA) 60-600 (ITR, CX)	4
Modified media (SGF-M1/ SIF-M2)	SGF+0.01%SLS	0-60	8
	Blank FaSSIF-V2+ 0.1% SLS	60-240 (CA) 60-600 (ITR, CX)	4
Modified media (SGF-M2/ SIF-M3) (CX only)	SGF+0.015% HTAB	0-60	8
	SIF+0.1% HTAB	60-600	4
Biorelevant media (Fasted state)	FaSSGF	0-60	8
	FaSSIF-V1	60-240 (CA, ITR) 60-300 (CX)	4
	FaSSGF	0-60	8
	FaSSIF-V2	60-240 (CA, ITR) 60-300 (CX)	4
Biorelevant media (Fed state)	FeSSGF	0-120	6
	FeSSIF-V1	120-360	6
	FeSSGF	0-120	6
	FeSSIF-V2	120-360	6

\*The flow rate is defined in steps in the piston pump. Their relation is given by the equation:  $y=0.0157x+0.7842$  (y: flow rate, x: steps).

Sampling times:

Every 10 min up until 240 min (fasted state studies for CA and ITR) and up until 300 min (fasted state studies for CX) (additional sampling at every 30 min until 600 min).

Every 10 min until 360 min (fed state studies).

Temperature:  $37\pm 0.5^{\circ}\text{C}$ .

Sampling procedure (USP apparatus 4):

The samples were collected in volumetric cylinders and an adequate volume was diluted with the dissolution medium (when appropriate) and injected into the HPLC system.

For the milk-based medium, 3 mL of the collected samples were diluted with acetonitrile (1:1 for CA or 1:2 for ITR and CX). The mixture was vortexed for 1 min and centrifuged (Centrifugation 8000 rpm, 10 min at 10 °C). The supernatant was filtered (0.45 µm nylon filter) before injecting into HPLC.

Formulations tested were:

1. CA: Zinnat<sup>®</sup>
2. ITR: Sporanox<sup>®</sup>
3. CX: CX formulations (Formulation 4, 5, 6, 7, 8, composition presented in Section 2.3.3). The types of experiment performed for CX formulations are presented in Table 15.

Table 15. The types of experiments performed for CX formulations

CX formulation	USP apparatus 4 experiment
F4	FaSSGF/FaSSIF-V2, FeSSGF/FeSSIF-V2
F5	FaSSGF/FaSSIF-V2, FeSSGF/FeSSIF-V2
F6	FaSSGF/FaSSIF-V2, FeSSGF/FeSSIF-V2
F7	FaSSGF/FaSSIF-V2, FeSSGF/FeSSIF-V2
F8	SGF-M1/SIF-M1, SGF-M1/SIF-M2, SGF-M1/SIF-M3, SGF-M1/SIF-M1, FaSSGF/FaSSIF-V1, FaSSGF/FaSSIF-V2, FeSSGF/FeSSIF-V2

#### 2.4.10 Drug precipitation study (Sample after media change with USP apparatus 4)

The aim of this study was to determine the drug concentration in the opaque/cloudy sample collected during media and flow rate change with USP apparatus 4. The results of the precipitation study should confirm whether the excipient or the drug precipitate causes the opaqueness/cloudiness. The precipitation study was performed by ITR and CX only because there was no precipitation observed in the dissolution experiment of CA. The discriminatory sample treatment methods for the opaque sample collected after media change were:

### Method one (Filtered sample)

The precipitate (or solid phase of the drug) dispersed in the medium was separated immediately after collection using a filtration technique. Firstly the sample collected at 70 min was shaken well and a fraction of this sample was withdrawn using a 5 mL Fortuna<sup>®</sup> Optima<sup>®</sup> syringe; then the sample was filtered through cellulose nitrate membrane filters (0.45 µm, Whatman) fitted within 13 mm stainless steel swinny filter holders. The first 1 mL of filtrate was discarded. The clear eluent was analysed using HPLC or diluted with a dissolution medium before analysis.

### Method two (Methanol diluted sample)

The precipitated sample (5 mL) was dissolved in methanol (45 mL, to dissolve any possible suspension of drug particles). The mixture was shaken well and filtered using nylon membrane disc filters (0.45 µm) fitted with 13 mm stainless steel swinny filter holders. The first 1 mL of filtrate was discarded. The clear eluent was analysed using HPLC or diluted with the dissolution medium before analysis.

Concentrations of both filtered and methanol diluted samples were calculated and the amount of drug dissolved (mg) was calculated based on the volume of the sample collected between 60 to 70 min. % of the dose precipitated (after media and flow rate change) in each cell was calculated accordingly:

$$\text{Percentage of the dose precipitated} = \frac{\text{Amt drug (diluted with methanol)} - \text{Amt drug (filtered)}}{\text{Dose}} \times 100\% \quad \text{Equation 13}$$

\* Dose of CA= 250mg, dose of ITR= 100mg, dose of CX= 240mg

Mean± SD values of % dose precipitated were plotted on bar charts for each formulation across all dissolution media.

#### 2.4.11 Statistical analysis: Dissolution profile comparison

Dissolution profile comparisons were performed with the use of difference factor  $f_{1,area}$  (Equation 14) (266):

$$f_{1,area}(\tau) = \frac{\int_0^\tau |W_R(t) - W_T(t)| dt}{\int_0^\tau W_R(t) dt} \quad \text{Equation 14}$$

Where  $W_R$  and  $W_T$  are the reference and test % cumulative profiles at time  $t$ , respectively.



Evaluation of  $f_{1,area}$  was considered up to the time corresponding to the first experimental datum after 85% of the plateau level of the reference data set. In cases where this datum point was not observed within the last time point of experimentation,  $f_{1,area}$  was evaluated up to 4 h, to reflect the maximum physiologically reasonable small intestinal residence period (63). The profile comparison index calculation could be based on the mean data sets if the data set involved has low variability (167) (% coefficient of variation of data points at every sampling time less than 20%). In this project  $f_{1,area}$  was applied from mean data sets and a suggested 20% average difference of a test from a reference data set ( $f_{1,area} = 0.20$ ) was used as the limit for identifying differences between the samples (266). In each dissolution profile comparison, one profile was chosen as the reference profile.

#### **2.4.12 Dissolution kinetics modeling**

Estimates for kinetic parameters were derived by fitting to the set of data in media simulating gastric and intestinal states. Full dissolution profiles as a whole were used for CA (Dissolution profile presented in Section 3.2). Meanwhile separate fitting for ITR and CX dissolution profile in the simulated gastric (first 1 and 2 h in simulated fasted and fed conditions, respectively) and intestinal phases (post 1 and 2 h in simulated fasted and fed conditions, respectively) were performed using first order kinetics and Power law models (Dissolution data presented in Sections 3.3 and 3.4). In that case, a model with lag time was applied whereby a lag time of 1 h and 2 h was used for simulated fasted and fed conditions respectively. The mathematical expressions used to describe the kinetics of drug release and the discernment of the dissolution and release mechanisms are shown in Table 16. The model used was based on the observation of the curve pattern and the type of formulations, for example Power law was applied for kinetic ITR because Sporanox<sup>®</sup> is a drug-HPMC polymeric coated multi-particulate formulation. Mean $\pm$  SD values of the fitted parameters were presented. In all cases the Sigma Plot 11.0 program was used.

Table 16. Dissolution kinetics model applied

Model	Equation	Reference
First order	$f_t = \text{Max}(1 - e^{(-ct)})$	(267)
First order with lag time	$f_t = \text{Max}\left(1 - e^{[c(t-T_{lag})]}\right)$	(268)
Power law	$\frac{M_t}{M_\infty} = kt^n$	(269)
Power law with lag time	$\frac{M_t}{M_\infty} = k(t - T_{lag})^n$	(270)
Single Weibull function	$\text{Max}\left(1 - \exp\left(-\frac{(t-T_{lag})^b}{a}\right)\right)$	(163)

First order kinetics:  $f_t$  is the percentage of drug dissolved in time  $t$ .  $\text{Max}$  and  $c$  are the maximum cumulative percentage dissolved and first order rate constant, respectively.  $T_{lag}$  denotes the lag time.

Power law: The Power law model is generally used to analyse the release of pharmaceutical polymeric dosage forms when the release mechanism is not well known or when more than one type of release phenomenon could be involved (271).  $M_t$  and  $M_\infty$  are cumulative percentage of drug dissolved at time  $t$  and infinite time, respectively ( $M_t/M_\infty$  is the percentage drug release at time  $t$ ).  $T_{lag}$  denotes lag time and  $k$  is a dimensionless constant incorporating diffusion coefficient of the compound and geometric characteristics of the drug dosage form;  $n$  is the dimensionless diffusion exponent that depends on the transport mechanism and the shape of the matrix tested (269, 272). For swellable (a characteristic of HPMC) spherical sample,  $n$  values of 0.43, 0.43–0.85, 0.85 and  $>0.85$  indicates Fickian, non-Fickian (anomalous), Case II (zero order) and Super Case II transport (269, 273). Furthermore, Ritger and Peppas proposed an additional interpretation that  $n < 0.43$ , diffusion controlled release;  $n > 0.85$ , erosion controlled (polymer relaxation) release;  $0.43 < n < 0.85$ , mixed mechanism (drug diffusion in the hydrated matrix and the polymer relaxation) (273). When pure diffusion is the controlling release mechanism,  $n = 0.5$  (274). Power law is short time approximations of complex exact relationships and therefore its use is confined to the description of the first 60% of the release curve (274, 275).

Weibull function: The Weibull function is a very versatile and commonly used model for fitting dissolution data of different curve shapes (272).  $\text{Max}$  is the maximum percentage of the drug dissolved,  $a$  is the time scale parameter, which provides information about the scale of dissolution process. Scale parameter ( $a$ ) also represents the time interval necessary to dissolve or release 63.2% of the drug.  $b$  is the shape parameter [ $1^{\text{st}}$  order

exponential ( $b = 1$ ), sigmoid or S-shaped with upward curvature followed by a turning point ( $b > 1$ ) or parabolic, with a higher initial gradient  $m$  and after that consistent with the exponential ( $b < 1$ ) (87, 271).  $T_{lag}$  denotes lag time which essentially is a location parameter which represents lag period before the actual onset of the dissolution process.

## **2.5 Methods of Part 2: Surface UV dissolution imaging**

### **2.5.1 Experiment setup and protocol**

*In vitro* surface ultraviolet (UV) imaging experiments were performed using Sirius SDI (Surface Dissolution Imager, Sirius Analytical Instruments, East Sussex, UK). The Sirius SDI includes ActiPix™ UV area imaging technology combined with a laminar flow-through sample holder, integrated syringe pump and software (Schematic of apparatus is presented in Figure 7 in Section 1.5). The light source was a pulsed xenon lamp and detection was performed at 280 nm (band width 10 nm). The utilised CADISS-2 quartz flow cell had a light path of 4 mm. The imaging system consists of  $1280 \times 1024$  pixels with dimensions of  $9 \times 7 \text{ mm}^2$  (total imaging area of  $9 \times 7 \text{ mm}^2$ ), and each pixel can be considered as a conventional single-beam spectrophotometer. Output from the sensor is connected to a computer at a rate of one snapshot every 0.5 s for processing and storage. A syringe pump (RS-232 integrated pump, Maxim Integrated Products, Inc, US) was used for infusion of dissolution media at constant and changing flow rates, with temperature controlled at 37°C using Techne DB-2D Dri-Block® digital heater (Staffordshire, UK). Dissolution experiments themselves were performed using ITR and CA reference standard, Sporanox® and Zinnat® compacts, as described below.

### **2.5.2 Preparation of compacts**

Compacts were prepared using ITR (4 mg) and CA (4 mg) reference standard powder, Sporanox® pellet (4 mg, the hard gelatin Sporanox capsule was removed beforehand) and grounded Zinnat® tablet powder (4 mg, Zinnat® tablet was grounded into fine powder using mortar and pestle). Samples were transferred into a stainless steel cylinder sample cup (2 mm ID x 2.4 mm height). The sample cup was fitted into the middle plate and was accurately positioned over the compression base and beneath the compression rod. After powder had been placed inside the middle plate, the top plate was fitted. A Quickset Minor® torque screwdriver was then used to compress the

weighted materials at a constant torque pressure of 0.6 Nm. The compression was held continuously for 1 min, then the compression rod and top plate were removed to allow recovery of the packed sample cup. The surface to be tested was in contact with the bottom plate thus great care was taken in order not to touch this surface once it had been removed from the bottom plate. Examples of prepared compacts are presented in Figure 13.



Figure 13. Examples of Sporanox pellet (A), ITR API (B) and CA API (C) compact used for the surface dissolution imaging studies.

### **2.5.3 Design of experiment**

#### **2.5.3.1 Media and flow rate change**

The design of the experiment with flow rate change was based on the setup used in USP apparatus 4 (flow through cell). Due to the diameter of the sample cup (in Actipix SDI) being 2 mm compared to the diameter of flow through cells of 22.6mm, the flow rate and time for media change was scaled down by one order magnitude. For example in the USP apparatus 4 setup the flow rates of 8 mL/min (gastric phase) in the first 60 min and 4mL/min (intestinal phase) were used whereas in surface UV imaging setup the flow rates of 0.8mL/min (gastric phase) in the first 6 min and 0.4mL/min (intestinal phase) were used.

#### **2.5.3.2 Flow rate and its correlation with physiological linear velocity**

A linear regression of linear velocity of ActiPix<sup>TM</sup>'s flow through cell from various flow rate can be made using the data presented in literature (124) (Table 17). The flow rate corresponding to the published nominal physiological linear velocity for stomach (2 cm/min) and intestine (1 cm/min) was determined from the linear regression (276).

Table 17. Linear velocity of ActiPix™'s flow through cell from various flow rates

Flow rate ( mL/min)	0.1	0.2	0.4	0.8	1.2
Linear velocity	0.7	1.4	2.9	5.7	8.6

### 2.5.3.3 Procedure for surface UV dissolution imaging

The procedure for surface UV dissolution imaging was as follows:

1. For the first 10 sec period of imaging, dark values (UV light is off) are measured to account for the electronic noise. An average dark value is then subtracted from each background value to negate contributions from electronic noise. The subsequent 10 sec are used to collect the background intensities from the buffer contained within the flow cell.
2. Dark images ( $I_0$ ; lamp turned off; 10 sec) and reference images ( $I_{ref}$ ; 10 sec) were recorded with the dissolution cell filled with the medium. During the reference period, a stainless steel cylinder was placed in the sample holder.
3. After 60 sec, data collection was paused and the sample compact was then fitted into the sample cell before the sample cell was inserted into the dissolution cell. The pre-set flow program and data collection was then started. The pre-set flow programs consist of (1) Changing flow rate; (2) Constant flow rate and (3) Media and flow rate change (Table 18). UV images were therefore collected for a total duration of 18 min.

Table 18. The periods the compact was exposed to the dissolution media and the flow rate of each medium pumped through the cell

Medium	Period (min) of each flow rate	Flow rate (mL/min)
ITR and CA reference standard compact		
Changing flow rate		
SGF/ FaSSGF/ SIF/ FaSSIF-V1	5 or 15	0.14, 0.28, 0.4, 0.6, 0.8, 1
Media and flow rate change		
SGF/ FaSSGF	0-6	0.8
SIF/ FaSSIF-V1	7-30	0.4
Sporanox <sup>®</sup> pellet compact		
Constant flow rate		
SGF/ FaSSGF/ SIF/ FaSSIF-V1	5 or 15	0.14, 0.28, 0.4, 0.6, 0.8, 1
Media and flow rate change		
SGF/ FaSSGF	0-6	0.8
SIF/ FaSSIF-V1	7-30	0.4

- Calibration curves were constructed by flowing drug standard solutions through the dissolution cell at a flow rate of 1 mL/min. Recording of UV images was performed while each of the standard solutions was infused for a period of 5 min. The buffer was infused before and after the series of reference standard solutions for 4 min in order to detect baseline drift. The standard solutions were prepared using CA and ITR reference standard in FaSSGF and SGF respectively. The concentration range used was 5-180 µg/mL). FaSSGF was chosen for CA because the degradation is lowest in FaSSGF among all FaSSIF-V1, FaSSGF, SGF and SIF (refer to CA degradation Section 3.2.1) and SGF was chosen for ITR mainly due to its relatively good solubility in SGF. Three UV readings were made at different time points at each concentration and the average values were used for the calibration plot.

The collected data were then used to calculate dissolution rates of tested compounds in the various media at 1 min intervals, using ActiPix<sup>™</sup> D100 software version 1.5. This function employs absorbance values read from pixels within a designated quantification region of each image, located downstream from the surface of the dissolving sample compact. Absorbance values at each pixel row within the quantification region were

combined with the corresponding flow rate profile (defined by the software), together with the surface area of the drug compact, the molar mass and the molar absorptivity (extinction coefficient) of CA and ITR (determined from calibration curves), in order to compute drug dissolution rates. The calculated dissolution rates were subsequently used by the software to calculate the cumulative amount of drug dissolved. The calculation of the amount of dissolved drug is based on the assumption that the UV absorbance for each pixel reading is within the linear range (following Beer Lambert's law, Appendix 2).

The absorbance of the dissolution medium is set to zero prior to the measurement of the samples. In the ActiPix™ D100 software the procedure for every experiment is to measure the reference ( $I_{ref}$ ) and the dark current ( $I_0$ , electronic noise measured with the lamp turned off) within the first 20 s of a measurement, which are subtracted from all sample absorbance signals ( $I_{sig}$ ).

The conversion of pixel intensities to absorbance values (A) was done using the ActiPix™ software based on Equation 15 (111). Absolute absorbance values were collected by reading each pixel intensity (mean value) during the background (or  $I_0$ ) collection and then applying the standard log formula for Absorbance. Each pixel records the absorbance of light by photons in the quartz cell 4 mm (width) above it. The same principles of Beer's law apply to this arrangement with the exception that (b) the path length is 0.4 cm instead of the normal 1 cm

$$A = \log \left( \frac{I_{ref} - I_0}{I_{sig} - I_0} \right) \quad \text{Equation 15}$$

Where  $I_0$ ,  $I_{ref}$ , and  $I_{sig}$  are the pixel intensity due to the dark current (electronic noise measured with the lamp turned off), pixel intensity measured with the dissolution medium in the cell (reference signal), and pixel intensity measured during the experiment, respectively.

The absorbance values for each pixel in the selected viewing area create a 2-D image, and the images collected for the duration of the experiment were used to create a film (continuous images). Thus, a high resolution 2-D film of UV absorbance is captured that provides a detailed view of the dissolution process at the solid–liquid interface. In order to extract the dissolution profiles from the UV absorbance film, the copyrighted software tools (ActiPix™ software) were used.

The Limit of Quantification (LOQ) for infusion of CA and ITR reference standard solutions was estimated from Equation 16 (111) :

$$LOQ = \frac{C}{AU} \times 10 \times SD \quad \text{Equation 16}$$

Where  $C$ ,  $AU$ , and  $SD$  are the concentration of the ITR and CA reference standard solution, the mean UV absorbance of the selected pixels and the standard deviation of the mean UV absorbance, respectively.



## **2.6 Methods of Part 3: Physiologically Based Pharmacokinetics (PBPK) Modeling**

The PBPK software used in this project is GastroPlus™. GastroPlus™ is a very useful modeling tool due to its broad functionalities such as predicting percentage absorbed, building drug-specific model, dosage formulations evaluation and design, drug metabolism and pharmacokinetic model fitting, optimisation for drug-specific models and PSA (127, 162, 164, 277-282). The collection of mathematical models and correlations that were applied in GastroPlus™ mimicked the effects of a variety of physicochemical, physiological and formulation parameters on the absorption of drugs in the gastrointestinal tract (GIT) (163).

The applications of GastroPlus™ to predict the absorption of three model compounds (CA, ITR and CX) were implemented in this study. A fundamental description of these mathematical models and the details of each parameter and its selection are presented in this section. The accuracy of the models developed using GastroPlus™ was validated by various published examples (126, 136, 164, 165).

### **2.6.1 Computer hardware and software**

The simulations were performed on a Dell desktop station with Intel® Pentium Dual CPU E2160(1.80 GHz) using GastroPlus™ version 8.0 software (Simulation Plus Inc., Lancaster, CA). GastroPlus™ utilises the ACAT model to predict the rate and extent of drug absorption from the GIT (Refer to Section 1.6.2 for further details on PBPK modeling). It also incorporates intestinal drug efflux and metabolism in its predictions of pharmacokinetic parameters (163).

### **2.6.2 Advanced Compartmental Absorption and Transit (ACAT) model description**

Input parameters in the ACAT model can be categorized into three classes: formulation properties (such as drug particle size distribution and density, dosage forms), physicochemical properties of drug substance (such as diffusion coefficient, lipophilicity, pKa, solubility and permeability) and pharmacokinetic parameters (such as

clearance, volume of distribution;  $V_d$  and  $f_{up}$ ). In addition, the ACAT model accounts for factors such as variation in the pH along the GIT.

### 2.6.2.1 Compound database and dissolution model

CA, ITR and CX were not included in the pre-built demo database of the GastroPlus™ thus a new individual compound database was built.

Two main dissolution models, Johnson (283) and Wang-Flanagan (284), are available in GastroPlus™. In the current project, the dissolution model based on the Wang-Flanagan model was used.

### 2.6.2.2 Diffusion coefficient

The diffusion coefficient (or diffusivity) is the “proportionality constant between the rate of change of concentration at a point and the spatial variation of the concentration at that point”. Theoretically, it indicates the rate of molecules in solution moving away from the surface of a dissolving particle into the free stream, and is a function of the viscosity of the surrounding fluid (163). The diffusion coefficient,  $\gamma$ , can be estimated using the Hayduk-Laudie formula whereby the  $V_A$  is calculated from the molecular weight of the molecule (285) (Equation 17):

$$\gamma = 13.26n_w^{-1.4}V_A^{-0.589} \quad \text{Equation 17}$$

Where:  $\eta_w$  = viscosity of water (cP) at 37°C.

$V_A$  = Solute molal volume at its normal boiling point ( $\text{cm}^3/\text{gmol}$ ).

$\gamma$  = binary diffusion coefficient at infinite dilution ( $\text{cm}^2/\text{s} \times 10^5$ ).

### 2.6.2.3 Compound tab

#### CA

The physicochemical characteristics and *in vivo* study parameters of CA are summarized in Table 19. CA is a neutral compound with poor solubility and good permeability. The physicochemical properties (the acid dissociation constant [pKa],

partition coefficient [LogP]), protein binding (based on the unbound fraction in plasma [ $f_{u,plasma}$ ] and blood/plasma (B/P) ratio) were taken from literature. The effective permeability ( $P_{eff}$ ) was derived from *in-situ* perfusion (rat) using conversion tools in GastroPlus™.

Table 19. Physicochemical characteristics and *in vivo* study parameters of CA

Parameters	Values	Comments/ references
MW	510.48	Merck Index (286)
logP	0.25	clogP value (203)
Solubility (mg/mL)	0.395 (FaSSIF-V2) 0.3719 (FeSSIF-V2)	Kinetic solubility value measured from dissolution experiment with USP apparatus 2 (Refer to Table 34 for other values used in solubility-based model)
pK <sub>a</sub>	- (neutral compound)	Merck Index (286)
Dose (mg)	300.27	The dose of CA corresponds to 250mg of Zinnat® tablet used in <i>in vivo</i> (humans) study (287)
Volume of water administered (mL)	200 (fast) 100 (fed)	<i>In vivo</i> (human) study, fast (287), fed (288))
Particle density (g/mL)	1.61	Scifinder™ data (289)
Particle size distribution	Mean radius:19.5±1.63µm	Input as raw data as fractional % vs radius with total bin no. of 16 (290)
Precipitation time (sec)	900	Default GastroPlus™ value
Diffusion coefficient (cm <sup>2</sup> /s)	0.5776x10 <sup>-5</sup>	Converted value from molecular weight using built-in GastroPlus™ convertor. (Refer Section 2.6.2.2: Diffusion coefficient)
Effective permeability	1.2472 ×10 <sup>-4</sup> cm/s	Converted from rat <i>in-situ</i> perfusion permeability value (290). (Refer to Section 2.6.3.1 for further details)

## ITR

The physicochemical characteristics and *in vivo* study parameters of ITR are summarized in Table 20.

Table 20. Physicochemical characteristics and *in vivo* study parameters of ITR

Parameters	ITR	Comments/ references
MW (g/mol)	705.65	(289)
logP	5.66	(291)
Solubility(mg/mL)	4.812x10 <sup>-3</sup> (fasted state) 2.25x10 <sup>-2</sup> (fed state)	Scaled from human intestinal fluid data (292) using FaSSIF-V1 and FeSSIF-V1 solubility value (Refer to text for details). Refer to Table 34 for other values used in solubility-based model.
pK <sub>a</sub> , acid/base species	3.7 (weak base)	(291)
Dose (mg)	100	(228)
Volume of water administered (mL)	100	(228)
Particle density (g/mL)	1.2	(289)
Mean particle radius (µm)	1	(244)
Precipitation time (sec)	900	Default GastroPlus™ value
Diffusion coefficient (cm <sup>2</sup> /s)	0.4855x10 <sup>-5</sup>	Converted value from molecular weight using built-in GastroPlus™ convertor (Refer to Section 2.6.2.2: Diffusion coefficient).
Effective permeability, cm/s	3.46 ×10 <sup>-4</sup>	Converted from MDCKII permeability value (293) (Refer to Section 2.6.3.1 for further details).

### ITR: Scaling of *in vitro* biorelevant solubility

As the pH of biorelevant intestinal media (FaSSIF-V1, FeSSIF-V1) and HIF is higher than or similar to pH 5, the solubility of ITR in these media was much lower than in

gastric media. In this case, the effects of mixed micelles found in human intestinal fluid and were reported to greatly enhance the solubility of ITR (30).

In order to correlate the solubility of ITR in biorelevant media (fasted and fed states) with the human intestinal fluid, the solubility of 5 weak basic compounds in FaSSIF-V1 vs fasted HIF as well as FeSSIF-V1 vs fed HIF were used to form the regression relationship (in log-log scale) (292). The solubility value of ITR in FaSSIF-V1 and FeSSIF-V1 (30) were then scaled using the established regression relationship (Appendix 3).

In fasted HIF and in FaSSIF-V1 the regression formed is  $y=0.6068x+1.0272$  ( $R^2=0.80$ , log-log scale). The scaled value of FaSSIF-V1 (pH = 6.5) is  $4.812 \times 10^{-3}$  mg/mL, almost 16 times higher compared with the solubility of ITR in FaSSIF-V1  $0.34 \times 10^{-3}$  mg/mL (30). Meanwhile, in fed HIF and in FeSSIF-V1 the regression formed is  $y=0.5391x+1.4963$  ( $R^2=0.78$ , log-log scale). The scaled value of FeSSIF-V1 (pH = 5) is  $22.53 \times 10^{-3}$  mg/mL, more than 30 times higher than the solubility of ITR in FeSSIF-V1,  $0.73 \times 10^{-3}$  mg/mL (30).

## CX

The physicochemical characteristics and *in vivo* study parameters of CX are summarised in Table 21. The physicochemical properties (the acid dissociation constant [pKa], partition coefficient [LogP]), protein binding (based on the unbound fraction in plasma [ $f_{u,plasma}$ ], blood/plasma (B/P) ratio were taken from literature and a drug review published by the Center for Drug Evaluation and Research of FDA (*in vivo* studies conducted in humans) (233). The effective permeability ( $P_{eff}$ ) was derived from Caco-2 cell using conversion tools in GastroPlus™.

Table 21. Physicochemical characteristics and *in vivo* study parameters of CX

Parameters	CX	Reference
MW	489.93	(233, 249)
Partition coefficient, logP (neutral, water)	3.0	(233, 249)
Solubility (mg/mL at pH=5)	0.37	From solubility experiment in FeSSIF (at 2 h using shake flask method, (252)) (Refer to Table 34 for other values used in Solubility-based model).
Dissociation constant pK <sub>a</sub>	7.9 and 11.1 (acidic compound)	(233)
Dose/tablet (mg)	240	The dose used in <i>in vivo</i> (dog) study (252)
Volume of water administered (mL)	15	In-vivo (dog) study (252)
Particle density (g/mL)	1.25	(235)
Particle size distribution	Mean radius:1.5 μm	(249)
Precipitation time (sec)	9000	Estimated value postulated from literature value (294) that there was no precipitation within 2.5 h
Diffusion coefficient (cm <sup>2</sup> /s)	0.5904x10 <sup>-5</sup>	Predicted value from molecular weight using built in GastroPlus™ convertor (Refer to Section 2.6.2.2: Diffusion coefficient).
Effective permeability (Dog)	1.282 x10 <sup>-4</sup> cm/s	Converted to P <sub>eff</sub> (dog) using built-in GastroPlus™ permeability convertor (Refer to Section 2.6.3.1).

### CX: Scaling of *in vitro* biorelevant solubility

Similar to ITR, in order to correlate the solubility of CX in biorelevant media (fasted and fed states) with the human intestinal fluid, the solubility of 6 weak acidic compounds in FaSSIF-V1 vs fasted HIF as well as FeSSIF-V1 vs fed HIF were used to form the

regression relationship (in log-log scale) (292). The solubility values of CX in FaSSIF-V1 and FeSSIF-V1 (252) were then scaled using the established regression relationship (Appendix 3).

In fasted HIF and in FaSSIF-V1 the regression formed is  $y=0.7933x+0.8385$  ( $R^2=0.958$ , log-log scale). The scaled value of FaSSIF-V1 (pH = 6.5) is 0.11mg/mL, almost three times higher than the solubility of CX in FaSSIF-V1 0.04 mg/mL (252). Meanwhile, in fed HIF and in FeSSIF-V1 the regression formed is  $y=1.04x+0.4093$  ( $R^2=0.9572$ , log-log scale). The scaled value of FeSSIF-V1 (pH = 5) is 1.08 mg/mL, almost three times the solubility of CX in FaSSIF-V1, 0.37mg/mL (252).

#### 2.6.2.4 Particle size distribution

The particle radius was normally kept constant in equations. Using GastroPlus™, the particle radius could be modelled by monodisperse (all particles have the same radius) or polydisperse (contains a mixture of different size particles) particle size distributions.

CA: Particle size distribution was entered as raw data as a fractional percentage vs particle size with total bin number of 16 (Figure 14). The initial mass of undissolved drug corresponding to each bin was calculated automatically by GastroPlus™ using the previously published data (290) (Figure 14).

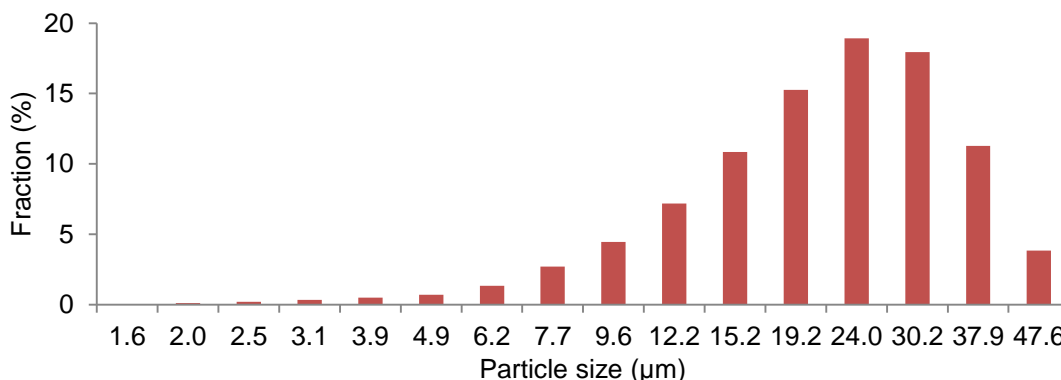


Figure 14. Particle size distribution of amorphous CA. Redrawn based on data available from PhD thesis by Ghazal (290).

ITR and CX: Due to the lack of particle size distribution of the raw material of Sporanox® and CX formulations, mean particle size was used. The mean particle size for the ITR and CX API are 1µm (244) and 1.5µm (249) respectively.

### 2.6.3 Effective permeability ( $P_{\text{eff}}$ )

GastroPlus™ provides a logD model, which scales regional permeability so that effective permeability decreases as the ionised fraction of a compound increases. The default Opt logD model, SAV 6.1 model and four coefficients, C1–C4, were used in the current study. All the physiology parameters were the default values in GastroPlus™.

The absorption rate coefficient  $k_{a(i)}$  for each compartment is the product of the effective permeability value for the absorption and the compartment scale factor ( $\alpha$ ) for the compartment (Equation 18).

$$k_{a(i)} = P_{\text{eff}} \alpha \quad \text{Equation 18}$$

In GastroPlus™,  $P_{\text{eff}}$  was inserted on the Compound tab and equations of the Optimisable log D model were applied to adjust the absorption scale factor for each of the other compartments of the small intestine and colon. The absorption scale factors justify changes in passive transcellular permeability primarily due to changes in ionisation and the distribution coefficient.

#### 2.6.3.1 Conversion of the intestinal permeability

In the absence of a measured  $P_{\text{eff}}$ , an estimated value can be used in the simulation. Estimated  $P_{\text{eff}}$  can come from an *in silico* prediction using software or from *in vitro* measurements. The programme also provides a convenient  $P_{\text{eff}}$  converter to input experimental permeability data from any source for a number of BCS reference compounds and the  $P_{\text{eff}}$  converter will generate a set of correlation models to estimate human  $P_{\text{eff}}$ . For interspecies conversion, GastroPlus™ incorporates an allometric model to estimate human  $P_{\text{eff}}$  from rat or dog  $P_{\text{eff}}$  measurements and vice versa

To the author's best knowledge, the actual measured  $P_{\text{eff}}$  values in humans for CA, ITR and CX are not available. Therefore, in this project, data from Caco-2 (CX) or MDCK cell cultures (ITR) and from a rat gut perfusion study (CA) were used. This was achieved by developing a correlation between  $P_{\text{eff}}$  in humans and the experimental models (163).

The “convert permeability” from user data function in GastroPlus™ (with “user permeability data” file extensions) was used to create a correlation function between



human  $P_{\text{eff}}$  and user-supplied data for permeability (Caco-2, rat gut perfusion and MDCK II).

## CA

The apparent permeability coefficient of CA measured using Caco-2 cell monolayer (apical to basolateral direction, pH 6 buffer solution) following the application of 1.0 mM CA was  $3.43 (\pm \text{SD } 0.15) \times 10^{-7} \text{ cm/s}$  (295). The apparent permeability coefficient was transformed using the built-in GastroPlus™ Caco-2 permeability conversion model (Caco-2 model convertor, the values are presented in Appendix 4) to an estimate of human  $P_{\text{eff}}$  value,  $0.55 \pm 0.21 \times 10^{-4} \text{ cm/s}$ . This value had underestimated the *in vivo* value because the CA concentration in the reservoir of Caco-2 was far lower than the *in vivo* condition and CA degradation was high in the phosphate buffer at pH 6 (206). On the other hand,  $P_{\text{eff}}$  of CA in rats measured using the *in situ* perfusion study was reported as  $0.3332 \times 10^{-4} \pm 0.16 \times 10^{-4} \text{ cm/s}$  (290).

These values were scaled to human  $P_{\text{eff}}$ ,  $0.9682 \times 10^{-4} \text{ cm/s}$  using a built-in model in GastroPlus™. This model correlates the *in situ* rat permeability values with human  $P_{\text{eff}}$  values using a regression relationship derived from example compounds where permeability values for such compounds were measured using both techniques for the same compounds (built-in data were not disclosed in the software) (163). The scaled values calculated from the GastroPlus™ model are very close to the value calculated from the conversion of  $P_{\text{eff,man}} = 3.6 * P_{\text{eff,rat}} + 0.03 \times 10^{-4}$  ( $R^2 = 1.00$ ),  $1.2477 \times 10^{-4} \text{ cm/s}$ , reported by Fagerholm *et al.* (296). This value ( $1.2477 \times 10^{-4} \text{ cm/s}$ ) was chosen and used in the CA model because the reported conditions of the experiment (where the raw data was generated (290)) applied the methods based on Fagerholm *et al.* (296).

## ITR

Monolayer efflux studies with multidrug resistance and MDR1-MDCKII cell permeability studies were available for 9 reference compounds and in the same study the  $P_{\text{app}}$  value of ITR was also reported,  $0.571 \pm 0.0261 \times 10^{-4} \text{ cm/s}$  (293, 297). A regression relationship that correlates the  $P_{\text{app}}$  permeability values of the 9 compounds with human  $P_{\text{eff}}$  values (built-in confidential GastroPlus™ data) was then established using the GastroPlus™ permeability convertor function. Thus, using this regression relationship, converted human permeability ( $P_{\text{eff}}$ ) of the ITR was  $3.48 \pm 0.515 \times 10^{-4} \text{ cm/s}$ .

## **CX**

$P_{\text{eff}}$  of CX measured using the Caco-2 cell monolayer (basolateral-to-apical direction) was reported as  $2.9 \times 10^{-6}$  cm/s (252). These values were converted to human  $P_{\text{eff}}$ ,  $1.1565 \times 10^{-4}$  cm/s using a built-in model in the GastroPlus™ Caco-2 permeability conversion model. This model correlates the Caco-2 cell permeability values with human  $P_{\text{eff}}$  values using a regression relationship derived from example compounds where permeability values for such compounds were measured using both techniques for the same compounds (163). Using the built-in GastroPlus™ convertor this value was then converted to  $P_{\text{eff}}$  (dog),  $2.801 \times 10^{-4}$  cm/s.

### **2.6.4 The pharmacokinetic model**

Plasma concentration profiles after IV administration of CA, ITR and CX (profiles presented in Appendix 5) were analysed using PKPlus™ to obtain the systemic clearance,  $V_d$  and distribution constants between central and peripheral compartments. Fitting of empirical PK models were performed using 1, 2 and 3 compartmental models.

$R^2$  and Akaike information criterion (AIC) was used to select the best fitted compartmental model which were subsequently used in simulations.

## **CA**

The plasma profiles of cefuroxime with IV administration were reported by Finn *et al.* (209). In that particular study 12 healthy male volunteers were given a single dose of 500mg cefuroxime IV injection and the reported mean cefuroxime plasma concentration profile was used in the compartmental analysis. Results of the compartmental analysis show cefuroxime IV profile was best represented by two compartmental model (Table 22).

Table 22. Compartmental analysis (1, 2 and 3 compartmental models) of cefuroxime in humans after administration of 500mg cefuroxime IV bolus (209)

Parameter	1 compartmental	2 compartmental	3 compartmental
$V_d$ (central compartment)(L)	15.23	7.28	4.56
$V_d$ (2 <sup>nd</sup> compartment)(L)	-	3.27	7.66
$V_d$ (3 <sup>rd</sup> compartment)(L)	-	-	37.09
Clearance (L/h)	6.76	7.63	7.51
$K_{10}$ (1/h)	0.44	0.71	1.65
$K_{12}$ (1/h)	-	0.08	5.26
$K_{21}$ (1/h)	-	0.17	3.13
$K_{13}$ (1/h)	-	-	0.30
$K_{31}$ (1/h)	-	-	0.04
$C_{max}$ ( $\mu\text{g/mL}$ )	33.00	46.50	109.50
$R^2$	0.68	0.99	0.91
AIC	-21.74	-68.63	-58.43

Subsequently, the disposition model (of CA in GastroPlus™) was constructed by using parameters from the fitted 2 compartmental model (best fitted compartmental model). Meanwhile, other IV pharmacokinetic parameters from the literature also were applied in the model:  $f_{up}$  [67% (197)]; simulation time [24h (287, 288)]; body weight [70kg (287, 288)] and blood to plasma concentration ratio [0.6315 (298)].

### ITR

The results of the compartmental pharmacokinetic data analysis for 100mg ITR post 1 h IV infusion in humans (291) are listed in Table 23.

Table 23. Compartmental analysis (1, 2 and 3 compartmental models) of ITR in humans after administration of 100mg ITR IV infusion (1 h) (291)

Parameter	1 compartmental	2 compartmental	3 compartmental
Clearance (L/h)	9.74	21.98	20.95
V <sub>d</sub> (L) (central compartment)	200.30	132.1	107.57
V <sub>d</sub> (L) (2 <sup>nd</sup> compartment)	-	5.43	162.83
V <sub>d</sub> (L) (3rd compartment)	-	-	289.56
C <sub>max</sub> (µg/mL)	4.97x10 <sup>-3</sup>	6.35x10 <sup>-3</sup>	6.78x10 <sup>-3</sup>
K <sub>10</sub> (1/h)	0.049	0.17	0.28
K <sub>12</sub> (1/h)		0.20	0.49
K <sub>21</sub> (1/h)	-	0.07	0.32
K <sub>13</sub> (1/h)	-	-	0.14
K <sub>31</sub> (1/h)	-	-	0.05
R <sup>2</sup>	0.72	0.94	1.00
AIC	-17.74	-45.75	-69.79

The results shows that the ITR IV concentration vs time curves were best fitted to 3 compartment model (R<sup>2</sup>: 1.00, AIC:-69.79). Subsequently, the disposition model (of ITR in GastroPlus<sup>TM</sup>) was constructed by using parameters from the fitted 3 compartmental model. Meanwhile, other IV pharmacokinetic parameters from the literature also were applied in the model (Table 24).

Table 24. Reported IV pharmacokinetic parameters of ITR applied in ITR model

Parameter	Value	Reference
$f_{up}$ (%)	0.2	(291)
Simulation time (h)	96	(228)
Body weight (kg)	74.77	(291)
Blood to plasma concentration ratio	0.58	(291)
Absolute bioavailability, F (%)	30 (fast) 25 (fed)	Observed values (fasted state) (299) and fed state (228)
$C_{max}$ ( $\mu\text{g/mL}$ )	0.112 (fast) 0.083 (fed)	
$T_{max}$ (h)	3 (fast) 4.47 (fed)	
$AUC_{0-\infty}$ (ng.h/mL)	1487 (fast) 1248.1 (fed)	

## CX

Following the oral administration of a single dose of 1 mg/kg of intravenous CX to four healthy beagle dogs, blood samples were collected to determine plasma concentration of CX (252). Besides linear pharmacokinetics compartmental analysis, non-linear pharmacokinetics compartmental analysis of IV CX administration was also performed. This is because there are no reported *in vitro* results of CX metabolism by Cytochrome P450 enzyme and P-gp and results of CX non-linear compartmental analysis could be used to determine  $V_{max}$  and  $K_m$  of enzyme and transporter metabolism. The fitted pharmacokinetic parameters are shown in Table 25 and 26.

Table 25. Mean± SD IV pharmacokinetics parameters of CX 240mg tablet orally in dogs using linear pharmacokinetic compartmental analysis

Parameter	1 compartmental	2 compartmental	3 compartmental
V <sub>d</sub> (L)(Steady state)	5.59	5.59	4.31
Clearance (L/h)	1.64	1.36	1.51
K <sub>10</sub> (1/h)	0.29	0.24	0.35
K <sub>12</sub> (1/h)	-	0.05	2.02
K <sub>21</sub> (1/h)	-	2.78x10 <sup>-6</sup>	5.87
K <sub>13</sub> (1/h)	-	-	0.038
K <sub>31</sub> (1/h)	-	-	1.65x10 <sup>-5</sup>
R <sup>2</sup>	0.96	0.96	0.96
AIC	-35.33	-31.33	-32.01

Table 26. Mean± SD IV pharmacokinetic parameters of CX 240mg tablet orally in dogs using non-linear pharmacokinetic compartmental analysis

Parameter	1 compartment	2 compartment	3 compartment
V <sub>d</sub> (L)(Steady state)	6.05	5.64	5.59
K <sub>12</sub> (1/h)	-	0.02	1.71
K <sub>21</sub> (1/h)	-	0.03	3.02
K <sub>13</sub> (1/h)	-	-	0.04
K <sub>31</sub> (1/h)	-	-	0.07
V <sub>max</sub> (mg/s)	25.63	2.40x10 <sup>-3</sup>	6.86x10 <sup>-4</sup>
K <sub>m</sub> (µg/mL)	63230.00	4.91	0.89
C <sub>max</sub> (µg/mL)	0.18	0.19	0.25
R <sup>2</sup>	0.87	0.90	0.96
AIC	-39.04	-63.57	-70.11

The results show that the CX IV concentration vs time curves were best fitted to 3 compartment non-linear model (R<sup>2</sup>: 0.96, AIC:-70.11). Subsequently, the disposition model (of CX in GastroPlus™) was constructed by using parameters from the fitted 3 compartment non-linear model. Meanwhile, other IV pharmacokinetic parameters from the literature also were applied in the model (Table 27).

Table 27. Reported IV pharmacokinetic parameters of CX applied in CX model

Parameter	Value	Reference
$f_{up}$ (%)	0.2 ( <i>in vivo</i> humans study)	(233)
Simulation time (h)	24	<i>In vivo</i> (dog) study (252)
Body weight (kg)	9.85±0.65	<i>In vivo</i> (dog) study (n=4, (252))
Blood to plasma concentration ratio	0.58 ( <i>in vivo</i> humans study)	(233)

## 2.6.5 Enzyme and transporter metabolism

The sophisticated mathematical model that has been developed for the Metabolism and Transporter Module in GastroPlus™ accounts for the important interactions among transit, release, dissolution, absorption/ exsorption, metabolism, transport, plasma protein binding and pharmacokinetic parameters in the humans or animals. The model had been tested extensively with a variety of drugs that had undergone various combinations of saturable metabolism and transport that had been found to be in excellent agreement with published observations in humans for the compounds tested (136, 278, 300). The contribution of efflux transport by P-gp (P-glycoprotein) on the absorption rate was also accounted for in building the GI absorption model, where the *in vitro* values of  $K_m$  and  $V_{max}$  for P-gp (various model compounds) were obtained from literature to simulate the *in vivo* nonlinear dose dependence gut efflux rate (147, 301).

### 2.6.5.1 Saturable gut and liver metabolism

The ACAT model in GastroPlus™ accounts for the relative distribution of P-gp based on studies describing experimental distribution in human tissues (as shown in Table 21-23). The contribution of passive diffusion and efflux transport were integrated

together to account for the total rate of absorption from the lumen to enterocytes. The contribution of the intestinal metabolism was also considered in the simulation by GastroPlus™ to calculate the gut metabolism rate by using the *in vitro*  $K_m$  and  $V_{max}$  values for CYPs. The distribution of P-gp in the GIT was not uniform, as it was shown by many studies in both animals and humans that the relative distribution of P-gp increases when approaching closer to the colon (302, 303). In contrast to P-gp, the distribution of CYP450 decreases when approaching closer to the colon. The relative distribution of CYP450 was also included in the calculation of the gut metabolism rate in each compartment (as shown in Tables 28-30). It is important to note that gut metabolism and apical membrane efflux will affect free drug concentration in the enterocyte, and the dynamic changes in concentration gradient will affect the rate of drug transport both into and out of the enterocytes to the intestinal lumen and portal vein.

Meanwhile in GastroPlus™ gut metabolism was assumed to follow Michaelis-Menten kinetics. The enzyme kinetic constants for each gut metabolising enzyme were entered into the “Enzyme Table” with the location “Gut”. Since the GIT was split into distinct compartments and each of these compartments could contain different amounts of enzyme, the regional distribution of the enzymes was required to calculate the rate of metabolic process in each compartment. When the enzyme already existed in the selected physiology, the column would hold the stored scale factor profile (as shown in Table 30-32).

#### **2.6.5.2 Enzyme metabolism**

Values for the maximum metabolic velocity,  $V_{max}$ , and the Michaelis-Menten constant,  $K_m$ ) were inserted into the “Metabolism and Transporter Module” to calculate saturable metabolism. The Enzymes table shows the database table that stores the values of  $V_{max}$  and  $K_m$  for each drug record (163). Different distribution profiles of enzymes had been built into the GastroPlus™ programme (301) as shown in Table 28-30. As with gut enzymes, GastroPlus™ will load the corresponding distribution factors for each compartment from the selected physiology into the “Physiology tab” for any transporter with Gut Location (Gut-Apical or Gut-Basolateral).

It must be stressed that the default enzyme distribution factors represent the relative amount of the enzyme in each intestinal compartment to the amount of that enzyme in the liver; the default transporter distribution factors represent only relative expression levels of that transporter across different intestinal compartments. These values are not related to the liver or any other tissue (163).



In fact, GastroPlus™ is the first commercial compartmental absorption and transit model to incorporate saturable gut and liver metabolism. In the “Physiology tab”, separate entries were used to clarify expression levels of influx and efflux transporters (Table 28-30).

## CA

Enzyme and transporter effects were not applied in the CA models because linear relationships between the dose of CA and both  $C_{max}$  and AUC were demonstrated in the bioavailability study designed to evaluate the dose proportionality of four oral doses of CA (125, 250, 500, and 1,000 mg) (209).

## ITR

Studies have reported that oral absorption and bioavailability of ITR are a function of dose (304-307). For example, after oral doses of 50, 100 and 200 mg, increases in the AUC and  $C_{max}$  follow nonlinear kinetics, suggesting a saturation of the first-pass metabolism process in the liver and the intestine. Furthermore, consistent with concentration, dose and time nonlinearity, the elimination of ITR was found to follow Michaelis–Menten kinetics and it was suggested that ITR and/or its metabolites saturate intestinal and hepatic CYP3A4 and thus their own CYP3A4-mediated elimination (224, 226). Based on all the clinical evidences, the nonlinear metabolism in the liver and the gut was included in the PBPK model.

The *in vitro*  $V_{max}$  and  $K_m$  of ITR were obtained from literature where the cDNA-expressed CYP3A4 (supersomes)-mediated metabolism of ITR was used (226). From this study, the reported *in vitro* value of  $V_{max}$  was 270 pmol/min/nmol CYP3A4 protein (226). However, this reported *in vitro*  $V_{max}$  value was unrealistically large because its corresponding intrinsic unbound clearance value ( $CL_{int(u)}$ ) is 69.3 mL/min/nmol CYP3A4 protein which was equal to an unreasonable total drug clearance of 33858 L/h (calculated using built-in “Enzyme and transporter convertor”). Thus it was necessary to scale the *in vitro*  $V_{max}$  value to a corresponding *in vivo* ITR clearance value of 20.95 L/h (determined using compartmental analysis with ITR IV profile) (291). Thus, a linear regression of *in vitro*  $V_{max}$  vs *in vivo* intrinsic clearance of ITR was established by generating ten *in vitro*  $V_{max}$  data using the metabolism and transporter units convertor (built-in GastroPlus™ software) with values of intrinsic clearance that were close to the real *in vivo* ITR clearance value (20.95 L/h). Using linear regression ( $y=0.095x+0.0001$ ,

$R^2=1$ ), the scaling of the *in vitro*  $V_{max}$  value was performed and the scaled *in vitro*  $V_{max}$  value of  $2.095 \times 10^{-2}$  pmol/min/mg protein was found (Figure 15).

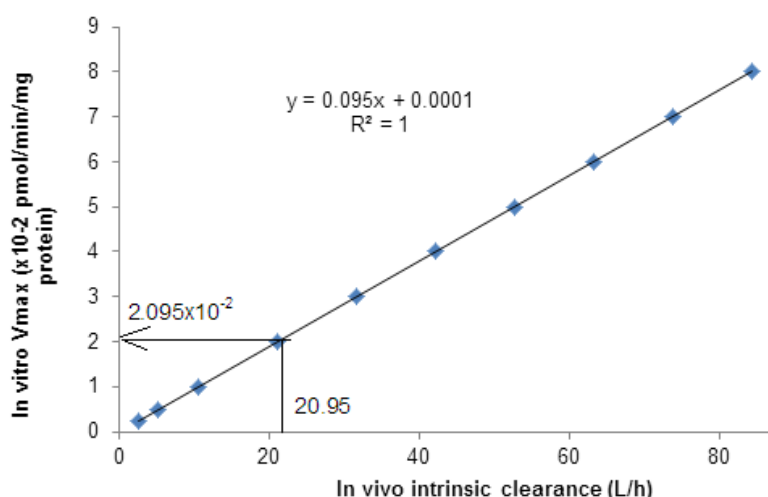


Figure 15. *In vitro*  $V_{max}$  ( $\times 10^{-2}$  pmol/min/mg protein) as a function of *in vivo* intrinsic clearance (L/h).

The scaled *in vitro*  $V_{max}$  value was converted to the equivalent *in vivo* values using the built-in “Enzyme and transporter convertor”. After conversion, an *in vivo*  $V_{max}$  value of  $1.685 \times 10^{-5}$  mg/s was obtained and applied in the hepatic metabolism of ITR models. Meanwhile, the  $K_m$  value for the hepatic metabolism of ITR by CYP3A4 is  $0.00275 \mu\text{g/mL}$  (226). This  $K_m$  value was taken from the same study as above by Isoherranen *et al.* where cDNA-expressed CYP3A4 (supersomes)-mediated metabolism of ITR was tested.

Likewise the  $V_{max}$  and  $K_m$  parameters of ITR due to gut metabolism of ITR by CYP3A4 also were taken from the same study by Isoherranen *et al.* (226). As recommended by literature (278), the same  $K_m$  value for the hepatic metabolism ( $0.00275 \mu\text{g/mL}$ ) could be used for gut metabolism but the *in vivo*  $V_{max}$  value for hepatic metabolism should be scaled with a scaling factor of two, giving an *in vivo*  $V_{max}$  gut metabolism value as  $8.425 \times 10^{-7}$  mg/s [ $1.685 \times 10^{-5}$  (the *in vivo*  $V_{max}$  value for hepatic metabolism) divided by 2].

## CX

It has been known that the major intestinal CYP3A isozyme is CYP3A4 for humans and CYP3A12 for dogs (308) and preliminary studies have indicated that the CYP3A12 is the major isozyme responsible for the metabolism of CX in dogs (233). Study also had shown that saturation of the first-pass metabolism process of CX occurred in the liver

and the intestine of the beagle dog (139). Based on these information, nonlinear metabolism of CX in the liver and the gut are included in the PBPK model (beagle dog).  $V_{max}$  and  $K_m$  of both liver and gut metabolism were determined from nonlinear kinetics compartmental analysis of *in vivo* (beagle dog) IV studies (252).  $V_{max}$  and  $K_m$  values obtained from the fitting were 0.00069 mg/s and 0.894 mg/L respectively.

### 2.6.5.3 P-glycoprotein transporter metabolism

#### ITR

The *in vitro*  $V_{max}$  and  $K_m$  values for P-gp were obtained from literature (137). P-gp transporter could be located in the “gut-apical” (at the apical enterocyte membrane) and “gut-basolateral” (at the basolateral enterocyte membrane) and an *in vitro* study using ITR determined that only efflux P-gp at the apical enterocyte membrane was responsive to ITR metabolism (137) thus the “efflux and gut-apical option” was selected in the GastroPlus™ model of ITR. The reported ATP hydrolysis (a parameter to determine the activity of P-gp) in the presence of ITR showed a  $V_{max}$  of  $69.1 \pm 1.5$  nmol/min/mg (137). As recommended by literature (278), scaling of *in vitro*  $V_{max}$  for P-gp metabolism is necessary before it can be used in PBPK modeling. It is because the ACAT model in GastroPlus™ uses the simulated concentration in the cytoplasm of the enterocyte for interaction with the binding site of P-gp (163). If the *in vitro*  $V_{max}$  value was not scaled then the ACAT model predicted a very low drug concentration because of the rapid efflux of the substrates in the enterocyte (278).

In order to perform the scaling, a correlation between *in vivo* intrinsic clearance and *in vivo*  $V_{max}$  was established. Firstly, *in vitro*  $V_{max}$  of the four model compounds reported in the study by Adachi *et al.* (309) was converted to its equivalent *in vivo*  $V_{max}$  using built-in GastroPlus™ metabolism and transporter unit convertor. Basically, the convertor converted the value from *in vitro* unit of (nmol /min/mg protein) to *in vivo* unit of mg/s. Then, the *in vivo* intrinsic clearance for the four model compounds was calculated using  $V_{max}$  and  $K_m$  of P-gp kinetics as reported in a study by Adachi *et al.* (309) (Note:  $V_{max}$  divided by  $K_m$  is equal to intrinsic clearance). Using the same equation, the *in vivo* intrinsic ITR clearance by P-gp was calculated using  $V_{max}$  and  $K_m$  value obtained from literature (137). Figure 16 shows that there is a good correlation between *in vivo*  $V_{max}$  (log scale) and *in vivo* clearance [ $\log Y = -2.22 \times 10^{-2} X + 1.57$ ,  $R^2 = 0.97$ ]. Using this linear regression function and the *in vivo* intrinsic ITR clearance by P-gp, the *in vivo* ITR  $V_{max}$  (P-gp) of  $2.2658 \times 10^{-5}$  mg/s was determined.

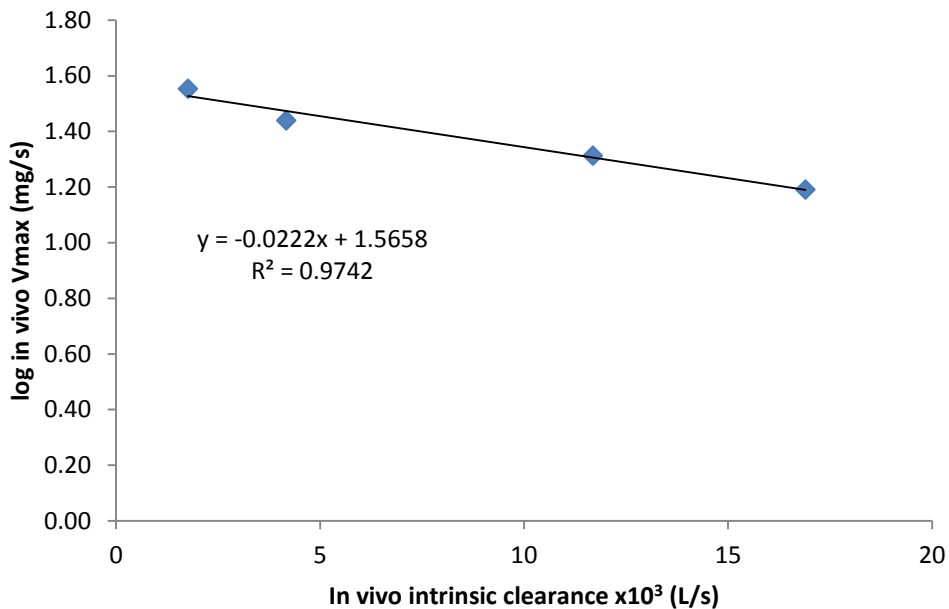


Figure 16. *In vivo*  $V_{\max}$  (mg/s) as a function of *in vivo* intrinsic clearance ( $\times 10^3$  L/h). The correlation line and correlation function between both parameters are indicated.

Meanwhile, the reported ATP hydrolysis in the presence of ITR showed an apparent  $K_m$  of  $0.8 \pm 0.2 \mu\text{M}$  (137). Considering the fraction unbound of ITR is 0.002, these values were inserted into the built-in GastroPlus™ metabolism and transporter unit convertor: the calculated *in vivo* unbound  $K_m$  was  $0.5642 \pm 0.1411$  mg/L.

It must be noted that the expression of P-gp in enterocytes exhibits similar intra and interpatient variability as seen with CYP3A4 and is not under synchronised regulation of CYP3A4 expression in the liver (310). Therefore, the  $K_m$  of the P-gp and CYP3A4 of ITR in humans might differ. Subsequently, these kinetic parameters for CYP3A4 and P-gp were then integrated into the ACAT model. The ACAT model assumed that P-gp and CYP3A4 were present in the same forms with similar intrinsic activity in all parts of the GIT; therefore any change in the rate of flux by P-gp or metabolism by CYP3A4 would be simulated.

## CX

*In vitro* studies conducted in transfected Madin-Darby canine kidney II (MDCK II) cells showed that the intracellular accumulation of CX was significantly restricted because of active efflux by P-gp (ABCB1/MDR1). Bidirectional flux studies indicated greater transport in the basolateral-to-apical direction than the apical-to-basolateral direction because of active efflux by P-gp. The P-gp inhibitor decreased the flux ratio by more than 50% thus the result strongly suggested that CX is a P-gp substrate (139). Similar

to CYP3A12,  $V_{\max}$  and  $K_m$  of gut efflux transportation by MDR-1 was determined using nonlinear kinetics compartmental analysis of *in vivo* (dog) IV studies (252), thus the same values of  $V$  (0.00069 mg/s) and  $K_m$  (0.894 mg/L) were applied in the CX models. The kinetic parameters for CYP3A4 and P-gp were then integrated into the “Physiology tab” of the ACAT model.

### **2.6.6 Physiology tab**

The GastroPlus™ contains built-in physiology models that can be selected. Each physiology model contains pH values, transit times, and geometric parameters (lengths, radii, volumes) that are appropriate to the selected physiology. For the fed-state models, the physiology input parameters for food-induced changes to GI physiology such as increased gastric residence, increased splanchnic blood flow, lower GI motility, bile salt/lecithin micellar solubilisation are considered and incorporated into the built-in database of the GastroPlus™ programme.

In this project, the default physiology models for the fasted (“Humans Physiological Fasted”) and fed state (“Humans Physiological Fed”) in humans were used for CA and ITR (humans *in vivo* data available). The default physiology models for the fasted (“Beagle Physiological Fast”) and fed state (“Beagle Physiological Fed”) in beagle dogs were used for CX (*in vivo* data available in beagle dogs).

#### **CA and ITR (Human physiology model)**

The default value of the parameter set in “Human physiological fast” and “Human physiological fed” is used for all CA and ITR models (fasted and fed states accordingly) (Tables 28 and 29).

Table 28. ACAT physiological model parameters for simulation of CA and ITR (fasted state humans)

Compartment data (CA and ITR)							Enzyme and transporter regional distributions (ITR)	
Compartment	ASF	pH	Transit time (h)	Volume (mL)	Length (cm)	Radius (cm)	P-gp (Apical) relative expression (301)	CYP3A4 relative expression (140)
Stomach	0.0	1.30	0.25	49.32	29.37	9.91	0.0	0.0
Duodenum	2.730	6.00	0.26	45.21	14.67	1.57	0.538	1.96x10 <sup>-3</sup>
Jejunum 1	2.675	6.20	0.94	169.3	60.63	1.49	0.645	3.10x10 <sup>-3</sup>
Jejunum 2	2.669	6.40	0.74	132.8	60.63	1.32	0.723	3.08x10 <sup>-3</sup>
Ileum 1	2.623	6.60	0.58	103.6	60.63	1.17	0.77	9.75x10 <sup>-4</sup>
Ileum 2	2.591	6.90	0.42	76.36	60.63	1.00	0.838	9.78x10 <sup>-4</sup>
Ileum 3	2.521	7.40	0.29	54.37	60.63	0.84	0.908	9.8x10 <sup>-4</sup>
Caecum	54.67	6.40	4.39	51.10	13.56	3.46	1.000	2.96x10 <sup>-4</sup>
Asc Colon	106.7	6.80	13.17	54.21	28.48	2.46	1.000	2.93x10 <sup>-4</sup>

Table 29. ACAT physiological model parameters for simulation of CA and ITR (fed state humans)

Compartment data (CA and ITR)							Enzyme and transporter regional distributions (ITR)	
Compartment	ASF	pH	Transit time (h)	Volume (mL)	Length (cm)	Radius (cm)	P-gp (apical) relative expression (301)	CYP3A4 relative expression (140)
Stomach	0.0	4.90	1.00	986.4	29.37	9.91	0.0	0.0
Duodenum	2.730	5.40	0.26	45.21	14.67	1.57	0.538	1.96x10 <sup>-3</sup>
Jejunum 1	2.675	5.40	0.94	169.3	60.63	1.49	0.645	3.10x10 <sup>-3</sup>
Jejunum 2	2.669	6.00	0.74	132.8	60.63	1.32	0.723	3.08x10 <sup>-3</sup>
Ileum 1	2.623	6.60	0.58	103.6	60.63	1.17	0.77	9.75x10 <sup>-4</sup>
Ileum 2	2.591	6.90	0.42	76.36	60.63	1.00	0.838	9.78x10 <sup>-4</sup>
Ileum 3	2.521	7.40	0.29	54.37	60.63	0.84	0.908	9.8x10 <sup>-4</sup>
Caecum	54.67	6.40	4.39	51.10	13.56	3.46	1.000	2.96x10 <sup>-4</sup>
Asc Colon	106.7	6.80	13.17	54.21	28.48	2.46	1.000	2.93x10 <sup>-4</sup>

## CX (Dog physiology model)

In the physiology tab, the default values (Beagle - Physiological – Fed) were used and the enzyme and transporter regional distribution were taken from literature (311) (Table 30).

Table 30. Physiological parameters for CX model (fed state)

Compartment data							Enzyme and transporter regional distributions	
Compartment	ASF	pH	Transit time (h)	Volume (mL)	Length (cm)	Radius (cm)	CYP3A12 expression (311)	MDR-1 apical expression (311)
Stomach	0.0	5.00	1.50	1000.0	15.00	1.00	0.0	0.0
Duodenum	11.23	6.20	0.28	6.083	12.43	0.62	$3.0 \times 10^{-4}$	0.410
Jejunum 1	12.66	6.20	0.85	18.58	66.64	0.47	$3.0 \times 10^{-4}$	0.530
Jejunum 2	10.38	6.20	0.63	13.74	66.64	0.41	$2.0 \times 10^{-4}$	0.660
Ileum 1	7.103	6.40	0.02	0.389	1.43	0.47	$2.0 \times 10^{-4}$	0.880
Ileum 2	6.960	6.60	0.02	0.396	1.43	0.47	$3.0 \times 10^{-4}$	0.990
Ileum 3	6.815	7.05	0.02	0.403	1.43	0.47	$4.0 \times 10^{-4}$	1.030
Caecum	9.147	7.50	3.81	0.538	1.99	0.93	$4.0 \times 10^{-4}$	0.530
Asc Colon	7.171	6.45	8.19	2.700	4.26	1.42	$5.0 \times 10^{-4}$	0.610

## 2.6.7 Intestinal first-pass effect and chemical degradation (CA)

Following oral administration, CA was absorbed from the GIT and was rapidly hydrolysed by non-specific esterases in the intestinal mucosa and blood, to cefuroxime (312). The loss in extent of the unabsorbed parent drug (CA) is the main reason for its moderate bioavailability (199, 313). Numerous investigations have focused on the effect of intestinal esterases in the hydrolysis of CA to the poorly absorbed cefuroxime in the GIT before CA is absorbed (212, 213, 313-315). For example, an *in vitro* study performed on the intestine of rats showed 21.44% CA hydrolysis (212).

### 2.6.7.1 Luminal degradation (CA)

The hydrolysis rate changes according to the pH environment of the GI lumen and was incorporated into the model as chemical degradation rate vs pH data. The chemical degradation data is presented in Table 31.

Table 31. Chemical degradation rate vs pH data: Hydrolysis rate of CA in physiological pH environment measured with USP apparatus 2 (50rpm, 500mL, 37°C, n=3)

Dissolution medium	pH	Half-life (mean± SD, min), n=3
SGF, pH1.2	1.20	1038.98±80.56
FaSSGF, pH 1.6	1.60	3960.00±1005.42
FaSSIF-V2, pH 6.5	6.50	1823.68±104.40
SIF, pH 6.8	6.80	376.02±53.74

Luminal degradation (chemical or metabolic) was modelled by interpolating from an input table of degradation rate as half-life (h) vs pH. At any time point in any compartment, the degradation rate constant was determined for the local pH while the loss of drug concentration through chemical degradation was calculated in GastroPlus™ using the degradation rate constant multiplied by the amount of dissolved material in the compartment.

In this study intestinal extraction of 46.8% was obtained using data from a degradation study performed on fasted state human intestinal fluid (264). Meanwhile, a CA food effect study found that 64% and 48% of CA was not absorbed in fasted state and fed state, respectively (209). The degradation of CA followed first order kinetics (264) thus the intestinal extraction in fed state could be postulated using the ratio of intestinal extraction and the % of CA not absorbed in fasted and fed states (Equation 19)

**Intestinal extraction (fed state) =**

$$\frac{\% \text{ of CA not absorbed (fasted state)} \times \text{Intestinal extraction (fasted state)}}{\% \text{ of CA not absorbed (fed state)}} \quad \text{Equation 19}$$

From the calculation using Equation 19, the intestinal extraction of CA in fed state was 35.1%. The fixed intestinal extraction input in GastroPlus™ gave a fixed percentage of the absorbed drug to be extracted before it reached the portal vein. This intestinal extraction % was constant at all times and all concentrations during a simulation.

### 2.6.8 Approach and design of simulation

In this project, prediction of *in vivo* performance based on PBPK models for Zinnat® (CA), Sporanox® (ITR) and CX formulation were performed using (i) solubility-based model and (ii) solubility combined with dissolution based model.



### 2.6.8.1 Solubility-based model

In the solubility-based model (Table 32), the solubility of the drug within the luminal contents was taken into account for absorption simulation. The absorption rate was restricted to the maximum possible luminal drug concentration based on the local (pH-dependent) solubility of the simulated compound calculated according to the Henderson–Hasselbalch equation (163). For the solubility based model, the IR tablet (CA, CX) and IR capsule (ITR) dosage forms in GastroPlus™ were selected for simulations. IR formulations begin dissolving in the stomach as soon as the dose is administered.

Table 32. Simulations using solubility-based model

Studies	Media used
Input as an individual solubility and pH (reference solubility)	<p style="text-align: center;">CA:</p> <p>Experimental solubility data in simulated fasted state media :SGF, SIF, FaSSGF, FaSSIF-V2 and in simulated fed state media : FeSSGF and FeSSIF-V2</p>
	<p style="text-align: center;">ITR:</p> <p>Solubility data using SGF, SIF, FaSSGF, FaSSIF-V1 and human gastric fluid, human intestinal fluid reported in literature (30) and scaled FaSSIF-V1 and FeSSIF-V1 values (Details in Section 2.6.2.3) were used.</p>
	<p style="text-align: center;">CX:</p> <p>Solubility data using FaSSIF-V1 and FeSSIF-V1 (252) and scaled FaSSIF-V1 and scaled FeSSIF-V1 values (Details in Section 2.6.2.3) were used.</p>
Input as a solubility over a pH range	<p style="text-align: center;">CA:</p> <p>Experimental solubility-pH data in simulated fasted state media :SGF and SIF; FaSSGF and FaSSIF-V2 and in simulated fed state media : FeSSGF and FeSSIF-V2</p>
	<p style="text-align: center;">ITR:</p> <p>Solubility-pH data using SGF and SIF; FaSSGF and FaSSIF-V1 (30) were used.</p>
	<p style="text-align: center;">CX:</p> <p>Solubility data using aqueous buffer (pH3) and FeSSIF-V1 (252) and aqueous buffers (233) were used.</p>

### 2.6.8.2 Solubility combined with dissolution based model

The dissolution profile determined using an *in vitro* dissolution method was inserted into the GastroPlus™ as a table of time and % dissolved. Simulations were performed using the Controlled Release (CR): Dispersed option (Table 33). In this CR: Dispersed option, unreleased material disperses by way of transit at the same rates as solid particles or drug in solution (used for other dosage forms such as oral suspension). This is especially applicable for Sporanox which consists of a capsule that releases coated pellets which then disperse throughout the GIT compartments (163).

Table 33. Simulation design using solubility combined with dissolution-based models

Study	Solubility used	Dissolution profile from	Media used
CA	FaSSIF-V2 (fasted state); FeSSIF-V2 (fed state)	a. USP apparatus 2 b. USP apparatus 4	Compendial and biorelevant media
ITR	Scaled FaSSIF-V1 (fasted state); Scaled FeSSIF-V1 (fed state)	a. USP apparatus 1 b. USP apparatus 4	Compendial and biorelevant media
CX	FeSSIF-V1 (fed state)	a. USP apparatus 2 b. USP apparatus 4	Biorelevant and modified media

There is no recommended dissolution medium simulating gastric and intestinal fluids of beagle dogs up to the time the dissolution experiment was conducted. Thus the modified media and biorelevant media (fasted and fed state) simulating human GI conditions were used for the study of CX (*in vivo* study performed on beagle dog) since literature had suggested that beagle dog GI conditions are close to humans (316). Thus dissolution profiles in simulated biorelevant media in fed state as well as fasted state were also inserted into the GastroPlus™ CX fed state model to test if these profiles could produce a predictive absorption model.

With GastroPlus™, a four-parameter single Weibull function (Equation 20) or an eight-parameter double Weibull function (Equation 21) (163) could be used for fitting the dissolution profiles.

$$\% \text{ dissolved} = \text{Max}\left(1 - \exp\left(\frac{-(t-T_{\text{lag}})^b}{a}\right)\right) \quad \text{Equation 20}$$

$$\% \text{ dissolved} = \text{Max}\left(1 - f_1 \exp\left(\frac{-(t-T_{\text{lag1}})^{b_1}}{a_1}\right) - f_2 \exp\left(\frac{-(t-T_{\text{lag2}})^{b_2}}{a_2}\right)\right) \quad \text{Equation 21}$$

Where Max is the % of maximum release,  $T_{lag}$  is the lag time, a is the scale factor, and b is the shape factor.

Due to the parabolic curve shape of the dissolution profiles in 2 stage dissolution experiments, instead of fitting with a Weibull function the dissolution profiles were inserted as raw dissolution data (CX). The single Weibull function was used for CA and CX but the double Weibull function was used for ITR due to the more complex nature of its dissolution curve shape. It is noteworthy that the use of Weibull distribution which does not have a physiological meaning was mainly due to its versatility to fit most curve shapes (sigmoidal or parabolic).

### 2.6.9 Prediction of *in vivo* performance based on PBPK models

In order to verify the capability of each PBPK model to predict accurately the *in vivo* profiles, the simulated profiles were compared with the observed *in vivo* profiles reported in literature.

#### CA

The observed *in vivo* plasma concentration–time data of CA in fasted and fed states were reported by Rojanasthien *et al.*(287) and Donn *et al.* (288) respectively. The *in vivo* plasma concentration–time profiles were obtained from the published graphs by digitalisation with a software tool (GetData<sup>®</sup> Graph Digitizer version 2.24).

In the fasted state study, a single immediate release (IR) Zinnat<sup>®</sup> 250mg/tablet (GlaxoSmithKline, Durham, UK) was given to 12 healthy volunteers together with 200mL of water. In the fed state study, a single immediate release (IR) Zinnat<sup>®</sup> 250mg/tablet was given to 24 healthy male volunteers together with 100mL of water after a standard breakfast.

#### ITR

*In vivo* plasma concentration–time profiles of Sporanox<sup>®</sup> (Janssen-Cilag, High Wycombe, UK) tablets were taken from the study of Yun *et al.* (228) (fed state). In the fasted state study, 12 healthy volunteers were given a single dose of Sporanox<sup>®</sup> containing 100mg of ITR/capsule. The dose was administered with 100 mL of water. In the fed state study, 80 healthy male volunteers were administered a single dose of

Sporanox<sup>®</sup> containing 100mg of ITR/capsule. The dose was administered 5 min after a standard bread meal (150g) recommended by FDA plus 150mL of low fat milk.

## CX

The observed *in vivo* plasma concentration–time data of CX were obtained from an interim company report (252) in which 7 formulations (F1, F2, F3, F4, F5, F6 and F7) of CX formulation 240mg/tablet was given separately to 4 healthy beagle dogs 1 h post meal (fed state) with 15mL of water (as a slurry mixture). The plasma concentration–time profiles are presented in Figure 17.

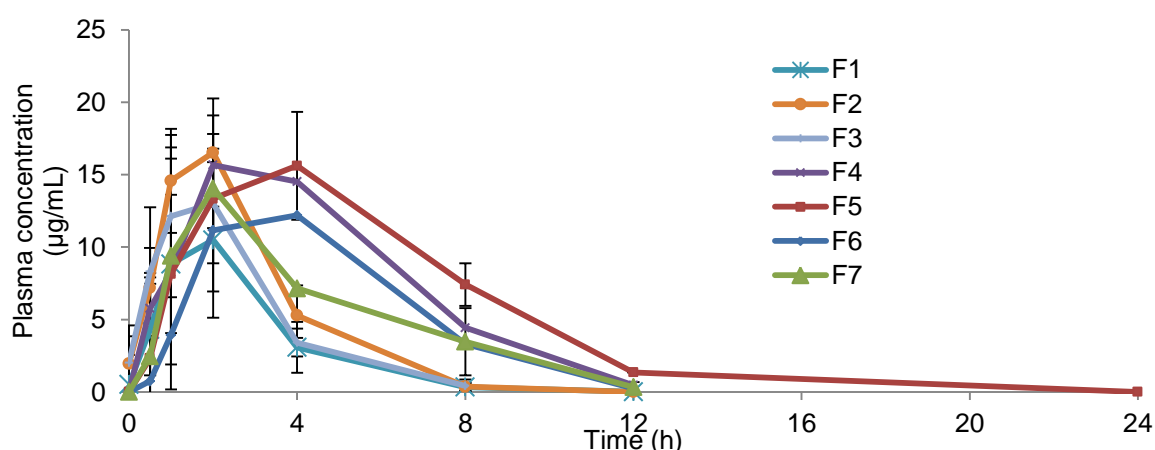


Figure 17. Mean ( $\pm$ SD) plasma concentration vs time profiles of CX in beagle dogs (n=4) after a single administration of F1, F2, F3, F4, F5, F6 and F7 of CX (252).

As only F4, F5, F6 and F7 were available for *in vitro* dissolution testing, the average plasma concentrations of these four formulations (n=16) were used as reference profiles in the model validation study.

### 2.6.10 Parameter sensitivity analysis

Parameter sensitivity analysis (PSA) was performed to analyse the effect of selected parameters on the predicted amount absorbed,  $C_{max}$  and AUC of simulated profiles. Three types of parameters were tested for sensitivity analysis. The first group was related to the absorption process and included parameters such as  $P_{eff}$  and dose of the drug given. The second group consisted of parameters that describe the physicochemical properties of the drug such as solubility, particle size distribution (PSD) and precipitation (prec) time. The third group related to physiological parameters, such as gastric emptying time, percentage of drug having undergone first pass extraction in the gut (% gut first pass extraction), stomach and duodenum pH.

During this analysis, one parameter was changed gradually within a realistic range. The parameter ranges used for the PSA are presented in Tables 34-36.

Table 34. The range of parameters used for the PSA of CA: simulating fasted state (A) and fed state (B) conditions.

A	% Gut first pass extraction	Ref solubility (mg/mL)	Prec time (s)
Baseline	46.8	0.443	900
Lower limit	23.4	0.044	90
Upper limit	93.6	4.429	9000

B	Ref solubility (mg/mL)	Prec time (s)	GI transit time	P <sub>eff</sub> (cm/s)	Gut 1st pass extraction %
Baseline	0.372	900	0	1.247	35.1
Lower limit	0.037	90	0	0.624	17.55
Upper limit	3.719	9000	10	2.494	70.2

Table 35. The range of parameters used for the PSA of ITR; simulating fasted state (A) and fed state (B) conditions.

A	Prec time (s)	Ref solubility (mg/mL)	P <sub>eff</sub> (cm/s)	PSD (µm)	Dose (mg)	Duodenum pH	Stomach pH
Baseline	900	0.00481	3.46	1	100	6	1.3
Lower limit	90	0.000481	1.73	0.1	10	0.5	0.5
Upper limit	9000	0.048	6.92	10	1000	8	8

B	Ref solubility (mg/mL)	Prec time (s)	P <sub>eff</sub> (cm/s)	PSD (µm)	Dose (mg)	Stomach pH	Duodenum pH
Baseline	0.023	900	3.46	0	100	4.9	5.4
Lower limit	0.00225	90	1.73	0	10	0.5	0.5
Upper limit	0.225	9000	6.92	10	1000	8	8

Table 36. The range of parameters used for the PSA of CX; simulating fed state condition.

	Ref solubility (mg/mL)	Dose (mg)	PSD (µm)	Prec time (s)	P <sub>eff</sub> (cm/s)
Baseline	0.37	240	1.5	9000	0.641
Lower Limit	0.037	24	0.15	900	1.282
Upper Limit	3.7	2400	15	90000	2.564

PSA was performed using the “solubility combined with dissolution based model” that showed the closest simulated profiles with the *in vivo* profiles (based on the simulated results performed in this study, Table 37).

Table 37. The solubility value and dissolution profiles used for PSA

	Simulating state	Solubility value	Dissolution profile
CA	Fasted	FaSSIF-V2	FaSSGF/FaSSIF-V2
	Fed	FeSSIF-V2	FeSSGF/FeSSIF-V2
ITR	Fasted	Scaled FaSSIF-V1	FaSSGF/FaSSIF-V1
	Fed	Scaled FeSSIF-V1	FeSSGF/FeSSIF-V2
CX*	Fed	FeSSIF-V1	FeSSGF/FeSSIF-V2

\*For CX, only PSA for fed state was performed because only *in vivo* data in fed state is available.

### 2.6.11 Analysis and comparison of plasma concentration vs time data

Differences in the simulated vs the observed profiles were assessed using the model-independent approach based on the similarity factor ( $f_1$ ) as follows (Equation 22) (43)

$$f_1 = \frac{\sum_{j=1}^n |R_j - T_j|}{\sum_{j=1}^n R_j} \times 100 \quad \text{Equation 22}$$

where  $n$  is the sample number, and  $R_j$  and  $T_j$  are the drug plasma concentration of the reference and test profiles, respectively, at different time intervals  $j$ .  $f_1$  value increases proportionally due to the dissimilarity between the two dissolution profiles.

The observed plasma concentration time data were used as a reference data set. Predicted profiles were compared in this manner so the equivalent time points to reference profiles could be selected for comparison. Entire profiles were taken into account. 20% average difference of a test from a reference data set was set as the limit for identifying differences between the profiles. The 20% is in agreement with the FDA guidance for industries where the difference in predicted means of  $C_{max}$  and AUC should be no more than 20% from that of the reference product (170).

## 2.7 Methods of Part 4: Deconvolution and development of *In vitro-in vivo* correlation

### 2.7.1 Deconvolution analysis

Essentially in numerical deconvolution, drug plasma data from oral formulations are used as a response and IV profile as a weighting function to estimate the *in vivo* drug absorption profiles.

In the current study, numerical deconvolution was performed using the PCDCON software (188). PCDCON enables the provision of absorption rate plots vs time and the cumulative amount absorbed over time as part of the output. An interpolating cubic spline was used to fit the serum concentration data for the intravenous formulation (as weighting function). Input rate function was the plasma concentration vs time profile following oral administration of CA, ITR and CX formulations (Refer to Section 2.3.3: CX formulations). The deconvolution result is expressed in terms of the cumulative percentage absorbed (%) and absorption rate (mg/h). Meanwhile, the input response was from the plasma concentration vs time profile following oral administration of the tested marketed amorphous formulations (Table 38).

Table 38. Input response used in the deconvolution

Drug	Formulation	Sample/Subject
CA	Zinnat <sup>®</sup> (Glaxo Wellcome) 250 mg/ tablet, fasted state (287) and fed state (288)	Humans (mean data, fasted state and fed state n=10)
ITR	Sporanox <sup>®</sup> (Jassen) 100mg/ capsule, fasted state (299) and fed state (228)	Humans (mean data, fasted state n=12, fed state n=80)
CX	240mg/tablet, fed state (252)	Dog (mean data, n=4)

For CA the plasma concentration profile of IV injection data (dose=500mg, mean data of n=12 healthy male volunteers, age 21-27 years, mean weight 80 kg) reported by Finn *et al.* was used as a weighting function for deconvolution (209).

For ITR, due to the unavailability of IV bolus profiles in the literature, an IV infusion (over 1 h, dose=100mg, mean data of n=6 health male volunteers) profile reported by Heykants *et al.* was used (291). PK parameters derived from compartmental analysis of this profile were used to construct a biexponential function (317). The concentration

time course for ITR administered as 1 h IV infusion (100mg) was fitted with the following bi-exponential equation (Equation 23):

$$\text{Plasma concentration (ng/ml)} = 838.2282e^{-0.4071t} + 78.9071e^{-0.0269t} \text{ Equation 23}$$

The parameters of biexponential Equation 23 were then used as the weighting function.

For CX the data after an IV injection (1mg/kg) were obtained from a crossover study in 4 healthy beagle dogs (252). The mentioned individual plasma concentration profiles post IV doses (weighting function) were entered as raw data and an interpolating cubic spline was used as a weighting function for deconvolution. The IV profile corresponding to each dog was used and then the mean deconvoluted profile was calculated. The calculated cumulative amount then was used to compare the critical manufacturing variables (CMV) of CX formulation such as the particle size of API and tableting strength.

## 2.7.2 Development of IVIVC

The percentage of *in vivo* absorption obtained with deconvolution (Section 2.7.1) was compared directly with the percentage of *in vitro* dissolution determined from *in vitro* dissolution experiments.

The Level A IVIVC (Point-to-point IVIVC) model was developed using a direct comparison method: % *in vivo* absorption (from deconvolution) vs % *in vitro* dissolved at time. Linear interpolation was used in cases where % *in vitro* dissolved was at different time points with % *in vivo* absorption. Linear regressions were used to develop a single time IVIVC model using data in each experimental *in vitro* dissolution profile. A linear mathematical equation (Equation 24) with intercept (a) and gradient (b) was applied to define the IVIVC model (192).

$$\% \text{absorption } in \text{ vivo} = b \cdot \% \text{dissolution } in \text{ vitro} + a \quad \text{Equation 24}$$

where % absorption *in vivo* and % dissolution *in vitro* are the mean percentage *in vivo* absorption and *in vitro* dissolution respectively; a is a constant additive term that accounts for a percentage delay *in vivo* as compared with *in vitro* and the gradient b is a transformation factor for the mean percentages. This gradient, b, compares the rate of the *in vivo* absorption and *in vitro* dissolution.



### 3. Results and discussion

#### 3.1 Results and discussion of Part 1: *In vitro* solubility and dissolution testing

##### 3.1.1 Validation of chromatographic methods

###### 3.1.1.1 Calibration curve linear range

Linear calibration curves for the three drugs were obtained throughout the concentration range studied. Regression analysis was performed for the area of the peak vs drug concentration and the results are presented in Table 39 and Table 40.

Table 39. Analytical parameters of calibration curve in aqueous media.

Drug	Concentration range ( $\mu\text{g/mL}$ )	$R^2$
CA	10-200	0.999
ITR	0.1-5	0.999
CX	0.1-4	0.999

Table 40. Analytical parameters of calibration curve in milk-based media.

Drug	Concentration range ( $\mu\text{g/mL}$ )	$R^2$
CA (FeSSGF)	0.4-50	1.00
ITR (FeSSGF)	0.1-6	1.00
ITR (Early FeSSGF)	0.2-6	0.999
ITR (Digested early FeSSGF)	0.2-5	0.999
CX (FeSSGF)	0.2-8	1.00

###### 3.1.1.2 Limit of detection (LOD) and limit of quantification (LOQ)

Based on the LOD and LOQ equations and calibration curves, LOD and LOQ values for the investigated drugs in aqueous media (Table 41) and milk-based media (Table 42) were calculated.

Table 41. LOQ and LOD ( $\mu\text{g/mL}$ ) for the investigated drugs in aqueous media

Drug	LOD ( $\mu\text{g/mL}$ )	LOQ ( $\mu\text{g/mL}$ )
CA	0.04	0.10
ITR	0.03	0.09
CX	0.03	0.07

Table 42. LOQ and LOD ( $\mu\text{g/mL}$ ) for the investigated drugs in milk-based media

Drug (Milk based media)	LOD ( $\mu\text{g/mL}$ )	LOQ ( $\mu\text{g/mL}$ )
CX (FeSSGF)	0.06	0.18
ITR (FeSSGF)	0.03	0.09
ITR (Early FeSSGF)	0.049	0.149
ITR (Digested early FeSSGF)	0.064	0.197
CA (FeSSGF)	0.11	0.32

### 3.1.1.3 Recovery

Accuracy of the developed method was examined by recovery studies at various concentration values. These results are summarised in Table 43. Recovery data were determined as ratios of drug concentration in standard solutions prepared in FeSSGF compared to the standard solution in blank FeSSGF (acetate buffer). An estimation of the recovery of the method can also be obtained using the standard addition method.

Table 43. Mean  $\pm$  SD of % recovery of the three investigated drugs

Drug (Milk based media)	Calculated using ratio of concentration	Calculated using standard addition method
CX (FeSSGF)	94.41 $\pm$ 0.87 to 99.52 $\pm$ 0.65	97.51 $\pm$ 1.1 to 103.41 $\pm$ 1.19
ITR (FeSSGF)	96.77 $\pm$ 0.32 to 103.01 $\pm$ 2.07	100.21 $\pm$ 0.78 to 104.76 $\pm$ 0.081
ITR (Early FeSSGF)	95.73 $\pm$ 1.48 to 101.89 $\pm$ 1.97	98.83 $\pm$ 0.16 to 103.51 $\pm$ 0.41
ITR (Digested early FeSSGF)	94.73 $\pm$ 4.74 to 105.56 $\pm$ 1.47	106.26 $\pm$ 0.15 to 115.45 $\pm$ 0.45
CA (FeSSGF)	94.42 $\pm$ 0.45 to 102.88 $\pm$ 1.32	97.63 $\pm$ 1.06 to 107.81 $\pm$ 1.16

### 3.1.1.4 Fat binding test

The binding of the drug to the fat content was clearly related to the hydrophobicity of the drug (Table 44). This agrees with a previous study which showed correlation between increasing octanol–water partition coefficient (log P) and increasing affinity of drug to fat in milk (318).

Table 44. Mean± SD of % fat partition of the three investigated drugs

Drug (Milk based media)	Log P	% fat partition ± SD
CX (FeSSGF)	3.84	51.49 ±2.30
ITR (FeSSGF)	4.3	45.23 ±2.72
ITR (Early FeSSGF)	4.3	35.12±4.23
ITR (Digested early FeSSGF)	4.3	4.33±1.70
CA (FeSSGF)	-1.4	11.60 ±0.99

### 3.1.1.5 Filter adsorption studies (Milk-based media)

The results showed that the drugs adsorption to the nylon filter was low and was within the accepted value (>95%) (Table 45). Therefore, this filter type was used.

Table 45. % recovery ± SD from filtrate for filter adsorption studies

Drug	1st filtration	2nd filtration
CX	95.12±0.092	100.84±0.604
ITR	95.12±1.86	95.19±1.86
CA	100.30±0.71	100.29±4.83

### 3.1.2 Development of modified media

In the current study, the addition of SLS (anionic surfactant) and HTAB (cationic surfactant) in the compendia media (SGF, SIF) and blank FaSSIF-V2 (FaSSIF-V2 without bile salt and lecithin) has been proposed to mimic the presence of bile salts *in vivo*, as in biorelevant media. These newly proposed modified media may be used for initial screening as an alternative to the BDM which are costly and time consuming to prepare (319).

#### 3.1.2.1 SLS-based modified media

##### Surface tension (ST) measurement

Endogenous surfactants such as bile salts and lecithin reduce the ST of GI fluids and affect the solubilisation of poorly water-soluble drugs (62, 320). Literature has shown that blank (without bile salt and lecithin) FaSSIF-V1 plus surfactant had a similar ST to FaSSIF-V1 and produced similar dissolution profiles (319). To mimic the surface tension in gastric fluid, SLS is included in SGF to reduce the ST of the medium to physiological values of 41.9-45.7 mN/m (73). The linear regression plot of ST in different concentrations of SLS in SGF showed that 0.01% SLS in SGF has an ST equivalent to the ST in fasted stomach fluid (Figure 18). Furthermore, in this study, critical micelle concentration (CMC) of different surfactants was estimated by identifying the concentration corresponding to the bend in the curve of ST plotted against surfactant concentration. This is determined graphically from the intersection of the two linear portions of the ST and concentration plot and the value determined from the graph is 0.103% SLS. As observed in the graph, the ST of the solution does not decrease further with an increase in surfactant concentration at concentrations greater than the CMC (321).

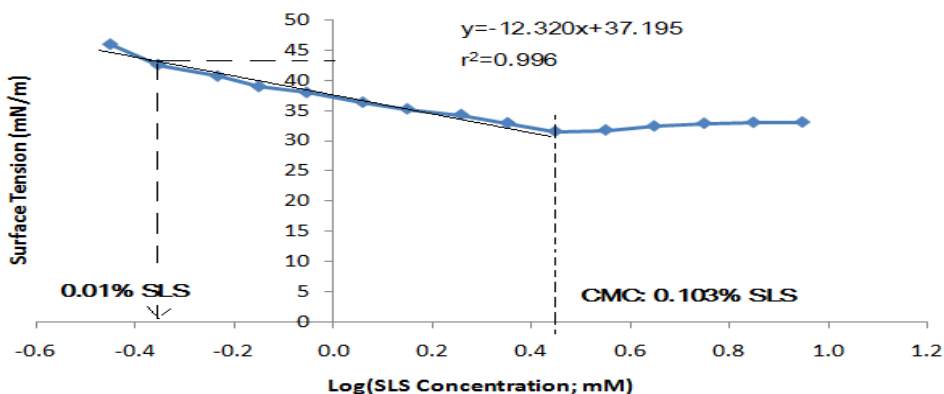


Figure 18. Surface tension vs log SLS concentration (mM) (CMC determination of SLS) in SGF at 25°C (data obtained in this project).

Therefore, a modified compendial medium simulating the contents in the stomach under fasted state conditions (SGF-M1) was proposed. It contains 0.2% NaCl and 0.01% (w/v) SLS with its pH adjusted to 1.2 with 1M hydrochloric acid. It achieved similar physicochemical properties to fasted state human gastric fluid (e.g. ST, ionic strength, pH value and osmolality) (Table 46).

Table 46. Comparison of physicochemical properties between modified compendial medium for the fasted stomach and fasted state human gastric fluid.

Property	Medium	
	Fasted state human gastric fluid	SGF-M1 (SGF +0.01% SLS)
Surface tension (mN/m)	41.9-45.7 (73)	42.8
Ionic strength (M)	0.1 (72) (Detailed calculation presented in Appendix 6)	0.136 (Detailed calculation presented in Appendix 6)
pH	1.7 (73)	1.2
Osmolality (mOsm/kg)	98.0 (Median value) (73)	~103.3*

\* Calculated using NaCl equivalence method (322):0.2% NaCl (from SGF) plus 0.125% NaCl (Equivalent value of 0.01% SLS)

Meanwhile, simulated intestinal fluid-modified 1 and 2 (SIF-M1 and SIF-M2) were developed by Tomaszewska and Fotaki (258), composed of 50mM sodium phosphate buffer plus 0.2% SLS (SIF-M1) and 19.12mM maleate buffer plus 0.1% SLS (SIF-M1), both at pH 6.8.

SIF-M5 consists of 1% SLS in 50mM phosphate buffer, pH6.8. The medium is used mainly as a controlled medium for SIF-M4 (1% HTAB in 50mM phosphate buffer, pH 6.8) to compare the effect of anionic and cationic surfactant. Due to its high surfactant content, this medium is regarded as being for quality control purposes for complete dissolution of test formulation.

It is important to note that the surfactant, when present at levels below the CMC, enhances the dissolution rate of low water soluble drug products, probably by increasing the wetting and lowering the interfacial tension (320). Since CMC in the other dissolution media is lower than that in water, more surfactants form micelles rather than moving to the surface. This will increase the solubility of the drug rather than just reducing the surface tension or wettability (323). For example, the SLS concentration in SGF<sub>SLS</sub> is 8.67 mM and the CMC of SLS in SGF<sub>SLS</sub> is 1.75 mM (54). If the concentration of SLS in the media is greater than its CMC, the potential for

overestimation of solubility exists due to the presence of an additional 6.92mM SLS in  $SGF_{SLS}$  (58).

Another reason for not having the surfactant exceeding the CMC concentration is that the natural surfactant in the stomach, pepsin, is not known to form micelles (58). The lower gastric ST has also been attributed to bile salts due to reflux. According to the literature (58), the concentration of bile salts found in the stomach is in an order of magnitude lower than the reported CMC values of bile salts (e.g. 20 mM, 18 mM, 13 mM, and 17mM for sodium cholate, sodium taurocholate, sodium deoxycholate and sodium taurodeoxycholate, respectively). Hence, one would not expect any significant bile salt micellar solubilisation in the stomach.

### 3.1.2.2 HTAB-based modified media

Unlike studies with SLS, the complete ST and CMC dataset of HTAB in SGF and SIF was presented in Stippler's PhD thesis (262). Therefore, the reported CMC plot of HTAB in SGF and SIF was used in this study (262) (Figure 19).

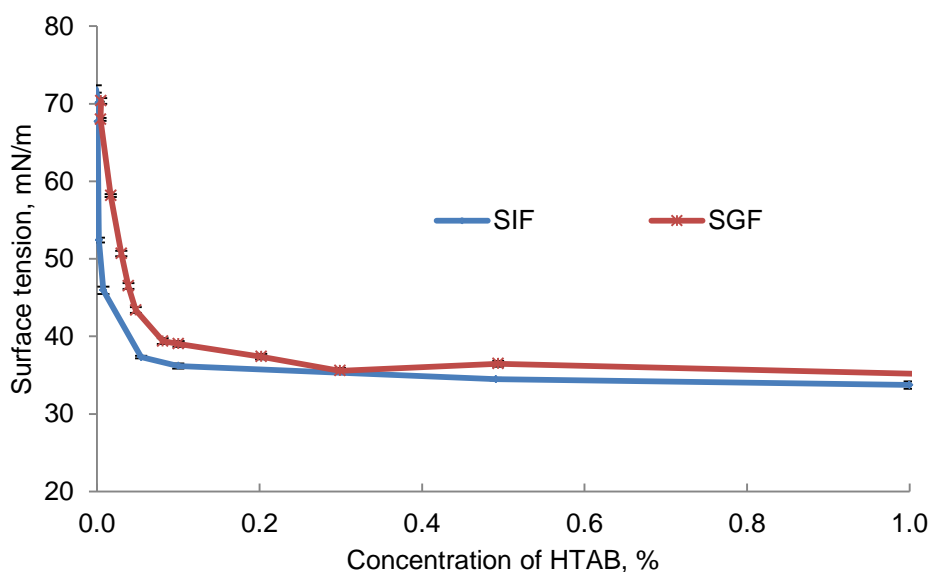


Figure 19. Mean  $\pm$  SD surface tension vs HTAB concentration (%) in SGF and potassium phosphate buffer (n=6) [values were extracted from a graph presented in Stippler's PhD thesis (262)].

Literature had reported that the ST in the human stomach and duodenum (fasted state) is 41.90-45.70  $mNm^{-1}$  and 33.30-46.00  $mNm^{-1}$  (83), respectively. Using the same principle as mentioned in SLS-based modified media, three new HTAB-based modified media were developed in this study.

Simulated gastric fluid-modified 2 (SGF-M2), consists of 0.015% HTAB in 2% sodium chloride aqueous solution with pH adjusted to 1.2 with concentrated hydrochloric acid,

corresponding to an ST of 43.99. Since the reported CMC of HTAB in SGF was 0.02%, at a concentration of 0.015% HTAB, it was expected that no HTAB micelle is formed, a condition also found in the human stomach.

Simulated intestinal fluid-modified 3 (SIF-M3), composed of 0.1% HTAB in 50mM phosphate buffer pH 6.8, corresponds to an ST of  $36.7 \text{ mNm}^{-1}$ , within the reported *in vivo* surface tension range of 33.30-46.00  $\text{mNm}^{-1}$  (83). As this concentration is the CMC value of HTAB (262), the HTAB micelle can be formed in agreement with the *in vivo* condition (83).

Lastly, simulated intestinal fluid-modified 4 (SIF-M4), composed of 1.0% HTAB in a 50mM phosphate buffer pH 6.8, has a concentration 100 times higher than its CMC. A study has shown that 1% HTAB provided a sink condition for CX dissolution and it is the recommended dissolution medium for the CX specification as suggested by the Center for Drug Evaluation and Research, US FDA (233).

## 3.2 Results and Discussion of Part 1: *In vitro* dissolution testing (Cefuroxime axetil)

### 3.2.1 Degradation study of cefuroxime axetil

As part of the characterisation of the *in vitro* dissolution behaviour, it is crucial to determine the experimental degradation during dissolution. In particular the first 4 h of the experiment, the same reaction could take place *in vivo* and the degradation could adversely reduce the amount of CA for absorption. The results of the degradation study are presented in Figure 20.

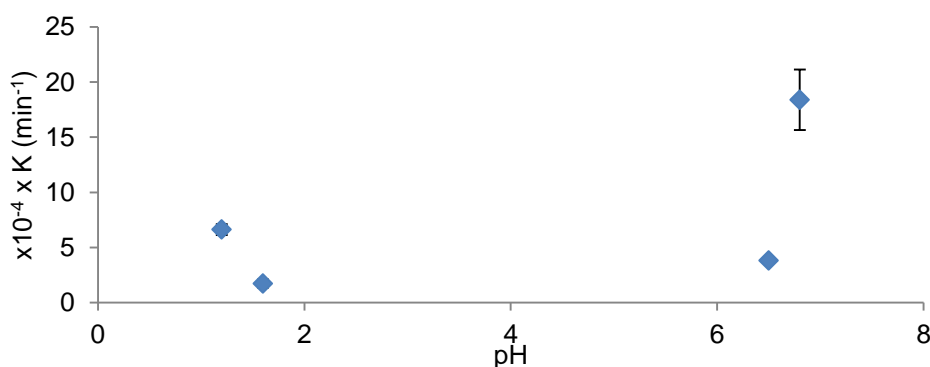


Figure 20. The relationship between the pH of the dissolution medium and the mean  $\pm$  SD degradation rate constant, K (n=3).

Based on Figure 20 which presents the degradation rate constant vs pH, a “U” shape curve indicates CA degradation is very pH dependent to the CA and it is most stable at pH 3.5-5.5 (324). CA degradation is highest in the phosphate buffer at pH 6.8 ( $18.40 \times 10^{-4} \text{ min}^{-1}$ ), followed by in acidic medium, SGF ( $6.62 \times 10^{-4} \text{ min}^{-1}$ ), FaSSIF-V2 ( $3.825 \times 10^{-4} \text{ min}^{-1}$ ) and FaSSGF ( $1.733 \times 10^{-4} \text{ min}^{-1}$ ).

It is noteworthy that for FaSSIF-V2 (pH 6.5), a maleate buffer is used. From a chemical point of view, two reactions (Michael addition) could occur between a primary amine group of the CA molecules and maleic acid: one undergoes nucleophilic attack at the carbonyl carbon with 1, 2-addition, and the other attacks at the  $\beta$ - carbon with 1, 4-addition. Michael addition is a common reaction mechanism in API–salt interaction which could lead to API degradation (325).



### 3.2.2 Dissolution testing in USP apparatus 2

#### Simulated fasted state conditions

The cumulative % CA dissolved from Zinnat<sup>®</sup> in various media with USP apparatus 2 is presented in Figure 21.

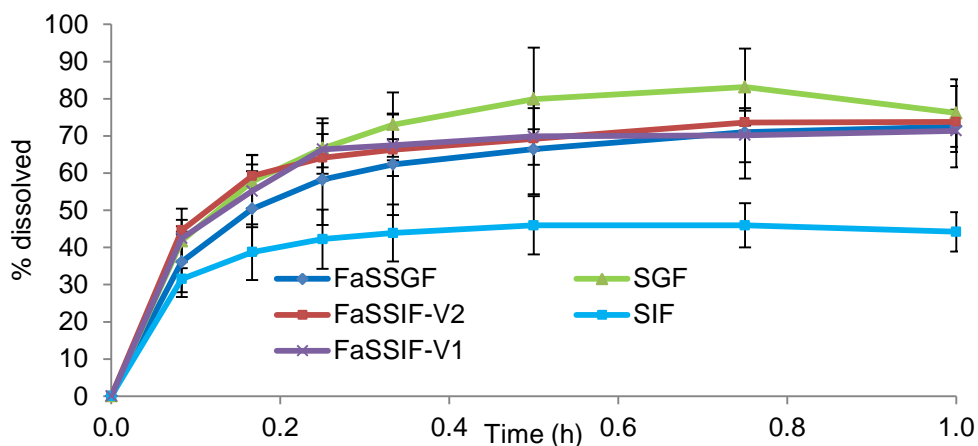


Figure 21. Mean  $\pm$  SD % cumulative CA dissolved from Zinnat<sup>®</sup> tablets in various media using the USP apparatus 2 (500mL, 50rpm, 37°C, n=3).

Studies have shown that the solubility of CA, which is a cephalosporin ester molecule, is highest at low pH values (SGF: pH 1.2 and FaSSGF: pH 1.6) and it reduces at higher pH (205). Meanwhile, CA was degraded at a higher rate in SIF therefore greatly reduced the amount of CA available for dissolution. As a result, dissolution profiles SGF vs SIF were different by 41% ( $f_{1,area}$ : 0.41). At pH 6.8, a considerable amount of croscarmellose sodium (anionic type disintegrant) forms sticky cellulose leading to coning effects that affect the CA dissolution (238). It is notable that biorelevant media produce very similar profiles (FaSSGF vs FaSSIF-V2:  $f_{1,area}$  0.03 or FaSSIF-V2 vs FaSSGF  $f_{1,area}$ :0.07).

## Simulated fed state conditions

The cumulative % CA from Zinnat<sup>®</sup> in FeSSGF and FeSSIF-V2 with USP apparatus 2 are presented in Figure 22.

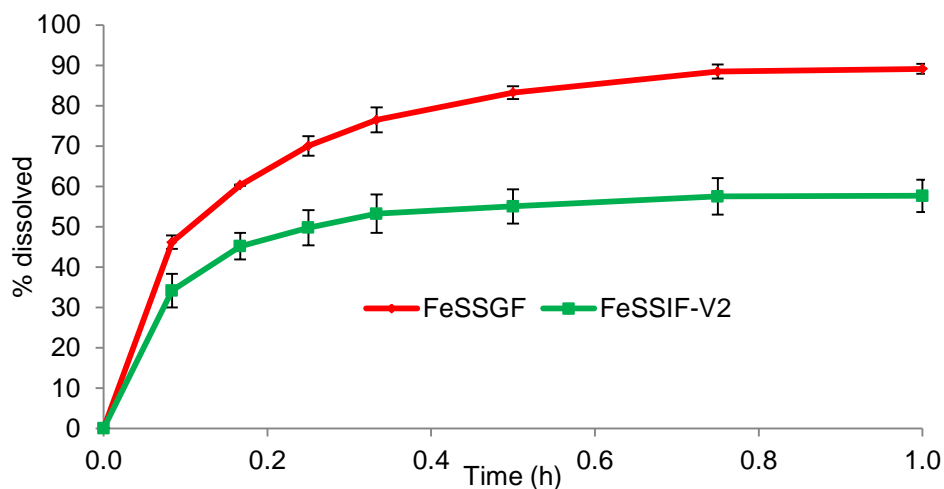


Figure 22. Mean $\pm$  SD % CA dissolved from 250mg Zinnat<sup>®</sup> tablet in FeSSGF and FeSSIF-V2 with USP apparatus 2 (500 mL medium, 37°C, 50rpm).

The CA dissolution profiles showed that the rate and the extent of dissolution was faster and higher in FeSSGF compared to FeSSIF-V2 (FeSSGF vs FeSSIF-V2;  $f_{1,area}$ : 0.48). This is probably due to glyceryl monooleate and sodium oleate in FeSSIF-V2 forming a glutinous aggregate with the croscarmellous sodium in Zinnat<sup>®</sup> tablet causing excessive gelling and cones at the bottom of the vessel.

## Dissolution kinetics of profiles with USP apparatus 2

The dissolution profiles of the CA tablet were fitted well with first order and single Weibull kinetics models. The fitted parameters in the fasted state and fed state experiments are presented in Table 47.

Table 47. Mean± SD dissolution kinetic parameters of CA dissolved from Zinnat<sup>®</sup> tablet in simulated fasted and fed states media with USP apparatus 2 (n=3).

	First order kinetics						
	SGF	FaSSGF	SIF	FaSSIF-V1	FaSSIF-V2	FeSSIF-V2	FeSSGF
Max (%)	81.36± 11.47	73.00± 11.26	44.85± 6.79	72.62± 2.45	71.03± 2.56	59.20± 3.16	86.65± 1.72
c (/h)	7.68± 0.83	6.80± 1.22	13.39± 1.49	10.19± 0.19	10.93± 0.28	8.66± 1.02	7.46± 0.44
R <sup>2</sup>	0.99± 0.00	0.98± 0.01	0.99± 0.01	0.99± 0.00	0.99± 0.00	0.98± 0.01	0.99± 0.00
	Single Weibull function						
Max (%)	86.62± 13.03	77.24± 9.38	45.81± 5.85	72.00± 4.80	73.90± 2.55	60.25± 2.80	88.03± 1.41
a (h)	0.24± 0.05	0.34± 0.11	0.15± 0.08	0.14± 0.07	0.20± 0.01	0.26± 0.05	0.21± 0.02
b	0.75± 0.10	0.62± 0.08	0.76± 0.18	0.87± 0.12	0.67± 0.03	0.60± 0.06	0.77± 0.03
R <sup>2</sup>	1.00± 0.00	1.00± 0.00	1.00± 0.00	1.00± 0.00	1.00± 0.00	1.00± 0.00	1.00± 0.00

According to first order kinetics, CA dissolution was higher but the dissolution rate was lower in SGF than SIF. Similarly, the same scenario was observed between FaSSGF and FaSSIF-V2. The higher dissolution is probably due to the higher equilibrium solubility of CA in SGF and FaSSGF than SIF and FaSSIF-V2— as in a closed dissolution system the dissolution of a poorly soluble drug is limited by the equilibrium solubility of the drug. Meanwhile, the first order kinetics showed that the maximum % dissolved and the dissolution rate between FaSSIF-V1 and FaSSIF-V2 are very similar; whereas, FeSSIF-V2 has a lower rate and extent of dissolution. The disparity is mainly due to the heavy coning effect observed in FeSSIF-V2 with USP apparatus 2.

The dissolution kinetics of CA from the amorphous formulation Zinnat<sup>®</sup>, was also analysed by the application of a single Weibull function. The shape factor (b) reveals that all media (simulating fasted and fed state) have a parabolic curve shape. Literally, the dissolution profiles show a steep initial dissolution and then plateau out at the maximum dissolution level. It is important to note that the time scale of the dissolution process for CA follows the sequence of FaSSGF (0.62 h), FaSSIF-V2 (0.67 h), SGF (0.75 h) and SIF (0.76 h) which is in agreement with the sequence of rate of CA degradation measured *in vitro* (results presented in Section 3.2.1). This seems to

indicate that the Weibull function could be a good fitting method to forecast the CA degradation rate.

### 3.2.3 2 stage dissolution studies

The cumulative % of dissolved CA from Zinnat<sup>®</sup> in 2 stage dissolution experiments with USP apparatus 2 are presented in Figure 23.

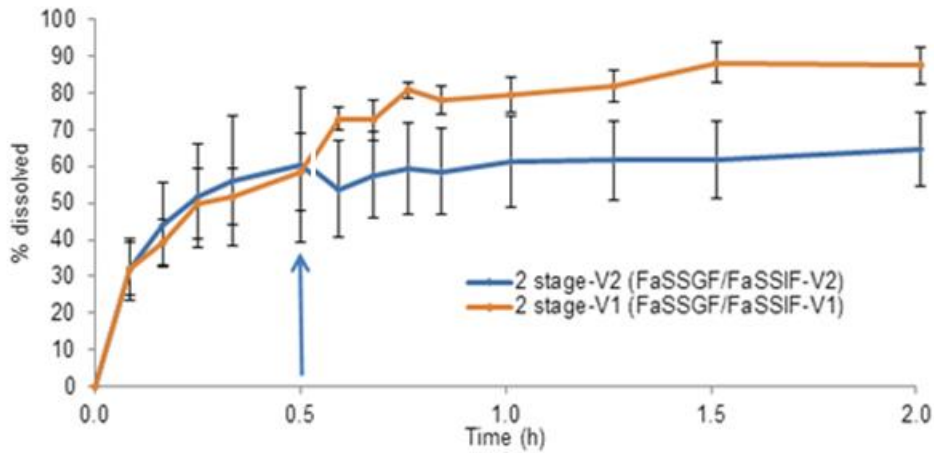


Figure 23. Mean $\pm$  SD % CA dissolved from 2 stage dissolution, 250 mL FaSSGF for 30min/500 mL FaSSIF-V1 or -V2 with USP apparatus 2 (37°C,50rpm). Blue arrow indicates time with media change. Gap after media change indicates short pause of paddle rotation.

The results of the 2 stage dissolution model in the simulated gastric phase compared to the conventional USP apparatus 2 (using FaSSGF) showed that the dissolution was lower, probably limited by the smaller volume of medium used (250mL) in the first 30 min of the experiment. The results showed that higher and faster CA dissolution occurring in FaSSIF-V1 (Max 78.03%, first order rate constant  $3.31\text{h}^{-1}$  vs 45.08% and  $2.73\text{h}^{-1}$  in FaSSIF-V2, respectively) could be due to FaSSIF-V1 containing almost four times more lecithin (a surfactant that acts as a solubilisation agent) compared to FaSSIF-V2.

### 3.2.4 Dissolution testing in USP apparatus 4 (with sequential change of media and flow rate)

#### Simulated fasted state conditions

The cumulative % of dissolved CA from Zinnat<sup>®</sup> in various media with USP apparatus 4 are presented in Figure 24.

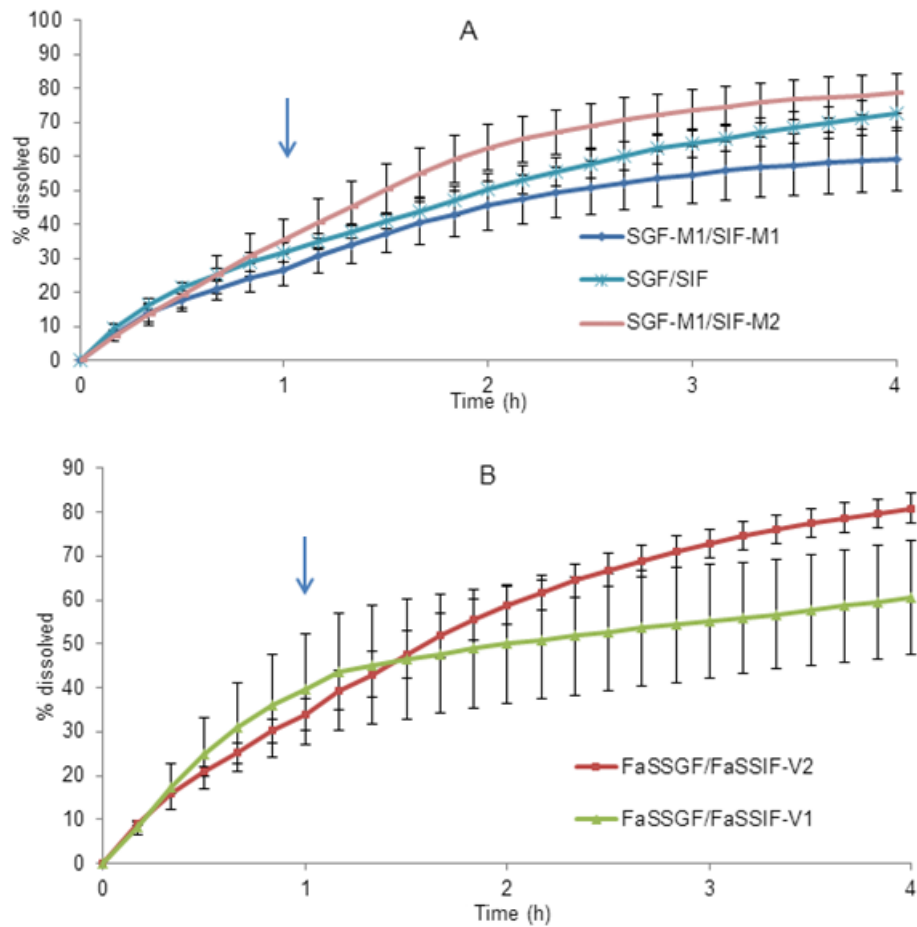


Figure 24. Mean $\pm$  SD % cumulative CA dissolved from Zinnat<sup>®</sup> tablet in (A) SGF-M1(8mL/min; 1h) then SIF-M1 and M2 (4mL/min; 5h) SGF (8mL/min;1h) then SIF (4mL/min; 5h) (B) FaSSGF(8mL/min; 1h) then FaSSIF-V1 and V2 (4mL/min; 3h) using the USP apparatus 4 (n=3). Blue arrows indicate time with media and flow rate change.

The dissolution curves indicated that CA remained solubilised when it was transferred from simulated gastric media into simulated intestinal media with USP apparatus 4. This condition was probably due to the solubility of CA in simulated gastric media being close to the simulated intestinal media. Therefore the issue of recrystallisation was not apparent in the dissolution of Zinnat<sup>®</sup> tablet.

The presence of SLS (part of the excipient of the tablet) caused more than 50% CA dissolution across all five experiments presented in Figure 24. The dissolution profiles comparison showed that the difference between the dissolution profiles of SGF-M1/SIF-M1 and SGF/SIF was 17% ( $f_{1\text{area}}: 0.17$ ) whereas the profiles between SGF-M1/SIF-M2 and FaSSGF/FaSSIF-V2 were very similar ( $f_{1\text{area}}: 0.05$ ).

The dissolution curve of CA in SIF-M1 reached a plateau in 2 h compared to the dissolution curve of SIF. This was because the type of buffer and its pH can change the rate of degradation of CA (206, 326). Even though both SIF and SIF-M1 were prepared using a phosphate buffer, lower dissolution was observed in SGF-M1/SIF-M1. The lower dissolution was an artifact due to the higher degradation of CA in the presence of SLS (324).

From the dissolution results, a few critical factors affecting CA dissolution were identified:

1. Effect of extent of disintegration and agglomeration/aggregation of tablet content

During the dissolution study of FaSSGF/FaSSIF-V1, one particular tablet formed a gelatinous mass that prevented free penetration of medium into the mass. Literature had demonstrated that the gelling effect of CA could affect its dissolution (241). Furthermore, mass formation also was shown to lead to a lower rate and extent of dissolution (59). Furthermore, it was observed during dissolution experiments with USP apparatus 4 that hard lumps were formed with SIF-M1 as a dissolution medium compared to compendial media where most of the tablet was dissolved. The reduced surface area decreased the dissolution of CA. As reported by Rohrs *et al.*, the changes in the disintegration/deaggregation behavior can cause occlusion of the drug in the aggregate that did not disperse during testing. The extent of dissolution would then be limited by the lack of drug surface exposed to the dissolution medium (327).

2. Effect of CA degradation on dissolution profile

A study reported that the degradation rate of CA was influenced by the type of buffer and its concentration (328). Its degradation rate was highest in phosphate (SIF, FaSSIF-V1) compared to acetate and carbonate and formate buffer (206).

During the experiment with modified media containing SLS, the colour of the powder in the cell was white. After changing media, the color of the powder turned yellowish gradually, indicating delta-3-isomers of CA had been formed (Delta-3-isomers of CA is

a clumpy tan or yellowish coarse powder). The clumpy powder increased clustering and agglomeration of the drug powder and affected the CA dissolution.

### Simulated fed state conditions

The cumulative percentage and mean amount of dissolved CA from Zinnat<sup>®</sup> in FeSSGF/FeSSIF-V2 and FeSSGF/FeSSIF-V1 with USP apparatus 4 are presented in Figure 25.

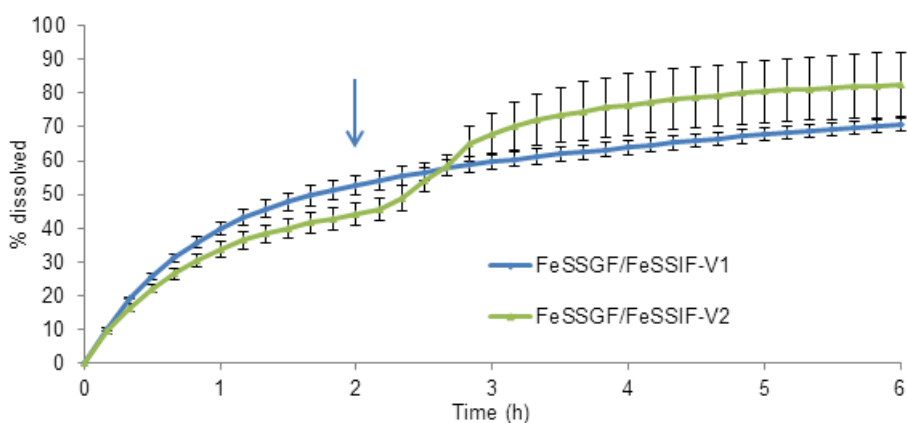


Figure 25. Mean  $\pm$  SD % CA dissolved from Zinnat<sup>®</sup> tablet in fed state FeSSGF(6mL/min; 2h)/FeSSIF-V1 and-V2 (6mL/min; 4 h) using the USP apparatus 4 (n=3). Blue arrow indicates time with media change.

The results of the dissolution test with USP apparatus 4 showed that the FeSSIF-V2 enhanced the dissolution of CA with 80% dissolved, compared to 70% in FeSSIF-V1. This was probably due to the presence of GMO and high concentrations of sodium oleate in FeSSIF-V2 increasing the dissolution of CA under the open dissolution setup.

### Dissolution kinetics of profiles with USP apparatus 4

The dissolution profiles of CA tablet were all fitted well with first order kinetics model. The maximum % dissolved (Max) and rate constants in fasted state and fed state are presented in Table 48.



Table 48. Mean± SD dissolution kinetic parameters of CA dissolved from Zinnat® tablet in simulated fasted and fed states media using the USP apparatus 4 (n=3).

	SGF/ SIF	FaSSGF/ FaSSIF-V1	FaSSGF/ FaSSIF-V2	SGF-M1/ SIF-M1	SGF-M1/ SIF-M2	FeSSGF/ FeSSIF-V1	FeSSGF/ FeSSIF-V2
First order kinetics							
Max (%)	92.1± 9.98	58.75± 15.10	97.67± 1.66	68.23± 0.07	85.84± 1.59	67.74± 11.66	91.12± 3.61
c (/h)	0.39± 0.03	1.06± 0.15	0.46± 0.05	0.53± 0.00	0.60± 0.07	0.81± 0.28	0.41± 0.03
R <sup>2</sup>	0.99± 0.01	0.99± 0.00	1.00± 0.00	0.99± 0.01	0.99± 0.01	0.99± 0.01	0.98± 0.01
Single Weibull function							
Max	96.88± 1.36	69.43± 2.68	97.24± 4.77	69.97± 9.97	83.88± 5.44	78.78± 4.31	93.91± 10.54
a (h)	2.46± 0.20	1.28± 0.82	2.21± 0.37	1.87± 0.09	1.76± 0.26	1.35± 0.20	2.56± 0.69
b	0.88± 0.13	0.69± 0.11	1.01± 0.05	0.91± 0.06	1.17± 0.10	0.62± 0.05	0.98± 0.17
R <sup>2</sup>	1.00± 0.00	1.00± 0.00	1.00± 0.00	1.00± 0.00	1.00± 0.00	1.00± 0.00	0.98± 0.02

As described in Section 3.2.1, the dissolution of CA was affected by the types of buffer, surfactant, pH and hydrodynamics of the system and the effect of degradation. These cumulative effects were shown in the Max (%) and dissolution rate of the applied models. The application of first order and single Weibull kinetic models in the analysis of dissolution data (simulating fasted state) showed that the mean values of Max (maximum percentage dissolved) followed the sequence of FaSSGF/FaSSIF-V2> SGF/SIF> SGF-M1/SIF-M2> SGF-M1/SIF-M1> FaSSGF/FaSSIF-V1.

Similarly, application of first order and single Weibull kinetic models in the analysis of dissolution data (simulating fed state) shows that the mean values of Max (maximum percentage dissolved) in FeSSGF/FeSSIF-V2 is higher than in FeSSGF/FeSSIF-V1. From the perspective of CA dissolution rate, the first order rate constant and time scale parameter of single Weibull function (simulating fasted state) followed the rank order of FaSSGF/FaSSIF-V1> SGF-M1/SIF-M2> SGF-M1/SIF-M1> FaSSGF/FaSSIF-V2> SGF/SIF. The results clearly showed that the rate of dissolution is higher in media containing a surfactant (Table 48). Meanwhile, in the simulated fed state experiments, a higher amount of lecithin in FeSSIF-V1 caused almost twice the increment of dissolution rate compared with FeSSIF-V2.

Comparing the first order rate constant of dissolution profiles of CA with USP apparatus 2 and 4 (Table 47 vs Table 48), the rate constant was at least 10 times higher in experiments with USP apparatus 2 (closed system) than the experiments with USP apparatus 4 (open system). It is appropriate to state that the dissolution process in dissolution experiments with USP apparatus 4 had mimicked the *in vivo* condition closer when compared with the dissolution profiles with USP apparatus 2 which showed a sharp rise to plateau in 5-10 min. Considering this factor, biorelevant media with USP apparatus 4 seem to be a good dissolution setup to characterise dissolution of CA formulation.

### 3.3 Results and Discussion of Part 1: *In vitro* solubility and dissolution testing (ITR)

#### 3.3.1 Equilibrium solubility studies

Solubility values (measuring solubility up to 72 h) of ITR API in FaSSGF and FaSSIF-V2 measured by the shake flask method (37°C) are shown in Figure 26.

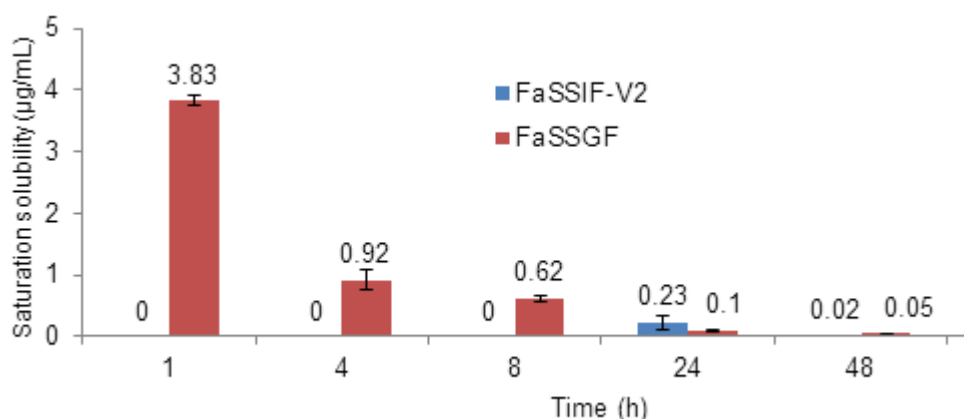


Figure 26. Equilibrium solubility ( $\mu\text{g/mL}$ , Mean  $\pm$  SD) of ITR in FaSSGF and FaSSIF-V2

#### Solubility of ITR in FaSSGF

ITR is a weak base ( $\text{pK}_a$  3.7). After the 1<sup>st</sup> h the solubility was enhanced mainly because ITR exists as an ionised (cationic) form in pH 1.6 medium. The concentration was reduced to 0.92 $\mu\text{g/mL}$ , 0.62 $\mu\text{g/mL}$  and 0.10 $\mu\text{g/mL}$  subsequently. The rapid precipitation of ITR in FaSSGF could be due to the acid-base reaction between the sodium taurocholate (329, 330) and weak base ITR leading to the charge neutralisation

of ITR that facilitate the nucleation of ITR. In the beginning of the experiment, the dissolution of the ITR molecules into the bulk solution probably exceeded the equilibrium solubility of the ITR in FaSSGF. This excess concentration or chemical potential, called the supersaturation, was the driving force for nucleation and crystal growth of ITR (36, 331).

### Solubility of ITR in FaSSIF-V2

In FaSSIF-V2 ITR mainly exist in an unionised form. The dissolution profile of ITR in the presence of FaSSIF-V2 compared to FaSSGF showed a very slow and steady dissolution; after the supersaturation state at 24 h the ITR slowly reached the equilibrium solubility of  $0.02 \pm 0.0023 \mu\text{g/mL}$  at 48 h. The supersaturated solution of ITR at 24h could be due to the micellar solubilisation effect of mixed micelles as a combination of bile salt and lecithin. The bile components exert their effect on solubility by forming different colloidal phases that could solubilise the ITR molecule better. The mixed micelle produced a transient higher solubility than FaSSGF before slowly nucleating and precipitating at 48 h.

### 3.3.2 Dissolution testing in USP apparatus 1

#### Simulated fasted state conditions

The cumulative % of ITR dissolved from Sporanox<sup>®</sup> in SGF, FaSSGF and FaSSIF-V2 with USP apparatus 1 is presented in Figure 27.

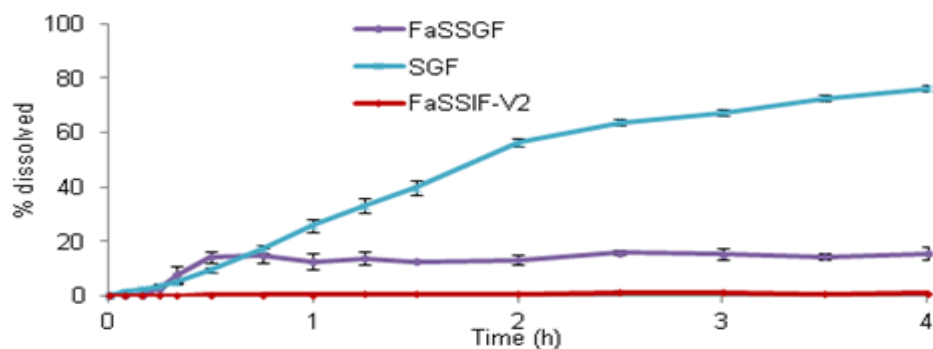


Figure 27. Mean  $\pm$  SD % ITR dissolved from Sporanox<sup>®</sup> capsule with USP apparatus 1 (500mL, 37°C, 75 rpm, n=3). Blue arrow indicates time with media change.

The Sporanox<sup>®</sup> capsule is a floating capsule therefore the basket apparatus (USP apparatus 1) is a better option compared with USP apparatus 2. Essentially, all dissolution profiles were very different depending on the pH of the dissolution media. As a weak base (pKa 3.7) (216, 219) the decrease in solubility in media above pH 3 confirms the changes in pH profoundly influenced both solubility and dissolution. Dissolution of ITR from Sporanox<sup>®</sup> was enhanced as the equilibrium solubility of ITR in SGF (3.9 µg/mL)(219 3.9 µg/mL) could only bring about 2% dissolution (Figure 27). It is due to Sporanox<sup>®</sup> being a solid dispersion formulation with molecular dispersion of ITR in HPMC. HPMC is an amorphous carrier that could form a high apparent concentration supersaturated solution of ITR and increases the solubilisation of ITR (332, 333). In agreement with the literature (30, 231) the supersaturation effect has been shown in this study (Figure 28).

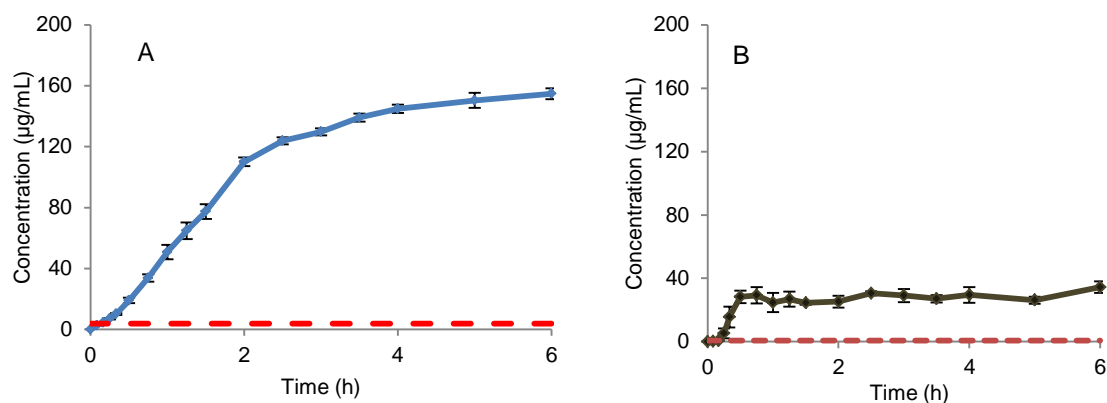


Figure 28. Mean $\pm$  SD ITR concentration yielded from 100mg Sporanox<sup>®</sup> capsule with USP apparatus 1 (500mL SGF: A and FaSSGF: B, 37°C, 75rpm) [Dashed line indicates the ITR equilibrium solubility in the medium (219)]

The dissolution data profile showed that the initial burst in FaSSGF was larger than in SGF with 14.2% dissolved in FaSSGF compared to 9.7% dissolved in SGF at 0.5 h. In the ITR dissolution study with USP apparatus 1 (closed dissolution system) a supersaturated solution of ITR was produced in FaSSGF and it is significantly higher in SGF (almost 90% of ITR dissolved in SGF and 16% of ITR dissolved in FaSSGF) (SGF vs FaSSGF;  $f_{1,area}=0.76$ ) The tendency to achieve supersaturation is higher in closed dissolution systems such as USP apparatus 1. This is due to the fact that poorly soluble compound tends to be in non-sink conditions in the closed system (334).

## Simulated fed state conditions

The cumulative % of ITR dissolved from Sporanox<sup>®</sup> in FeSSIF-V2, FeSSGF, early FeSSGF and digested early FeSSGF with USP apparatus 1 are presented in Figure 29.

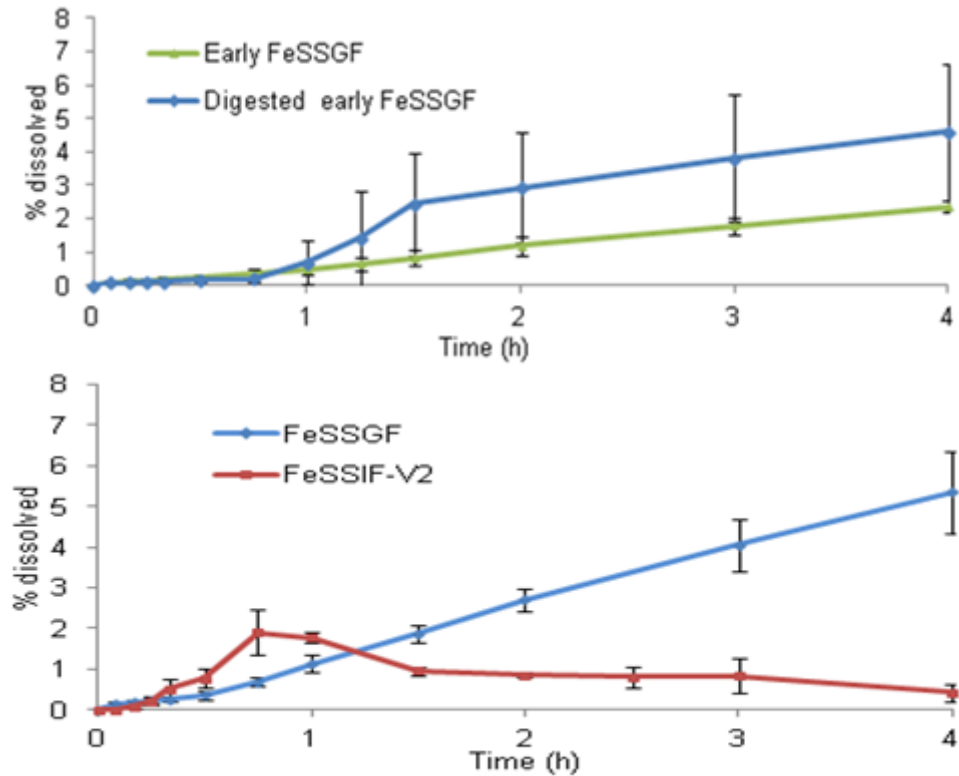


Figure 29. Mean  $\pm$  SD % ITR dissolved from 100mg Sporanox<sup>®</sup> capsule with FeSSIF-V2, FeSSGF, early FeSSGF and digested early FeSSGF with USP apparatus 1 (500mL medium, 37°C, 75rpm, n=3).

In FeSSGF (pH 5) ITR mainly exists as unionised form. Compared with FaSSGF the dissolution rate in FeSSGF is slower. It is noted that the initial slow dissolution could be partially contributed by the fact that milk (a major component of early, digested early FeSSGF and FeSSGF is milk) influences disintegration of drug products and the formulation disintegration was more than five times longer in milk than in fasted state simulated gastric media (335).

In this study, gastric secretions in the fed stomach were simulated using digested early FeSSGF. Meanwhile, the dissolution experiment in early FeSSGF served as a control study. In the digested milk ITR exists mainly in an ionised (cationic) form (pH of medium reduces due to the pepsin solution added into the medium throughout the experiment) and has better solubility in digested early FeSSGF. The observed larger

variability in digested early FeSSGF compared to FeSSGF and digested early FeSSGF is probably due to the highly viscous digested milk formed when pepsin was added causing non-uniformity of drug concentration distribution. The  $f_{1,area}$  value for the comparison of dissolution data profiles of Sporanox<sup>®</sup> in digested and undigested early FeSSGF using the USP apparatus 1 is 0.52. The results show that milk digestion (pH and digested protein) could lead to about 50% difference in *in vitro* dissolution studies.

On the other hand, the presence of lecithin and sodium taurocholate in FeSSIF-V2 produced a greater dissolution in the first 1 h of the experiment compared with FeSSGF (FeSSGF vs FeSSIF-V2,  $f_{1,area}=0.85$ ). The bile components exert their effect on solubility by forming different colloidal phases that could solubilise lipophilic drugs. *In vivo*, food stimulates the release of bile salts and phospholipids; this highlights the importance of the fed state in solubilising this lipophilic compound.

### 3.3.3 2 stage dissolution studies

In this section the biorelevant 2 stage dissolution model with composition and volume of the fluids that have a closer simulation of the *in vivo* conditions is discussed. The cumulative % of dissolved ITR from Sporanox<sup>®</sup> in 2 stage dissolution experiments with USP apparatus 1 are presented in Figure 30.

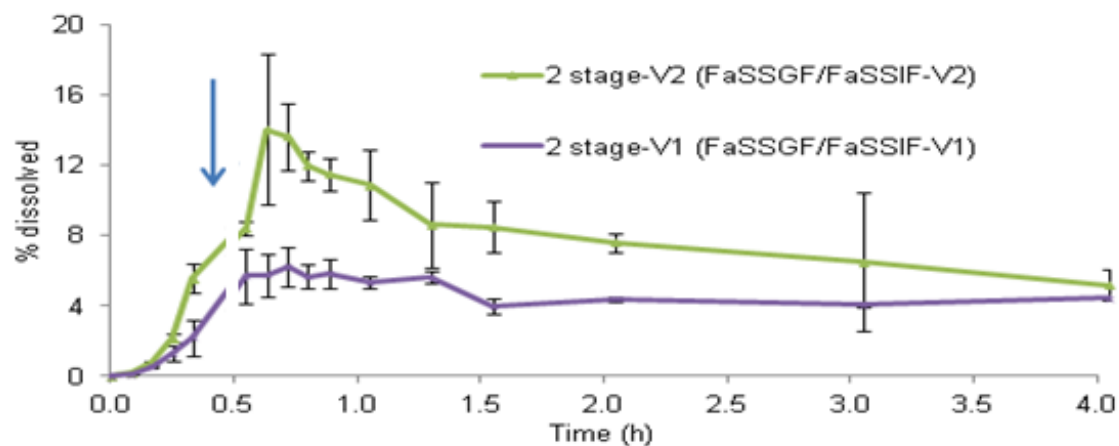


Figure 30. Mean  $\pm$  SD % ITR dissolved from 100mg Sporanox<sup>®</sup> capsule from 2 stage dissolution, 250 mL FaSSGF for 30 min/500mL FaSSIF-V1 or -V2 with USP apparatus 1 (37°C, 75 rpm). Blue arrow indicates time with media change. Gap after media change indicates short pause of paddle rotation.

This experimental setup using closed system optimises dissolution conditions for the ITR because the simulated gastric medium FaSSGF enables a potentially higher

amount of ITR to dissolve prior to the simulated intestinal medium, FaSSIF-V1 and -V2 which has a physiological relevant amount of bile salts and lecithin.

In the first 0.5 h FaSSGF was used and close to 5% and 8% ITR dissolution were recorded. Then FaSSIF-V1 and FaSSIF-V2, the biorelevant dissolution media simulating the physiological conditions in the small intestine in the fasted state were used in two separate 2 stage dissolution experiments. Dissolution experiments resulted in a maximum dissolution of approximately 14% in FaSSGF/FaSSIF-V2 and 6% in FaSSGF/FaSSIF-V1. It was observed that the level of ITR dissolved was maintained better in FaSSIF-V1 compared to FaSSIF-V2 mainly due to a lower supersaturation and better solubility of ITR in FaSSIF-V1.

In the two stage dissolution, highly supersaturated ITR solution in FaSSIF-V2 was produced after medium change and maintained up to 3h-4h. The combination of high concentration of ITR in FaSSGF and micellar solubilisation of ITR by the mixed micelle in FaSSIF-V2 provided the high “spring effect” (29) and the HPMC acts as a precipitation inhibitor to sustain the “parachute effect”, preventing the nucleation and fast precipitation of ITR in FaSSIF-V2.

## Dissolution kinetics of profiles with USP apparatus 1

The dissolution profiles of Sporanox<sup>®</sup> capsule were fitted with first order, single Weibull and Power law kinetics models. The fitted parameters in the fasted state and fed state experiments are presented in Table 49.

Table 49. Mean± SD dissolution kinetic parameters of ITR dissolved from Sporanox<sup>®</sup> 100mg capsule in simulated fasted and fed states media using the USP apparatus 1 (n=3)

	Simulating fasted state				Simulating fed state		
First order kinetic							
	SGF	FaSSGF	FaSSIF-V2	FeSSGF	Early FeSSGF	Digested early FeSSGF	FeSSIF-V2
Max	96.78± 1.82	15.27± 0.68	0.97± 0.21	60.00± 70.87	-*	6.70± 0.78	0.83± 0.14
k <sub>1</sub>	0.37± 0.02	2.03± 0.71	0.80± 0.31	0.06± 0.03	0.04± 0.07	0.28± 0.20	3.81± 0.45
R <sup>2</sup>	0.99± 0.00	0.83± 0.05	0.59± 0.03	0.99± 0.01	0.99± 0.00	0.92± 0.03	0.24± 0.03
Single Weibull function							
Max(%)	89.20± 1.00	14.02± 2.54	2.73± 3.13	21.27± 52.52	6.30± 0.55	4.93± 0.89	1.54± 0.09
a (h)	2.89± 0.23	0.01± 0.01	6.32± 8.79	16.71± 72.37	12.13± 3.00	7.33± 5.76	0.13± 0.05
B	1.30± 0.08	4.88± 0.40	1.97± 1.14	0.98± 1.72	1.21± 0.19	2.24± 0.55	3.16± 0.48
R <sup>2</sup>	1.00± 0.00	0.98± 0.01	0.76± 0.14	1.00± 0.00	1.00± 0.00	0.97± 0.02	0.84± 0.06
Power law							
Rate (unit-less)	24.67± 1.50	69.97± 25.81	0.48± 0.07	1.26± 0.11	0.57± 0.18	0.66± 0.71	3.31± 1.14
Exponential (unit-less)	1.10± 0.07	2.21± 0.54	1.60± 0.27	0.96± 0.14	0.99± 0.15	3.73± 1.28	1.94± 0.34
R <sup>2</sup>	1.00± 0.00	0.98± 0.02	0.99± 0.01	1.00± 0.00	0.99± 0.00	0.94± 0.08	0.99± 0.01

\*the model could not fit the data satisfactorily

A study has shown that the release mechanisms of ITR from Sporanox<sup>®</sup> were controlled by diffusion, swelling, and/or erosion which depends on the HPMC:ITR ratio. For example, in the beginning of the experiment the weight ratio of HPMC:ITR was 1.15:1 and as the experiment progressed, the ratio increased or decreased depending on the rate of HPMC swelling and ITR diffusion to the bulk media (336). Meanwhile, the



surfactant used in dissolution (bile salt, lecithin, SLS) can assist in transferring the drug molecules out of the diffusional layer.

The application of Power law in the analysis of dissolution data showed that the values of kinetic constant are very different in the simulated fasted state conditions compared to the values of 0.57-3.31 in the simulated fed state conditions. The kinetic modeling using Power law also shows that the dissolution of ITR from Sporanox<sup>®</sup> with USP apparatus 1 is associated with an erosion controlled mechanism (exponent >0.85, except FeSSIF-V1 at borderline of 0.82). Studies have shown that for a swellable (a characteristic of HPMC) spherical sample, the values of n of more than 0.85 indicate Super Case II transport (erosion controlled and polymer relaxation release mechanisms) (269, 273). This was due to the increase in HPMC matrix erosion, which can be attributed to slow relaxation of HPMC after exposure to the *in vitro* USP apparatus 1 system. Furthermore, the erosion mechanism is predominant because of the much different hydrodynamics inside the USP apparatus 1 vessel (Reynolds number of more than 1500) compared with in USP apparatus 4 (Reynolds number approximately 10) (337).

On the other hand, application of first order and single Weibull kinetic models in the analysis of dissolution data shows that the mean values of maximum % dissolved (Max) in SGF is higher than in FaSSGF. However, the time scale parameter of Weibull function and first order rate constant shows that the ITR dissolution rate with FaSSGF is at least 5 times higher than in SGF. It indicates that the use of lecithin and bile salt, even at below the CMC value is still able to increase the ITR dissolution rate considerably. Similarly, the time scale parameter of Weibull function and first order rate constant show that the rate of ITR dissolution with digested early FeSSGF is much greater than the early FeSSGF and FeSSGF. For instance, the first order rate constant with digested early FeSSGF is almost 5 times higher than early FeSSGF and FeSSGF. This showed that the milk digestion process also contributed to increasing the ITR dissolution rate.

### 3.3.4 Dissolution testing in USP apparatus 4

#### Simulated fasted state conditions

The cumulative % of ITR dissolved from Sporanox<sup>®</sup> in various simulated fasted state media with USP apparatus 4 is presented in Figure 31.

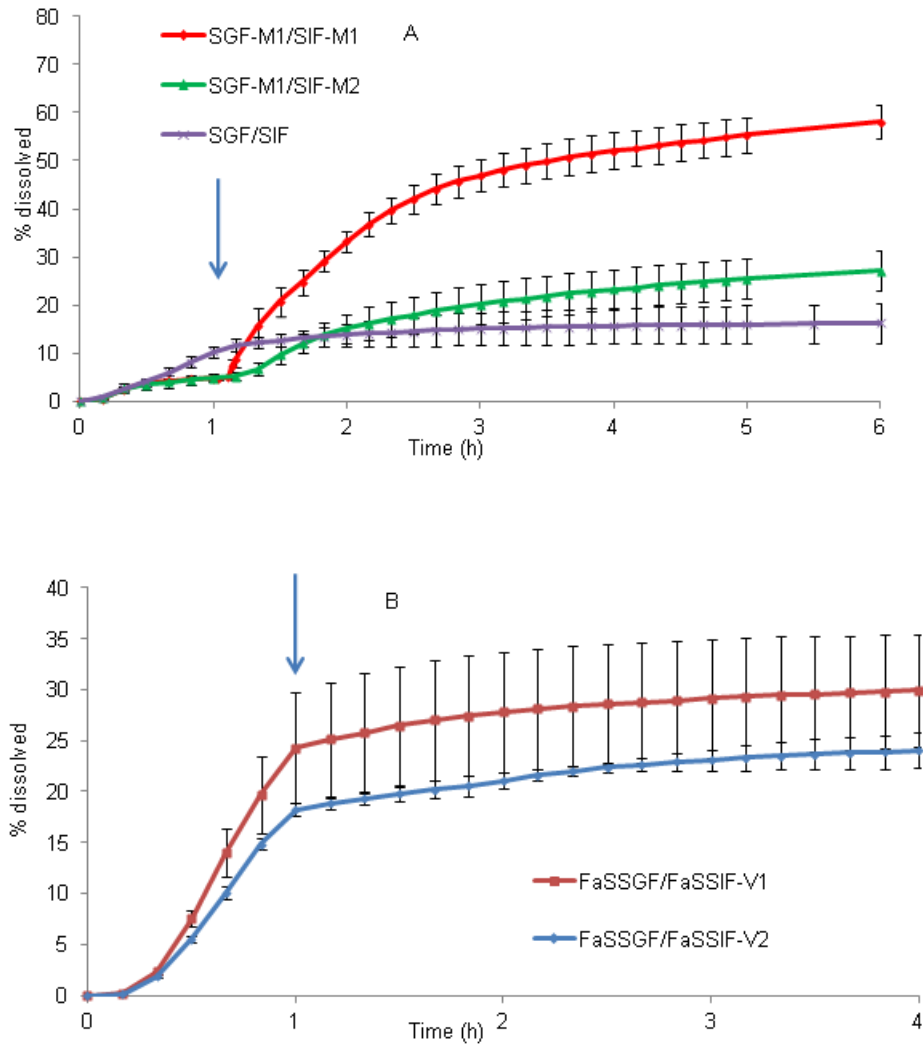


Figure 31. Mean  $\pm$ SD % ITR dissolved from Sporanox<sup>®</sup> capsules in (A) SGF-M1(8mL/min; 1h) then SIF-M1 and M2 (4mL/min; 5h) SGF (8mL/min;1h) then SIF (4mL/min; 5h) (B) FaSSGF (8mL/min; 1h) then FaSSIF-V1 and V2 (4mL/min; 3h) using the USP apparatus 4 (n=3). Blue arrows indicate time with media change.

ITR is a weak base and it is important to test the formulation of ITR with change of media that reflect the human GI system to characterise the degree of supersaturation and dissolution behaviour. One of the main dissolution setups with sequential change of media and flow rate that is accepted by the regulatory agency such as FDA and

EMA is USP apparatus 4. Firstly, in order to characterise the dissolution of ITR from Sporanox<sup>®</sup> in compendial media, experiments with media change using SGF/SIF were conducted. Figure 31A demonstrates that % dissolved in SGF was far greater than the % dissolved in SIF which reflects also in the solubility of ITR in both media (solubility of ITR in SGF and SIF are 3.9 µg/mL and 0.003 µg/mL respectively) (219). As a result, the dissolution of ITR in SGF (8mL/min) was relatively fast initially but slowed down after conditions changed to SIF (Figure 31A).

Secondly, in order to characterise the dissolution of ITR from Sporanox<sup>®</sup> using biorelevant media, experiments with media change using FaSSGF/FaSSIF-V1 and FaSSGF/FaSSIF-V2 were conducted. The results clearly show that the presence of lecithin and sodium taurocholate produced an enhancement in dissolution compared with the compendial media. It is important to note that FaSSIF-V1 which contains more bile salts and lecithin may give a false impression that it has better dissolution of ITR than FaSSIF-V2. This is mainly attributed to the fact that approximately 8% more dissolution in the gastric phase of FaSSGF/FaSSIF-V1 compared to gastric phase of FaSSGF/FaSSIF-V2.

There are a few possible mechanisms of the observed supersaturation and dissolution behavior of ITR from Sporanox<sup>®</sup>. A comprehensive explanation for the mechanism of stabilisation of supersaturated ITR solutions has not been reported (338). Several studies had suggested the factors related to the improved supersaturation of ITR: (1) through incorporating polymers to solutions is the result of intermolecular interactions in solution (hydrogen bonding) (338); (2) steric hindrance of recrystallisation (338); (3) viscosity that influence the stability of supersaturation (338); (4) the effect of elevated glass transition temperature (T<sub>g</sub>) of the binary system (the incorporation of the drug and the polymer) which would slow down the molecular mobility rendering greater physical stability (37). Related to that, it was observed that ITR concentration levels increased sharply to above 80.8 µg/mL (FaSSIF-V1) and 60.9 µg/mL (FaSSIF-V2). This phenomenon of a higher level of supersaturation tends to cause greater driving force for ITR precipitation (51, 339). Upon media change to intestinal media, the ITR concentration reduced immediately and slowly decreased over the next 3 h of the experiment.

It is noteworthy that when the media was changed to simulated intestinal media, the solution in the cells turned opaque which was a strong indicator that the ITR precipitation occurred (340, 341). The processes involved are summarised in Figure 32.

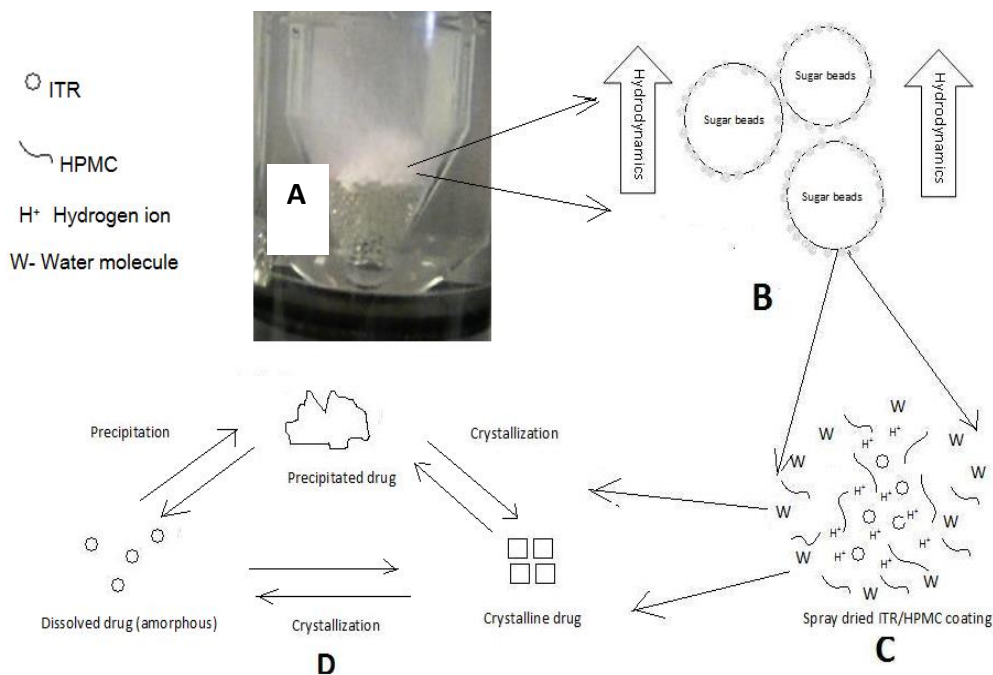


Figure 32. Proposed dissolution and precipitation mechanisms of ITR dissolved from Sporanox<sup>®</sup>. The capsule dissolved in dissolution medium in flow-through cell (A), the pellet/beads dissolving in the medium flushing through (B), the coating dissolving with the polymer carried away by medium causing phase separation, exposing the ITR molecules which eventually leads to nucleation/crystallisation and precipitation (C, D).

A study has found that the ITR dissolution from Sporanox<sup>®</sup> was controlled by the dissolution of its HPMC matrix (341). The spray-dried layers of HPMC and ITR solid dispersion dissolved along with the erosion process. HPMC, the hydrophilic carrier of Sporanox<sup>®</sup> in this case acted as a precipitation inhibitor and prevented the plasticizer effect of the water molecules. Other studies also have shown that once the phase separation between HPMC and ITR occurred the nucleation and precipitation of ITR occur almost immediately (338, 339). In the event of phase separation, a colloidal dispersion of ITR in the aqueous dissolution medium was generated (observed as an opaque solution in Figure 32A) which eventually crystallised (332).

## Simulated fed state conditions

The cumulative % ITR dissolved from Sporanox<sup>®</sup> in FeSSGF/FeSSIF-V2 and FeSSGF/FeSSIF-V1 with USP apparatus 4 are presented in Figure 33.

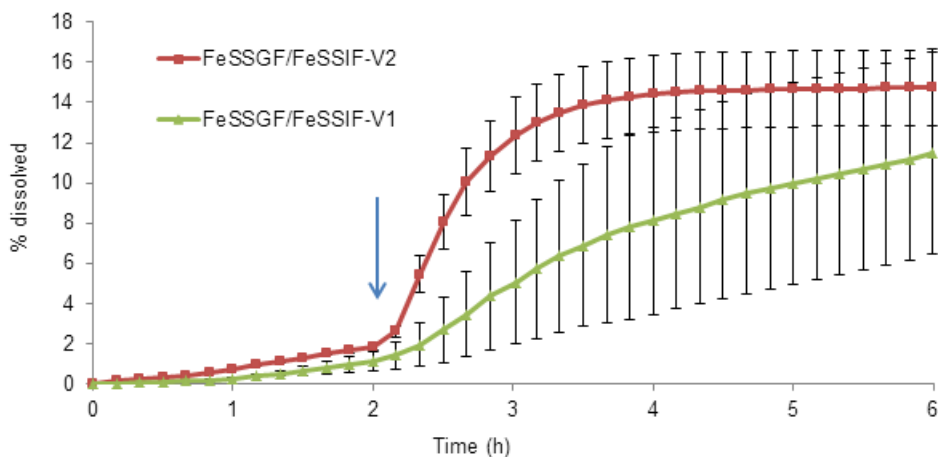


Figure 33. Mean $\pm$  SD % ITR dissolved from Sporanox<sup>®</sup> capsule in fed state media FeSSGF/FeSSIF-V2 and FeSSGF/FeSSIF-V2 (6mLmin<sup>-1</sup>; 2h/ 6mLmin<sup>-1</sup>; 4h) using the USP apparatus 4 (n=3). Blue arrow indicates time with media change.

In FeSSGF, designed to simulate the fed state conditions in the small intestine, the percentage of ITR dissolved is considerably low, with dissolution of the drug in the first 2 h of up to 1.83%. The observed slow and delayed ITR dissolution in FeSSGF could be due to the milk albumin or drug binding mechanism. The albumin could interact with ITR through hydrophobic and electrostatic interaction (342) as in the case with human serum albumin where ITR exhibited significant protein binding *in vivo* (99.8%) (343). There was a faster dissolution of ITR in FeSSIF-V2 compared with FeSSIF-V1. Also, the initial burst in FeSSIF-V2 was far greater than in FeSSIF-V1 (Figure 33) ( $f_{1,area}$ : 0.42). Apparently, the presence of 5mM of glyceryl monooleate in FeSSIF-V2 produced an enhancement in dissolution rate even though FeSSIF-V1 contains up to 50% more bile salts and lecithin than FeSSIF-V2. It is noteworthy that the high variation was observed in the FeSSGF/FeSSIF-V1 mainly due to one of the triplicate experiments showing much slower and lower dissolution.

## **Dissolution kinetics of profiles with USP apparatus 4**

### **Simulated fasted state conditions**

Swelling facilitates drug release and dissolution through Fickian diffusion, whereas erosion results in anomalous diffusion (co-dominated by both diffusion and polymer erosion in the release mechanism), and these have been reported as Case 1 (Higuchi model) and Case 2 transport (zero-order release) (274). A study has shown that the erosion process and diffusion through the gel layer (transfer of drug molecules into solution) are the main mechanisms that control the dissolution and release rate from coated beads (344). The ITR coated pellet is in the amorphous state before the dissolution experiment (244). To investigate the mechanism involved in the drug diffusion process (Fickian, non-Fickian, Case II or Super Case II transport), the dissolution data in simulating gastric and intestinal phases was fitted to the Power law equation (269) (Table 50). Similarly, the dissolution data in simulating gastric and intestinal phases was fitted with first order kinetic model and the whole profile was fitted with a single Weibull function (Table 50).

Table 50. Mean± SD dissolution kinetic parameters of ITR dissolved from Sporanox® 100mg capsule in simulating fasted state media using the USP apparatus 4 (n=3)

	SGF/SIF	FaSSGF/ FaSSIF- V1	FaSSGF/ FaSSIF-V2	SGF-M1/ SIF-M1	SGF-M1/ SIF-M2
First order kinetics (Gastric phase at first 1 h)					
Max (%)	-*	-*	-*	6.71± 0.19	8.50± 3.57
c (/h)	4.82X10 <sup>-3</sup> ± 2.53X10 <sup>-3</sup>	2.06X10 <sup>-3</sup> ± 9.19X10 <sup>-4</sup>	1.58X10 <sup>-3</sup> ± 2.94X10 <sup>-4</sup>	1.52± 0.32	1.40± 0.87
R <sup>2</sup>	0.99± 0.01	0.95± 0.01	0.95± 0.01	0.96± 0.01	0.97± 0.01
First order kinetics (Intestinal phase post 1 h)					
Max (%)	11.64± 2.65	30.48± 5.13	29.91± 11.62	62.60± 3.16	38.91± 2.66
c (/h)	0.40± 0.03	0.83± 0.25	0.78± 0.55	0.64± 0.04	0.39± 0.07
R <sup>2</sup>	0.99± 0.01	1.00± 0.00	0.99± 0.01	0.99± 0.01	0.97± 0.01
Single Weibull function (Whole profile)					
Max(%)	10.50± 2.09	28.36± 5.73	20.99± 0.58	60.16± 2.72	37.83± 2.99
a (h)	0.59± 0.06	0.59± 0.06	0.55± 0.07	5.69± 0.35	3.37± 0.03
b	1.73± 0.18	2.35± 0.35	2.51± 0.12	1.92± 0.14	1.23± 0.06
R <sup>2</sup>	0.99± 0.00	0.99± 0.00	0.99± 0.00	0.98± 0.00	0.98± 0.01
Power law kinetics (Gastric phase at first 1 h)					
Rate (unit-less)	10.31± 1.29	37.36± 9.27	21.09± 1.06	37.55± 15.72	8.37± 2.01
Exponential (unit-less)	1.30± 0.14	2.37± 0.23	1.99± 0.04	2.43± 0.47	1.21± 0.14
R <sup>2</sup>	1.00± 0.00	1.00± 0.00	0.97± 0.01	1.00± 0.00	0.97± 0.01
Power law kinetics (Intestinal phase post 1 h)					
Rate (unit-less)	13.79± 2.38	26.06± 6.51	20.95± 0.63	32.54± 2.95	21.28± 2.03
Exponential (unit-less)	0.10± 0.06	0.14± 0.05	0.13± 0.11	0.70± 0.04	0.44± 0.04
R <sup>2</sup>	0.98± 0.01	1.00± 0.00	0.99± 0.01	1.00± 0.00	0.99± 0.01

\* the model could not fit the data satisfactorily

The first 60min of the dissolution curve (in fasted state simulating gastric condition) obeyed the Power law model. The analysis of the release mechanism in SGF, FaSSGF and SGF-M1 followed Super Case II transport ( $n > 0.85$ ) which implied that ITR dissolution in these media could have occurred by a combination of several processes like diffusion, swelling of HPMC component (polymer relaxation), and erosion of the HPMC matrix.

The Power law kinetic constants ( $k$ ) (Table 50) show that initial dissolution rates occur in the following sequence: FaSSGF > SGF > SGF-M1 (simulating gastric state with USP 4 apparatus) and SIF-M1 > FaSSIF-V1 > SIF-M2 > FaSSIF-V2 > SIF (simulating intestine state with USP apparatus 4). The trends are in agreement with the concept that the kinetics constant increases with increasing total solubility of the matrix (269).

In Fickian diffusion the solvent diffusion rate is slower than the polymer relaxation rate and the increase of kinetics constant ( $k$ ) reflects the decrease of the disorder of the medium (274). The sequential change of medium and flow rate simulating intestinal conditions after 60min with USP apparatus 4 lead to dissolution associated with diffusion controlled release in SIF and FaSSIF-V1 and -V2 ( $n$ , exponent  $< 0.43$ , Fickian diffusion). The kinetic modeling also shows that the dissolution mechanism transformed to Fickian diffusion of ITR through the HPMC matrix upon changing to SIF and FaSSIF-V1 and -V2 concurrently, with a reduction in flow rate from 8 mL/min to 4 mL/min. It indicated that the amorphous matrix had transformed to a rubbery state. This was due to the fact that the polymer is in a rubbery state and polymer chains have a higher mobility that allows easier penetration of the solvent. Furthermore, water acts as a plasticizer, and its presence has caused a decrease of the polymer glass transition temperature ( $T_g$ ) (345). The exponent,  $n$ , increases as the solubilisation capacity of the surfactant/micelle increases (Table 50). This may be attributed to the fact that as the HPMC and drug matrix swelled, the soluble drug was also removed by the micelle systems, thus decreasing the resistance of the gel layer to diffusion of the drug (269). These findings suggest that the nature of the soluble fraction of the tablet is as important a factor as the drug loading (269). On the other hand, the exponent constant ( $n$ ) data indicated mixed mechanism of diffusion and erosion controlled release ( $0.43 < \text{exponent} < 0.85$ ; non-Fickian) in SIF-M1 and SIF-M2. In the dissolution of the polymeric system the polymer chains are not sufficiently mobile to permit immediate penetration of the solvent into the polymer core. This could lead to a non-Fickian diffusion process which also includes anomalous diffusion whereby the rate of diffusion is close to the rate of polymer relaxation.



Meanwhile, application of first order kinetic models in the analysis of dissolution data (simulating gastric phase) shows that the mean first order rate constant is in the following sequence: SGF-M1/SIF-M2> SGF-M1/SIF-M1> FaSSGF/FaSSIF-V2> FaSSGF/FaSSIF -V1> SGF/SIF. This is strongly supportive of the effect of SLS (in SGF-M1) and bile salt and lecithin (in FaSSGF). Likewise, the mean first order rate constant (simulating intestinal phase) is in the following sequence: SGF-M1/SIF-M2> SGF/SIF> SGF-M1/SIF-M1> FaSSGF/FaSSIF-V2> FaSSGF/FaSSIF-V1. It shows that SIF-M2 could allow faster ITR dissolution compared to other media.

### Simulated fed state conditions

The dissolution profiles of ITR from Sporanox<sup>®</sup> 100mg capsule in simulating fed state media using the USP apparatus 4 were fitted well with Power law, first order, and single Weibull kinetics models. The fitted parameters are presented in Table 51 and 52.

Table 51. Mean± SD dissolution kinetic parameters (first order and Power law with gastric and intestinal phase) of ITR from Sporanox<sup>®</sup>

	Gastric phase at first 2 h		Intestinal phase post 2 h	
	FeSSGF/ FeSSIF-V1	FeSSGF/ FeSSIF-V2	FeSSGF/ FeSSIF-V1	FeSSGF/ FeSSIF-V2
First order kinetics				
Max (%)	-*	-*	60.49±76.42	14.80±1.85
c (h)	8.36x10 <sup>-4</sup> ±6.59x10 <sup>-4</sup>	1.67x 10 <sup>-3</sup> ±6.18x10 <sup>-4</sup>	0.36±0.34	1.89±0.17
R <sup>2</sup>	0.93±0.06	0.98±0.01	1.00±0.00	1.00±0.00
Power law kinetics				
Rate (unit-less)	0.28±0.04	0.78±0.04	5.00±3.02	11.94±1.80
Exponential (unit-less)	1.96±0.62	1.25±0.14	0.82±0.07	0.64±0.03
R <sup>2</sup>	1.00±0.00	1.00±0.00	0.99±0.00	0.96±0.01

\*the model could not fit the data satisfactorily

Table 52. Mean± SD dissolution kinetic parameters (single Weibull with whole curve) of ITR dissolved from Sporanox

	FeSSGF/FeSSIF-V1	FeSSGF/FeSSIF-V2
Single Weibull function		
Max (%)	14.51±1.84	11.65±3.64
a (h)	264.76±142.06	63.79±9.93
b	5.60±0.63	3.05±0.59
R <sup>2</sup>	1.00±0.00	1.00±0.00

The dissolution data in simulating gastric and intestinal condition was fitted to the Power law equation (269). The dissolution profiles obeyed the Power law model. The kinetic constants show that ITR initial dissolution rates in FeSSIF-V2 are higher than in FeSSIF-V1 (simulating intestinal stage with USP 4 apparatus).

The mean value of n changed from 1.96± 0.62 (in FeSSGF) to 0.82± 0.07 (in FeSSIF-V1) and from 1.25± 0.14 (in FeSSGF) to 0.64± 0.03 (in FeSSIF-V2). It indicates that with the change of medium and hydrodynamics, release mechanism shifted from Super Case 2 release ( $n > 0.85$ ) to non-Fickian release ( $0.43 < n < 0.85$ ).

Interestingly, the dissolution of ITR in FeSSIF-V1 with USP apparatus 4 at 6 mL/min is very close to zero order kinetic (mean,  $n=3$ , Power law exponent parameter is  $0.82 \pm 0.07$ ). From a kinetic viewpoint, the term “zero-order release” occurs when the transport of a drug is sustained at a constant thermodynamic activity gradient across the diffusional layer for an extended period of time (under steady state conditions) (346). Furthermore, Korsmeyer *et al.* suggested that zero order kinetic (Case 2 transport) is a case of anomalous (non Fickian) diffusion, in which a solvent front penetrates the initially glassy polymer at a constant velocity (269). At high coating levels the drug is forced to diffuse through the membrane. The coating layers effectively seal the pores and channels in the coating. Hence dissolution of the drug from coated beads exhibits zero release.

The dissolution mechanism is more erosion driven in FeSSIF-V1 because the Power law exponential (n) is  $0.82 \pm 0.07$  and closer to Super Case II transport compared with more diffusion driven in FeSSIF-V2 ( $n: 0.64 \pm 0.03$ ). It is proposed that the higher concentration of lecithin and bile salt in FeSSIF-V1 affects also the characteristic of the

HPMC system found in the Sporanox<sup>®</sup> pellet. The high viscosity in the pellets retards the diffusion of the drug at the early stages of release in FeSSIF-V1. At the later stages of release the polymer solution becomes dissipated and resistance to diffusion is decreased. The net effect of this process is a decrease in release rate, which is normally observed as the drug concentration in the drug content within the flow through the cell decreases (269).

The role of a polymer such as HPMC in controlling drug release is determined by its hydration, swelling and dissolution. The latter process involves steps including absorption or adsorption of water at the most accessible sites on the polymer, breaking of polymer–polymer bonds via the creation of water–polymer bonds, separation of the polymer chains and finally dispersion of the polymer chains in the dissolution media (345). It seems that the polymer relaxation (swelling of HPMC) was less complete after 2 h (at 6mL/min) in viscous colloidal solution (FeSSGF; Table 51) than 1 h in FaSSGF solution (at 4mL/min; results as shown in Table 50). Therefore kinetic fitting using the Power law shows that drug release and dissolution of ITR from Sporanox<sup>®</sup> are affected by the rate of dissolution of the API, the diffusion through the coating polymer as well as gelling, swelling and erosion of the coating polymer.

In this study, first order and single Weibull kinetic models were also applied to analyse the ITR dissolution data (simulating fed state). From the perspective of the ITR dissolution rate, the first order rate constant and time scale parameter of a single Weibull function showed that a higher rate was achieved in FeSSGF/FeSSIF-V2 compared to FeSSGF/FeSSIF-V1. Furthermore, the shape factor of the Weibull function also implies that the curve shape of FeSSGF/FeSSIF-V2 is steeper (in terms of sigmoidal curve) than FeSSGF/FeSSIF-V1. The results indicate that FeSSIF-V2 which contains lipolytic products caused at least 4 times the increment of the dissolution rate compared to FeSSIF-V1.

### **3.3.5 Simulation of physiological relevant *in vivo* precipitation**

It is generally believed that the drug precipitation in the GIT affects the drug absorption. This is especially true for weakly basic drugs that have a high solubility in the gastric medium but low solubility at high pH values (347). ITR, a weak base has shown a high solubility and dissolution rate in the acidic environment of the stomach (Figure 34). It is possible that as it moves down the GIT and the pH rises, its solubility and dissolution rate decreases and it may precipitate out. This possible *in vivo* precipitation was

investigated using a drug precipitation study design with USP apparatus 4, in which the drug precipitation was calculated when the media was changed from simulated gastric to simulated intestinal media.

The % of dose and sample precipitated after media change with USP apparatus 4 are shown in Figure 34.

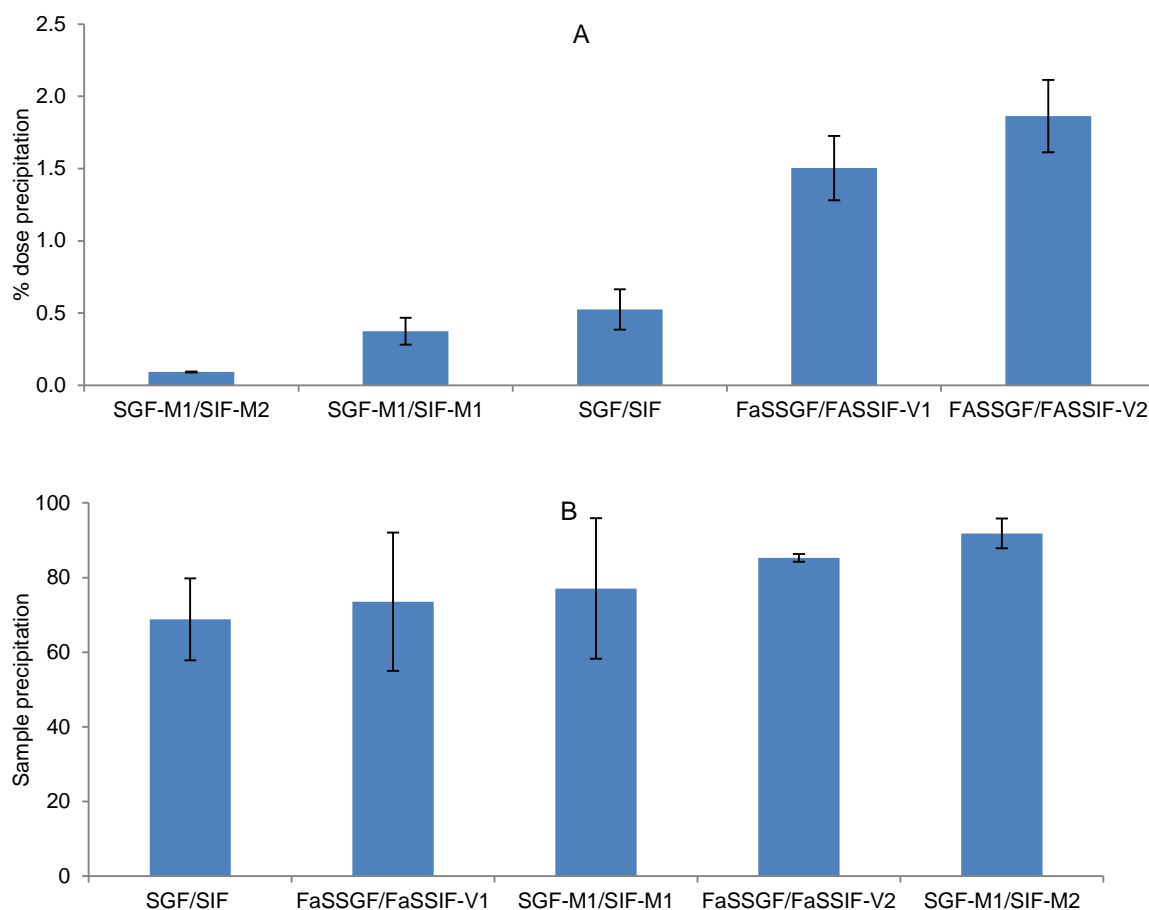


Figure 34. (A) Mean  $\pm$  SD % dose precipitation of ITR from Sporanox<sup>®</sup> with various media with USP apparatus 4; (B) Sample precipitation at 70 min.

The solubility of ITR is 3.9  $\mu\text{g/mL}$  in SGF in contrast to 0.003  $\mu\text{g/mL}$  in SIF (219). Precipitation of the ITR occurred during a change of media from 1.2 to 6.8. The precipitation level is mainly controlled by two factors, the solubility of ITR in the gastric and intestinal phase and the composition of the medium simulating intestinal phase. The better solubility of ITR with SIF-M1 and SIF-M2 caused lower precipitation of ITR from the Sporanox<sup>®</sup> capsule. Interestingly, the higher solubility of ITR in SGF leading to lower precipitation in SIF and the lower solubility of ITR in FaSSGF compared to the one in SGF caused higher precipitation even though both FaSSIF-V1 and FaSSIF-V2 contain bile salt and lecithin that could solubilise ITR better. The results suggested that

pH is the more dominant factor influencing the precipitation compared with the micellar solubilisation with bile salt and lecithin.

### 3.4 Results and Discussion of Part 1: *In vitro* dissolution testing (CX)

#### 3.4.1 Dissolution testing in USP apparatus 2

Compound X (CX) is a highly lipophilic, poorly soluble compound. CX has weak acidic (pKa 10) functional groups and its pKa at 10 renders it essentially neutral under the GI physiological pH range. Due to its high lipophilicity (log P= 5.42) its solubility is very low (less than 5 µg/mL in water and SGF and 40 µg/mL in FaSSIF-V1) (252). Owing to the extremely low solubility and dissolution of CX in media such as FaSSGF, FaSSIF-V2 analysis with USP apparatus 2 (a closed dissolution system) was not performed. In this case the use of a surfactant is necessary in order to facilitate the characterisation of the CX dissolution profile.

The cumulative % of dissolved CX from CX F8 in FeSSGF and SIF-M4 and –M5 with USP apparatus 2 are presented in Figure 35.

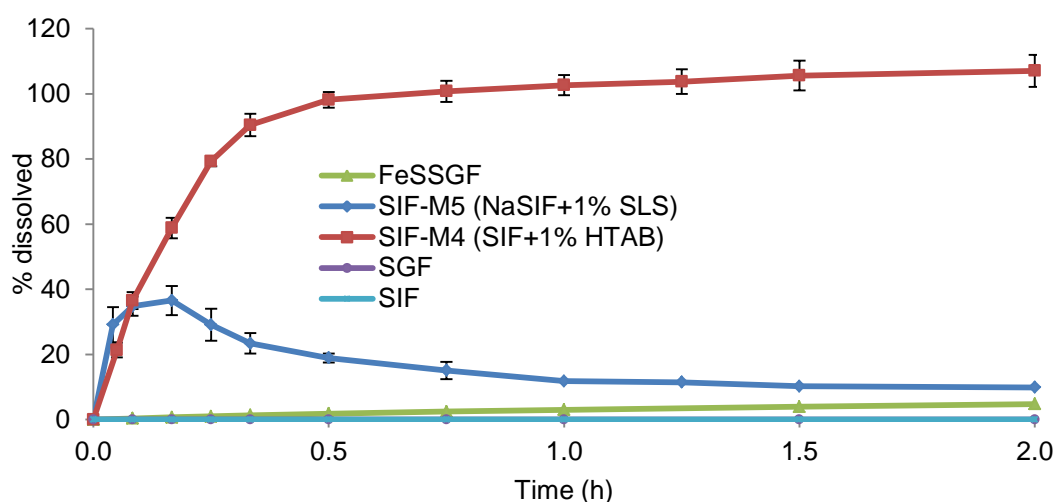


Figure 35. Mean± SD % CX dissolved from CX formulation (F8) with various media with USP apparatus 2 (500 mL medium, 37°C, 75 rpm).

Dissolution of CX from CX formulation (F8) in FeSSGF, which is the acetate buffer solution containing 50% milk, is 4.7% at 2 h. Considering that the dissolution was almost zero in SGF and SIF under the same conditions (Figure 35), the composition of milk seems better able to solubilise this highly lipophilic compound compared to SGF and SIF. Shono *et al.* proposed that poorly water soluble drugs could possibly be incorporated into casein micelles (55). However, it must be noted that casein micelles have a net negative charge and are quite stable in the usual pH of milk (pH 6.6). The

isoelectric point (IEP; the pH at which the protein is least soluble and is precipitated) of casein is approximately 4.6 (348) a value very close to the pH of FeSSGF (pH 5.0). Therefore it is highly probable that the casein precipitated in FeSSGF and hence the main mechanism of the solubilisation of CX in milk is through emulsification by milk lipids and fat globules. This is supported by the dissolution profile closely following a first order kinetic model where the drug dissolution depends on the amount of drug remaining.

### 3.4.2 2 stage dissolution studies

The cumulative % of dissolved CX from CX formulation (F8) with 2 stage dissolution experiments with USP apparatus 2 are presented in Figure 36.

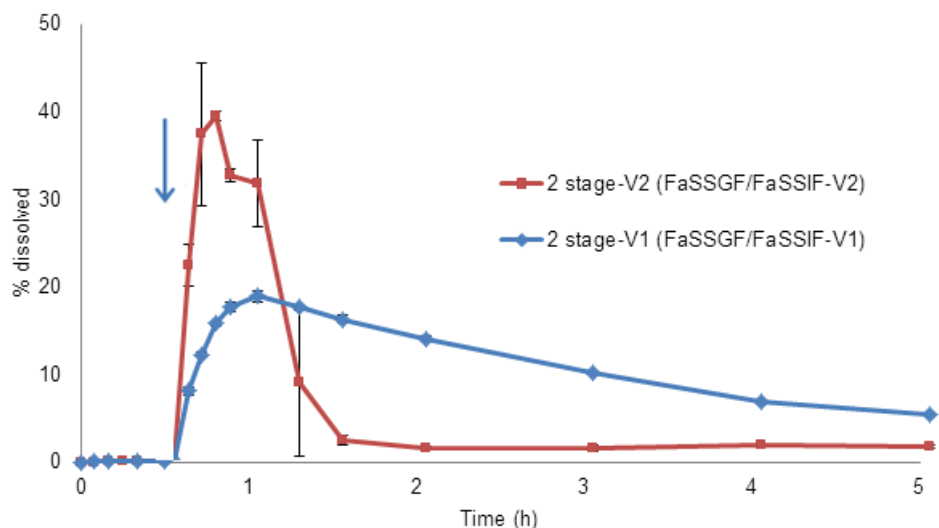


Figure 36. Mean $\pm$  SD % CX dissolved from CX formulation (F8) using 2 stage dissolution, 250 mL FaSSGF for 30min/500 mL FaSSIF-V1 or -V2 with USP apparatus 2 (500 mL medium, 37 °C, 75 rpm). Blue arrow indicates time with media change. Gap after media change indicates short pause of paddle rotation.

A high percentage of CX was dissolved after medium change and maintained up to 1 h before the precipitation rate exceeded the dissolution rate of CX, leading to a fast descending dissolution curve. This solid dispersion formulation exhibited the so-called “spring” and “parachute” dissolution profile (29). The amorphous compound served as the “spring” that brings the dissolved drug concentration above the equilibrium solubility and the polymer (precipitation inhibitor) served as a “parachute”, slowly settling down the concentration to the equilibrium solubility.

Dissolution of CX in FaSSGF (in the first 0.5 h) was almost zero (Figure 62). Upon the medium change to FaSSIF-V1 or FaSSIF-V2 a marked increase in dissolution occurred. The extent and rate of dissolution was much higher in FaSSIF-V2 than in FaSSIF-V1. This is mainly due to the change of the properties and capacity of the lecithin/bile salt micelle which is influenced by the ionic strength of the medium (349).

### 3.4.3 Dissolution testing in USP apparatus 4

#### Simulated fasted state conditions

The cumulative % of dissolved CX from CX formulation in modified media (F8), FaSSGF/FaSSIF-V1 (F8) and FaSSGF/FaSSIF-V2 (F4-F8) are presented in Figure 37. Formulation 8 of CX was tested in all conditions (modified media, FaSSGF/FaSSIF-V1 and FaSSGF/FaSSIF-V2) to characterise its dissolution profiles in these media. Furthermore, formulation 4, 5, 6 and 7 of CX were also tested in FaSSGF/FaSSIF-V2 to study the formulation effects on dissolution of CX.

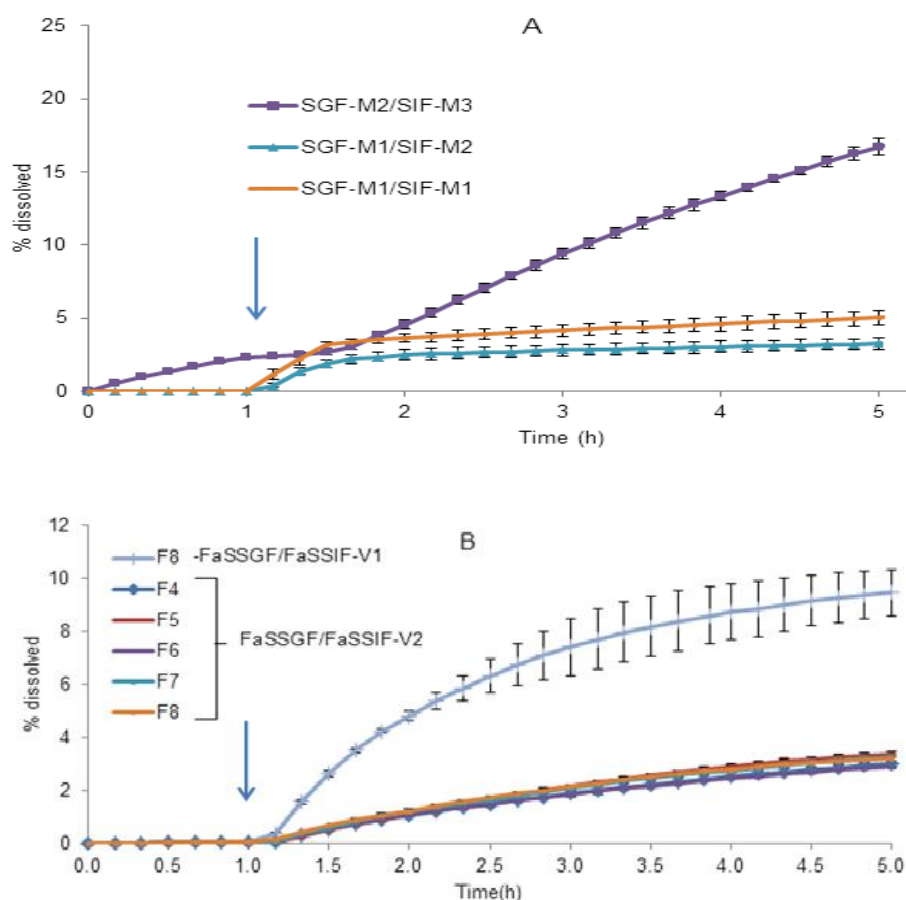


Figure 37. Mean  $\pm$  SD % CX dissolved from CX formulations (A): modified media (B):F4-F8 with FaSSGF/FaSSIF-V2 and F8 with FaSSGF/FaSSIF-V1 (8 mL/min; 1 h; 4 mL/min; 4h) using the USP apparatus 4 (n=3). Blue arrow indicates time with media change.



The dissolution of CX in simulated gastric media was extremely poor mainly due to the fact that the polymer used in CX solid dispersion formulation is HPMCAS, which does not dissolve in an acidic medium. On the other hand, when media were changed to simulated intestinal fluids (SIF-M3, FaSSIF-V1 and FaSSIF-V2), the dissolution of CX increased gradually with the modified media with 0.1% HTAB (SIF-M3) yielding 16.73% CX dissolved; whereas, in FaSSIF-V1 and V2 less than 10% and 5% of CX were dissolved at 5 h, respectively.

Immediately after the medium change to simulated intestinal media with a physiological amount of SLS (SIF-M1 and SIF-M2), the presence of SLS micelle with high solubilisation capacity was able to solubilise CX molecules available in the system thereby producing a sudden increase of dissolution. Due to twice higher the content of SLS in SIF-M1 (0.2%) than in SIF-M2 (0.1%) the dissolution of CX is almost double in the SIF-M1 compared to SIF-M2.

Comparing FaSSGF/FaSSIF-V1 and FaSSGF/FaSSIF-V2 (F8), it is obvious that FaSSIF-V1 solubilises CX better than FaSSIF-V2. A sharper rise in the FaSSIF-V1 phase seems to suggest that a mixed micelle of bile salt and lecithin in FaSSIF-V1 has a better solubilisation capacity. The lower ratio of bile salt: lecithin (4:1) in FaSSIF-V1 vs 15:1 in FaSSIF-V2 proved to be superior for dissolution of this poorly soluble compound with USP apparatus 4 (open system). In the open dissolution system, fresh FaSSIF-V1 containing mixed micelle of bile salt and lecithin was able to solubilise the drug molecules and 9.5% of the drug was dissolved after 5h. Profile comparison among different CX formulations (F4, F5, F6, F7 and F8) with FaSSGF/FaSSIF-V2 shows that these profiles are similar ( $f_{1,area}$ =F4: 0.08 F5:0.06, F6:0.07, F7:0.08, F8 as reference formulation). It must be stressed that a medium with a non-physiological surfactant such as HTAB could potentially mask supersaturation of the amorphous form especially under non-sink conditions (350). Supersaturation of the CX from its amorphous formulation was clearly observed in FaSSIF-V1 that was not apparent in SIF-M3 (CX solubility in SIF-M3 of 480 µg/mL (233) is not shown in Figure 38 due to the high scale value for clarity in the graph). Therefore, FaSSIF-V1 is superior for characterising the dissolution profile of CX. Literature has also suggested that FaSSIF-V1 can be a useful tool for examining the dissolution profile of CX (249).

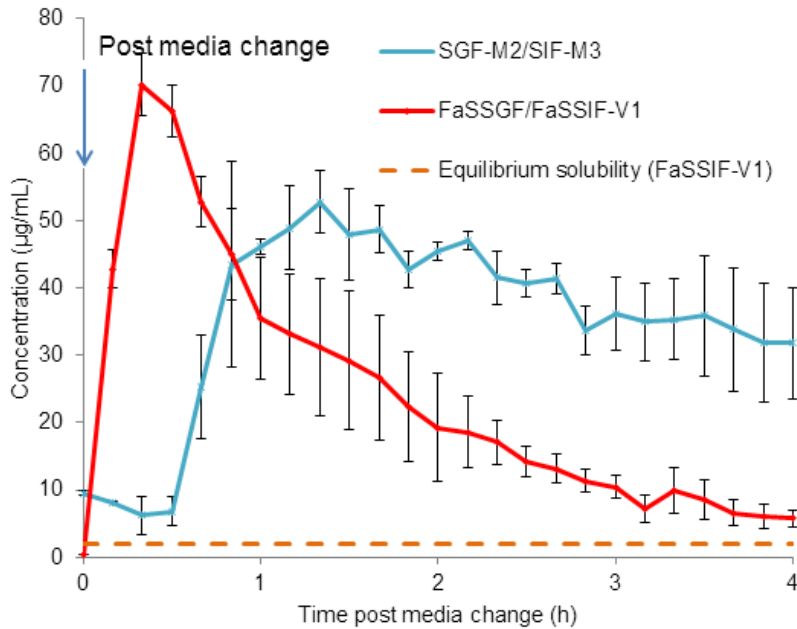


Figure 38. Mean  $\pm$  SD % CX concentration yielded from CX formulation in post media change (SGF-M2/SIF-M3, FaSSGF/FaSSIF-V1 (8mL/min 1 h then 4 mL/min; 4 h) using the USP apparatus 4 (dissolution profiles were presented in Figure 38). Equilibrium solubility of each media is shown except SIF-M3, 480  $\mu$ g/mL. Blue arrow indicates time with media change.

### Simulated fed state conditions

The cumulative percentage dissolved of CX from CX formulation (F4-F8) in FeSSGF/FeSSIF-V2 and FeSSGF/FeSSIF-V1 with USP apparatus 4 is presented in Figure 39.

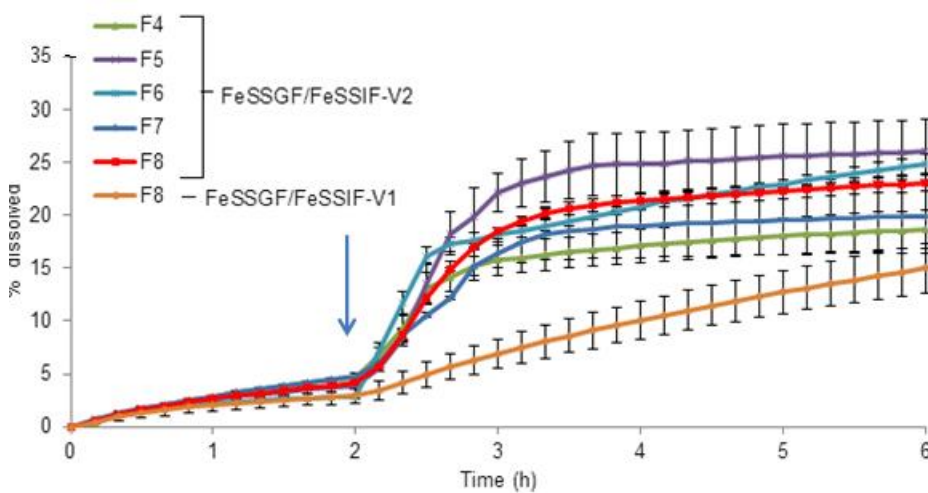


Figure 39. Mean  $\pm$  SD % of CX dissolved from CX tablet in fed state media FeSSGF (6 mL/min; 2 h)/ FeSSIF-V1 or -V2 (6 mL/min; 4 h) using the USP apparatus 4 (n=3). Blue arrow indicates time with media change.

Drug solubility and dissolution can be considerably enhanced in the mixed micelles found in GIT and especially fatty substances and products of fat digestion (lipolytic product) such as monoglycerides and fatty acids (57). Studies have confirmed that the combination of bile salt and monoglycerides in the medium could increase the dissolution and capacity for supersaturation for a poorly soluble compound (351). Furthermore, partitioning of poorly soluble drugs between the different colloidal phases (mixed micelles and vesicles) formed in aqueous media containing bile acids and phosphatidylcholine with the addition of monoglycerides and free fatty acids could also greatly increase drug dissolution (352).

Similar to the FaSSGF/FaSSIF-V1 and -V2 dissolution profile, immediately after the medium change to simulate fed state intestinal media, there is an apparent increase of CX dissolution. These results again indicate that the bile salt, lecithin and lipolytic products found in FeSSIF-V2 have a significant effect on CX dissolution. It is interesting to note that the percentage of CX dissolved in FeSSIF-V2 is 15% higher than in FeSSIF-V1, a pattern that was observed also in the ITR dissolution profile (another model drug used in this project). For the purposes of profile comparison, in agreement with the comparison in FaSSGF/FaSSIF-V2, for the dissolution studies with different formulations (F4, F5, F6, F7 and F8) the profiles are deemed to be similar ( $f_{1,area}$ =F4:0.14, F5:0.0.13, F6:0.09, F7: 0.10, F8 as a reference compound).

## **Dissolution kinetics of profiles with USP apparatus 4**

### **Simulated fasted state conditions**

HPMCAS (an enteric polymer) consists of more than 50% of the bulk content of the CX tablet (235). It must be noted that due to its high polymer content, the dissolution behaviour tend to be influenced and affected by the polymer (HPMCAS) used. When placed in medium with a pH greater than 4, HPMCAS would dissolve and act as the water-filled pores (251). A study has also shown that drug molecules diffuse through pores and channels in the membrane according to first order kinetics (251). In agreement with that, the dissolution profiles of CX formulations all fitted well with a first order kinetics model. For comparison purposes, the dissolution profiles were also fitted with a single Weibull function. The fitted parameters of CX dissolved from CX formulations in simulated fasted state media using the USP apparatus 4 (n=3) are presented in Tables 53 and 54.

Table 53. Mean± SD dissolution kinetic parameters (first order with intestinal phase and single Weibull function) of CX from CX formulations with biorelevant media

	FaSSGF/ FaSSIF-V2 (F4)	FaSSGF/ FaSSIF-V2 (F5)	FaSSGF/ FaSSIF-V2 (F6)	FaSSGF/ FaSSIF-V2 (F7)	FaSSGF/ FaSSIF-V1 (F8)	FaSSGF/ FaSSIF-V2 (F8)
First order (Intestinal phase post 1 h)*						
Max (%)	4.74± 0.21	6.20± 0.84	4.25±0.54	4.99±1.25	10.43±1.48	4.47±0.36
c (/h)	0.25± 0.01	0.21±0.04	0.30±0.05	0.29±0.10	0.61± 0.05	0.33±0.03
R <sup>2</sup>	1.00± 0.00	1.00± 0.00	1.00± 0.00	1.00±0.00	0.99± 0.00	1.00±0.00
Single Weibull function						
Max (%)	3.05±0.11	3.40±0.16	2.98±0.16	3.27±0.23	9.06±0.94	3.23±0.17
a (h)	12.95±0.88	15.93±0.93	11.30±0.74	12.45±3.28	9.26±2.28	11.33±0.88
b	2.30±0.16	2.52±0.04	2.20±0.07	2.31±0.19	2.58±0.31	2.31±0.06
R <sup>2</sup>	0.99±0.00	1.00±0.00	0.99±0.00	0.99±0.00	0.99±0.01	1.00± 0.00

Table 54. Mean± SD dissolution kinetic parameters (first order with intestinal phase and single Weibull function) of CX from CX formulations with modified media

	SGF-M1/SIF-M1	SGF-M1/SIF-M2	SGF-M2/SIF-M3
First order kinetics (Intestinal phase post 1 h)*			
Max (%)	11.69± 8.19	3.21± 0.16	71.71± 28.69
c (/h)	0.08± 0.05	0.18± 0.05	0.07± 0.06
R <sup>2</sup>	1.00± 0.00	0.98± 0.01	1.00± 0.00
Single Weibull function			
Max (%)	4.12±0.43	2.79±0.38	59.08±37.32
a (h)	8.33±3.17	9.11±1.84	27.97±16.09
b	5.78±1.76	5.28±0.66	1.43±0.13
R <sup>2</sup>	0.97±0.00	0.98±0.00	1.00± 0.00

(\*Due to the extremely low dissolution (less than 2%) of CX formulation in the simulated gastric phase (SGF-M1, SGF-M2 and FaSSGF) only the dissolution profiles in the simulated intestinal phase were characterised)

The application of a first order kinetics and single Weibull model in the analysis of dissolution data shows that the mean values of maximum percentage dissolved (Max) followed the sequence of SGF-M2/SIF-M3>SGF-M1/SIF-M1 >FaSSGF/FaSSIF-V1 > FaSSGF/FaSSIF-V2> SGF-M1/SIF-M2. This indicates that HTAB-based modified

media (SGF-M2/SIF-M3) have greater solubility capacity for CX than SLS-based modified media and biorelevant media.

According to the first order kinetic model, the first order rate constant suggested that the dissolution rates are FaSSGF/FaSSIF-V1 > FaSSGF/FaSSIF-V2 > SGF-M1/SIF-M2 > SGF-M1/SIF-M1 > SGF-M2/SIF-M3. The results clearly show that FaSSIF-V1 and FaSSIF-V2 which contain physiological surfactants (bile salt and lecithin) gave a faster dissolution rate. However, the biorelevant micelle system has less solubilisation capacity compared to an artificial surfactant such as SLS and HTAB.

The dissolution profiles of CX formulations (F4, F5, F6, F7 and F8) in FaSSGF/FaSSIF-V2 show quite similar first order rate constant and maximum percentage dissolution. Likewise, the Weibull fitting also shows a very similar value of time scale and shape factor parameters. For example, the shape factor parameters (b) range from 2.20-2.58. This can be attributed to the fact that the CX formulations tested (F4-F8) do not vary much in the critical manufacturing attributes thus it is expected that the dissolution profiles would be very similar. The Max values show the same rank order according to the particle size distribution of CX proprietary microprecipitated bulk powder (MBP). The radius of MBP in the formulation of CX is F5 (37.2  $\mu\text{m}$ ) > F4 (48  $\mu\text{m}$ ) > F6 (60.9-64.9  $\mu\text{m}$ ) (Compositions presented in Section 2.3.3). It is generally accepted that the dissolution rate is proportional to the particle size of the powder (353, 354), indicating the importance of particle size as a critical manufacturing variable that indirectly affects the absorption of poorly soluble drugs. However, the rank order of Max does not translate into the ranking of first order rate constant between F4, F5 and F6. This could be due to the fact that the difference in particle size is too small to be discriminated in an *in vitro* experiment. For instance, literature indicates that the dissolution rate for a micronised particle would not be affected even by changing the stirring conditions because the thickness of the boundary layer is too small (355). Furthermore during dissolution, the volume of a particle decreases at a faster rate than the surface area. Thus, surface area is one of the critical factors affecting dissolution especially for relatively small particle sizes like the MBP for CX (249).

### **Simulated fed state conditions**

Similar to the dissolution profiles of CX from CX formulations (F4-F8) of the simulated fasted state conditions, the dissolution profiles of the simulated fed state conditions were fitted well with a first order kinetic and single Weibull model. The fitted parameters

of CX dissolved from CX formulations in simulated fed state media using the USP apparatus 4 (n=3) are presented in Table 55.

Table 55. Mean± SD dissolution kinetic parameters (first order with gastric and intestinal phase and single Weibull function) of CX from CX formulations

	FeSSGF/ FeSSIF-V2 (F4)	FeSSGF/ FeSSIF-V2 (F5)	FeSSGF/ FeSSIF-V2 (F6)	FeSSGF/ FeSSIF-V2 (F7)	FeSSGF/ FeSSIF-V2 (F8)	FeSSGF/ FeSSIF-V1 (F8)
First order kinetics (Gastric phase first 2 h)						
Max (%)	7.69± 0.60	4.41± 0.63	2.96± 0.24	8.63± 0.60	5.92± 0.65	3.64± 0.32
c (h)	0.47± 0.06	0.99± 0.12	1.56± 0.20	0.40± 0.04	0.59± 0.04	0.88± 0.31
R <sup>2</sup>	1.00± 0.00	1.00± 0.00	1.00± 0.01	1.00± 0.02	1.00± 0.03	1.00± 0.04
First order kinetics (Intestinal phase post 2 h)						
Max (%)	18.55± 1.67	26.35± 3.02	23.37± 0.09	19.24± 2.58	22.85± 0.67	16.19± 1.69
c (h)	1.47± 0.05	1.50± 0.00	1.49± 0.02	1.81± 0.46	1.50± 0.01	0.53± 0.07
R <sup>2</sup>	0.88± 0.04	0.97± 0.01	0.85± 0.04	0.66± 0.57	0.99± 0.00	0.96± 0.01
Single Weibull function						
Max (%)	18.05± 1.65	25.36± 2.90	22.82± 0.88	19.68± 3.24	22.27± 0.77	24.96± 8.21
a (h)	16.81± 4.72	174.84± 93.22	40.77± 22.47	27.96± 13.50	52.99± 20.72	17.95± 2.05
b	3.06± 0.38	5.19± 0.57	3.71± 0.81	3.34± 0.37	3.97± 0.42	1.62± 0.25
R <sup>2</sup>	0.98± 0.00	0.99± 0.00	0.97± 0.00	0.98± 0.01	0.99± 0.00	0.99± 0.00

Like the FaSSGF/FaSSIF-V2 dissolution profiles of CX formulations (F4, F5, F6, F7 and F8), FeSSGF/FeSSIF-V2 show a fairly consistent time scale parameter of single Weibull function and maximal percentage dissolution apart from the one tested using Formulation 5. Higher dissolution rate and extent achieved in Formulation 5 could be due to its smaller PSD of 37.2 µm compared to other formulations that range from 48.0- 64.9 µm. Likewise, the Weibull fitting also shows a very similar time scale and shape factor parameters. For example, the shape factor parameters (b) range from 3.06-3.97 except 5.19 from Formulation 5. This shows that FeSSGF/FeSSIF-V2 is a

more discriminating testing media compared to FaSSGF/FaSSIF-V2 because FeSSGF/FeSSIF-V2 could differentiate Formulation 5 with other formulations.

The Max values show the same rank order according to the particle size distribution of CX proprietary microprecipitated bulk powder (MBP). The radius of MBP in the formulation of CX is F5 >F4> F6 (Compositions presented in Section 2.3.3). The application of a first order kinetics and single Weibull function in the analysis of this dissolution data showed that the mean values of Max in FeSSGF/FeSSIF-V2 is higher than in FeSSGF/FeSSIF-V1. On the same note, the dissolution rate fitted using first order and Weibull model (in the intestinal phase) is almost 3 times higher in FeSSGF/FeSSIF-V2 compared to FeSSGF/FeSSIF-V1.

### 3.4.4 Simulation of physiological relevant *in vivo* precipitation

CX has shown a very low solubility and dissolution rate across the physiological pH in the GIT, reflected also in the drug precipitation after media change. *In vitro* precipitation was observed due to the properties of the compound and its formulation effect. The whole dissolution setups are designed based on the physiological conditions (pH, media and hydrodynamics used); thus, similar *in vivo* precipitation could also be observed. The percentage of dose precipitation after media change with USP apparatus 4 is shown in Figure 40.

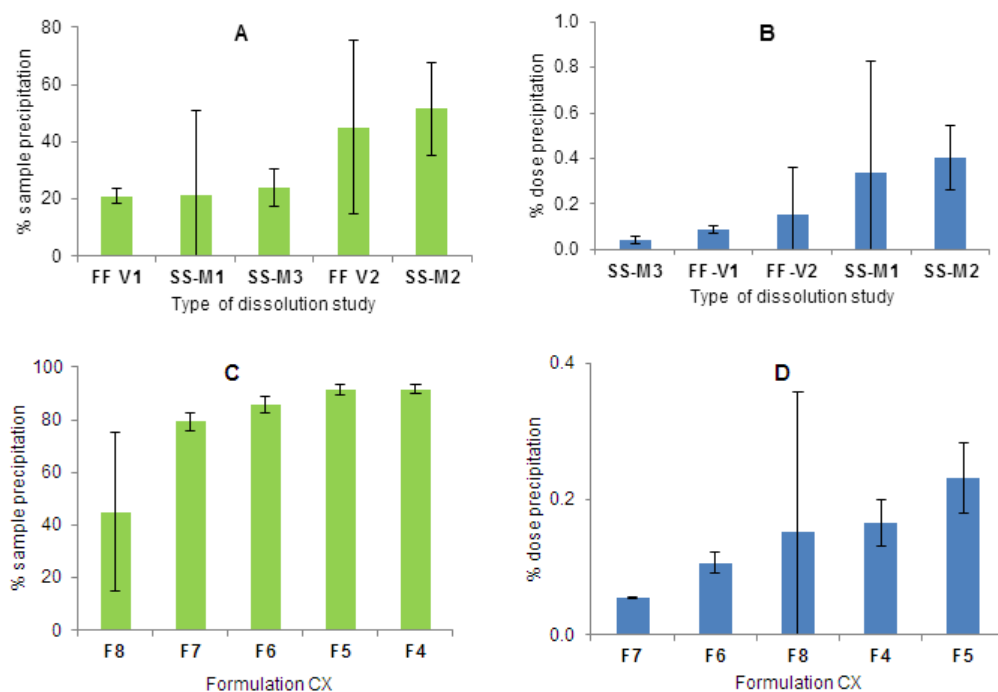


Figure 40. Mean± SD % precipitation (A: sample precipitated; B: dose precipitated) of CX from its formulations in various media with USP apparatus 4. Graphs C and D show precipitation from FaSSGF/FaSSIF-V2 (FF: FaSSGF/FaSSIF; SS: SGF-M1/SIF).

Drug precipitation after media and flow rate change ranged from 20% to 90% in the sample collected, which accounted for less than 1% of the dose tested (240 mg of CX per tablet). Relatively higher dose precipitation was observed after change of medium using modified compendial media with SLS and less with HTAB. This is in agreement with the dissolution results of the modified media with SLS, that reported fast precipitation compared to media with HTAB (Figure 40). The high variability observed in some experiments was mainly due to the difference in the dispersion of the content inside the flow through cells especially during media change, which led to a difference in drug dissolution. Furthermore, there was no significant difference in the percentage dose precipitation among the various formulations (F4, F5, F6, F7 and F8) and dissolution media of FaSSIF-V1 and FaSSIF-V2, which show that these formulations are very similar in terms of their critical manufacturing variables.



### 3.5 Results and Discussion of Part 2: Surface UV dissolution imaging

#### 3.5.1 Calibration curves

Calibration curves for ITR and CA were constructed and the quantitative performance of the UV imager was verified before conducting the *in vitro* release experiments. For this purpose, the phosphate buffer followed by a series of ITR and CA reference standard standard solutions were flowed through the laminar flow cell (2 mL/ min) with continuous image data collection. In this project the area selected for imaging was 9.0 mm × 4.3 mm as suggested in the literature (111). In principle, 4× 4 pixel binning was applied and produced approximately  $5 \times 10^4$  individual UV spectrophotometers.

From the gradients of calibration curves (Figure 41), the molar absorption coefficient (molar absorptivity) of CA and ITR were determined to be 2057.65 m<sup>2</sup>/mol and 363.56 m<sup>2</sup>/mol respectively.

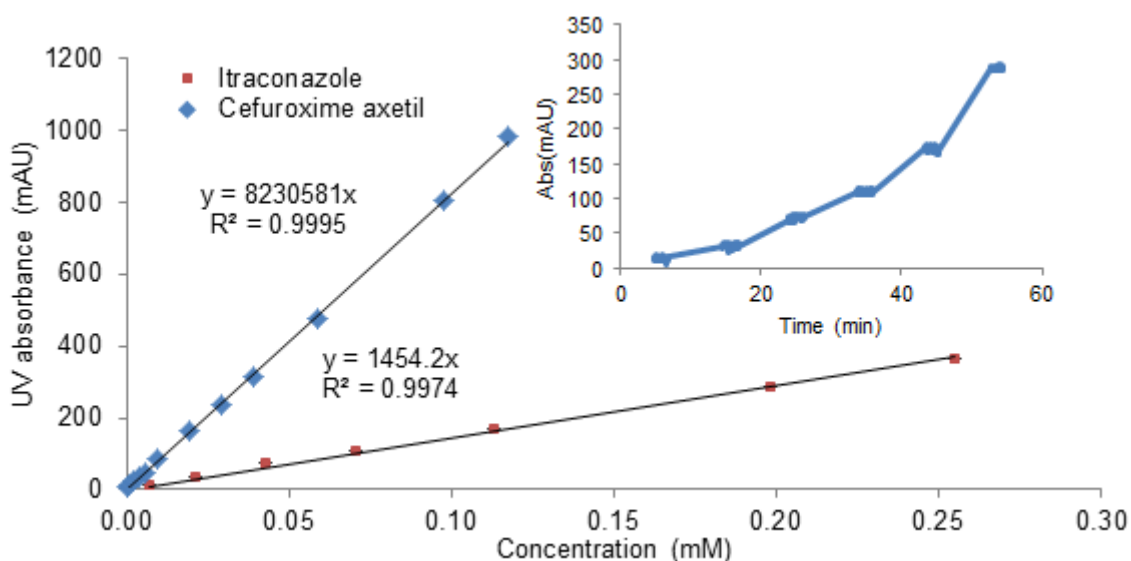


Figure 41. Mean absorbance values as a function of concentration for pixel subselection obtained by flowing ITR and CA standard solutions through the laminar flow cell. Insert shows the UV absorbance vs time profile obtained by flowing ITR standard solutions through the cell.

The UV imaging ITR and CA reference standard calibration curve at 280 nm was considered linear within the investigated range. The LOQ was estimated to be  $2.4 \times 10^{-5}$  mM (ITR) and  $1.10 \times 10^{-6}$  mM (CA).

### 3.5.2 *In vitro* surface UV dissolution imaging studies

In the current study, two particular low flow rates of 0.14mL/min and 0.28 mL/min are chosen based on the linear regression of linear velocity and flow rate (Figure 42). The results of linear velocity (cm/min) of ActiPix™'s laminar flow cell at various flow rates and in the human stomach and intestine have been reported in the literature (124, 276). Without taking into account the cross-sectional water loss, the flow rates of ActiPix™'s flow cell that correspond to the linear velocity reflecting the human stomach and intestinal section are 0.28 mL/min and 0.14 mL/min respectively. Based on the facts that both ActiPix™'s flow cell and USP apparatus 4's flow through cell provided unilateral laminar flow and the former generates lower hydrodynamics, a one-order magnitude scale-down of the current project's USP apparatus 4 setup was used. Hence, flow rates of 0.8mL/min and 0.4mL/min reflecting the human stomach and intestine respectively were used in the experiment with media and flow rate change.

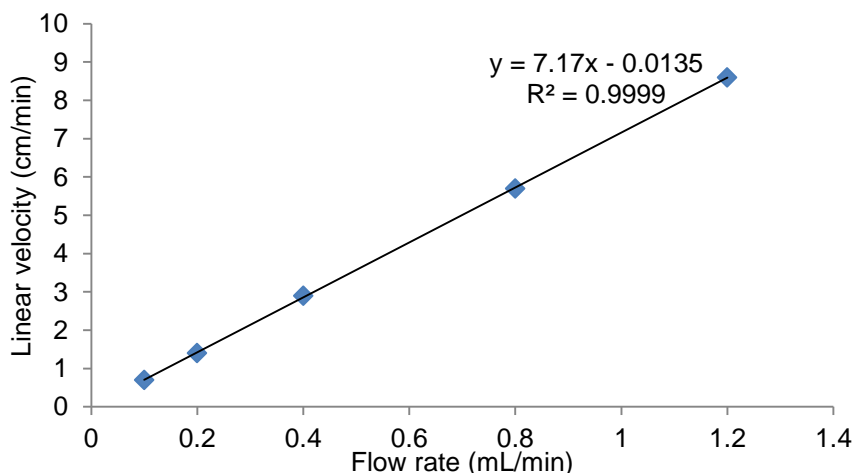


Figure 42. Linear velocity of ActiPix™'s flow cell vs flow rate. Data were available from literature (124).

### CA

First, it must be noted that an initial dissolution test using Zinnat® (amorphous formulation of CA) compact was not satisfactory because the high loading of super-disintegrant croscarmellose sodium in Zinnat® became a dense layer after being exposed to the dissolution medium (Figure 43). This layer caused physical blocking of the light and yielded a large amount of debris that clogged the flow cell thus preventing further testing.

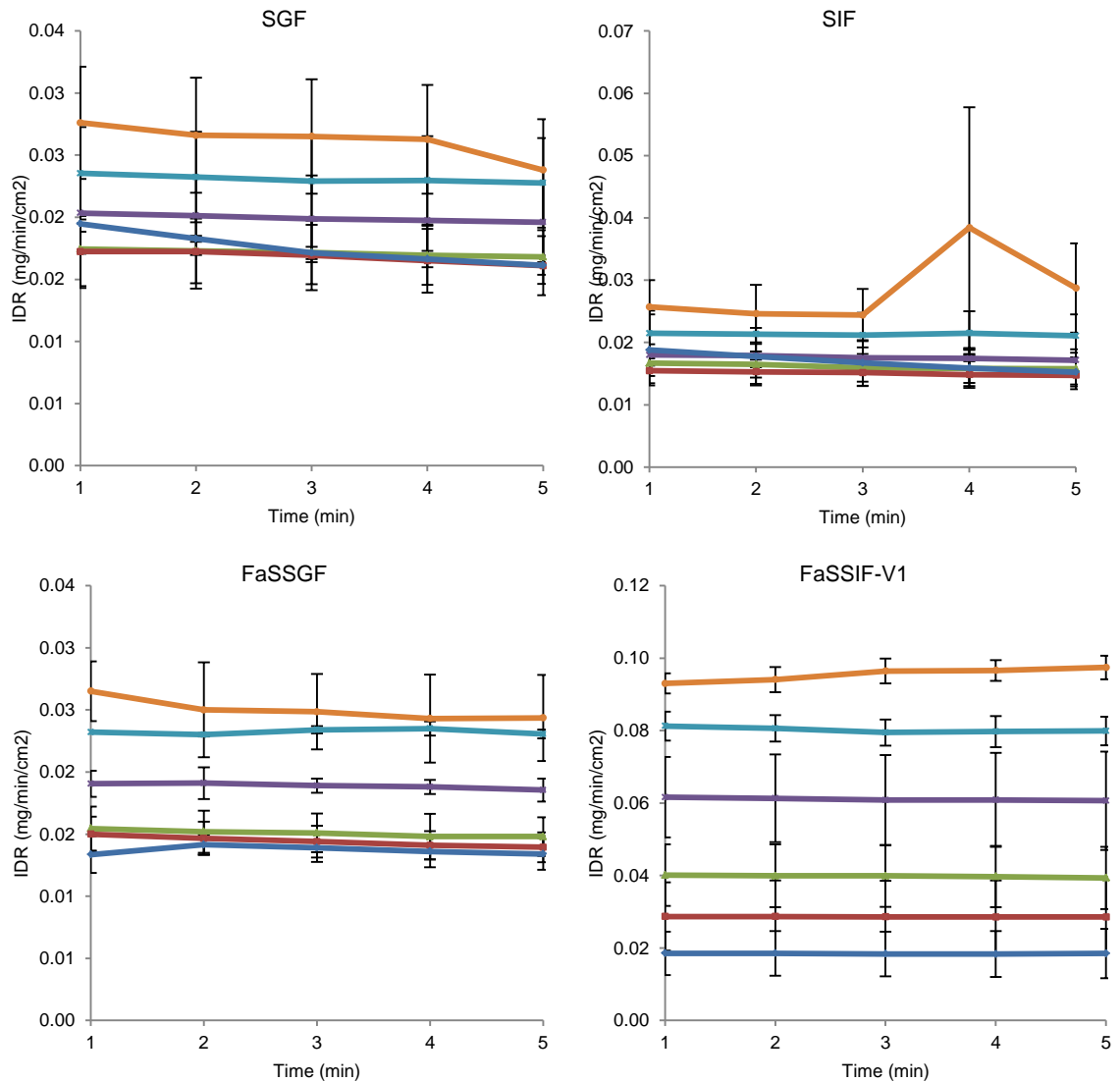


Figure 43. Dense layer formed immediately after Zinnat<sup>®</sup> compact exposure to dissolution medium.

The intrinsic dissolution rate (IDR) was calculated using the built-in programme available in the ActiPix<sup>™</sup> software using the absorbance values from the quantification region during dissolution of drug compacts. The calculation program integrates information such as the absorbance reading, the molar absorptivity calculated from the calibration curves of each drug, the surface area of compacts and the flow rate profile to estimate the IDR value.

## Single medium and flow rate study

IDRs of CA API in compendial and biorelevant media vs time profiles with single media and flow rate are presented in Figure 44.



### Legend

— 1 ml/min — 0.8 ml/min — 0.6 ml/min — 0.4 ml/min — 0.28 ml/min — 0.14 ml/min

Figure 44. Mean ± SD IDR of CA from its API compact in compendial and biorelevant media.

The impact of reducing the flow rate from 1 mL/min to 0.14 mL/min on the CA IDR profiles was evident (Figure 44). The dissolution experiment setup with FaSSIF-V1 showed a clear stepwise IDR reduction in tandem with flow rate decrease from 1 mL/min (0.097 mg/min/cm<sup>2</sup>) to 0.14 mL/min (0.018 mg/min/cm<sup>2</sup> at 5 min). In contrast, the IDR profiles in SGF, SIF and FaSSGF showed a very dense IDR profile pattern especially at lower flow rate.

A compilation of all measured IDR results vs flow rate is shown in Figure 45. The graph profiles formed in SGF, FaSSGF and SIF are almost straight and suggest that the dissolution mechanism is predominantly swelling or erosion; whereas, with the FaSSIF-V1 profiles the graph profile shows an apparent gradient which indicates dissolution in convective flow as the main dissolution mechanism. The difference is a good indicator for the effect of mixed micelles that facilitate and enhance the dissolution of a poorly water soluble compound.

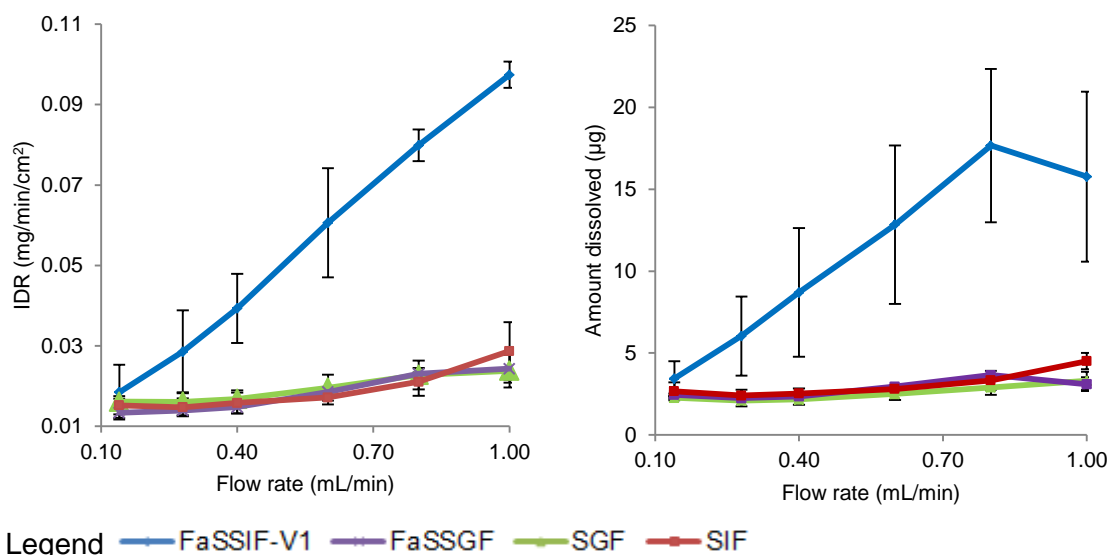


Figure 45. Mean  $\pm$  SD IDR and amount of CA dissolved at 5 min from its API compact with compendial and biorelevant media (n=3, except FaSSGF n=2).

All IDR profiles, regardless of the media used, yielded a plateau IDR vs time profile which clearly showed zero order dissolution kinetic. This verified that sink conditions for CA dissolution possibly exist in the channel flow cell and literature has suggested that this sink condition is an important factor in the simulation of the human *in vivo* condition (117, 124).

### Media and flow rate change study

Dissolution behaviour of CA was monitored by the surface UV dissolution imager with SGF (0.8 mL/min;6 min)/ SIF (0.4 mL/min;18 min). The UV images of absorbance maps of dissolved CA at different selected time points are shown in Figure 46. A contour concentration line is presented in the concentration scale bar. The measured concentrations in the UV map shown were all within the linear range of the calibration curve (below 35 µg/mL). It can be observed that the dissolution layer is thin with a wide hydrodynamic boundary layer as reported by Prandtl (356).

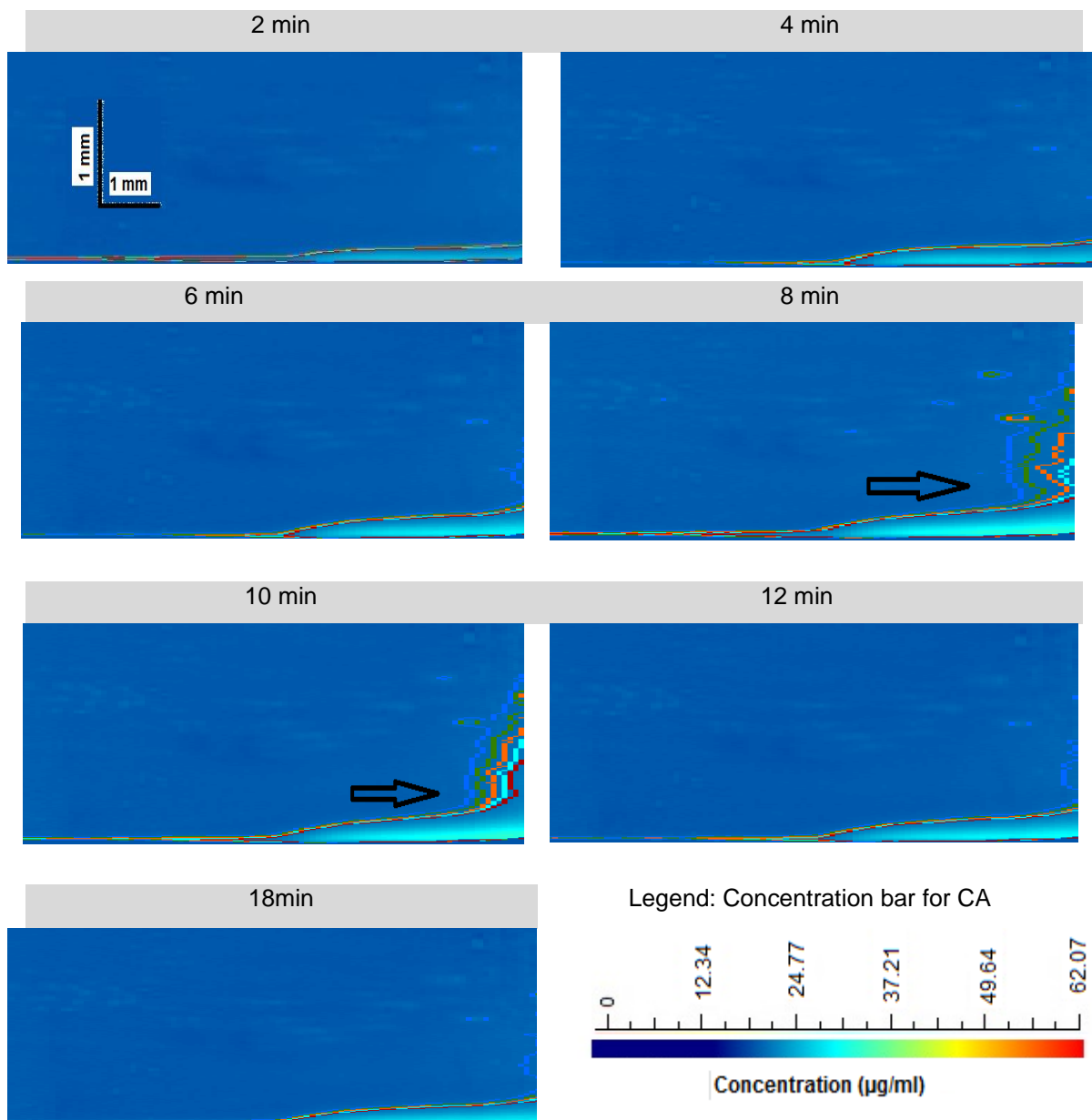


Figure 46. UV concentration maps of CA dissolved from API compacts with SGF (0.8 mL/min;6 min)/ SIF (0.4 mL/min;18 min) using surface UV imaging apparatus (Time point: 2,4,6,8,10,12 and 18 min). Colour-concentration banding: red 62.07; orange 49.64; green 37.21; light blue 24.77; dark blue 12.34 µg/mL.

The results point out that soon after media and flow rate change the drug concentration peak at 8 min forms a supersaturated solution and then gradually reduces. As indicated by the arrow in Figure 46, there was an apparent turbulent pattern contour which could probably imply a dispersion of the recrystallised particle at 8 and 10 min corresponding to the crystal growth post supersaturation.

The dissolution layer thickness at the surface is approximately 0.05mm to 0.1mm under both flow rate at 0.8mL/min and 0.4mL/min, whereas the boundary layer thickness is  $4.34 \times 10^{-3}$  mm (0.8mL/min) and  $8.66 \times 10^{-3}$  mm (0.4mL/min), respectively.

The boundary layer thickness is calculated based on the CA diffusion coefficient value of  $5.776 \times 10^{-6} \text{ cm}^2/\text{s}$  (calculated value based on molecular weight using GastroPlus™). The measured values using surface UV imaging apparatus is far higher than the value projected using a diffusion coefficient. According to the literature (116), this phenomenon suggests that CA dissolved from the surface as aggregate, initially forming a supersaturated solution; this is in agreement with the observed IDR and amount of CA dissolved from its API compact with media and flow rate change from SGF (0.8 mL/min) to SIF (0.4 mL/min) (Figure 47). Figure 47 indicates that there are two supersaturated solutions formed in SGF and SIF before particle precipitation and decrease of IDR.

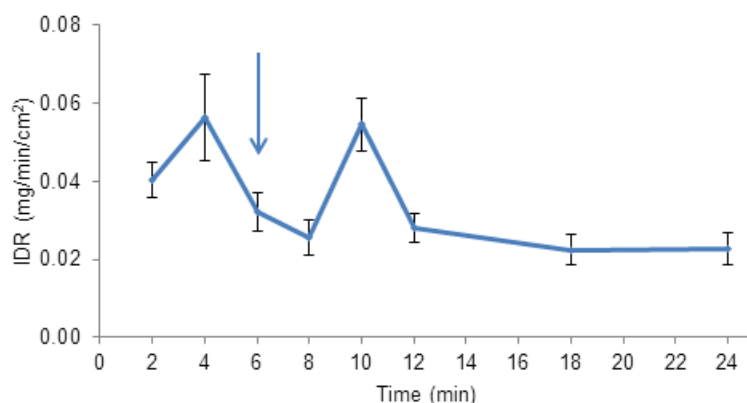
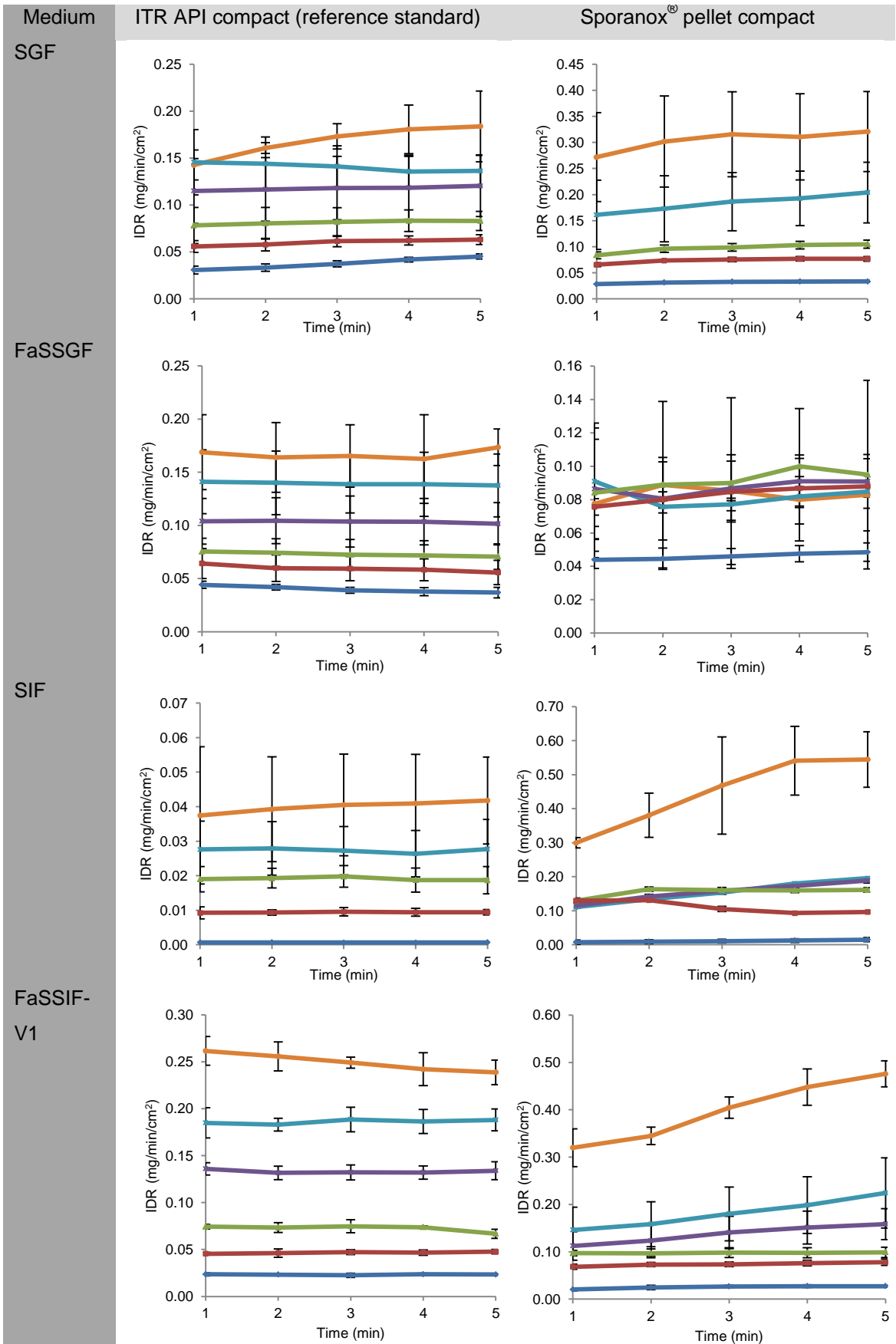


Figure 47. Mean  $\pm$  SD IDR of CA dissolved from its API compact with SGF (0.8 mL/min; 6 min)/ SIF (0.4 mL/min; 18 min) (n=2). Blue arrow indicates time with media change.

## ITR

### Single medium and flow rate study

IDR of ITR from ITR API and Sporanox® in compendial and biorelevant media vs time profiles are presented in Figure 48.



Legend: Flow rate — 1 ml/min — 0.8 ml/min — 0.6 ml/min — 0.4 ml/min — 0.28 ml/min — 0.14 ml/min

Figure 48. Mean ± SD IDR of ITR from its API compact and Sporanox® compact in compendial and biorelevant media.



A stepwise decrease in dissolution rate corresponding to the stepwise reduction in flow rate was obtained from the imaging data (Figure 48). This trend was expected according to the convective diffusion theory (357). The impact of reducing the flow rate from 1 mL/min to 0.14 mL/min on the IDR profiles was evident in ITR API in the compendial and biorelevant media and Sporanox<sup>®</sup> formulations with SGF and FaSSIF-V1. In Sporanox<sup>®</sup>, the IDR profiles in FaSSGF and SIF showed no obvious rank order, probably due to the interference of surface dissolution characterisation in the presence of excipients and polymers, such as HPMC and PEG.

In order to determine the dissolution mechanism of ITR from both compacts, the same IDR results were plotted against flow rate (Figure 49).

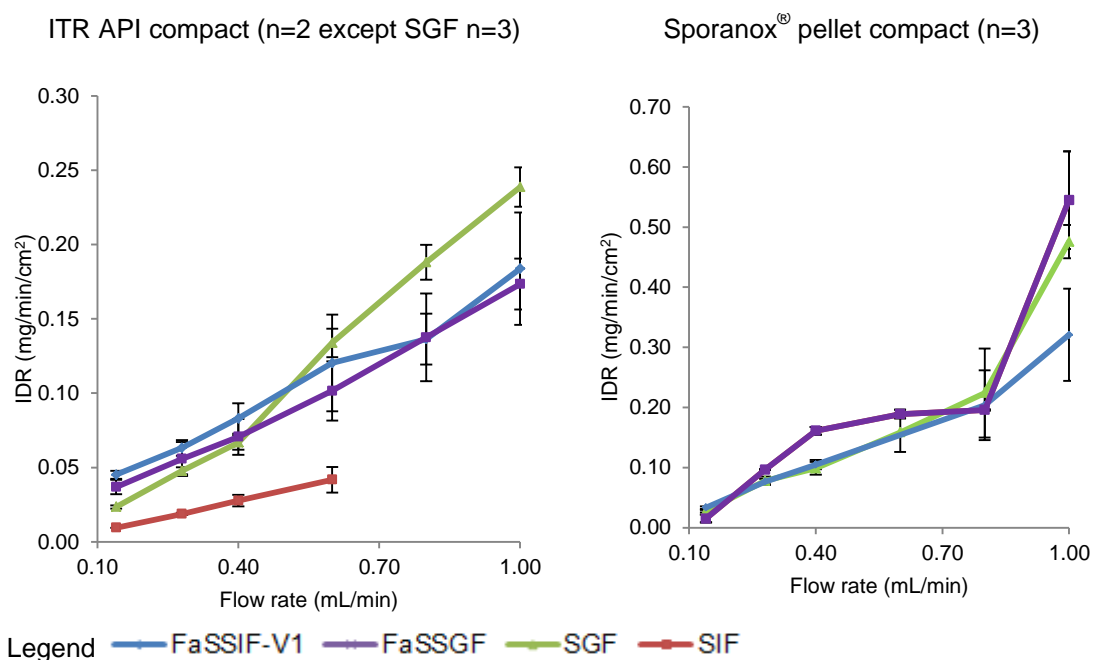


Figure 49. Mean  $\pm$  SD IDR and amount of ITR dissolved at 5 min from its API compact and Sporanox<sup>®</sup> compact with compendial and biorelevant media.

Literature has suggested that the flat and gradient IDR profiles indicate that the dissolution mechanism is predominantly erosional (swelling) and convective, respectively (116). The dissolution mechanism of ITR from Sporanox<sup>®</sup> (SIF and FaSSIF-V1 at 1 mL/min) showed a higher gradient curve than from the ITR API, denoting a higher convective dissolution of ITR from the HPMC gel matrix. This is in agreement with the dissolution kinetic of ITR characterised with USP apparatus 4 showing that the dissolution in convective flow is the main process determining the dissolution of ITR formulated as a solid dispersion coating pellet. The IDR trends with biorelevant media did not reveal the advantage of the surfactants in terms of enhancing the dissolution rate. This is in agreement with the results presented in Section 3.3.1

whereby bile salt was shown to potentially undergo an acid-base reaction with ITR molecules leading to slower ITR dissolution (329, 330).

The content of HPMC in Sporanox<sup>®</sup> pellet coating is 60% w/w (ratio of 1:1.5 ITR to HPMC), thus at this high concentration the release of ITR is controlled by HPMC. The multiparticulate drug coated Sporanox<sup>®</sup> pellet was also coated with the PEG membrane at its outer most layer. The rate of ITR dissolution in convective flow to the dissolution media is dependent not only on the thickness of the membrane but also on the composite of the HPMC-ITR solid solution matrix itself which sustains the dissolution. Furthermore, HPMC has a gelling property upon hydration which has been identified as a variable affecting drug dissolution (358). Hence, the dissolution of ITR from Sporanox<sup>®</sup> compact was delayed due to drug particles having to diffuse out from the HPMC matrix before undergoing dissolution.

Due to the poor solubility of ITR in SIF and without the interference of bile salt and lecithin, SIF was able to discriminate Sporanox<sup>®</sup> formulation (amorphous formulation) and ITR API (crystalline compact). For example, the IDR of Sporanox<sup>®</sup> pellet in SIF was nearly 10 times higher than the same measurement in the ITR API compact. The results seem to suggest that this experiment setup and conditions could be used to discriminate critical manufacturing variables of such formulations.

### **Media and flow rate change study**

Dissolution behaviour of ITR from its API and Sporanox<sup>®</sup> compacts were monitored by the surface UV dissolution apparatus with SGF (0.8 mL/min;6 min)/ SIF (0.4 mL/min;18 min) and FaSSGF (0.8 mL/min;6 min)/ FaSSIF-V1(0.4 mL/min;18 min). IDR and cumulative amount of ITR dissolved are presented in Figure 50.

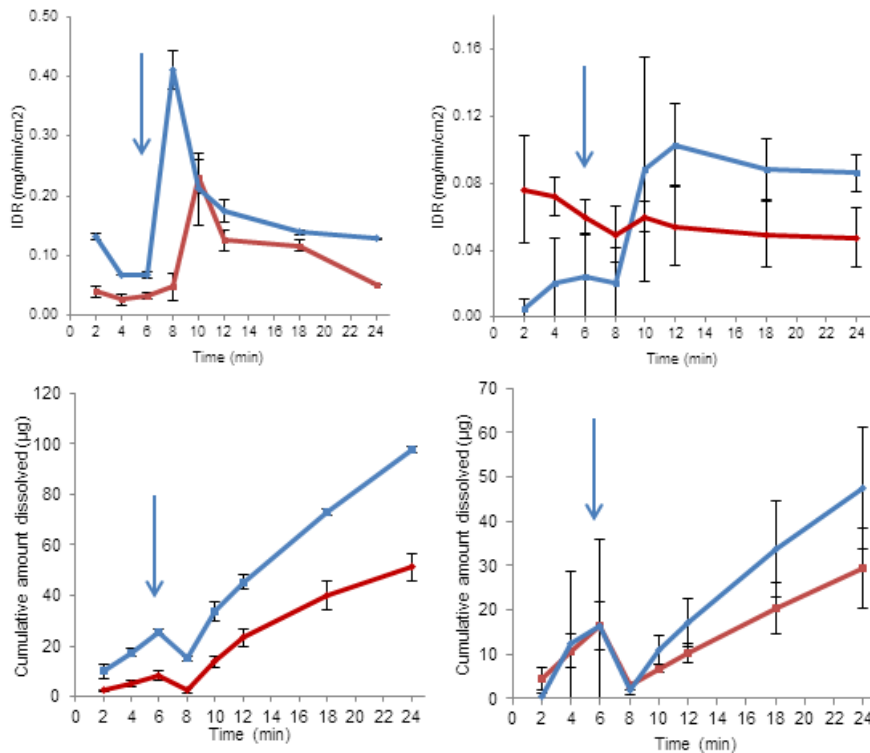


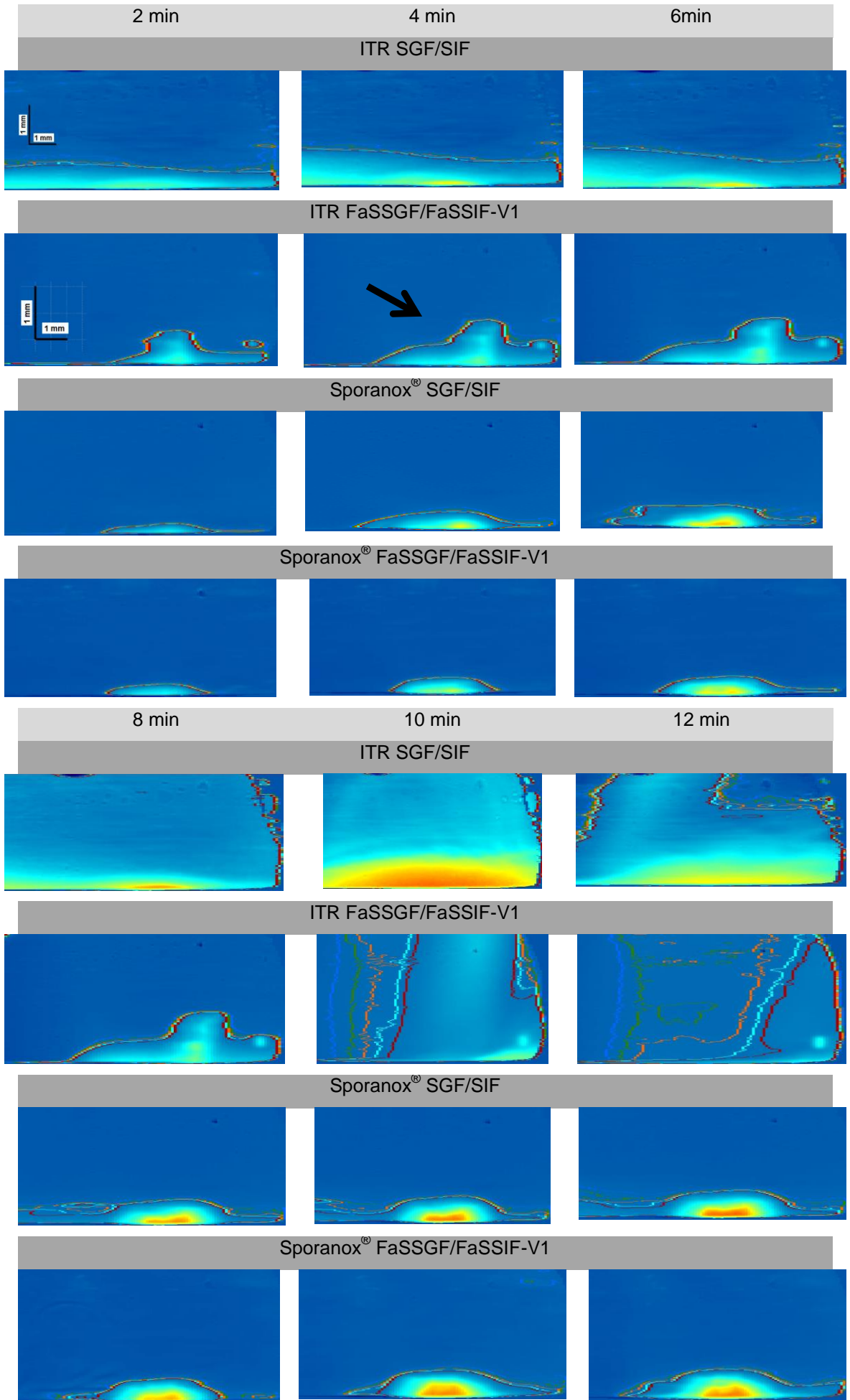
Figure 50. Mean $\pm$  SD IDR and amount of ITR dissolved from its API and Sporanox<sup>®</sup> compact with SGF(0.8 mL/min;6 min)/ SIF (0.4 mL/min;18 min) and FaSSGF(0.8 mL/min;6 min)/ FaSSIF-V1(0.4 mL/min;18 min, n=3)

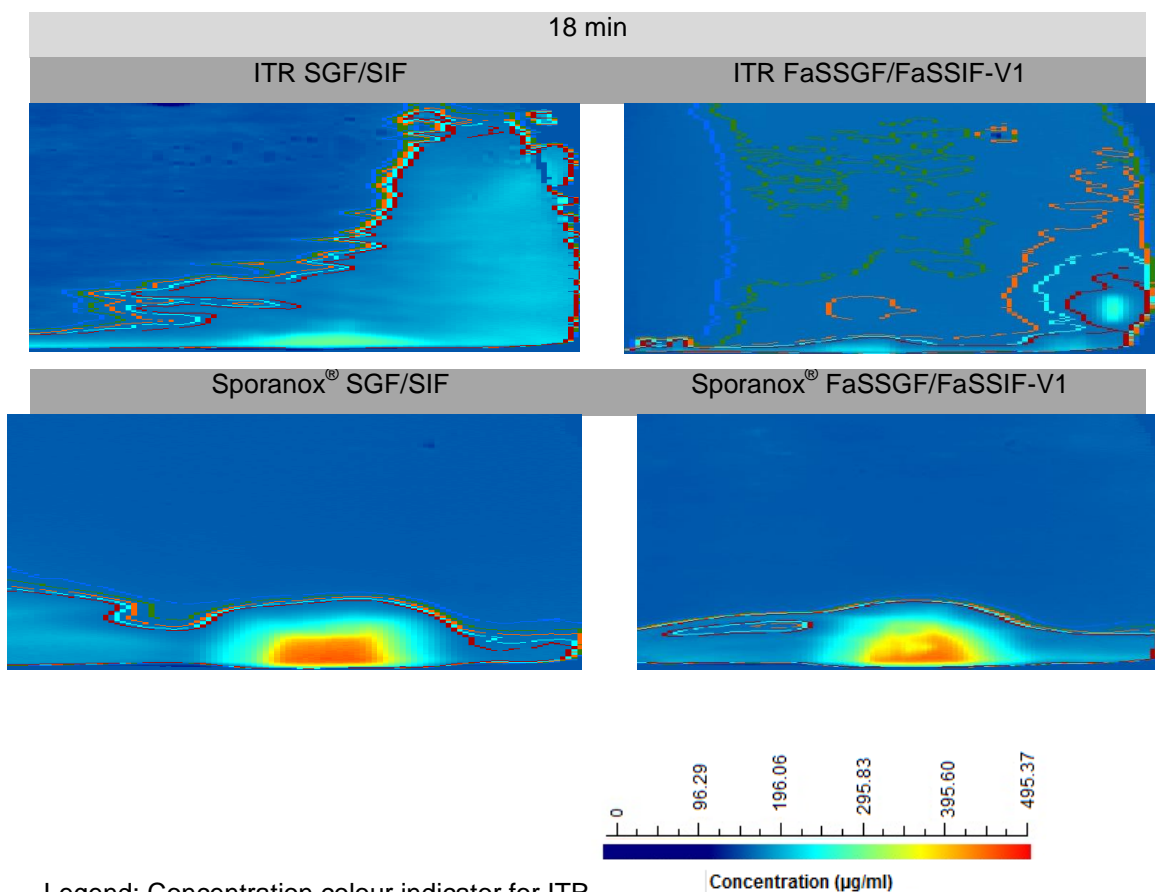
Compared to the graphs in individual media such as FaSSGF, FaSSIF-V1, SGF and SIF (Figure 50) that showed a flat and linear graph, the curve experiments with media change have exhibited their own characteristic gradient. The dissolution profiles of experiments with media change using surface UV imaging resembled those of USP apparatus 4. For example, the biphasic curve was apparent, with a sudden increment after media change from simulated gastric medium to simulated intestinal medium. Similar to USP apparatus 4, due to media change to FaSSIF-V1 with micellar solubilisation, higher supersaturation could be observed with the media change from FaSSGF to FaSSIF-V1. The same dissolution rate enhancement was observed in the Sporanox<sup>®</sup> pellet compact with FaSSGF/FaSSIF-V1 also but not in SGF/SIF.

The IDR profile of ITR API compact in SGF/SIF and FaSSGF/FaSSIF-V1 also showed that after medium and flow rate changes from simulating gastric condition to simulating intestinal condition the IDR and amount dissolved increased significantly forming a transient supersaturated solution of ITR. After 5 to 8 min the supersaturation ratio reduced steadily toward the equilibrium dissolution rate of 0.128 mg/min/cm<sup>2</sup> in FaSSIF-V1 and 0.051 mg/min/cm<sup>2</sup> in SIF yielding a total amount of ITR dissolved of 98  $\mu$ g and 51 $\mu$ g respectively.

The IDR of ITR from its API and amorphous formulation (Sporanox<sup>®</sup>) showed that the IDR and amount dissolved were twice as high in the ITR API compact than Sporanox<sup>®</sup> compact (Figure 50). This does not reflect the fact that amorphous formulation generally has a higher dissolution. The results were probably due to the interaction of bile salt (found in FaSSIF-V1) and potassium salt (found in SIF) with PEG which had been proposed in the literature (359). The PEG coating was used in Sporanox<sup>®</sup> pellet to prevent agglomeration which in surface UV imaging hindered the ITR dissolution. The effect of PEG on the surface UV imaging was also shown in the individual Sporanox<sup>®</sup> dissolution test using FaSSGF and FaSSIF-V1 (Figure 50). Probably for the aforementioned reason, the supersaturated solution produced from FaSSGF/FaSSIF-V1 was less obvious with a peak IDR of 0.103 mg/min/cm<sup>2</sup> compared with the equilibrium rate of 0.086 mg/min/cm<sup>2</sup> which yields a total of 48 µg of ITR dissolved.

The concentration curves of ITR dissolved from ITR API compact and Sporanox<sup>®</sup> pellet compact relative to the compact surface axis are presented as concentration contours within the UV absorbance maps of ITR dissolved at different selected time points (Figure 51; please note that Figure 51 is displayed over 2 pages).





Legend: Concentration colour indicator for ITR

Figure 51. UV concentration maps of ITR dissolved from API and Sporanox<sup>®</sup> pellet compacts with SGF (0.8 mL/min;6 min)/ SIF (0.4 mL/min;18 min) and FaSSGF (0.8 mL/min;6 min)/ FaSSIF-V1 (0.4 mL/min;18 min) using surface UV imaging apparatus (Time point: 2,4,6,8,10,12 and 18 min).

The area in blue shows the background (without drug solute) absorbance and tense light colour indicates high absorbance at the lower right corner. The sample compact was located at the bottom of each image and the contours represent curves with the same concentration. The absorbance map in each image indicates the spatial concentration distribution of the dissolved ITR in the flow cell at the recording time, which was affected by the flow rate and diffusion coefficient of ITR.

Generally, the contours based on concentration bands show that laminar flow conditions are obvious in the flow cell. However, when approaching downstream, the more turbulent flow was observed due to the hydrodynamic boundary layer built up, leading to slowing down of more drug and fluid molecules. The contours of Sporanox<sup>®</sup> pellet compacts (Figure 51) showed that density gradients in the proximity of compact surface affect the concentration distribution of the surrounding solutions. Accumulation of dissolved ITR was slightly skewed toward the left part of the contour images for the

sample due to a higher density of the HPMC and PEG gel matrix as compared to the solvent (Figure 51). This is in agreement with the previous results showing that the ITR dissolution from the Sporanox<sup>®</sup> compact was affected by the PEG gelling layer and HPMC matrix thus showing a steady convectonal and erosional dissolution pattern.

On the other hand the contour in ITR API compact has contour lines that show a flat and broad laminar layer. ITR API compact with FaSSGF/FaSSIF-V1 form the least concentrated solution in the dissolution layer compared with the experiments in SGF/SIF, Sporanox<sup>®</sup> compact with SGF/SIF and FaSSGF/FaSSIF-V1. There was a clear upward movement of the dissolved ITR into the bulk buffer solution as the downstream distance increases to form a stable dissolution layer. Furthermore, it is observed that a distorted curve and abnormal shifting of contour lines strongly indicated ITR dissolution followed by recrystallisation of the ITR particle at the compact surface (black bold arrow in Figure 51).

For ITR with compendial media, although a thicker dissolution layer was observed throughout the whole experiment, the size of the dissolution layer quickly dissipated to the minimum layer at 18 min. Likewise for the ITR compact with biorelevant media, there was a significant decrease in the dissolution layer after 10 min of the dissolution test that slowly relaxed at a low concentration layer. It is safe to conclude that the fast supersaturation formed on the surface after media change drastically increased the recrystallisation of ITR on the surfaces of the compacts which could also lead to crystal growth on the surface.

### 3.6 Results and Discussion of Part 3: PBPK modeling (CA)

#### 3.6.1 Prediction of *in vivo* performance based on PBPK models

In the first part of this section, the PBPK predictions of the *in vivo* behaviour of the amorphous CA formulation (Zinnat<sup>®</sup>) using GastroPlus<sup>®</sup> are presented. Profile comparison was performed using plasma concentration vs time profile obtained in clinical *in vivo* study.

Firstly, the predictions were made based on solubility based models in which the results showed that these models were not able to simulate closely the observed *in vivo* profile (results presented in Appendix 7). Secondly, the predictions were made based on the solubility combined with the dissolution based model whereby *in vitro* drug dissolution profiles obtained with USP apparatus 2 and 4 were included.

##### 3.6.1.1 Solubility combined with dissolution based model

###### Simulated fasted state condition

The plasma concentration-time of simulated (solubility and dissolution-based model) and observed (human) profiles after an oral administration of Zinnat<sup>®</sup> in fasted state with USP apparatus 2 are presented in Figure 52 (single stage dissolution models) and Figure 53 (2 stage dissolution models).

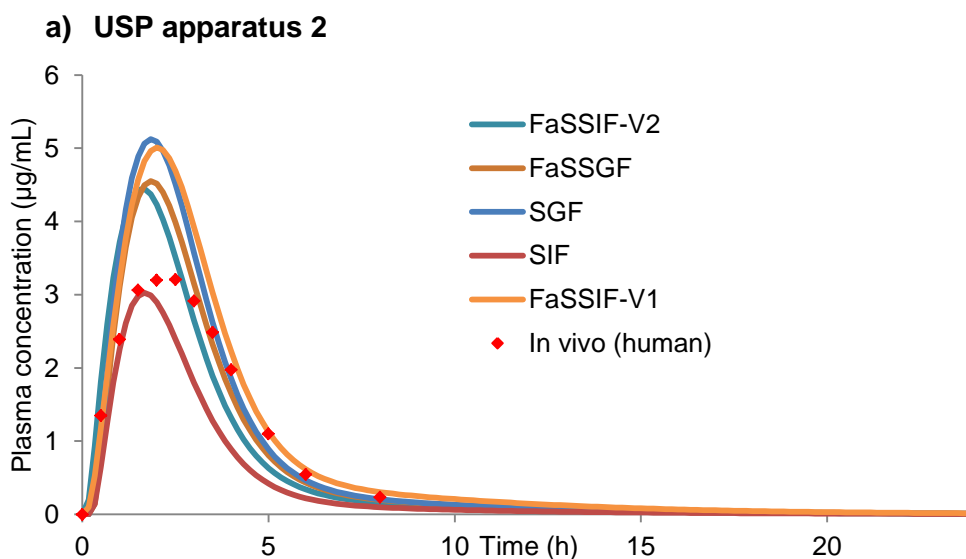


Figure 52. Simulation (line) of oral Zinnat<sup>®</sup> profiles in humans with various media with USP apparatus 2 and reference solubility in FaSSIF-V2 compared to the observed *in vivo* profile (human, fasted; ♦) (287).



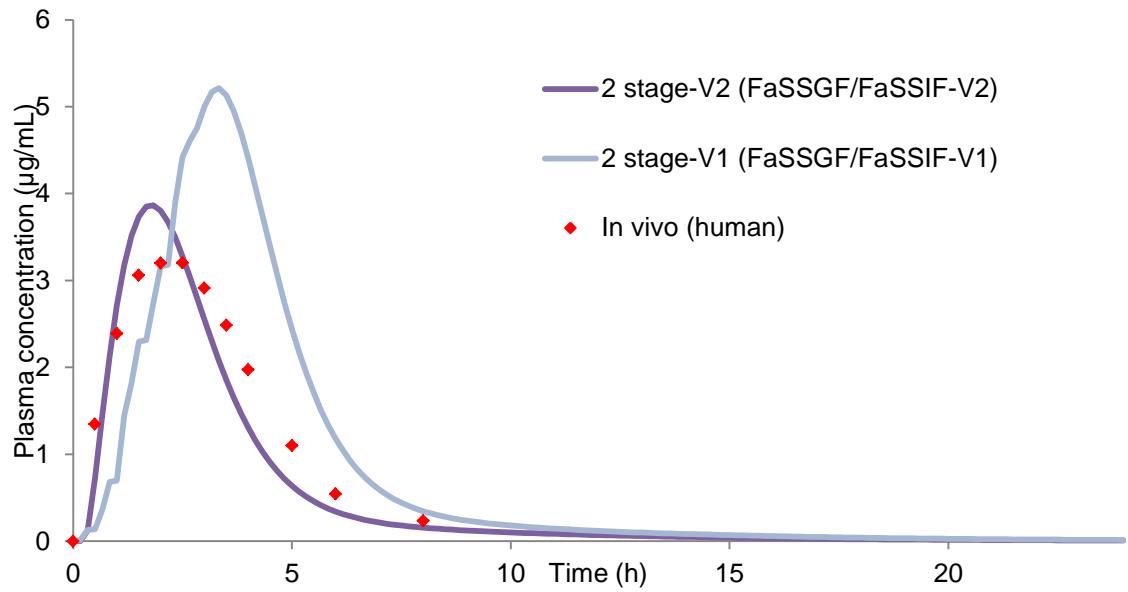


Figure 53. Simulation (line) of oral Zinnat<sup>®</sup> profiles in humans with various media with USP apparatus 2 and reference solubility in FaSSIF-V2 compared to the observed *in vivo* profile (human, fasted; ♦) (287)

#### b) USP apparatus 4

The plasma concentration-time of simulated (solubility and dissolution-based model) and observed (human) profiles after an oral administration of Zinnat<sup>®</sup> in fasted state with USP apparatus 4 are presented in Figure 54.

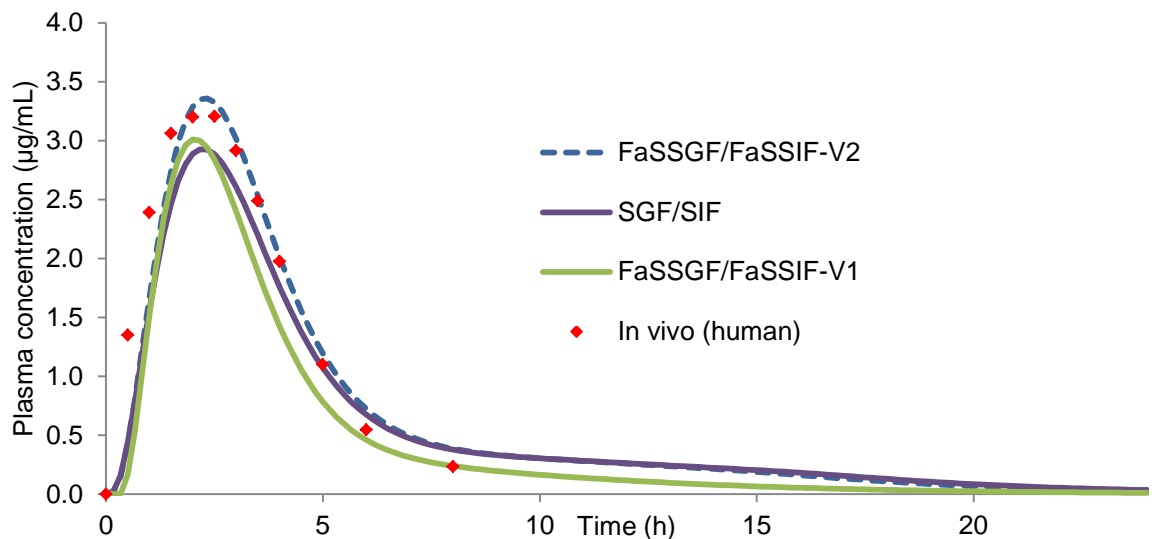


Figure 54. Simulation (line) of oral Zinnat<sup>®</sup> profiles in humans with various media with USP apparatus 4 and reference solubility in FaSSIF-V2 compared to the observed *in vivo* profile (human, fasted; ♦) (287)

In the case of CA, plasma concentration–time profiles of the immediate release tablet could be predicted after integrating the corresponding dissolution functions into the model. The simulated profiles' curve characteristics mimicked the *in vivo* profiles well, except the dissolution profile in 2 stage-V1 (FaSSGF/FaSSIF-V1) with USP apparatus 1. The dissolution profile of CA in FaSSGF/FaSSIF-V2 closely simulated the *in vivo* (human) data with almost identical plasma concentration–time profiles compared with the other dissolution profiles ( $f_1$  FaSSGF/FaSSIF-V2:12.28,  $f_1$  SGF/SIF:18.19,  $f_1$  FaSSGF/FaSSIF-V1: 22.70). This shows that physiological relevant hydrodynamics and medium change with USP apparatus 4 combined with solubility value in FaSSIF-V2 could be used to develop a predictive human absorption model.

### Simulated fed state condition

The plasma concentration-time of simulated (Solubility combined with dissolution-based model) and observed (human) profiles after an oral administration of Zinnat<sup>®</sup> in fed state are presented in Figure 55 (USP apparatus 2) and Figure 56 (USP apparatus 4).

#### a) USP apparatus 2

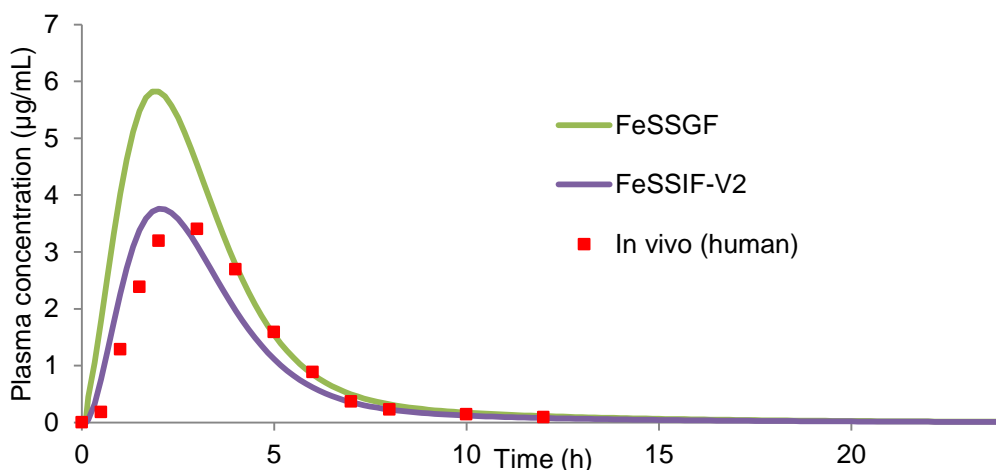


Figure 55. Simulation (line) of oral Zinnat<sup>®</sup> profiles in humans using reference solubility in FeSSIF-V2 and dissolution profiles measured in FeSSGF and FeSSIF-V2 with USP apparatus 2 compared to observed *in vivo* (human, fed; ■) (288).

In the FeSSGF model, a higher simulated peak concentration was observed. Nevertheless, the curve was well characterised by FeSSGF. As seen in Figure 55, the simulation using dissolution profile with FeSSGF overestimated the *in vivo* profile while the dissolution profile with FeSSIF-V2 shows a much closer simulation ( $f_1$  FeSSGF: 71.46 and FeSSIF-V2: 30.62).

### b) USP apparatus 4

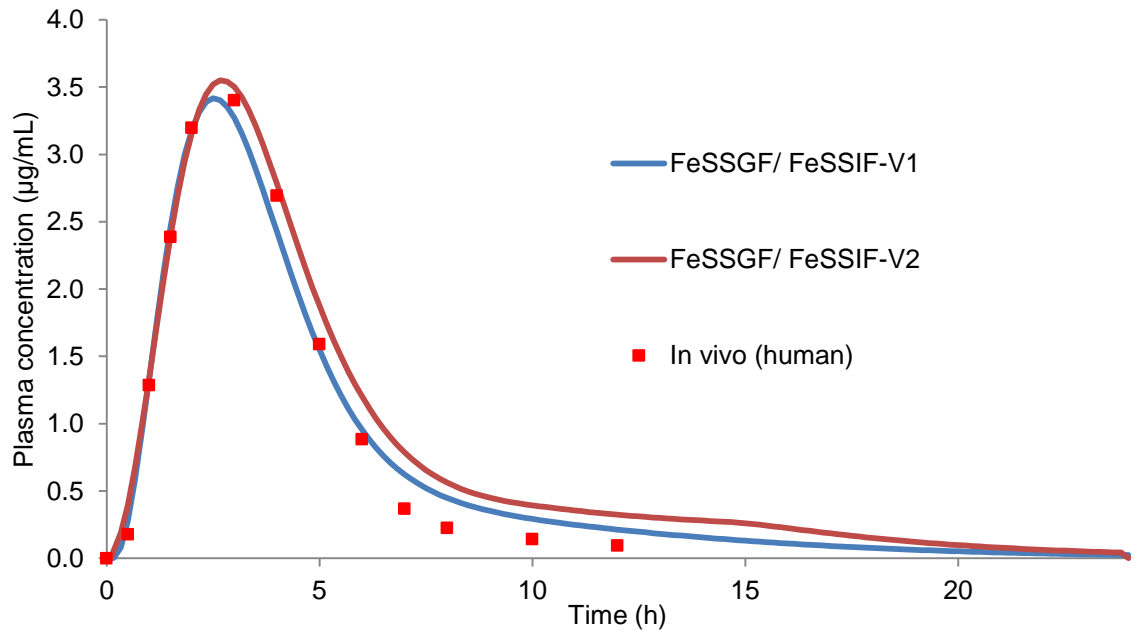


Figure 56. Simulation (line) of oral Zinnat<sup>®</sup> profiles in humans using reference solubility in FeSSIF-V2 and dissolution profiles measured in FeSSGF/FeSSIF-V1 and FeSSGF/FeSSIF-V2 with USP apparatus 4 compared to the observed *in vivo* profile (human, fed; ■) (288).

The simulated profiles show that plasma concentration–time profiles of the Zinnat<sup>®</sup> could be predicted after integrating the corresponding dissolution profiles. FeSSGF/FeSSIF-V2 closely simulated the *in vivo* (human) data with almost identical plasma concentration–time profiles compared with other dissolution profiles ( $f_1$  FeSSGF/FeSSIF-V2: 11.98,  $f_1$  FeSSGF/FeSSIF-V1: 7.79).

In this project, robust and validated PBPK models for fasted and fed states were developed. These models incorporate *in vitro* degradation, particle size distribution of CA, *in vitro* solubility and *in vitro* dissolution data. The inclusion of these elements into PBPK models proved their capability to predict accurately *in vivo* dissolution in terms of the rate as well as the absorption process.

### 3.6.2 Parameter sensitivity analysis

Parameter sensitivity analysis (PSA) is useful for continuous improvement of formulation development. In the scenario that the effect of changing certain parameters is uncertain, the PSA could be used for forecasting the impact of changes in key properties than to make precise quantitative experimental study.

#### Simulated fasted state conditions

The results of the PSA of CA in the human model (fasted state) are presented in Figure 57.

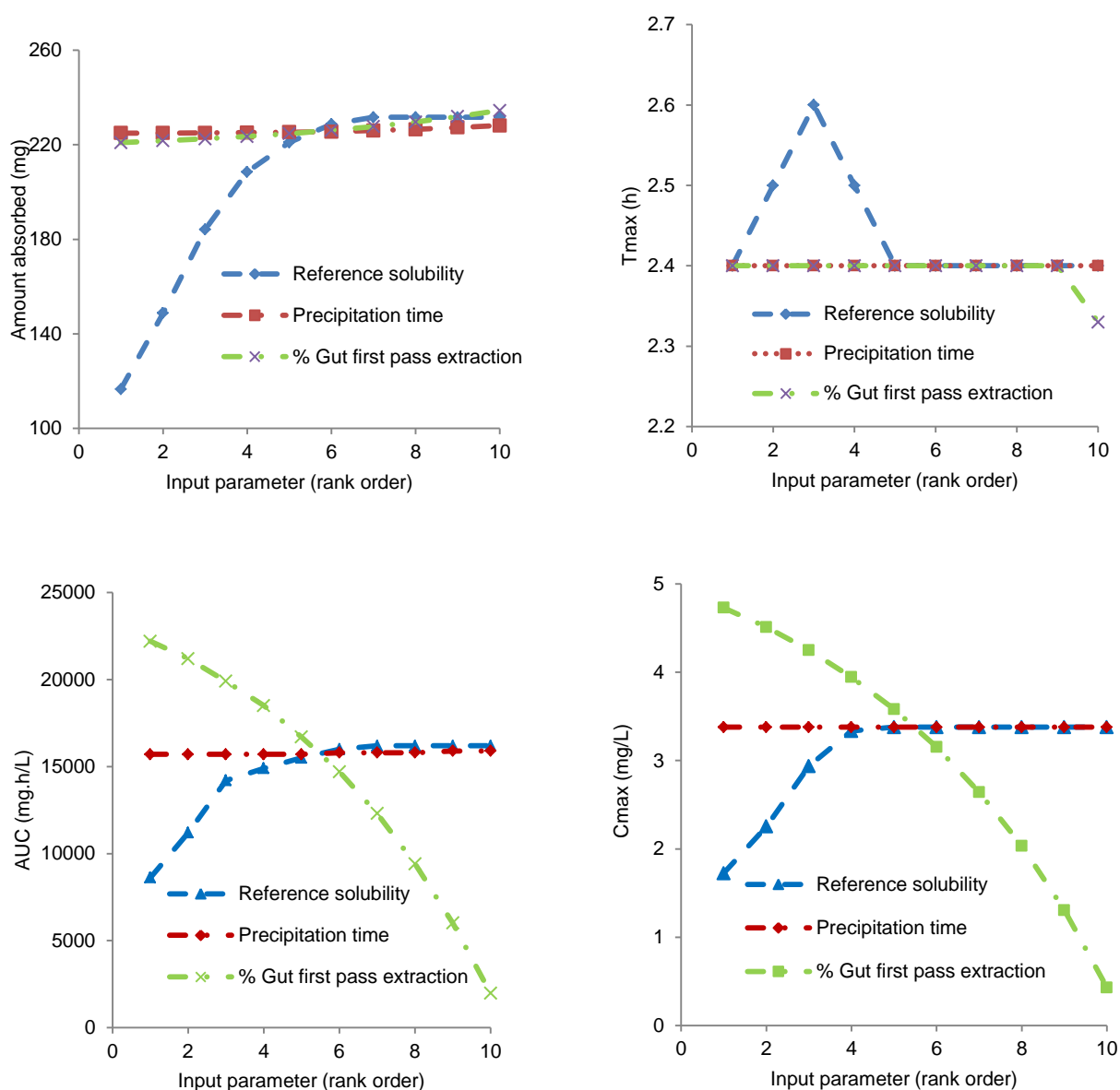


Figure 57. PSA of absorption and pharmacokinetic parameters of CA (fasted state)

The results of PSA show that the precipitation time and percentage of gut first pass extraction does not affect the absorption and pharmacokinetic of CA in the fasted state.

This is in agreement with *in vitro* dissolution testing where no precipitation occurred during media change from simulated gastric media to simulated intestinal media. The range of CA solubility analysed in this study was 0.044-4.43 mg/mL. The wide range of solubility applied was based on the consideration that the solubility of CA in the biorelevant media and aqueous media were different. The PSA results show that increasing CA solubility from 0.044 to 0.572 mg/mL (rank order 1 to 6) would have greater effects on the  $C_{max}$ , AUC and  $T_{max}$  (Figure 57). However, if the CA solubility is increased beyond 0.572 mg/mL, no effect on the pharmacokinetics of cefuroxime is observed. It seems to suggest that 0.527 mg/mL is the maximum solubility that might limit the absorption of CA. Furthermore, an increase in percentage of gut extraction of CA (from 23.4- 93.6 %) primarily caused by chemical degradation of CA would greatly reduce the  $C_{max}$  and AUC, albeit to a smaller extent for  $T_{max}$  and amount absorbed.

## Simulated fed state conditions

The results of the PSA of CA formulation in a human model (fed state) are presented in Figure 58.

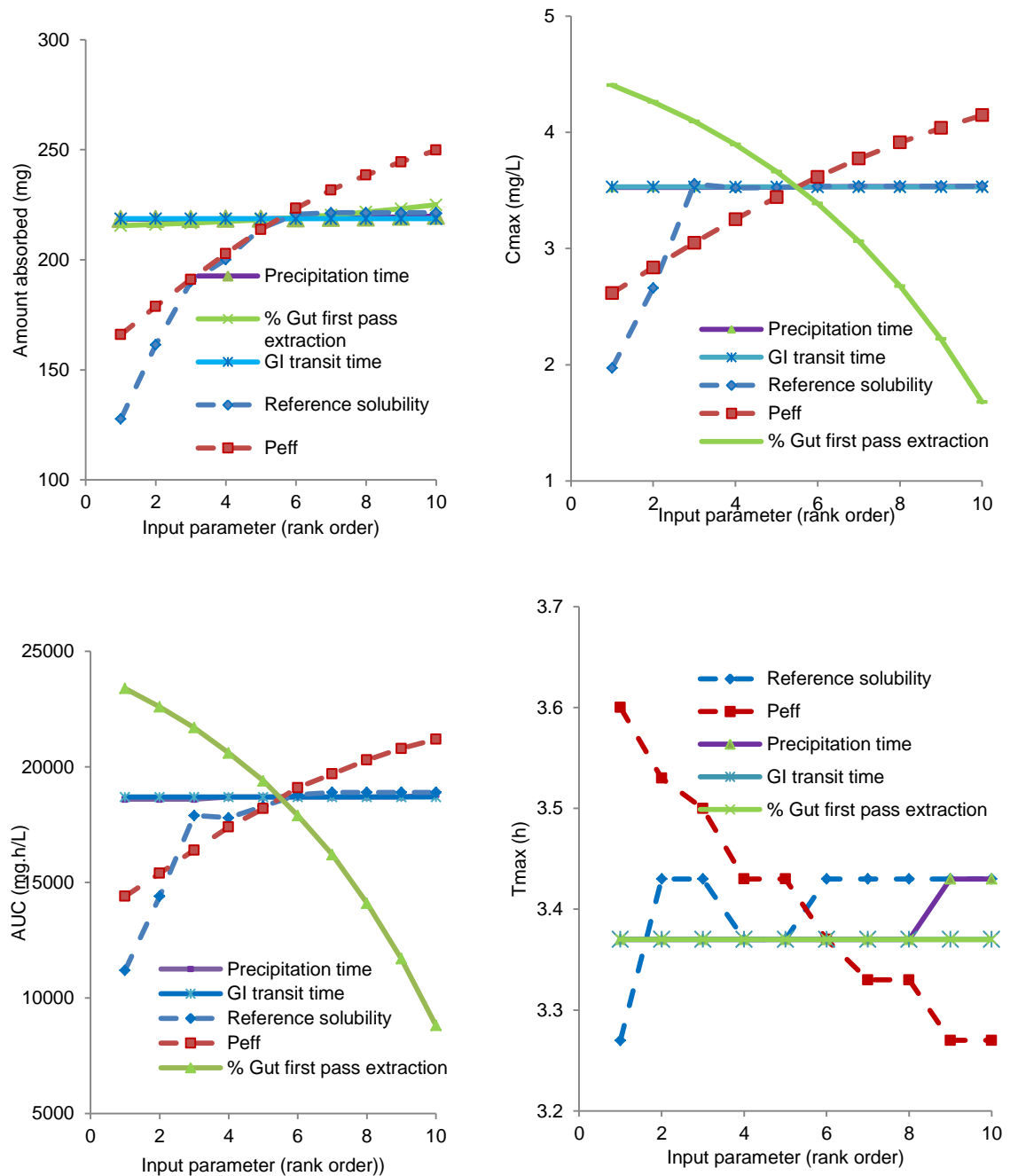


Figure 58. PSA of absorption and pharmacokinetic parameters of CA (fed state).

Parameter sensitivity analysis (PSA) using built-in GastroPlus™ software showed that the oral absorption of CA is very sensitive to solubility changes (Figure 58). For example, if the solubility increased from 0.037 to 0.48 mg/mL, the  $C_{max}$  would increase from 1.98 to 3.65 mg/L before it plateaued out. Likewise, the amount absorbed also achieved an absorption range of 125-225 mg and AUC of 11000-19000 mg·h/L before

it plateaued out when solubility of CA increased from 0.037 to 0.48 mg/mL. Interestingly, when the same range of solubility was tested, the  $T_{max}$  fluctuated around 3.28-3.44 h and then from 3.88 to 3.44 h (Figure 58). The small difference (0.16 to 0.44 h) was probably due to the changes of degradation rate with a fluctuating dissolution rate caused by the changes in solubility values (163).

The results of PSA indicate that the change of first pass extraction arises mainly due to chemical degradation within the stomach and intestine. This is important evidence to support that enhanced absorption of CA in the fed state is due to a low degradation by first pass extraction in the gut.

Similarly, human effective permeability,  $P_{eff}$ , may affect the amount absorbed,  $C_{max}$ , AUC and  $T_{max}$  if the  $P_{eff}$  range of  $0.624-2.494 \times 10^{-4}$  cm/s was applied. For example, the amount absorbed increased from 160 to 250mg,  $C_{max}$  increased from 2.6 to 4 mg/mL as well as AUC from 14500 to 21000 mg·h/L when  $P_{eff}$  was increased from 0.624 to  $2.494 \times 10^{-4}$  cm/s. On the other hand, the amount of CA absorbed was independent of the GI transit time indicating that CA was absorbed mainly in the intestine, which is as expected because Zinnat<sup>®</sup> is an immediate release formulation.

### **3.7 Results and Discussion of Part 3: PBPK modeling (ITR)**

#### **3.7.1 Prediction of *in vivo* performance based on PBPK models**

In this section, the PBPK predictions of the *in vivo* behaviour of the amorphous ITR formulation (Sporanox<sup>®</sup>) using GastroPlus<sup>®</sup> were presented. Firstly, the predictions were made based on solubility based models in which the results showed that these models were not able to simulate closely the observed *in vivo* profile (results presented in Appendix 8). Secondly, the predictions were made based on the solubility combined with the dissolution based model whereby *in vitro* drug dissolution profiles obtained with USP apparatus 2 and 4 were included.

### 3.7.1.1 Solubility combined with dissolution based model

#### Simulated fasted state conditions

##### a) USP apparatus 2

The plasma concentration-time of simulated (solubility and dissolution-based model) and observed (human) profiles after an oral administration of Sporanox<sup>®</sup> in fasted state with USP apparatus 1 are presented in Figure 59 (single stage dissolution models) and Figure 60 (2 stage dissolution models).

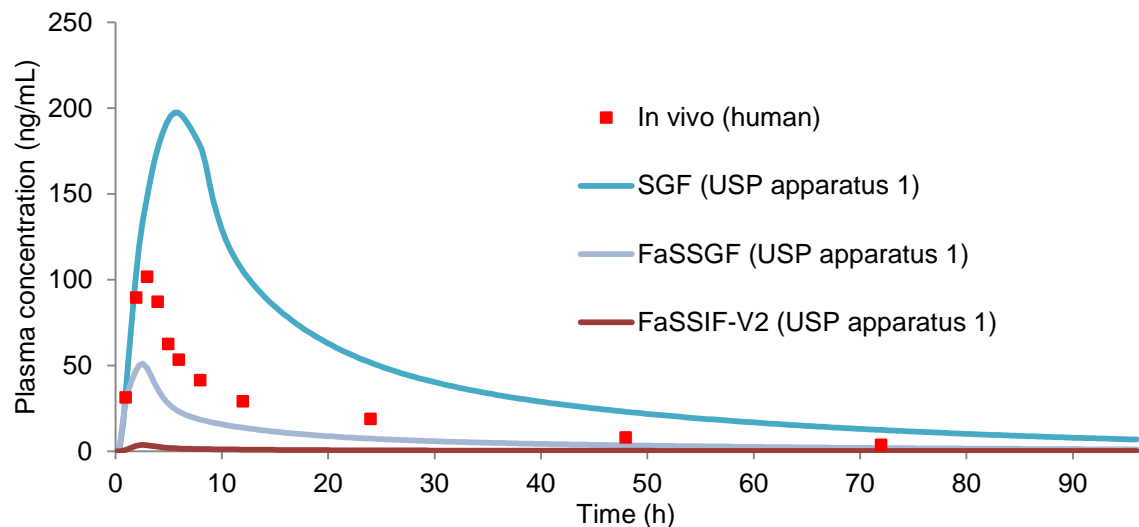


Figure 59. Simulation (line) of oral Sporanox<sup>®</sup> profiles in humans using dissolution profiles measured in FaSSIF-V2, SGF and FaSSGF with USP apparatus 1 compared to observed *in vivo* profile (human, fasted; ■)(299).

The plasma concentration–time profile of ITR was overpredicted by the models with dissolution profile with SGF with USP apparatus 1. SGF is the compendial dissolution medium recommended by USP (42) which yields more than 50% dissolution in 2 h and more than 90% dissolution in 8 h. Apparently, this dissolution profile was higher than that of *in vivo* thus led to an overestimated simulated profile ( $f_1$  SGF:123.20). However, other media such as FaSSGF and SIF led to an underestimated model ( $f_1$  SGF:123.20;  $f_1$  FaSSIF-V2:98.10;  $f_1$  FaSSGF:44.50). As a BCS Class 2 compound (360), the rate limiting step for absorption of ITR from Sporanox<sup>®</sup> is its dissolution. Apparently, the intraluminal dissolution rate was underestimated from the *in vitro* dissolution results with FaSSGF and FaSSIF-V2 with USP apparatus 1.



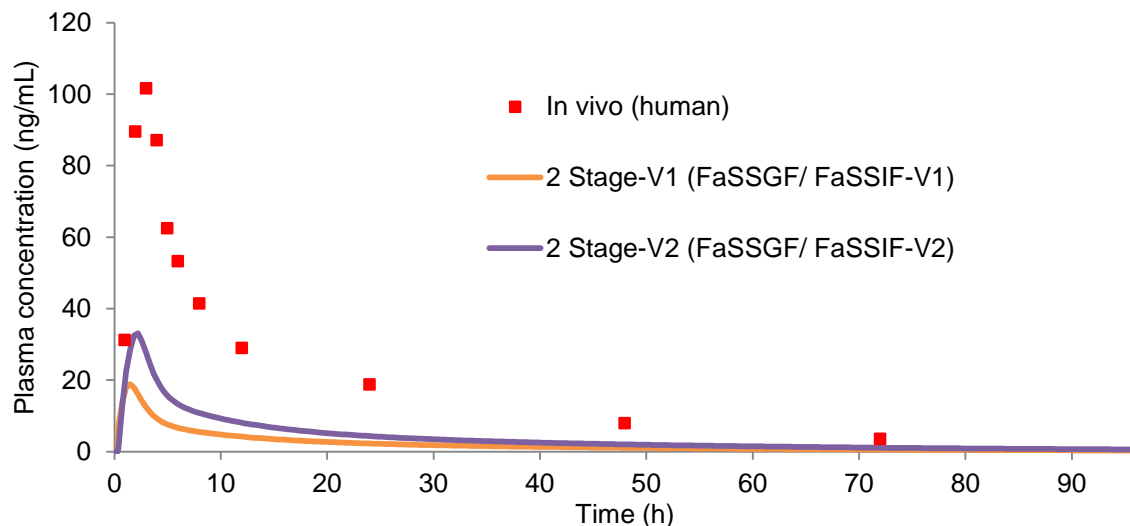


Figure 60. Simulation (line) of oral Sporanox<sup>®</sup> profiles in humans using dissolution profiles measured in 2 stage media experiments with USP apparatus 1 compared to the observed *in vivo* profile (human, fasted; ■) (299).

As depicted in Figure 60, simulated plasma concentration time profiles with 2 stage-V2 (FaSSGF/ FaSSIF-V1) dissolution data are more representative relative to the *in vivo* data compared with 2 stage-V1 (FaSSGF/ FaSSIF-V2) ( $f_1$  2 stage-V1 (FaSSGF/ FaSSIF-V1):79.50;  $f_1$  2 stage-V2 (FaSSGF/ FaSSIF-V2):40.70). The result suggested that a different degree of precipitation of ITR during pH change from stomach to intestine has a significant impact on the simulation. Due to higher dissolution as well as lower precipitation of ITR observed in 2 stage-V2, this result was translated into a higher simulated plasma concentration time profile. However, due to higher solubility of ITR in FaSSIF-V1, the supersaturation level was maintained for a longer period of time and subsequently decreased at a lower rate.

#### b) USP apparatus 4

The plasma concentration-time of simulated (solubility and dissolution-based model) and observed (human) profiles after an oral administration of Sporanox<sup>®</sup> in fasted state with USP apparatus 4 are presented in Figure 61.

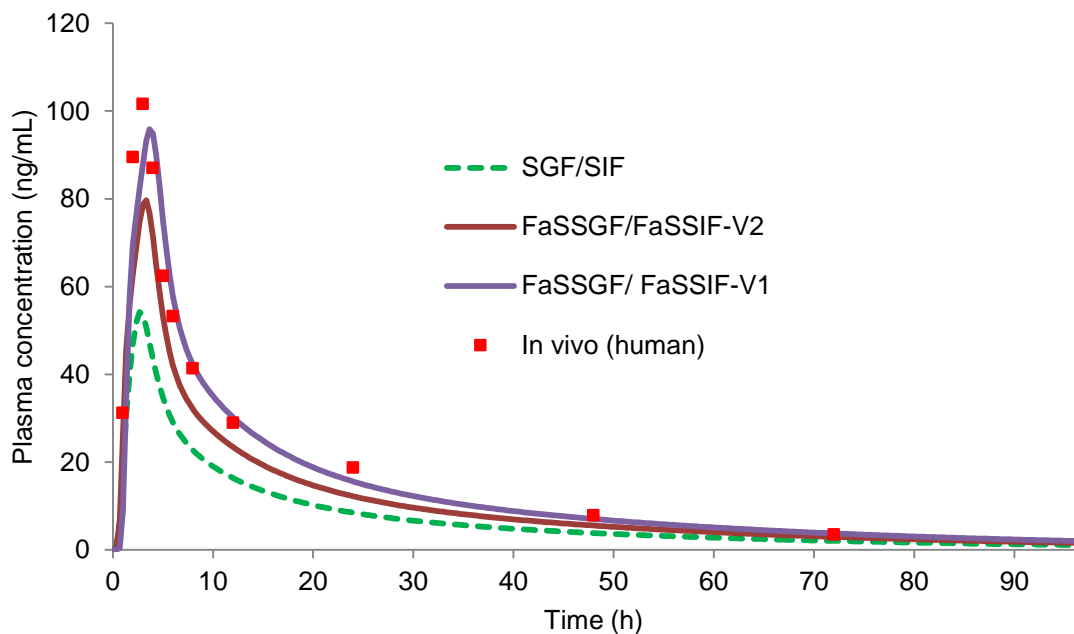


Figure 61. Simulation (line) of oral Sporanox<sup>®</sup> profiles in humans using scaled FaSSIF-V1 solubility and dissolution profiles obtained with USP apparatus 4 compared to the observed *in vivo* profile (human, fasted; ■) (299).

Based on the dissolution profiles with USP apparatus 4 as input functions, *in vivo* profile of Sporanox<sup>®</sup> was best predicted by FaSSGF/FaSSIF-V1 compared to FaSSGF/FaSSIF-V2 and SGF/SIF ( $f_1$  FaSSGF/FaSSIF-V1:16.50;  $f_1$  FaSSGF/FaSSIF-V2:21.90;  $f_1$  SGF/SIF:46.90). The results seem to suggest that FaSSIF-V1 could mimic the *in vivo* intestinal fluid better than FaSSIF-V2 and SIF. The main reason could be that FaSSIF-V1, which had a higher content of bile salt and lecithin than FaSSIF-V2, could prevent ITR from precipitation upon exit from the stomach (50, 51). This is in agreement with the results of the ITR precipitation study (Presented previously in Section 3.3.5) which showed different ITR (from Sporanox<sup>®</sup>) recrystallisation rates upon transfer to the conditions simulating the small intestine.

## Simulated fed state conditions

### a) USP apparatus 2

The plasma concentration-time of simulated (Solubility combined with dissolution based model) and observed (human) profiles after an oral administration of Sporanox<sup>®</sup> in fed state with USP apparatus 1 are presented in Figure 62 and Figure 63.

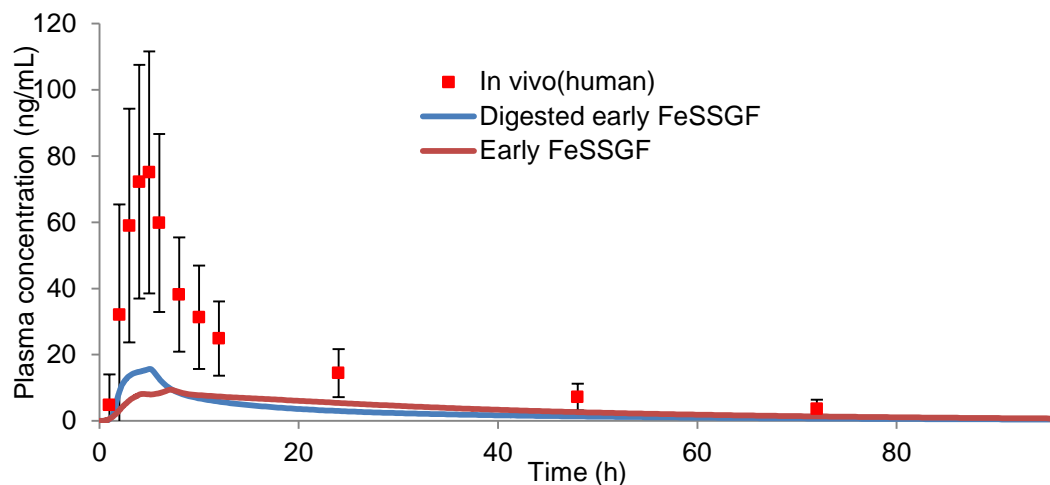


Figure 62. Simulation (line) of oral Sporanox<sup>®</sup> profiles in humans using reference solubility in scaled FeSSIF-V1 and dissolution profiles measured in digested early FeSSGF and early FeSSGF with USP apparatus 1 compared to the observed *in vivo* profile (human, fed; ■) (228).

As depicted in Figure 62, digested early FeSSGF (milk with pH adjusted to 6.4) has an impact on the simulation. Compared to early FeSSGF, digested early FeSSGF produced a higher peak concentration. This could be due to the higher rate and extent of ITR dissolution in digested early FeSSGF than early FeSSGF, which translated into a higher simulated plasma concentration.

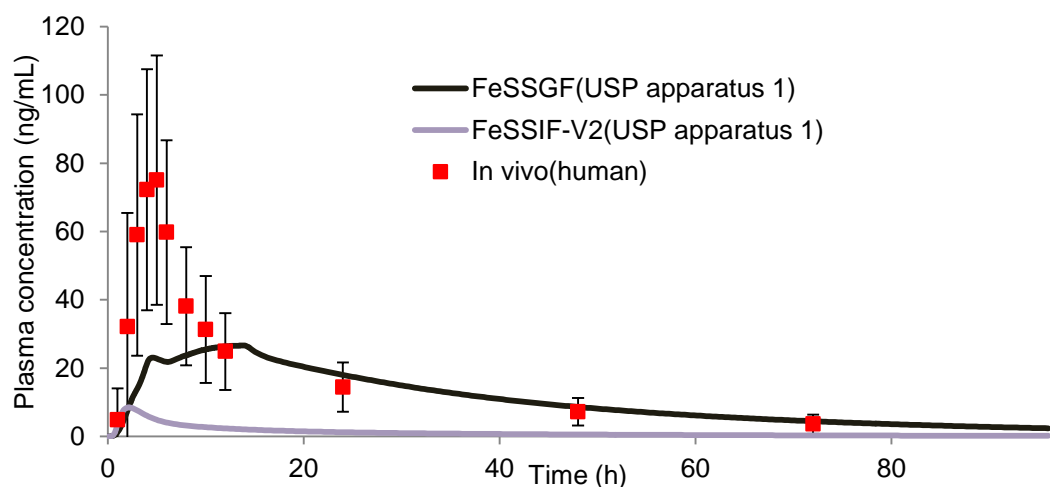


Figure 63. Simulation (line) of oral Sporanox<sup>®</sup> profiles in humans using reference solubility-pH in scaled FeSSIF-V1 and dissolution profiles measured in FeSSGF and FeSSIF-V2 with USP apparatus 1 compared to the observed *in vivo* profile (human, fed; ■) (228).

Based on the dissolution profiles with USP apparatus 1 as input functions (Figure 63), the *in vivo* profile of Sporanox<sup>®</sup> is comparatively better predicted by FeSSGF than FeSSIF-V2 ( $f_1$  FeSSIF-V2:90.8;  $f_1$  FeSSGF:59.74). For FeSSGF, the profile was not successful in simulating the *in vivo* plasma profile which has a prominent feature of a peak concentration of 75 ng/mL.

#### b) USP apparatus 4

The plasma concentration-time of simulated (Solubility combined with dissolution based model) and observed (human) profiles after an oral administration of Sporanox<sup>®</sup> in fed state with USP apparatus 4 are presented in Figure 64.

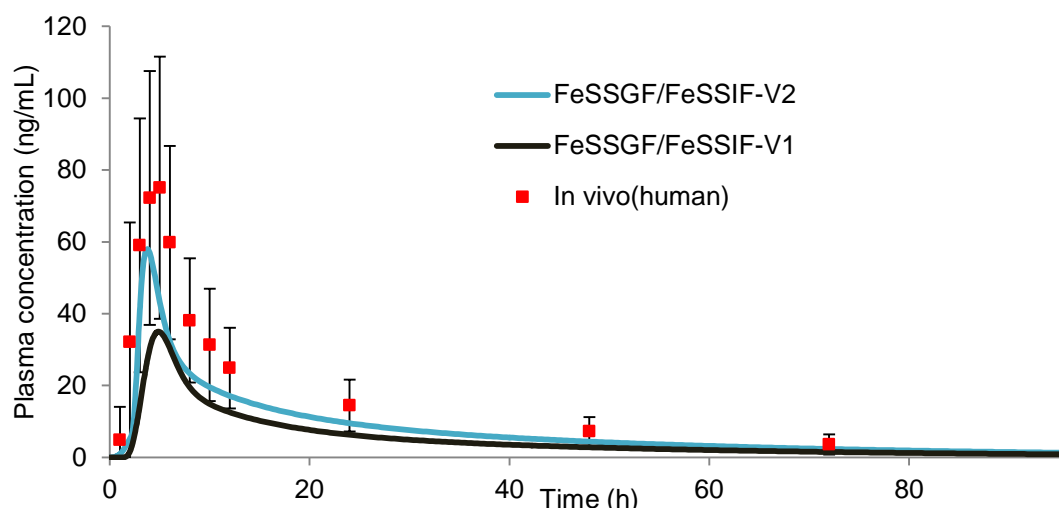


Figure 64. Simulation (line) of oral Sporanox<sup>®</sup> profiles in humans using dissolution profiles with FeSSGF/FeSSIF-V1 and FeSSGF/FeSSIF-V2 (reference solubility: scaled FeSSIF-V1) with USP apparatus 4 compared to the observed *in vivo* profile (human, fed; ■) (228).

Figure 64 shows that the predicted ITR plasma concentration profiles with FeSSGF/FeSSIF-V1 underestimated the *in vivo* profile ( $f_1$ :63.0). Meanwhile, in this project, the best predicted ITR plasma concentration profile was obtained with FeSSGF/FeSSIF-V2 ( $f_1$ :39.57). The dissolution profile in FeSSGF/FeSSIF-V2 indicated a better % dissolved of ITR compared to FeSSGF/FeSSIF-V1 (dissolution profiles presented in Figure 33), indicating the effect of the lipolytic product such as monoglycerides and fatty acids (57) on the dissolution of ITR. The simulated profiles also suggest that FeSSIF-V2 could mimic the *in vivo* intestinal fluid in the fed state better than FeSSIF-V1.

In sum, we successfully developed a validated PBPK model for amorphous ITR formulations in fasted and fed states using solubility combined with dissolution profile models. The results demonstrated how the knowledge generated by integrating biorelevant *in vitro* solubility, *in vitro* dissolution data, enzyme and transporter data ( $K_m$  and  $V_{max}$ ), with *in vivo* humans pharmacokinetics and clinical data, could create a predictive model for dissolution and absorption of amorphous ITR formulation.

### 3.7.2 Parameter sensitivity analysis

#### Simulated fasted state conditions

The results of the PSA of ITR in a human model (fasted state) are presented in Figure 65.

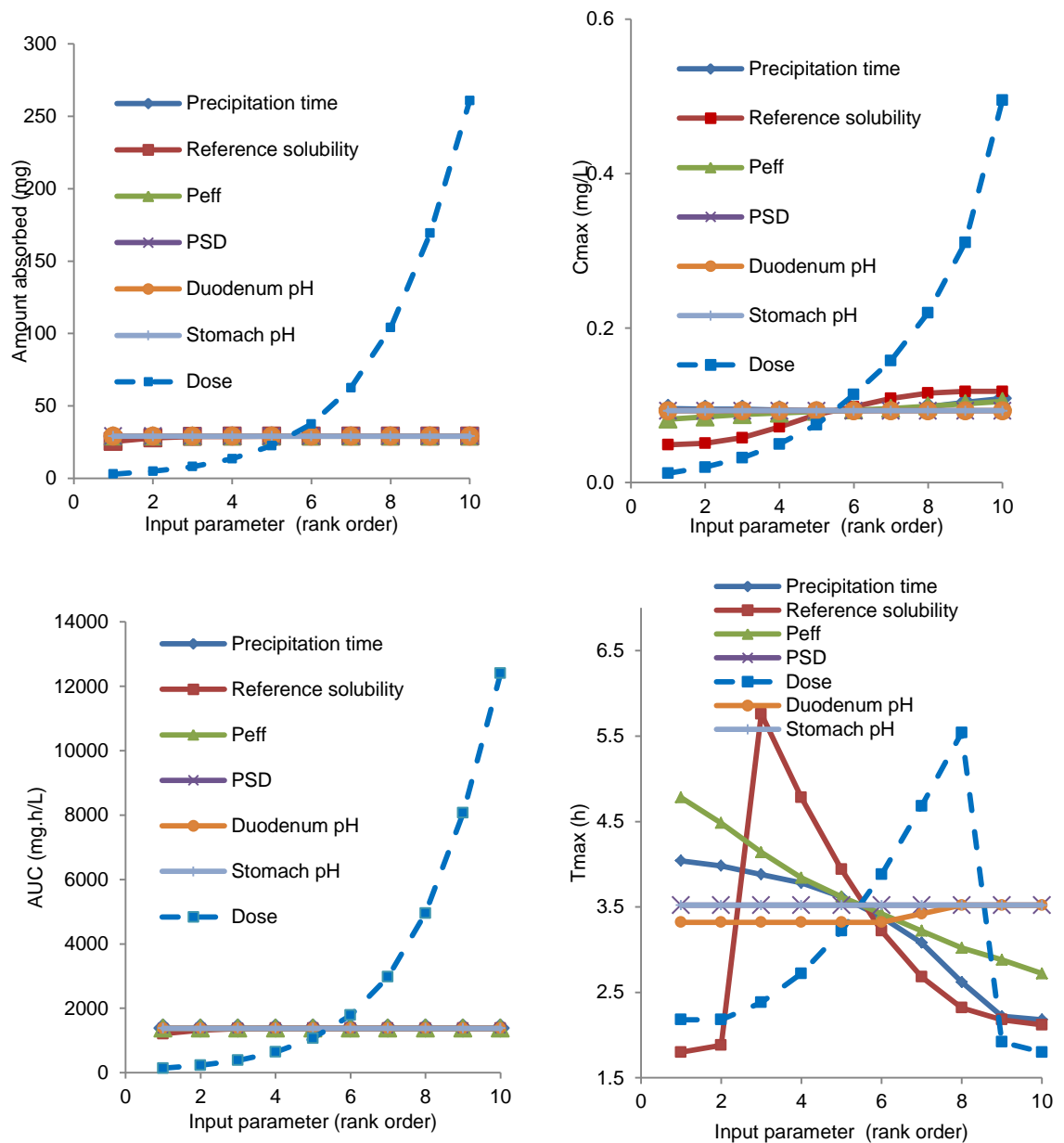


Figure 65. PSA of absorption and pharmacokinetic parameters of ITR (fasted state).

By using the ACAT model in GastroPlus™, it was assumed that only drug in solution could undergo luminal degradation, carrier-mediated influx transport and absorption

into the intestinal wall. Once the drug had been absorbed, it was assumed to remain in solution (in enterocytes, plasma and all pharmacokinetic compartments). Thus, both the rate at which solid drug particles dissolved and the total amount of drug that could be dissolved in any compartment at any one time (solubility) had a direct effect on the degradation, efflux, metabolism and absorption of the drug (361). Since ITR is a weak base, theoretically both the absorption and precipitation of ITR is influenced by the pH of the environment. If the drug in solution transits from a compartment of high solubility to one of lower solubility, precipitation can occur and indirectly affect the plasma concentration vs time profile. However, according to the PSA, the precipitation time, duodenum pH and stomach pH have less influence on the pharmacokinetic of ITR compared to the amount of dose administered. This is probably due to the formulation effect of ITR whereby the HPMC and ITR solid dispersions are more resistant to the changes in pH. Thus, the PSA suggested that the dose could be modified to enhance the pharmacokinetics of ITR (361).

According to Figure 65,  $T_{max}$  was mainly affected by dose, solubility and  $P_{eff}$  of ITR. For instance, by changing the dose administered from 10.0 to 359.4 mg, the  $T_{max}$  was delayed from 2.18 to 5.54 h. Interestingly, when solubility of ITR was increased from 0.802 to 1.34  $\mu\text{g/mL}$ , the  $T_{max}$  increased sharply. However, when the solubility was further increased from 1.34 to 48.0  $\mu\text{g/mL}$ , the  $T_{max}$  decreased drastically. This seems to indicate that after surpassing the solubility threshold of 1.34  $\mu\text{g/mL}$ , the dissolution of ITR in GIT is optimised, leading to a peak absorption in a shorter time. Similarly, when  $P_{eff}$  was increased from 1.73 to  $6.92 \times 10^{-4}$  cm/s, the corresponding  $T_{max}$  decreased from 4.48 to 2.72 h mainly due to enhanced permeability of ITR across the enterocytes, thus the increase in the rate of achieving peak concentration.

## Simulated fed state conditions

The results of the PSA of ITR formulation in a human model (fed state) are presented in Figure 66.

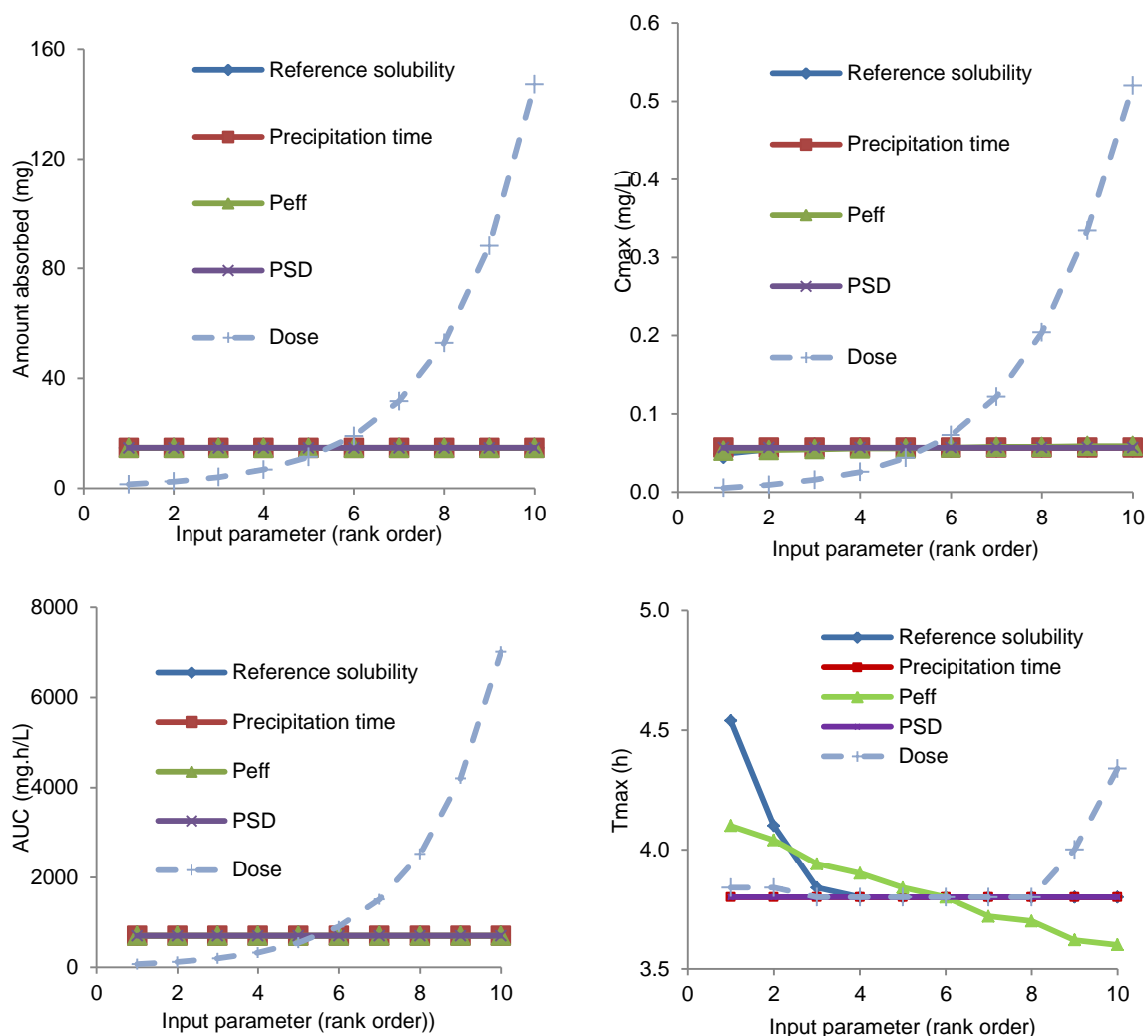


Figure 66. PSA of absorption and pharmacokinetic parameters of ITR (fed state).

Figure 66 illustrates that dose is the most susceptible parameter to any changes. The main parameter affecting absorption and pharmacokinetics is the change of dose (the amount of ITR administered). Since absorption is a first order process, the increased amount of ITR administered can affect greatly the absorption and pharmacokinetics. For instance, when the dose was increased from 10 to 1000 mg, the corresponding amount absorbed increased from 2.46 to 147.2 mg,  $C_{max}$  increased from 0.0006 to 0.52 mg/mL and AUC increased from 117 to 7009 mg.h/L. The PSA results suggest that increasing solubility by 100 fold (0.00225 to 0.225mg/mL) would have a minimal effect on the  $C_{max}$ , AUC and amount absorbed.



### 3.8 Results and Discussion of Part 3: PBPK modeling (CX)

In the first part of this section, the PBPK predictions of the *in vivo* behaviour of the amorphous CX formulations using GastroPlus® are presented. Predictions were made based on the solubility based model (with single solubility value and pH-solubility range value) as well as the solubility combined with the dissolution based model, whereby *in vitro* drug dissolution profiles obtained with USP apparatus 2 and 4 were included. Profile comparison was performed using plasma concentration vs time profile obtained in a clinical *in vivo* study.

#### 3.8.1 Prediction of *in vivo* performance based on PBPK models

The plasma concentration-time of simulated and observed (dog) profiles after oral administration of 240 mg/tablet CX formulations (Formulation 8 unless indicated otherwise as Formulation 4, 5, 6 or 7) in fed state conditions are presented in the following sections.

##### 3.8.1.1 Solubility-based model

The plasma concentration-time of simulated (solubility based model) and observed (beagle dog) profiles after oral administration of one CX F8 formulation in fed state are presented in Figures 67 and 68.

##### Single solubility value model

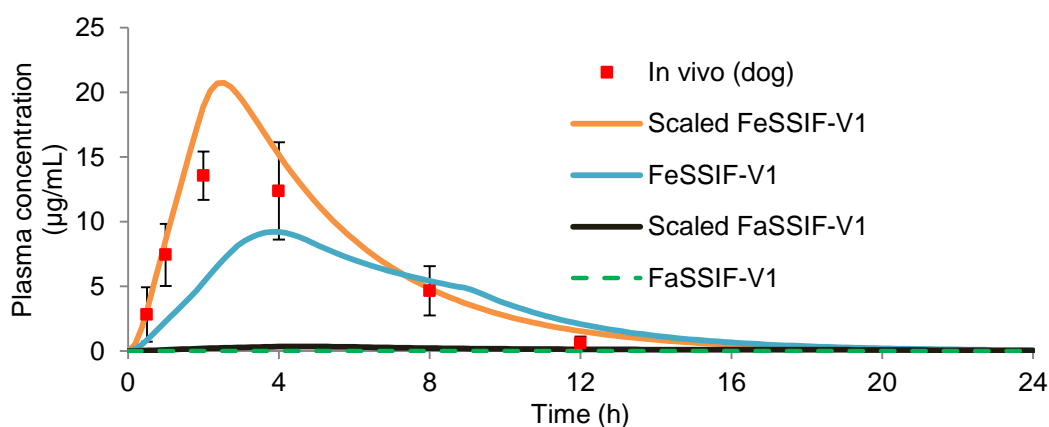


Figure 67. Simulation (line) of oral CX profiles in dogs using reference solubility measured in FaSSIF-V1, FeSSIF-V1, scaled FaSSIF-V1 and scaled FeSSIF-V1 compared to observed *in vivo* profile (dog, fed; ■) (252).

According to Figure 67, the simulation based on solubility of scaled FeSSIF-V1 is very similar to the *in vivo* profile ( $f_1$ :29.40). This seems to suggest that solubility of scaled FeSSIF-V1 mimicked CX solubility of *in vivo* fed state conditions well and CX solubility in intestinal fluid of beagle dogs is likely to be similar to the solubility in the fed state human intestinal fluid (equivalent to solubility in scaled FeSSIF-V1). In contrast to scaled FeSSIF-V1, the solubility values in FeSSIF-V1, FaSSIF-V1 and scaled FaSSIF-V1 produced simulated profiles that underestimated the *in vivo* profile ( $f_1$  FeSSIF-V1: 49.18,  $f_1$  FaSSIF-V1:99.50 and  $f_1$  scaled FaSSIF-V1: 97.50). This is expected as the *in vivo* data are from the fed state and FeSSIF-V1 does not contain lipolytic products that are commonly found in dog's GIT (362). The simulated profile developed using various solubility values also shows that solubility is one of the main rate-limiting physiological variables for *in vivo* absorption of CX. An appropriate biorelevant solubility value could accurately simulate the conditions in the dog GIT leading to closer prediction of *in vivo* performance.

#### pH solubility range model

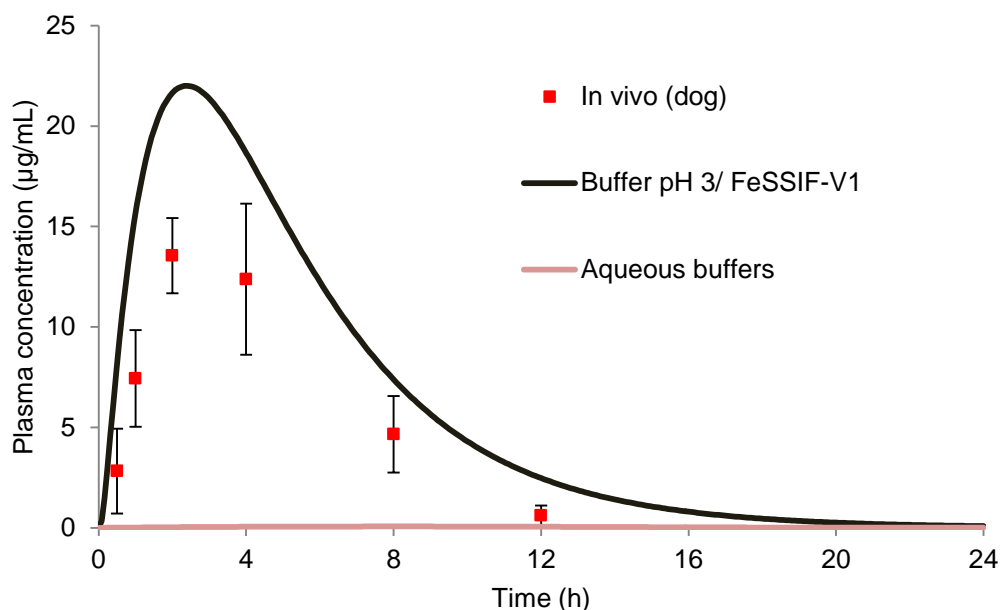


Figure 68. Simulation (line) of oral CX profiles in dogs using reference solubility-pH range in aqueous buffer pH 3/FeSSIF-V1 and aqueous buffers at pH 1.1, 3, 4.5, 6.8, 7.5 and 8.5 compared to observed *in vivo* profile (dog, fed; ■) (252).

According to Figure 68, using solubility-pH range as an input, *in vivo* solubility profile of buffer at pH 3 plus FeSSIF-V1 was overestimated ( $f_1$ :99.20), whereas the *in vivo* solubility profiles of aqueous buffers (233) were greatly underestimated ( $f_1$ :99.60). The results suggest that the solubility-pH range using FeSSIF-V1 and aqueous buffers are insufficient for generating a predictive PBPK model for CX.

### 3.8.1.2 Solubility combined with dissolution based model

#### Simulated fed state condition

##### a) USP apparatus 2

The plasma concentration-time of simulated (solubility and dissolution-based model) and observed (dog) profiles after oral administration of a CX tablet with USP apparatus 2 are presented in Figures 69 (single stage dissolution models) and 70 (2 stage dissolution models).

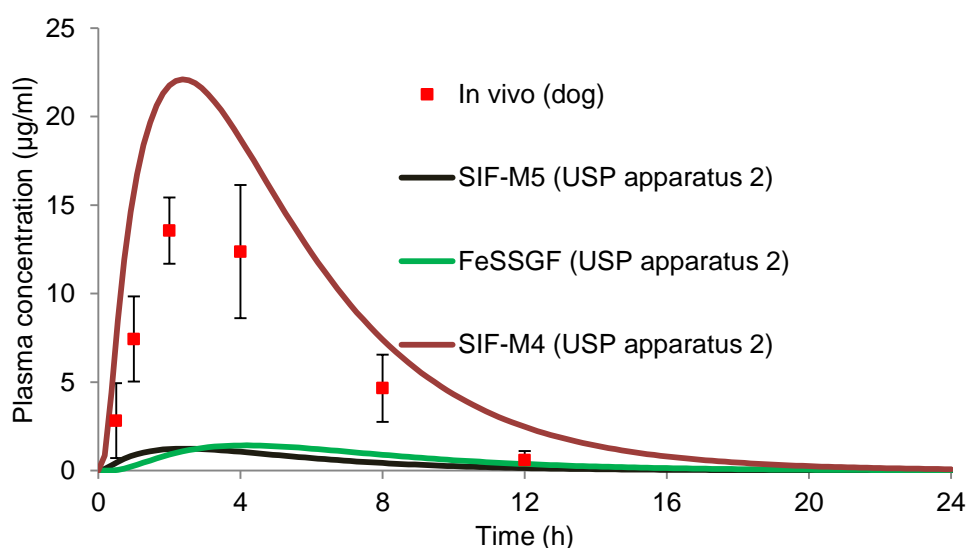


Figure 69. Simulation (line) of oral CX profiles in dogs using reference solubility in FeSSIF-V1 and dissolution profiles measured in SIF-M4 and SIF-M5 with USP apparatus 2 compared to observed *in vivo* profile (dog, fed; ■) (252).

According to Figure 69, the simulated plasma profiles using SIF-M5 (sodium based SIF +1% SLS) underestimated the *in vivo* profile ( $f_1$ : 47.40). This is in agreement with its dissolution profile that showed a fast precipitation after 1 h of the experiment. The simulation seems to indicate that CX in the media containing micelles at pH 6.8, nucleation and growth kinetics of CX out of solution may decrease the bioavailability of CX. Since the primary site for CX absorption is the proximal small intestine, the decreased soluble CX amount due to nucleation and growth out of solution at pH 6.8 is expected to be an important parameter in PBPK simulation.

Meanwhile, the proposed dissolution model for CX (233) (with SIF-M4: SIF+ 1% HTAB, dissolution profiles presented previously in Figure 35) seems to have overpredicted  $C_{max}$  and AUC of the *in vivo* profiles. It must be noted that 1% of HTAB which provides

a sink condition for CX dissolution (233) could probably have higher micellar solubilisation of the bile salt and lecithin in dogs ( $f_1$ :43.60).

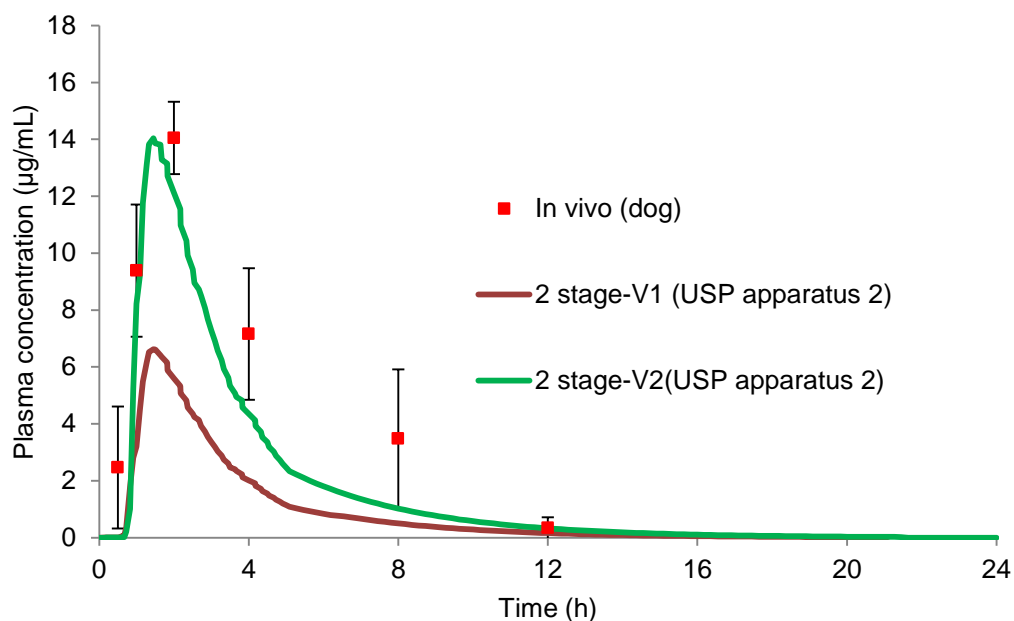


Figure 70. Simulation (line) of oral CX profiles in dogs using reference solubility in FeSSIF-V1 and dissolution profiles measured in 2 stage-V1 (FaSSGF/FaSSIF-V1) and 2 stage-V2 (FaSSGF/FaSSIF-V2) dissolution models with USP apparatus 2 compared to observed *in vivo* profile (dog, fed; ■) (252).

According to Figure 70, the simulation using dissolution profiles of CX in 2 stage-V2 is considerably closer to the *in vivo* profiles compared to 2 stage-V1 ( $f_1$  2 stage-V2=46.10,  $f_1$  2 stage-V1=75.40). The difference in the two simulated profiles is mainly due to much higher extent and rate of dissolution in FaSSIF-V2 than in FaSSIF-V1 (Dissolution profiles presented in Figure 36).

#### **b) USP apparatus 4**

The plasma concentration-time of simulated (solubility and dissolution-based model) and observed (dog) profiles after oral administration of a CX tablet with USP apparatus 4 are presented in Figures 71-75.

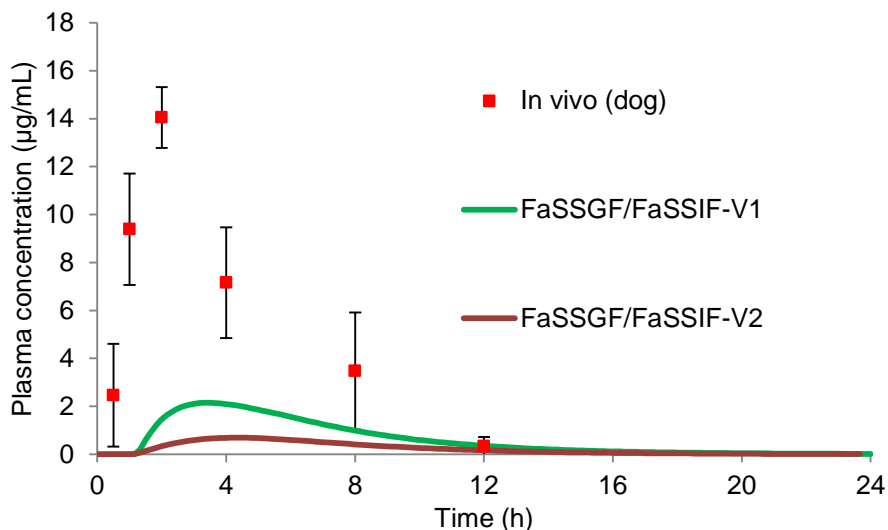


Figure 71. Simulation (line) of oral CX profiles in dogs using reference solubility in FaSSIF-V1 and dissolution profiles measured in FaSSGF/FaSSIF-V1 and FaSSGF/FaSSIF-V2 with USP apparatus 4 compared to observed *in vivo* profile (dog, fed; ■) (252).

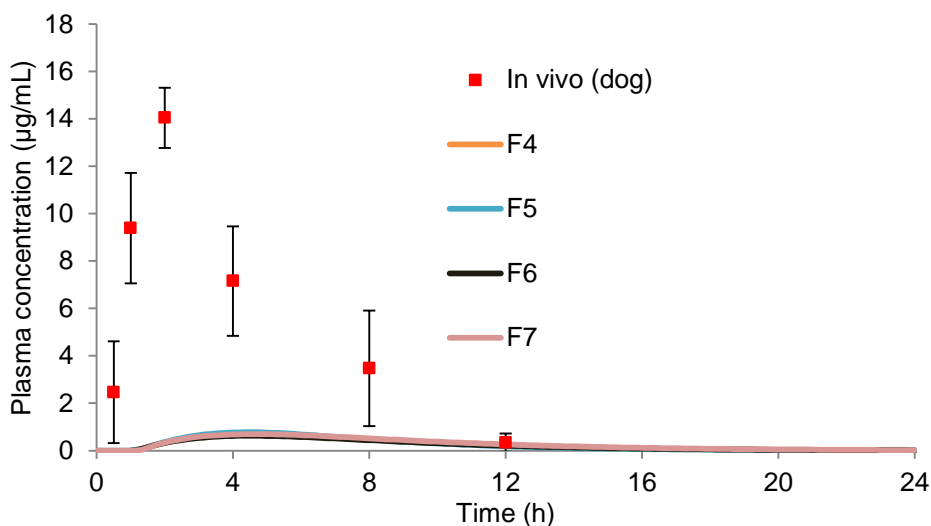


Figure 72. Simulation (line) of oral CX profiles of F4, F5, F6 and F7 in dogs using reference solubility in FaSSIF-V1 and dissolution profiles measured with FaSSGF/FaSSIF-V2 with USP apparatus 4 compared to observed *in vivo* profile (dog, fed; ■) (252).

To the best of the author's knowledge, there is no literature values published on the amount of bile salt and lecithin in the GI fluids of the beagle dog. It is known that there are differences in the composition of intestinal fluid in dogs and humans, including the concentration of bile salts. However, it is known that the amount of bile salt and lecithin in dog GI fluids is higher than the human GI fluids (363-365). Although the *in vivo* data was tested in the fed state, it is observed that the FaSSIF-V2 is closer to the intestinal fluid of the beagle dog ( $f_1$  FaSSGF/FaSSIF-V1:90.10; FaSSGF/FaSSIF-V1:95.70).

Meanwhile, the F4, F5, F6 and F7 of CX showed very similar simulated plasma profiles (Figure 72). It was expected because these formulations have very similar dissolution profiles in FaSSGF/FaSSIF-V2.

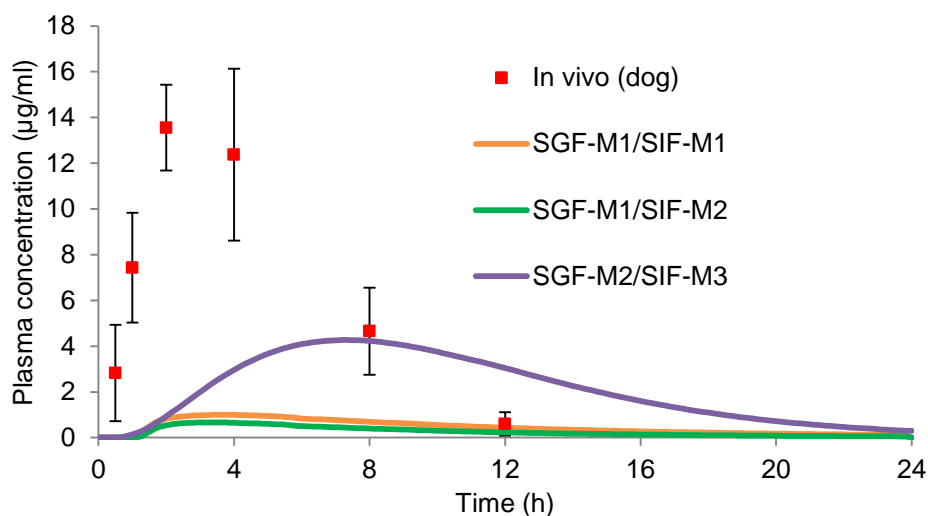


Figure 73. Simulation (line) of oral CX profiles in dogs using reference solubility in FeSSIF-V1 and dissolution profiles measured in SGF-M1/SIF-M1, SGF-M1/SIF-M2, SGF-M2/SIF-M3 with USP apparatus 4 compared to observed *in vivo* profile (dog, fed; ■) (252).

Similar to the simulated profiles in biorelevant media, the modified media do not simulate the *in vivo* dissolution in beagle dogs well (fed state). This is probably due to the solubilisation capacity of these modified media that do not match with the bile salt micellar solubilisation effect in dogs ( $f_1$ : SGF-M1/SIF-M1:92.97; SGF-M1/SIF-M2: 95.27 and  $f_1$ : SGF-M2/SIF-M3:84.19) (Figure 73).

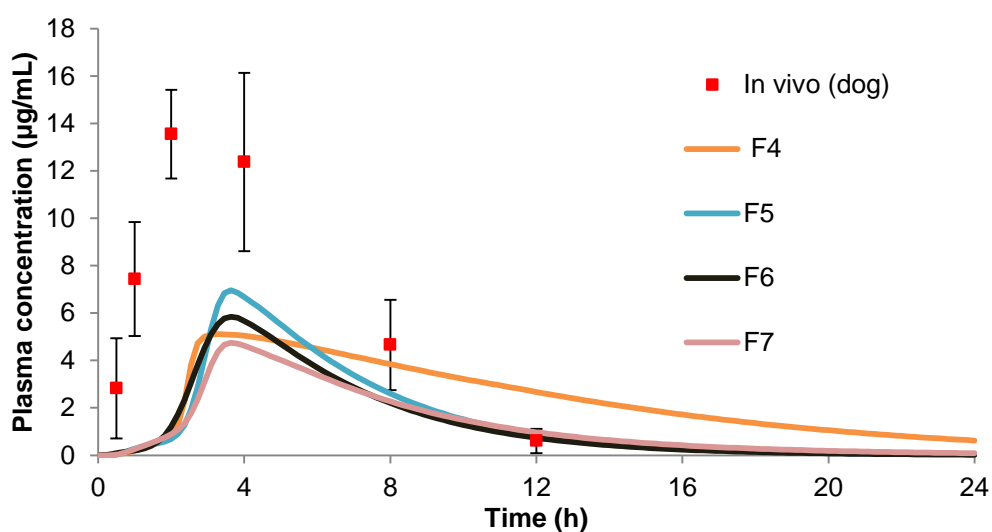


Figure 74. Simulation (line) of oral CX profiles in dogs using reference solubility in FeSSIF-V1 and dissolution profiles measured in FeSSGF/FaSSIF-V2 with USP apparatus 4 with F4, F5, F6 and F7 compared to observed *in vivo* profile (dog, fed; ■) (252).

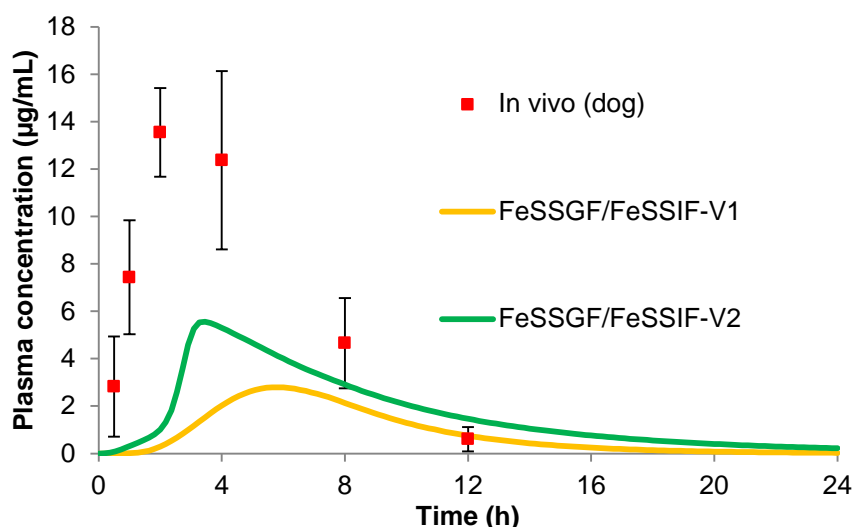


Figure 75. Simulation (line) of oral CX profiles in dogs using reference solubility in FeSSIF-V1 and dissolution profiles measured in FeSSGF/FeSSIF-V1 and FeSSGF/FeSSIF-V2 with USP apparatus 4 with F8 compared to observed *in vivo* profile (dog, fed; ■) (252).

Similar to FaSSGF/FaSSIF-V2 (presented in Figure 72), F4, F5, F6 and F7 of CX showed very similar simulated plasma profiles (Figure 74) and the dissolution profiles of these formulations in FeSSGF/FeSSIF-V2 were very similar (Dissolution profiles presented previously in Figure 39).

According to Figure 75, FeSSGF/FeSSIF-V2 is more predictive compared to -V1 because the lipolytic products in FeSSIF-V2 mimicked the true *in vivo* conditions and were capable of solubilising the poor water soluble CX molecules. The biorelevant dissolution media designed to simulate human conditions does not seem to be able to simulate the plasma concentration in dogs well, probably due to the higher amount of bile salt and lecithin content of dogs' GI fluid. The FeSSIF-V2 media indicated a better percentage of drug release compared to FeSSIF-V1 media, indicating the effect of the lipolytic product on the dissolution of CX and also reflecting on the absorption of the drug.

For compounds with highly pH-dependent solubility such as CX, changes in GI pH due to, for example, food intake, can have a large impact on the dissolution and hence absorption of the drug (366). Poorly soluble compounds often show an increased solubility in the presence of surfactants; for example, bile acid concentration is different in the fasted and fed states (54, 366). Therefore, the dissolution profiles in fed state with USP apparatus 4 provide a better prediction compared with the fasted media ( $f_1$ : FeSSGF/FeSSIF-V1=88.67, FeSSGF/FeSSIF-V2=82.06).

Generally, dissolution profiles with USP apparatus 4 give better simulations compared to single dissolution profiles with USP apparatus 2 ( $f_1$  FeSSGF=93.55). This shows that combining the physiological relevant hydrodynamics and medium change can mimic the human GI tract to achieve a predictive model.

In sum, in order to simulate better drug dissolution in the dog intestine, biorelevant dissolution testing taking into account interspecies differences in terms of the higher concentrations of bile salts and lecithin in dogs, and dog GIT hydrodynamic and gastric emptying time also need to be considered. On the other hand, simulations performed using simple aqueous buffers or modified buffers failed to provide a predictive property of CX formulations. This further validates the superiority of biorelevant media in solubility and dissolution testing of CX formulations than the compendial and simple aqueous buffers. Furthermore, preclinical dog data and appropriate physiology input parameters are crucial for the successful development of the PBPK model for CX amorphous formulation.



### 3.8.2 Parameter sensitivity analysis

The results of the PSA of CX in a dog model (fed state) are presented in Figure 76.

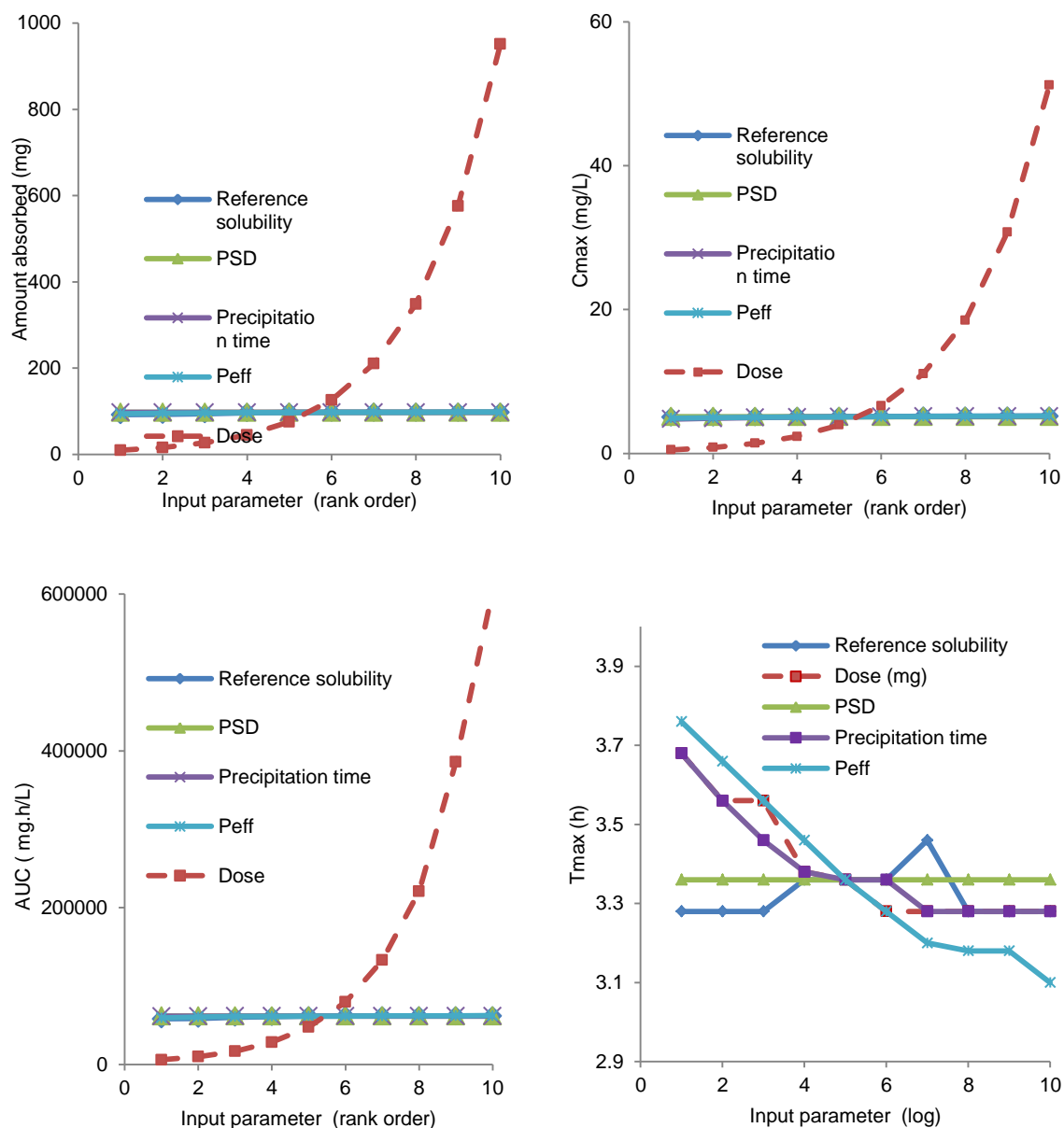


Figure 76. PSA of absorption and pharmacokinetic parameters of CX (fed state)

Based on the PSA GastroPlus<sup>TM</sup>, the oral absorption of this compound is very sensitive to the dose administered. This is expected because absorption of CX is a first order process, thus the increased amount of CX administered can affect greatly the absorption and pharmacokinetics. For instance, the amount absorbed greatly increased from 15.82 to 951 mg, C<sub>max</sub> increased from 0.83 to 51.23 mg/L and AUC increased from 10000 to 604000 mg·h/L. According to Figure 76, P<sub>eff</sub> and solubility are the two main parameters that influenced T<sub>max</sub>. For instance, changes in the P<sub>eff</sub> value

from  $1.4$  to  $5.6 \times 10^{-4}$  cm/s facilitated permeation of CX and enhanced the rate of achieving peak concentration, thus reducing  $T_{\max}$  from 3.66 to 3.10 h.

In sum, it appears that the rate, extent and gastrointestinal location of oral absorption of the CA, ITR and CX could be predicted well using the solubility combined with dissolution based models. Using the PBPK model, the experimental data of the drug was incorporated into the prediction (e.g., Caco-2 permeability, solubility, dissolution) along with the built-in physiological values (such as pH and transit time of each intestinal segment in humans and dogs) to increase the reliability of the absorption prediction. Other absorption related factors, including the time for the rate of precipitation, particle size, chemical degradation, were also considered in the predictions. In the current study, first pass effect, enzymes and transporter metabolism were also included. The PSA performed also increased the understanding of the correlations between absorption and associated parameters, such as solubility, dose, particle size, permeability, and pharmacokinetic parameters.

### 3.9 Results and Discussion of Part 4: Deconvolution analysis

#### 3.9.1 CA

Deconvolution of plasma concentration-time profiles after an oral 250mg Zinnat<sup>®</sup> tablet was implemented. The mean cumulative amount absorbed and absorption rate after oral administration of a CA 250mg/tablet are presented in Figure 77.

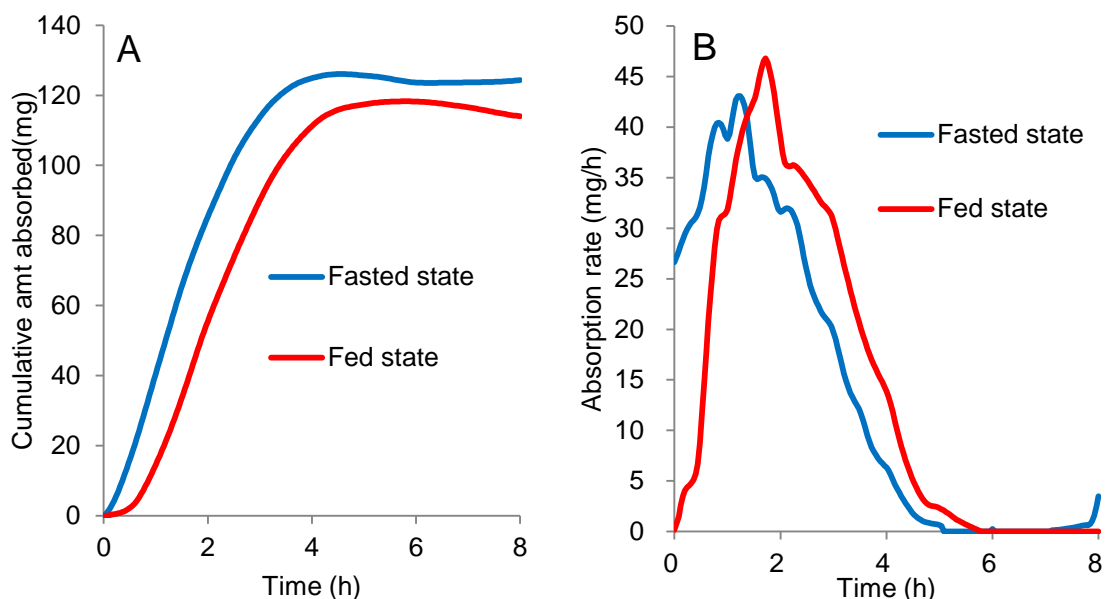


Figure 77. Mean cumulative CA absorbed (A) and absorption rate (B) in fasted and fed state (Deconvolution data).

The observed *in vivo* plasma concentration–time data of CA in fasted and fed states were reported by Rojanasthien *et al.* (287) and Donn *et al.* (288) respectively. The cumulative amount absorbed profiles show the absorption completed in the first 4 h after drug administration corresponding to the time passing through the intestine of human GIT both in fasted and fed states. The mean amount absorbed was approximately 50% in fasted state and 47% in fed state, both reaching a plateau around 4 h post administration (Figure 77). The result is close to the reported median absorption (30-50%) from the Zinnat<sup>®</sup> tablets taken during the fasted state (287). Similarly, this result is close to the reported median absorption (50-55%) from the Zinnat<sup>®</sup> tablets taken after food (198). Only half of CA was absorbed in the fasted state mainly due to the large amount of CA degraded upon exposure to the gastric fluid (pH 1.6- pH3) (199), especially as the CA degradation follows first order kinetics and CA has relatively better solubility in the acidic medium.

Generally administering poor water-soluble drugs in the postprandial state had shown increased absorption compared to when administered in the fasting state due to a longer residence time and changes in the composition of the gastro-intestinal fluids as a consequence of pancreatic and bile secretions (316). An increase in bile salt concentrations was shown to increase the solubility of poorly soluble drugs (75, 367). However, this enhanced effect in the fed state was not apparent in CA due to other confounding factors such as CA degradation and formulation effects (gelling of tablets) (240). Evidence from the literature using different model drugs confirmed that gastric motility and mixing of stomach content were mild such that different foods ingested consecutively were inclined to remain in layers until being emptied from the stomach (368). Thus it was highly likely that the full disintegration of the Zinnat<sup>®</sup> tablet in the stomach was hindered leading to gelling of CA itself and limiting absorption. Furthermore, the absorption rate profiles indicate that absorption occurs earlier in the fasted compared with the fed state, in agreement with the longer gastric transit time in the fed state.

### 3.9.2 ITR

Deconvolution of plasma concentration-time profiles after an oral 100mg Sporanox<sup>®</sup> capsule was implemented. The mean cumulative amount absorbed and absorption rate after oral administration of an ITR 100mg/capsule are presented in Figure 78.

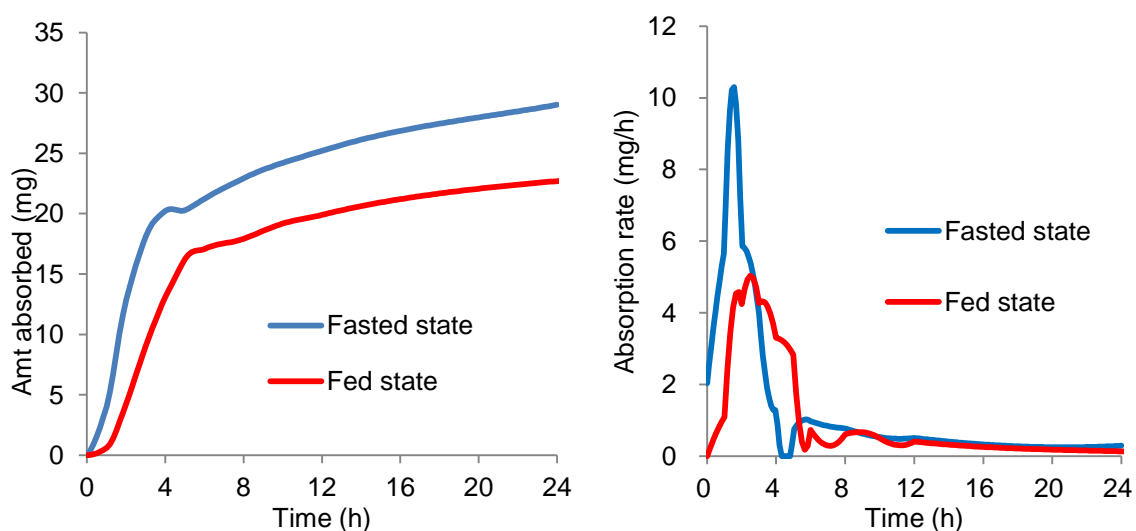


Figure 78. Mean cumulative ITR absorbed (A) and absorption rate (B) in fasted and fed state (Deconvolution data).

*In vivo* plasma concentration-time profiles of Sporanox<sup>®</sup> tablets were taken from the study of Yeates *et al.* (299) (fasted state) and Yun *et al.* (228) (fed state). The absorption rate profiles indicated that the major portion of ITR in the capsule was absorbed within 4-6 h post dose and absorption after 15 h post-dose was relatively low (Figure 80). Meanwhile, the cumulative percentage absorbed profiles showed that the absorption was mainly taking place in the first 4 h in fasted state and 6 h in the fed state. The mean percentage absorbed was approximately 28.78% in the fasted state. When dosed with a high-fat meal supplement (comprising 150 mL low fat milk), the percentage absorbed decreased to about 22.6%. The potential contributing factor for the decrease was the change of gastric pH to a less acidic condition with the ingestion of a milk based product (369) which adversely affects the dissolution of a weak base compound like ITR. The effect of gastric pH on the absorption of ITR from Sporanox<sup>®</sup> was confirmed in a randomised, parallel group, single dose study in 24 healthy subjects (229, 230).

### 3.9.3 CX

Deconvolution of plasma concentration-time profiles after a CX oral tablet formulations (240mg/tablet; F1-F7) was performed.

Figure 79 and Figure 80 present the average (n=4 dogs) cumulative CX absorption and rate after administration of Formulation 1, 2, 3, 4, 5, 6 and 7 (F1-F7; *in vivo* data of F8 was not provided thus deconvolution was not performed for F8). The range of CX absorbed from F1-F7 was from 100mg to 200mg. Meanwhile, the absorption rate profiles indicated that the major portion of CX in the tablet was absorbed within 5 h post dose and absorption after 8 h post-dose was almost zero.

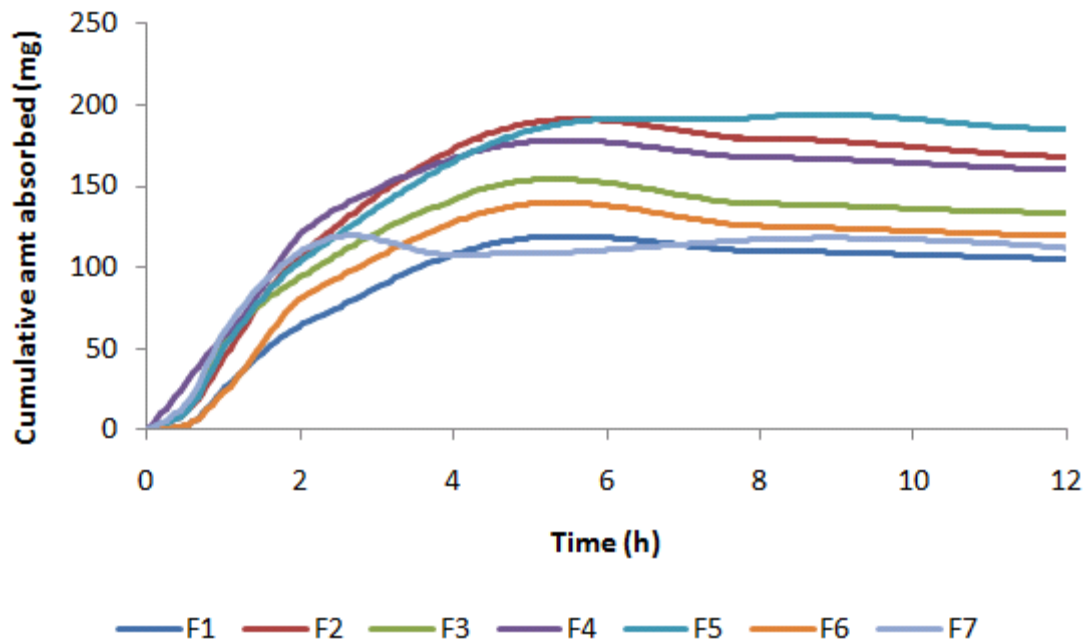


Figure 79. Summary of mean (n=4) cumulative amount absorbed (mg) CX Formulation 1,2,3,4,5,6 and 7 in beagle dogs.

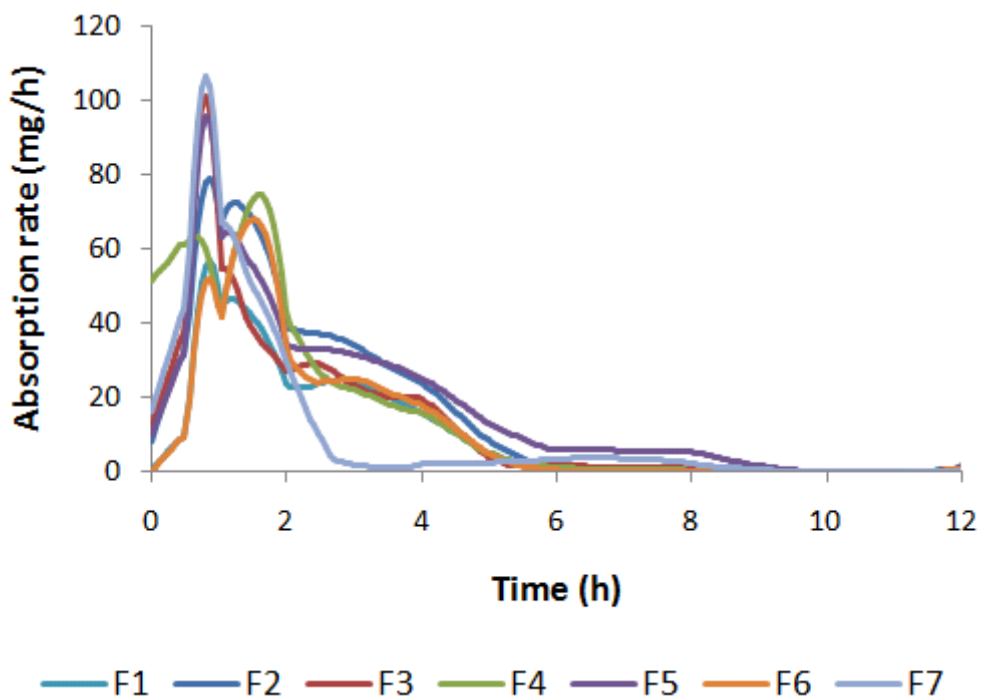


Figure 80. Summary of mean (n=4) absorption rate (mg/h) CX Formulation 1,2,3,4,5,6 and 7 in beagle dogs.

The cumulative amounts of CX absorbed (data from deconvolution using PCDCON) are shown in Figure 81.

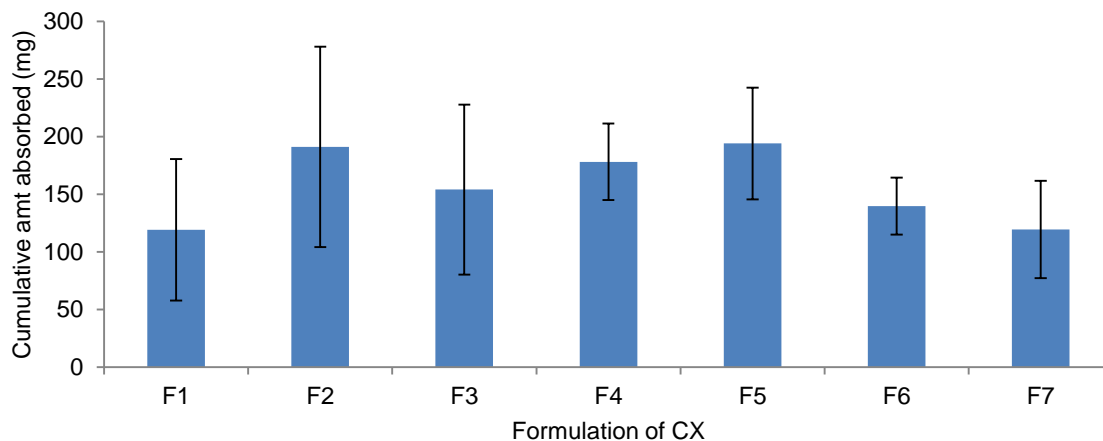


Figure 81. Mean  $\pm$  SD cumulative amount absorbed (deconvolution using PCDCON).

F1 is the first MBP amorphous formulation produced and its particle size distribution data was not given. Since F1 yielded low absorption it is prudent to assume that its particle size distribution is larger than the other formulation causing less dissolution and absorption. Meanwhile, the absorption of CX from F3, F6 and F7 was lower than other MBP formulations (F2, F4 and F5) partly because the particle size distribution was higher than F2, F4 and F5. For instance, the particle size distribution is 93.8  $\mu\text{m}$  for F3 compared to 37.2  $\mu\text{m}$  for F2 and F5 (Details of CX formulations presented previously in Section 2.3.3).

On the other hand, the tableting strength and hardness did not seem to affect the absorption of CX. For example F2, hardness 295N and F5 with hardness 341N showed similar AUC values, 191.09 and 194.05  $\mu\text{g}\cdot\text{h}/\text{mL}$  and a similar amount absorbed 101.28 and 114.25mg, respectively (the tableting strength and hardness for other formulations were not given).

In sum, a cumulative amount of drug absorbed and absorption rate vs time profiles were successfully generated using numerical deconvolution with PCDCON software. These data are useful for the development of IVIVC/IVIVR (Discussed later in Section 3.10). Meanwhile, the results suggested that absorption of CX is not significantly influenced by the drug particle size or compression hardness of tablets.

### 3.10 Results and Discussion of Part 4: Development of IVIVR/IVIVC models

It is well-known that the bioavailability studies in animals and man are time consuming and costly. To the best knowledge of the author, so far there has been no IVIVC /IVIVR of CA, ITR or CX reported in the literature. In this section, the qualitative IVIVRs are first presented and then the mathematical IVIVCs are presented

#### 3.10.1 Qualitative IVIVRs

The results of % absorbed *in vivo* were compared qualitatively with the % dissolved *in vitro* (Figures 82-84)

#### CA

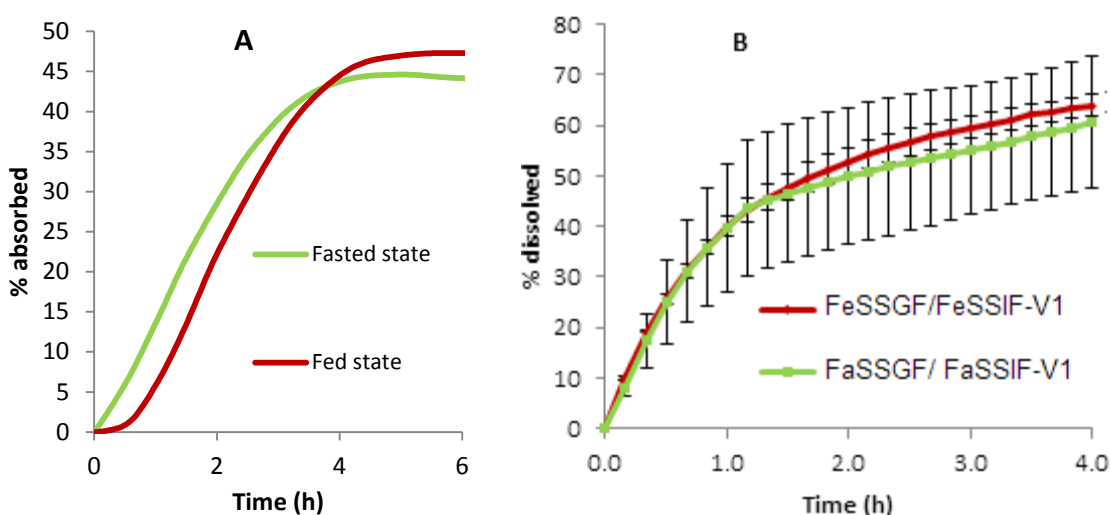


Figure 82. A: % CA absorbed; B: Mean  $\pm$  SD % of CA dissolved from Zinnat<sup>®</sup> 250mg tablet in fasted state FaSSGF (8mL/min;1h)/FaSSIF-V1 (4mL/min;3h) and fed state FeSSGF (6mL/min; 2h)/FeSSIF-V1 (6mL/min;4h) using the USP apparatus 4 (n=3).

The CA dissolution profile in fasted and fed state exhibited the same trend as the absorption profiles of CA. For example after 4 h the % absorbed (*in vivo* study) was around 45% in both the fasted and fed states. Likewise, after 4 h of experiment the % dissolved from FaSSGF/FaSSIF-V1 and FeSSGF/FeSSIF-V1 studies was around 60%. This showed that the use of biorelevant media that mimic the human *in vivo* condition are predictive and applicable for IVIVCs (Figure 82).



## ITR

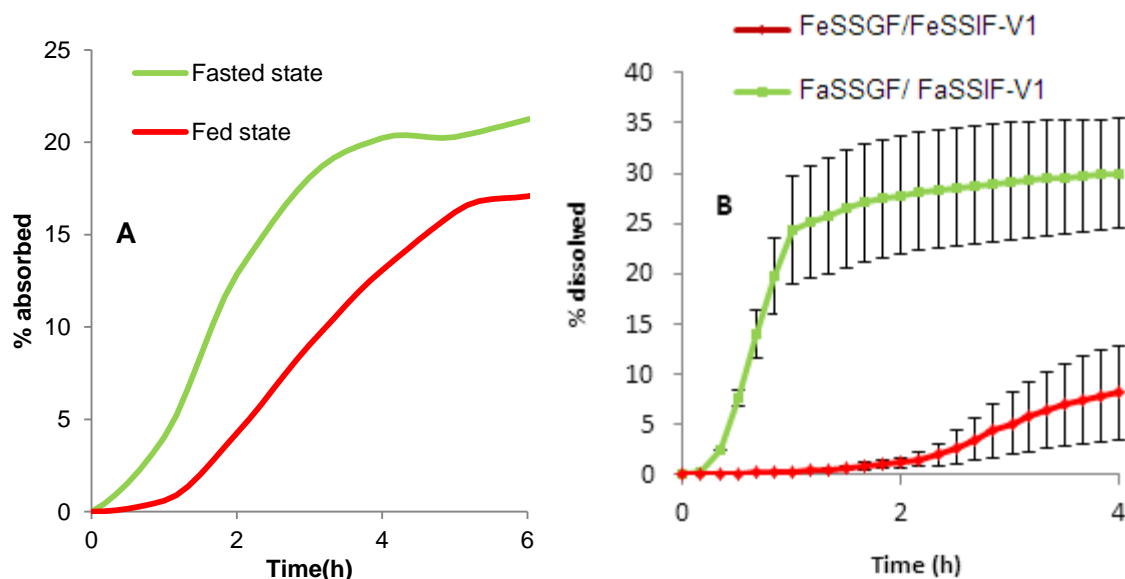


Figure 83. A: % ITR absorbed; B: Mean  $\pm$  SD % of ITR dissolved from Sporanox<sup>®</sup> capsule in fasted state media FaSSGF (8mL/min; 1h)/FaSSIF-V1 (4mL/min; 3h) and fed state media FeSSGF (6mL/min; 2h)/FeSSIF-V1 (6mL/min; 4h) using the USP apparatus 4 (n=3).

The *in vitro* results were translated into the *in vivo* condition because both fasted and fed experiment conditions showed the correct rank order of dissolution and absorption (Figure 83). Both *in vitro* and *in vivo* results showed higher dissolution/absorption in the fasted state. For *in vivo* condition, the highly supersaturated ITR solution produced in the acidic gastric fluid in the fasted state produced a fast absorption of ITR (29). Even though in the fed state a higher content of bile salt existed compared to the fasted state, still the bile components did not produce sufficient solubility enhancement or solubilisation of ITR (219).

## CX

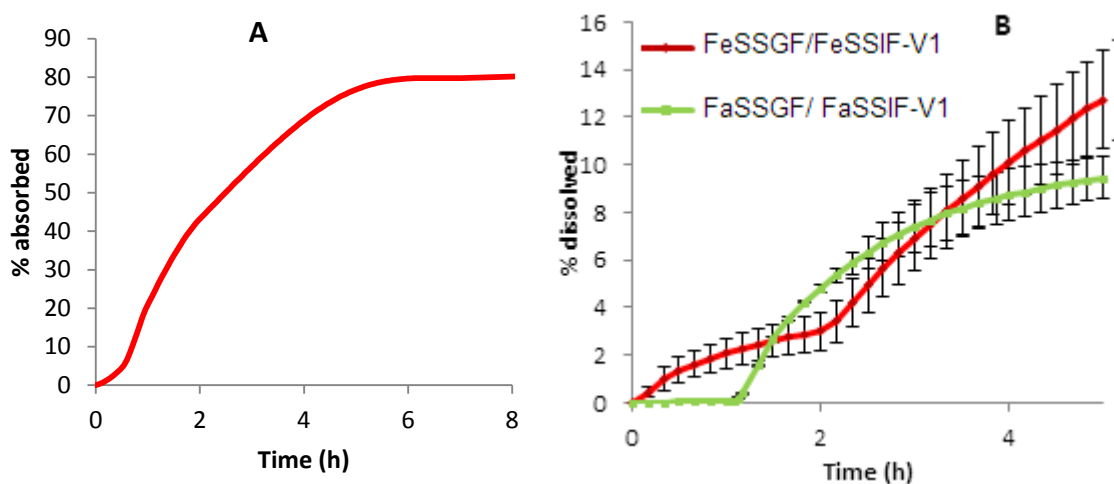


Figure 84. A:% CX absorbed (fed state); B:Mean± SD % of CX dissolved from CX formulation (F8) in fasted state media FaSSGF (8mL/min; 1h)/ FaSSIF-V1 (4mL/min; 3h) and fed state media FeSSGF (6mL/min; 2h)/ FeSSIF-V1 (6mL/min; 4h) using the USP apparatus 4 (n=3).

By comparing the *in vivo* (only fed state data available) and *in vitro* results, it seems that FeSSGF/FaSSIF-V1 dissolution profile of CX does not correlate well with the *in vivo* absorption profile in the gastric phase (Figure 84). Probably FeSSGF does not represent the fed conditions in the beagle dog well thus causing the discrepancy between the *in vitro* and *in vivo* conditions.

### 3.10.2 Mathematical IVIVC

In this section IVIVC using linear regression is presented according to the simulating fasted and fed state conditions.

#### CA

##### Simulating fasted state conditions

*In vivo* percentage of CA absorbed was compared to the corresponding percentage dissolved obtained from experiments with USP apparatus 4. The IVIVCs of CA are presented in Figure 85.

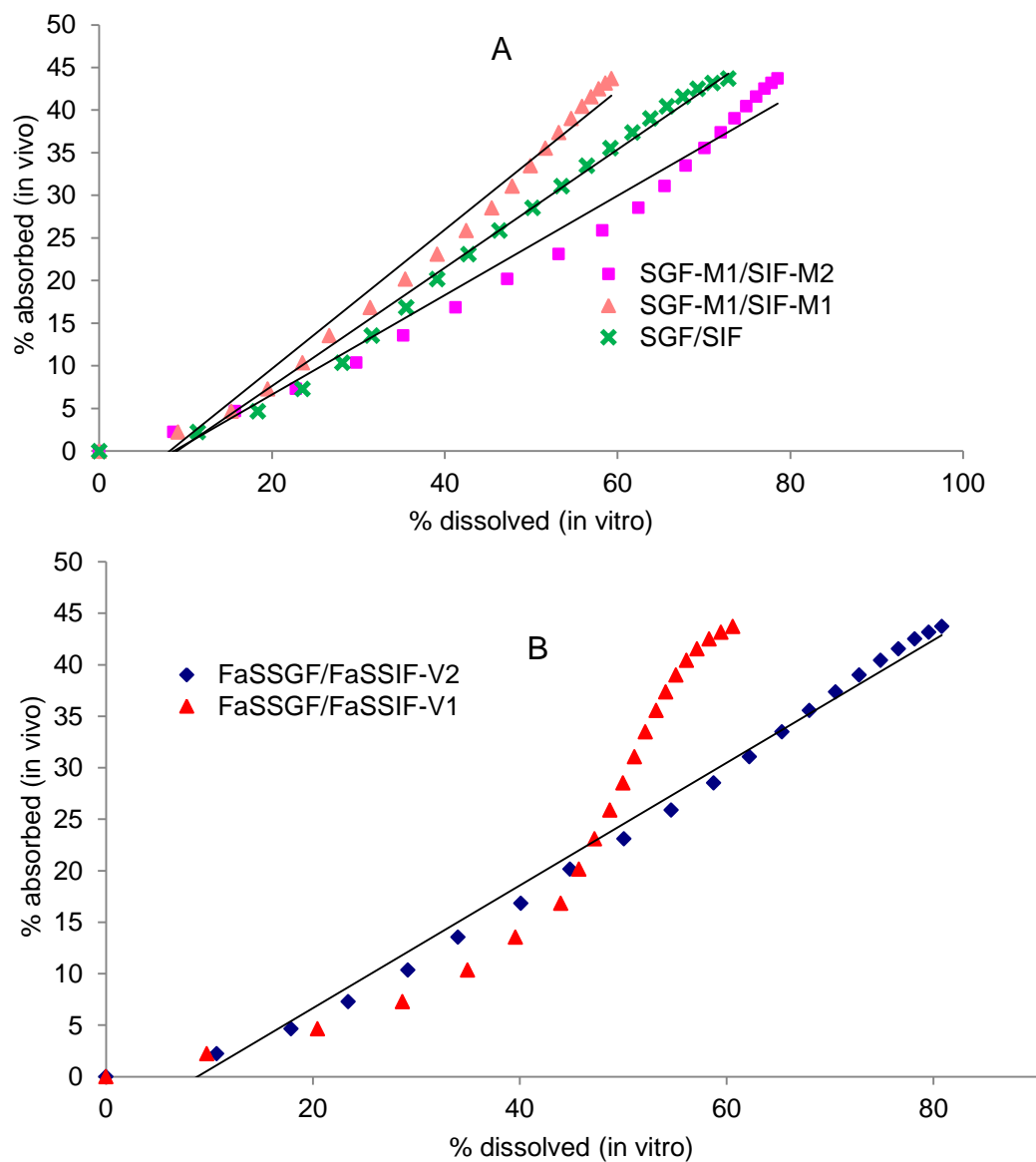


Figure 85. Mean % CA absorbed in humans vs mean % CA dissolved *in vitro* with USP apparatus 4. (A) Modified and compendial media (B) Biorelevant media

Summary of the obtained parameters derived from linear regression of the relation between % *in vivo* absorbed and % *in vitro* dissolved data of CA from 250mg Zinnat<sup>®</sup> tablet is presented in Table 56.

Table 56. Obtained regression parameters from relations between *in vivo* absorption and *in vitro* dissolution data (USP apparatus 4)

	SGF-M1/SIF-M1	SGF-M1/SIF-M2	SGF/SIF	FaSSGF/ FaSSIF-V1*	FaSSGF/ FaSSIF-V2
R <sup>2</sup>	0.98	0.98	0.98	-	0.99
Gradient	0.82	0.58	0.69	-	0.60
Intercept	-6.66	-5.04	-6.26	-	-5.24

\*A linear correlation is not obtained because profile shows more of sigmoidal shape

Table 56 shows that a linear response (R<sup>2</sup> close to 1) had been achieved for these simulating fasted state experiments apart from FaSSGF/FaSSIF-V1. IVIVC formed with *in vitro* dissolution profile performed with FaSSGF/FaSSIF-V2 with USP apparatus 4 exhibited a coefficient correlation of R<sup>2</sup>: 0.99 which shows a good correlation between the *in vitro* dissolution of CA and *in vivo* absorption of CA. The gradient of 0.60 denotes that the *in vitro* dissolution rate is higher than the *in vivo* absorption rate. For instance 80.80% of CA was dissolved whereas only 43.71% of CA was absorbed at 4 h. Meanwhile, the negative intercept of -5.24 implies that possibly the Zinnat<sup>®</sup> formulation is able to disintegrate and dissolve faster in the *in vitro* dissolution experiment with FaSSGF thus leading to *in vitro* dissolution before the corresponding *in vivo* absorption.

The correlation results of SGF-M1/SIF-M2, SGF/SIF, SGF-M1/SIF-M1 indicated a faster *in vitro* dissolution process than the *in vivo* absorption process. A rank order of gradient value (SGF-M1/SIF-M1 > SGF/SIF > SGF-M1/SIF-M2) shows that SGF-M1/SIF-M1 (gradient: 0.82) is closer to the *in vivo* conditions. The results seem to suggest that the best Level A correlation observed was obtained using FaSSGF/FaSSIF-V2. The intercept of this linear regression is the closest to zero among all five experiments with USP apparatus 4.

## Simulating fed state conditions

The IVIVCs of CA with *in vitro* dissolution performed with USP apparatus 4 are presented in Figure 86.

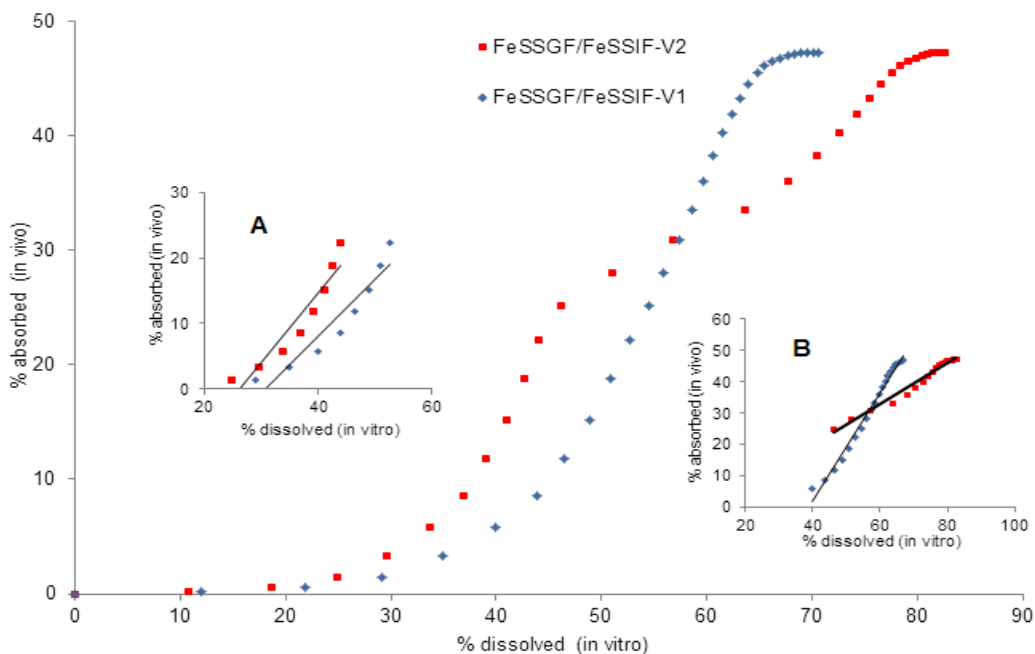


Figure 86. Mean % CA absorbed in humans vs mean % CA dissolved *in vitro* with USP apparatus 4 (fed state models). Inset A: Gastric phase (*in vitro* time 0-2 h) Inset B: Intestinal phase (*in vitro* 2-6 h).

Summary of the obtained parameters derived from linear regression of the relation between % *in vivo* absorbed and % *in vitro* dissolved data of 250mg Zinnat<sup>®</sup> tablet in the fed state is presented in Table 57.

Table 57. Obtained regression parameters from relations between *in vivo* absorption and *in vitro* dissolution data (simulating fed state condition)

	Gastric phase		Intestinal phase	
	<u>FeSSGF/</u> <u>FeSSIF-V1</u>	<u>FeSSGF/</u> <u>FeSSIF-V2</u>	<u>FeSSGF/</u> <u>FeSSIF-V1</u>	<u>FeSSGF/</u> <u>FeSSIF-V2</u>
R <sup>2</sup>	0.91	0.90	0.99	0.98
Gradient	0.87	1.06	1.73	0.66
Intercept	-26.60	-27.87	-67.37	-6.46

By applying IVIVC, *in vitro* dissolution profiles were compared to the corresponding *in vivo* absorption profiles in two phases. IVIVC for CA in FeSSGF/FeSSIF-V1 and FeSSGF/FeSSIF-V2 with USP apparatus 4 exhibit two phases in which the time of media change setup (*in vitro*) is at 1 h and 2 h respectively corresponding to 43.96% of

CA dissolution and 16.84% of CA absorbed (FaSSGF/FaSSIF-V1) and 43.96% of CA dissolution and 22.23% of CA absorbed (FeSSGF/FeSSIF-V2). The dissolution of CA in fed state simulated gastric medium, FeSSGF in FeSSGF/FaSSIF-V1 (gradient: 1.06) and FeSSGF/FeSSIF-V2 (gradient: 0.87) experiments shows that the dissolution and absorption processes occurred at a very similar rate. Nevertheless, the initial Zinnat<sup>®</sup> dissolution was faster before the corresponding absorption could occur (*i.e.*, intercept of -26.60 and -27.87 in FeSSGF/FeSSIF-V2 and FeSSGF/FaSSIF-V1 respectively). Whereas in the simulating intestinal media, the dissolution rate of CA with FeSSIF-V2 (gradient: 0.66) was higher and with FeSSIF-V1 (gradient: 1.73) was lower than the *in vivo* absorption rate.

On the other hand, regression of SGF/SIF, SGF-M1/SIF-M1,-M2 and FaSSGF/FaSSIFV2 exhibited a gradient lower than 1. This shows that these experiments had a higher *in vitro* dissolution than the corresponding *in vivo* absorption. These results seem to suggest that the *in vivo* absorption is slower than expected. This is in agreement with the findings from the *in vitro* dissolution which showed that the gelling of formulation and fast degradation of CA in GIT could potentially affect absorption (238) (gastric emptying lag time is indicated as negative intercept, Table 57).

## **ITR**

### **Simulated fasted state conditions**

The IVIVC of ITR with USP apparatus 1 and USP apparatus 4 are presented in Figures 87 and 88 respectively.

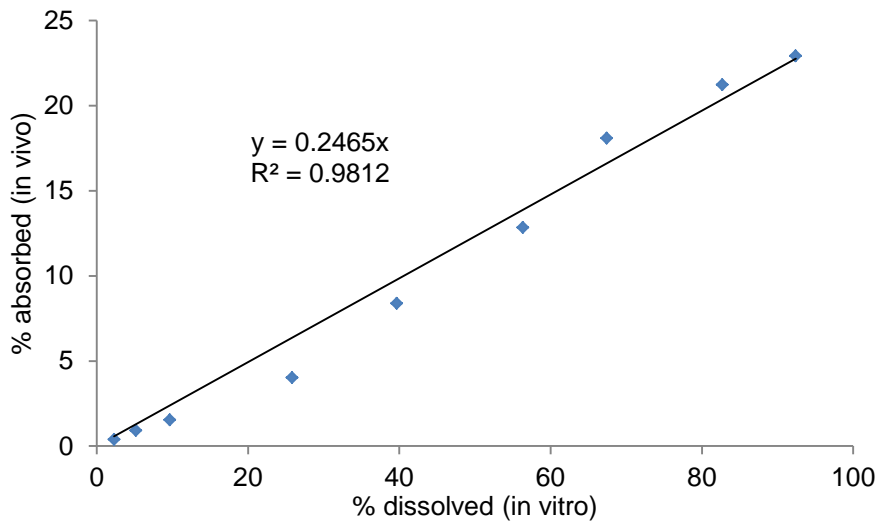


Figure 87. Mean % ITR absorbed in humans vs mean % ITR dissolved with SGF with USP apparatus 1.

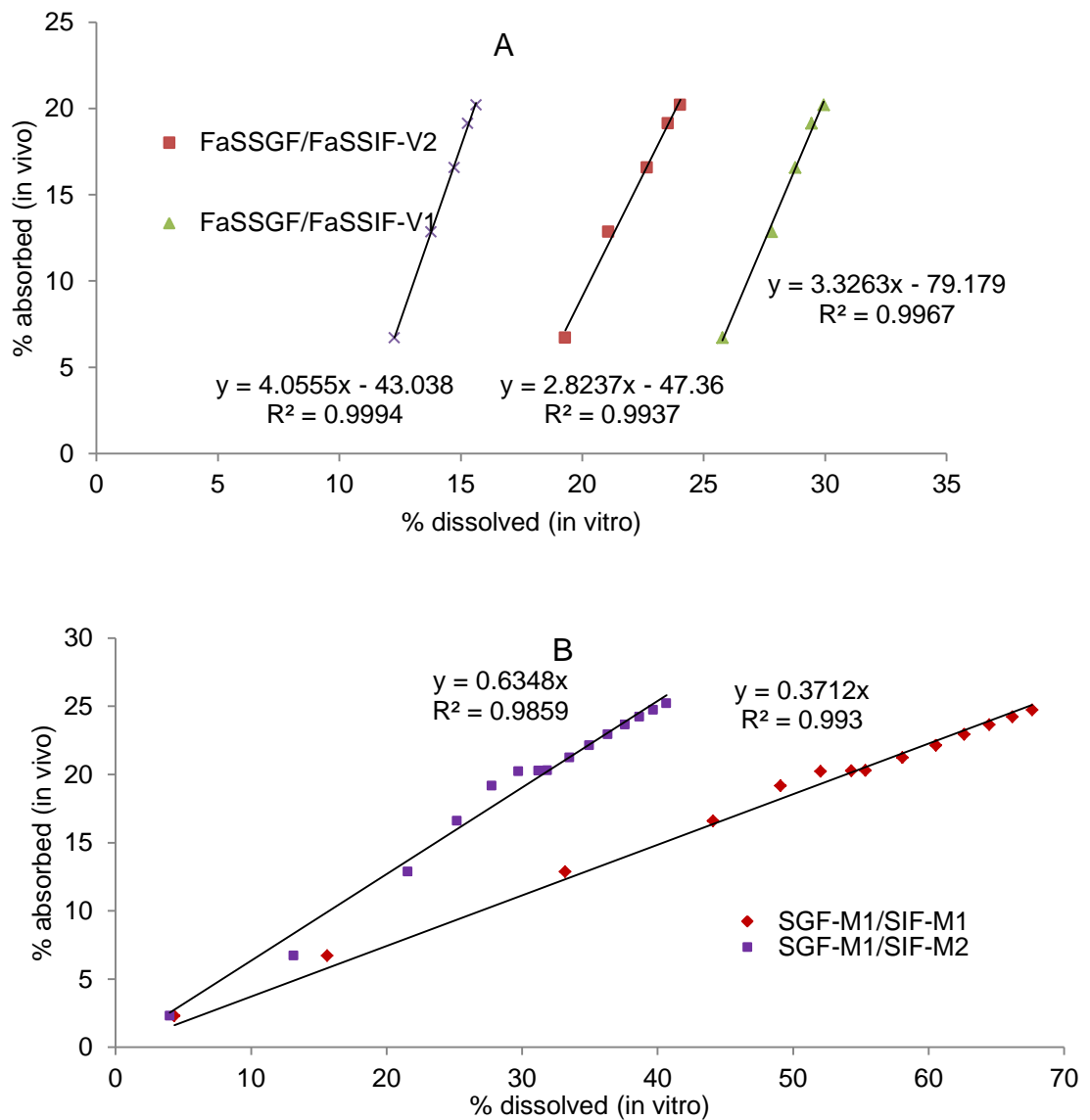


Figure 88. Mean % ITR absorbed in fasted state humans vs mean % ITR dissolved with USP apparatus 4 (A) Biorelevant and compendial media; (B) Modified media.

Summary of the obtained parameters derived from linear regression of the relation between % *in vivo* absorbed and % *in vitro* dissolved data of ITR from 100mg Sporanox<sup>®</sup> capsule is presented in Table 58.

Table 58. Obtained regression parameters from relations between *in vivo* absorption and *in vitro* dissolution data (fasted state)

A	SGF (USP apparatus 1)	FaSSGF/ FaSSIF-V1	FaSSGF/ FaSSIF-V2	SGF/ SIF	SGF-M1/ SIF-M1	SGF-M1/ SIF-M2
R <sup>2</sup>	0.98	0.99	0.99	0.99	0.99	0.99
Gradient	0.26	3.33	2.82	4.06	0.35	0.65
Intercept	-1.11	-79.18	-47.36	-43.04	1.15	-0.41

Table 58 shows that a linear response had been achieved for these simulating fasted state experiments. IVIVC formed with *in vitro* dissolution profile performed with SGF with USP apparatus 1 exhibited a coefficient correlation of R<sup>2</sup>: 0.98 which shows that there is a good correlation between the *in vitro* dissolution of ITR with SGF with USP apparatus 2 and *in vivo* absorption of ITR. The gradient of the regression for SGF is 0.26 which means that the *in vitro* dissolution process occurred at a higher rate than the *in vivo* absorption process. It is noteworthy that no IVIVR/IVIVC could be established for the dissolution profile of ITR with FaSSIF-V2 and FaSSGF with USP apparatus 1 because of its low percentage dissolved.

IVIVC formed with *in vitro* dissolution profile performed in FaSSGF/FaSSIF-V2, FaSSGF/FaSSIF-V1, SGF/SIF with USP apparatus 4 show a rank order of gradient that follows the sequence of SGF/SIF > FaSSGF/FaSSIF-V1 > FaSSGF/FaSSIF-V2. All these experiments yielded IVIVC with negative intercept which denotes that initial ITR dissolution from the Sporanox<sup>®</sup> capsule was faster than the corresponding *in vivo* absorption. Regression coefficients for SGF-M1/SIF-M1 and SGF-M1/SIF-M2 are both 0.99; this highlighted a good correlation; however the gradients of the regression are 0.37 and 0.63 which means that the use of artificial surfactant (SLS) at 0.2% (SIF-M1) and 0.1% (SIF-M2) caused a greater dissolution process than the corresponding *in vivo* absorption.

For the fasted state model, based on regression coefficient and gradient the best Level A correlation observed was obtained using SGF-M1/SIF-M2 and FaSSGF/FaSSIF-V2.



## Simulated fed state conditions

The correlations of ITR with USP apparatus 1 and USP apparatus 4 are presented in Figure 89A and Figure 89B respectively.

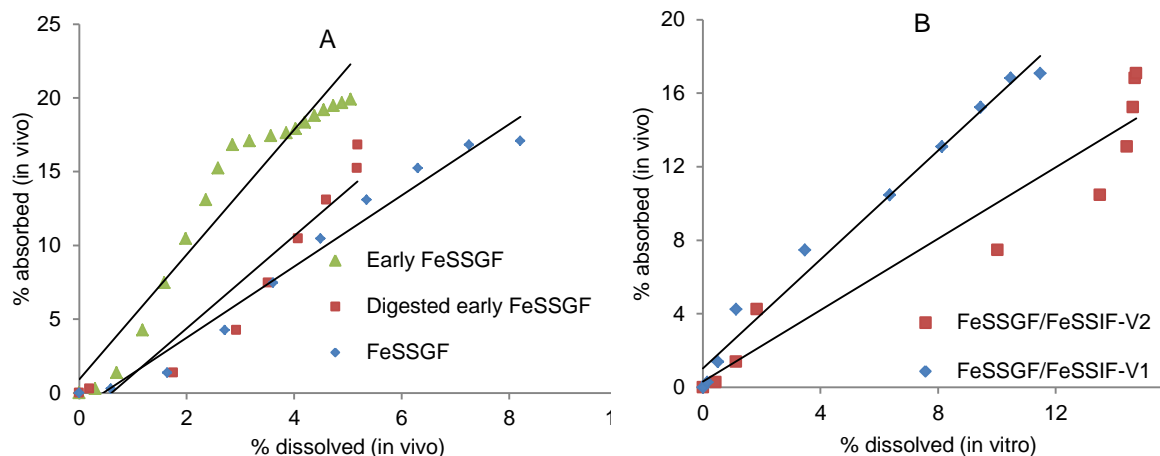


Figure 89. Mean % ITR absorbed in humans (fed state) vs mean % ITR dissolved *in vitro* with USP apparatus 1 (A) and USP apparatus 4 (B).

A summary of the obtained parameters derived from linear regression of the relation between % *in vivo* absorbed and % *in vitro* dissolved data of 100mg of Sporanox<sup>®</sup> is presented in Table 59.

Table 59. Obtained regression parameters from relations between *in vivo* absorption and *in vitro* dissolution data in the fed state

	USP apparatus 4		USP apparatus 1		
	FeSSGF/ FeSSIF-V1	FeSSGF/ FeSSIF-V2*	Early FeSSGF*	Digested early FeSSGF	FeSSGF
R <sup>2</sup>	0.98	-	-	0.97	0.91
Gradient	1.48	-	-	2.41	3.13
Intercept	1.04	-	-	-1.08	-1.87

\*A linear correlation is not obtained because profile shows more of sigmoidal shape

For the dissolution setup with USP apparatus 1, intercept for the correlation with digested early FeSSGF is smaller than with FeSSGF, indicating that *in vitro* dissolution for digested early FeSSGF simulated better than the *in vivo* stomach fluid in the fed state. The overall linear regression with *in vitro* experiments performed with USP

apparatus 1 (Table 59) showed that the best Level A correlation observed was obtained using digested early FeSSGF.

In this project we used milk based dissolution media such as FeSSGF, digested early FeSSGF, FeSSIF-V1 and FeSSIF-V2 with USP apparatus 1 and 4 for making correlations with the relevant *in vivo* data (228). However, compared to dissolution study of ITR with USP apparatus 4, study with USP apparatus 1 yielded a much lower rate and extent of ITR dissolution which led to a correlation's gradient greater than 1. Thus the best fed state model with the best Level A correlation observed was obtained using FeSSGF/FeSSIF-V2.

## CX

### Simulated fed state conditions

The correlations of CX with USP apparatus 2 are presented in Figure 90.

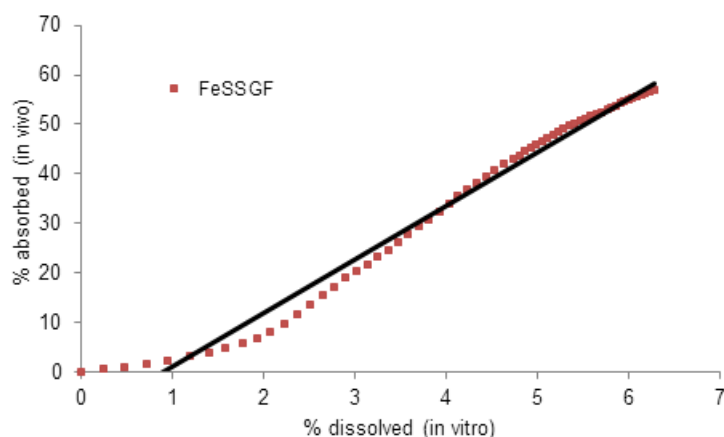


Figure 90. Mean % CX absorbed in dogs vs mean % CX dissolved *in vitro* with FeSSGF with USP apparatus 2.

According to Figure 90, dissolution data in biorelevant medium simulating the stomach in the fed state (FeSSGF) allowed development of point-to-point Level A IVIVC with goodness of fit value ( $R^2$ : 0.98). It is possible that this dissolution setup with USP apparatus 2 could be an alternative to the dissolution setup with USP apparatus 4 (discussed later in this section) as the desired dissolution specifications.

The correlations of CX Formulation 4, 5, 6 and 7 with FeSSGF/FeSSIF-V2 with USP apparatus 4 are presented in Figure 91.

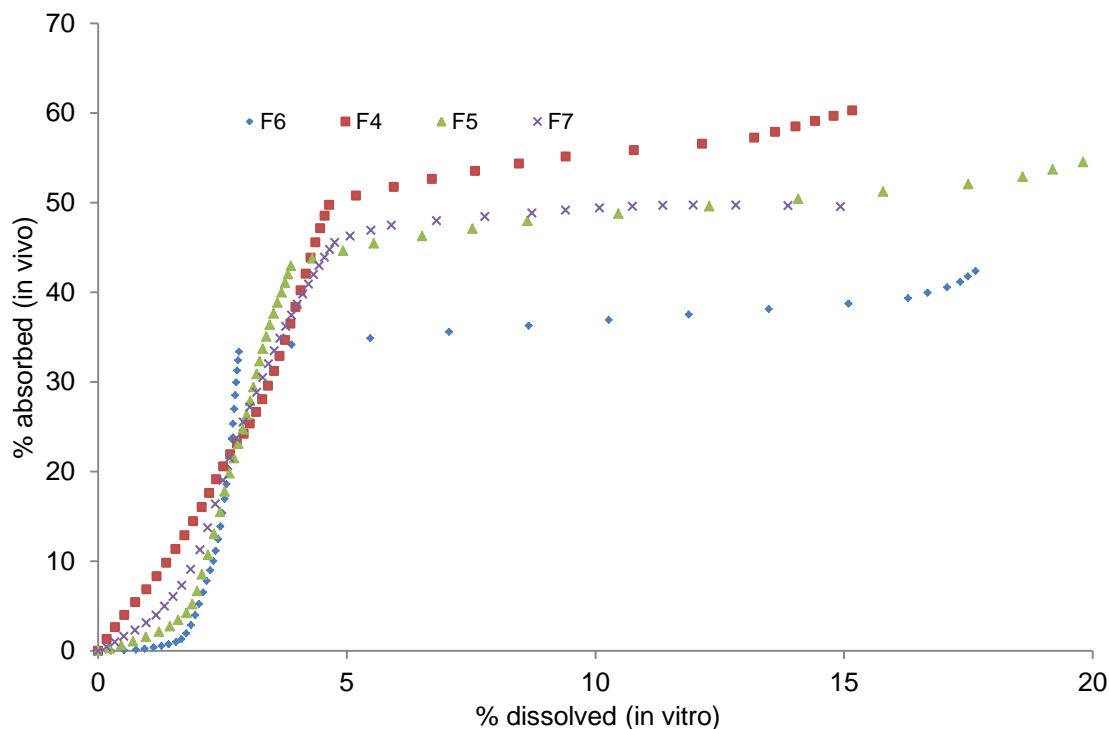


Figure 91. Mean % CX Formulation 4, 5, 6 and 7 absorbed in dogs (fed state) vs mean % CX dissolved *in vitro* with FeSSGF/FeSSIF-V2 with USP apparatus 4.

The lower and upper linear portions in Figure 91 indicate that the *in vitro* and *in vivo* release profiles are superimposable, but only up to a certain duration. The biphasic *in vitro*–*in vivo* correlation of CX may have many causes. One of the possible reasons is the change of dissolution kinetics of CX formulation (both *in vitro* and *in vivo*) when exposed to a different medium and hydrodynamics.

In our case, clearly the dissolution between 0-120 min in FeSSGF/FeSSIF-V1 and V2 was low but the corresponding period *in vivo* had fast absorption (as observed in deconvoluted profiles presented previously in Figure 79). As a result, the IVIVR/C for CX in FeSSGF/FeSSIF-V1 and –V2 with USP apparatus 4 exhibit two phases in which the time of media change setup (*in vitro*) is at 2 h, corresponding to 3% of drug dissolution and 33.4% of drug absorbed (FeSSGF/FeSSIF-V1) and 4% of drug dissolution and 32.4% of drug absorbed (FeSSGF/FeSSIF-V2). Since the time of transition from the first linear section to the second occurs after about 2 h, it is highly likely that this change occurs when the formulation enters the duodenum.

The correlations of CX Formulation F8 with SGF-M2/SIF-M3, FeSSGF/FeSSIF-V1 and FeSSGF/FeSSIF-V2 with USP apparatus 4 are presented in Figures 92 and 93.

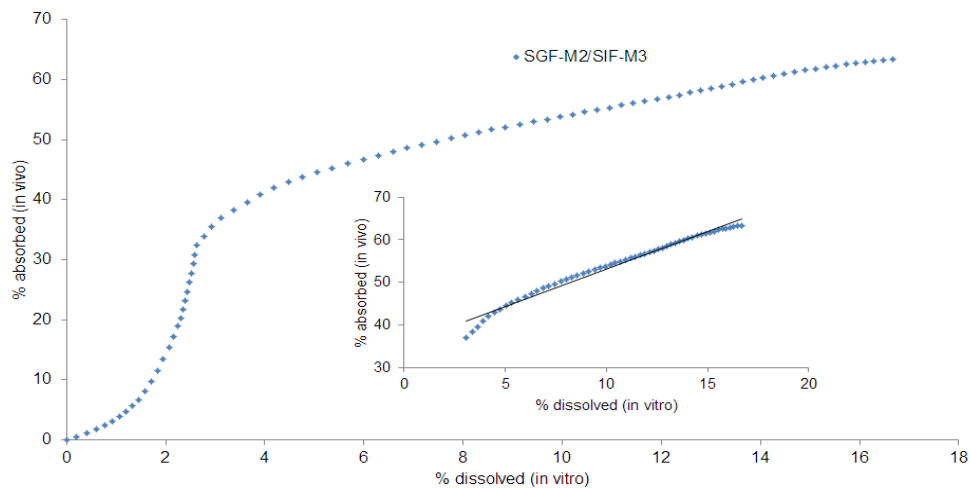


Figure 92. Mean % CX absorbed in dogs vs mean % CX dissolved *in vitro* with SGF-M2/SIF-M3 with USP apparatus 4. Inset: Intestinal phase (*in vitro* 2- 6 h).

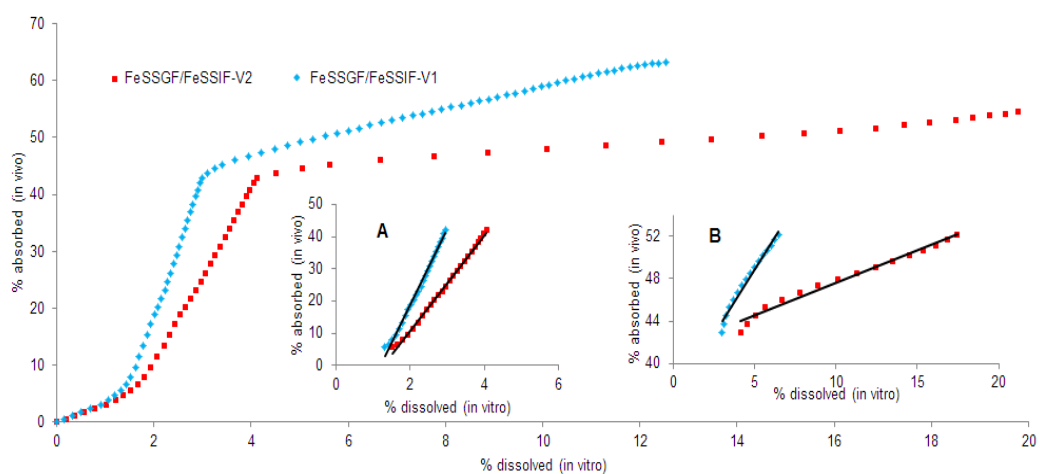


Figure 93. Mean % CX absorbed in dogs vs mean % CX dissolved *in vitro* with USP apparatus 4 (F8). Inset A: Gastric phase (*in vitro* time 0-2 h) Inset B: Intestinal phase (*in vitro* 2-6 h).

A summary of the obtained parameters derived from linear regression of the relation between % *in vivo* absorbed and % *in vitro* dissolved data of CX is provided in Table 60.

Table 60. (A) Obtained regression parameters from relations between *in vivo* absorption\* and *in vitro* dissolution data (Formulation 8) (B) *in vivo* absorption<sup>#</sup> and *in vitro* dissolution data with FeSSGF/ FeSSIF-V2 with USP apparatus 4 of Formulation 4, 5, 6 and 7.

A	USP apparatus 2	USP apparatus 4					
		Gastric phase			Intestinal phase		
Media	FeSSGF	<u>FeSSGF/</u> <u>FeSSIF-</u> V1	<u>FeSSGF/</u> <u>FeSSIF-</u> V2	<u>SGFM2/</u> <u>SIF-M3</u>	<u>FeSSGF/</u> <u>FeSSIF-</u> V1	<u>FeSSGF/</u> <u>FeSSIF-</u> V2	<u>SGFM2/</u> <u>SIF-M3</u>
R <sup>2</sup>	0.98	0.99	0.99	0.92	0.98	0.98	0.98
Gradient	10.81	23.18	14.8	5.91	2.47	0.62	1.77
Intercept	-9.65	-27.48	-18.68	-1.42	36.54	41.43	35.39

\*Mean *in vivo* absorption profiles of Formulation 4, 5, 6 and 7, total n=16 were used

B	USP apparatus 4							
	Gastric phase				Intestinal phase			
	F4	F5	F6	F7	F4	F5	F6	F7
R <sup>2</sup>	0.9789	0.99	0.9	0.9922	0.9797	0.98	0.93	0.7378
Gradient	12.31	19.63	25.61	12.99	0.894	0.64	0.54	0.33
Intercept	-10.37	-32.06	-45.43	-13.63	46.26	41.61	31.63	45.39

<sup>#</sup>Mean *in vivo* absorption profiles of corresponding formulation were used, n=4 of each formulation

Linear regression of FeSSGF/FeSSIF-V1, FeSSGF/FeSSIF-V2 (Gastric phase) and FeSSGF (USP apparatus 2) gradient values of greater than 1 were observed (*in vitro*: F8). These gradient values indicated that a high degree of CX was absorbed *in vivo* but this is not in tandem with the same degree of CX dissolved *in vitro* with FeSSGF using both USP apparatus 2 and 4.

On the other hand, in the regression of FeSSGF/FeSSIF-V2 (Intestinal phase) a gradient of 0.87 was observed in this study. This shows that FeSSIF-V2 gave a higher *in vitro* dissolution than the corresponding *in vivo* absorption value. Thus it seems that the concentration of GMO in FeSSIF-V2 is higher than the one in dogs leading to greater dissolution. Furthermore, in regressions of FeSSGF/ FeSSIF-V1, FeSSGF/ FeSSIF-V2 (Intestinal phase) and SGF-M2/SIF-M3 a significant positive intercept was noted. This pointed out that a considerable amount of CX was absorbed *in vivo* but the same degree of *in vitro* dissolution did not occur. As a summary, the correlation of

dissolution with drug absorption largely relies on the biorelevant conditions and discriminatory nature of the dissolution experiment settings.

For these five formulations (F4, F5, F6, F7 and F8) the *in vitro* dissolution of CX both in the gastric and intestinal phase was very similar. The linear regressions produced gradients of  $17.07 \pm 5.57$  and  $0.60 \pm 0.20$  in the gastric and intestinal phases respectively. The gradient in the gastric phase is greater than 1 indicating that for a small amount dissolved (e.g., only 4.65% dissolved after 2 h for formulation 4 in FeSSGF/ FeSSIF-V2 with USP apparatus 4), a large amount was absorbed at the same time point (49.74% absorbed). In contrast, the gradient in the intestinal phase is smaller than 1 which denotes the opposite of the gastric phase.

#### 4 Conclusions and future work

The results of the dissolution tests performed demonstrated that the effect of pH, content of media, pH change, flow rate and ST changes could affect dissolution of amorphous formulations of CA, ITR and CX. The results showed that biorelevant media combined with USP apparatus 4 provided dissolution profiles that simulated closely physiological *in vivo* profiles. Furthermore, dissolution kinetic modeling dissolution models (such as Power law, Weibull, first order) were successfully applied to describe the rate and mechanism of CA, ITR and CX dissolution from its amorphous formulations.

From the surface UV dissolution testing, the UV images of absorbance maps and contour concentration lines of the dissolved CA during the experiment with media and flow rate change (SGF/SIF) revealed that CA dissolved from the compact surface as aggregates and formed a supersaturated CA solution that subsequently precipitated out. Similarly for ITR, supersaturation of ITR after media change drastically increased the recrystallisation of ITR on the surfaces of the ITR and Sporanox<sup>®</sup> compacts which could lead to ITR crystal growth.

In this project, successful cases of PBPK models and IVIVCs development describing physiology of fasted state (CA, ITR) and fed state (CA, ITR and CX) of amorphous formulations were presented. The differences in predictions mediated by *in vitro* drug dissolution as input profiles and the importance of biorelevant dissolution tests for more accurate prediction of *in vivo* performance were also shown and verified.

As an overall conclusion, this project successfully provides a comprehensive methodology which a pharmaceutical scientist could follow to characterise the dissolution profiles of the compound of interest, develop PBPK models and IVIVCs simulating fasted and fed states for orally administered amorphous formulations. In this study, the hypothesis of biorelevant dissolution media combined with USP apparatus 4 could achieve a good PBPK model and IVIVC were proven correct.

Future work that is worth performing includes using dissolution media with higher concentrations of bile salts, lecithin and lipolytic products than FeSSIF-V2 to simulate better CX dissolution in the dog intestine. A closer simulation of human and dog differences in terms of the content and hydrodynamic and gastric emptying time could be investigated too. Meanwhile, future work for surface UV dissolution imaging is to perform surface UV dissolution experiments for CA (with media change using biorelevant dissolution media) and CX. These were not performed in the current study

due to time limitation. Lastly, future work that could be performed for PBPK modeling includes further refinement of the developed models based on the latest clinical data and better *in vitro* results.



## 5.0 References

### 5.0 References

1. R. Hilfiker, F. Blatter, and M. Raumer. Chapter 1: Relevance of solid-state properties for pharmaceutical products. In R. Hilfiker (ed.), *Polymorphism in the pharmaceutical industry*, Wiley VCH, Weinheim 2006, pp. 1-19.
2. H.G. Brittain, S.J. Bogdanowich, D.E. Bugay, J. DeVincentis, G. Lewen, and A.W. Newman. Physical characterization of pharmaceutical solids. *Pharm Res.* 8:963-973 (1991).
3. P.M. Ossi. Structural changes induced by swift heavy ions in non-metallic compounds. *Nucl Instr and Meth B.* 209:55-61 (2003).
4. S. Petit and G. Coquerel. The Amorphous State. In H. Rolf (ed.), *Polymorphism: in the Pharmaceutical Industry*, Wiley-VCH Verlag GmbH, Weinheim, 2006, pp. 259-285.
5. E. Shalaev and G. Zografi. The concept of structure in amorphous solids from the perspective of the pharmaceutical sciences. *Amorphous Food and Pharmaceutical Systems*, The Royal Society of Chemistry, Cambridge, 2002, pp. 11-30.
6. J. Zarzycki. Preface to Volume 9. In J. Zarzycki (ed.), *Amorphous materials Vol. 9*, VCH, Weinheim, 1991.
7. Y. Guo. Impact of Solid-State Characteristics to the Physical Stability of Drug Substance and Drug Product. 2009, pp. 241-261.
8. A.T.M. Serajuddin. Solid dispersion of poorly water-soluble drugs: Early promises, subsequent problems, and recent breakthroughs. *J Pharm Sci.* 88:1058-1066 (1999).
9. W.L. Chiou and S. Riegelman. Pharmaceutical applications of solid dispersion systems. *J Pharm Sci.* 60:1281-1302 (1971).
10. O.I. Corrigan, E.M. Holohan, and M.R. Reilly. Physicochemical properties of indomethacin and related compounds co-spray dried with polyvinylpyrrolidone. *Drug Dev Ind Pharm.* 11:677 - 695 (1985).
11. C. Brough, Williams III, R.O.,. Amorphous solid dispersions and nano-crystal technologies for poorly water-soluble drug delivery. <http://dx.doi.org/10.1016/j.ijpharm.2013.05.061>. *Int J Pharm*(2013).
12. D. Law, S.L. Krill, E.A. Schmitt, J.J. Fort, Y.H. Qiu, W.L. Wang, and W.R. Porter. Physicochemical considerations in the preparation of amorphous ritonavir-poly(ethylene glycol) 8000 solid dispersions. *J Pharm Sci.* 90:1015-1025 (2001).
13. I. Kushida, M. Ichikawa, and N. Asakawa. Improvement of dissolution and oral absorption of ER-34122, a poorly water-soluble dual 5-

- lipoxygenase/cyclooxygenase inhibitor with anti-inflammatory activity by preparing solid dispersion. *J Pharm Sci.* 91:258-266 (2002).
14. V. Tantishaiyakul, N. Kaewnopparat, and S. Ingkatawornwong. Properties of solid dispersions of piroxicam in polyvinylpyrrolidone. *Int J Pharm.* 181:143-151 (1999).
  15. C. Leuner and J. Dressman. Improving drug solubility for oral delivery using solid dispersions. *Eur J Pharm Biopharm.* 50:47-60 (2000).
  16. B.C. Hancock and G. Zografi. Characteristics and significance of the amorphous state in pharmaceutical systems. *J Pharm Sci.* 86:1-12 (1997).
  17. P. Gupta, G. Chawla, and A.K. Bansal. Physical stability and solubility advantage from amorphous celecoxib: The role of thermodynamic quantities and molecular mobility. *Mol Pharm.* 1:406-413 (2004).
  18. H. El-Zein, L. Riad, and A.A. El-Bary. Enhancement of carbamazepine dissolution: *in vitro* and *in vivo* evaluation. *Int J Pharm.* 168:209-220 (1998).
  19. F. Fawaz, F. Bonini, M. Guyot, J. Bildet, M. Maury, and A.M. Lagueny. Bioavailability of norfloxacin from PEG 6000 solid dispersion and cyclodextrin inclusion complexes in rabbits. *Int J Pharm.* 132:271-275 (1996).
  20. A.A. Ali and A.S. Gorashi. Absorption and dissolution of nitrofurantoin from different experimental formulations. *Int J Pharm.* 19:297-306 (1984).
  21. N. Kohri, Y. Yamayoshi, H. Xin, K. Iseki, N. Sato, S. Todo, and K. Miyazaki. Improving the oral bioavailability of albendazole in rabbits by the solid dispersion technique. *J Pharm Pharmacol.* 51:159-164 (1999).
  22. B.C. Hancock and M. Parks. What is the true solubility advantage for amorphous pharmaceuticals? *Pharm Res.* 17:397-404 (2000).
  23. M.J. Pikal, A.L. Lukes, J.E. Lang, and K. Gaines. Quantitative crystallinity determinations for  $\beta$ -lactam antibacterials *J Pharm Sci.* 67:767-773 (1978).
  24. G.G.Z. Zhang, D. Zhou, Q. Yihong, C. Yisheng, G.Z.Z. Geoff, L. Lirong, and R.P. William. Crystalline and amorphous solids. *Developing Solid Oral Dosage Forms*, Academic Press, San Diego, 2009, pp. 25-60.
  25. P.T. Cardew and R.J. Davey. The kinetics of solvent-mediated phase transformations. *Proc R Soc Lond A.* 398:415-428 (1985).
  26. G.G.Z. Zhang, C. Gu, M.T. Zell, R.T. Burkhardt, E.J. Munson, and D.J.W. Grant. Crystallization and transitions of sulfamerazine polymorphs. *J Pharm Sci.* 91:1089-1100 (2002).
  27. N. Rodriguez-Hornedo, D. Lechuga-Ballesteros, and H.J. Wu. Phase transition and heterogeneous/epitaxial nucleation of hydrated and anhydrous theophylline crystals. *Int J Pharm.* 85:149-162 (1992).
  28. T. Wei-Qin (Tony). Salt screening and selection: New challenges and considerations in the modern pharmaceutical research and development

- paradigm. *Developing Solid Oral Dosage Forms*, Academic Press, San Diego, 2009, pp. 75-86.
29. J. Brouwers, M.E. Brewster, and P. Augustijns. Supersaturating drug delivery systems: the answer to solubility-limited oral bioavailability? *J Pharm Sci.* 98:2549-2572 (2009).
  30. J. Bevernage, J. Brouwers, S. Clarysse, M. Vertzoni, J. Tack, P. Annaert, and P. Augustijns. Drug supersaturation in simulated and human intestinal fluids representing different nutritional states. *J Pharm Sci.* 99:4525-4534 (2010).
  31. A.L. Sarode, H. Sandhu, N. Shah, W. Malick, and H. Zia. Hot melt extrusion for amorphous solid dispersions: temperature and moisture activated drug-polymer interactions for enhanced stability. *Mol Pharm*(2013).
  32. N. Blagden, M. de Matas, P.T. Gavan, and P. York. Crystal engineering of active pharmaceutical ingredients to improve solubility and dissolution rates. *Adv Drug Deliv Rev.* 59:617-630 (2007).
  33. C.A. Lipinski, F. Lombardo, B.W. Dominy, and P.J. Feeney. Experimental and computational approaches to estimate solubility and permeability in drug discovery and development settings. *Adv Drug Deliv Rev.* 46:3-26 (2001).
  34. L.F. Huang and W.Q. Tong. Impact of solid state properties on developability assessment of drug candidates. *Adv Drug Deliv Rev.* 56:321-334 (2004).
  35. H. Gamsjager, J.W. Lorimer, P. Scharlin, and D.G. Shaw. Glossary of terms related to solubility. *Pure Appl Chem.* 80:233-276 (2008).
  36. R.G. Strickley, R. Oliyai, P. Augustijns, and M.E. Brewster. *Solvent Systems and Their Selection in Pharmaceuticals And Biopharmaceutics*, Biotechnology: Pharmaceutical Aspects 2007.
  37. K. Six, G. Verreck, J. Peeters, M. Brewster, and G. Van Den Mooter. Increased physical stability and improved dissolution properties of itraconazole, a class II drug, by solid dispersions that combine fast- and slow-dissolving polymers. *J Pharm Sci.* 93:124-131 (2004).
  38. B. Abrahamsson. Dissolution testing in the development of oral drug products. In J. Dressman and H. Lennernäs (eds.), *Oral Drug Absorption: Prediction and Assessment*, Marcel Dekker Inc., New York, Basel, 2000, pp. 197-228.
  39. V.P. Shah. The role of dissolution testing in the regulation of pharmaceuticals: the FDA perspective. In J. Dressman (ed.), *Pharmaceutical dissolution testing*, Taylor and Francis 2005.
  40. V. Gray, G. Kelly, M. Xia, C. Butler, S. Thomas, and S. Mayock. The Science of USP 1 and 2 dissolution: Present challenges and future relevance. *Pharm Res.* 26:1289-1302 (2009).
  41. V.P. Shah. Progressive applications of dissolution, its impact, and implications in the pharmaceutical world. *J Pharm Sci.* 102:2895-2897 (2013).

42. United States Pharmacopeial Convention. The United States Pharmacopeia : USP32. The National Formulary: NF27, United States Pharmacopeial Convention, Rockville, Maryland, 2009.
43. CDER/FDA. Guidance for industry: Waiver of *in vivo* bioavailability and bioequivalence studies for immediate-release solid oral dosage forms based on a Biopharmaceutics Classification System. Available from: <http://www.fda.gov/downloads/Drugs/GuidanceComplianceRegulatoryInformation/Guidances/ucm070246.pdf>. Accessed Date: September 11, 2012, U.S. Department of Health and Human Services Food and Drug Administration Center for Drug Evaluation and Research (CDER), Rockville, MD, 2000.
44. G. Levy. Effect of certain tablet formulation factors on dissolution rate of the active ingredient. I. Importance of using appropriate agitation intensities for *in vitro* dissolution rate measurements to reflect *in vivo* conditions. J Pharm Sci. 52:1039-1046 (1963).
45. M. Kamba, Y. Seta, A. Kusai, and K. Nishimura. Comparison of the mechanical destructive force in the small intestine of dog and human. Int J Pharm. 237:139-149 (2002).
46. M. Vertzoni, J. Dressman, J. Butler, J. Hempenstall, and C. Reppas. Simulation of fasting gastric conditions and its importance for the *in vivo* dissolution of lipophilic compounds. Eur J Pharm Biopharm. 60:413-417 (2005).
47. E.S. Kostewicz, M. Wunderlich, U. Brauns, R. Becker, T. Bock, and J.B. Dressman. Predicting the precipitation of poorly soluble weak bases upon entry in the small intestine. J Pharm Pharmacol. 56:43-51 (2004).
48. G.L. Amidon, H. Lennernas, V.P. Shah, and J.R. Crison. A theoretical basis for a biopharmaceutic drug classification: The correlation of *in vitro* drug product dissolution and *in vivo* bioavailability. Pharm Res. 12:413-420 (1995).
49. G. Garbacz, B. Golke, R.-S. Wedemeyer, M. Axell, E. Söderlind, B. Abrahamsson, and W. Weitschies. Comparison of dissolution profiles obtained from nifedipine extended release once a day products using different dissolution test apparatuses. Eur J Pharm Sci. 38:147-155 (2009).
50. D.A. Miller, J.T. McConville, W. Yang, R.O. Williams, and J.W. McGinity. Hot-melt extrusion for enhanced delivery of drug particles. J Pharm Sci. 96:361-376 (2007).
51. K. Six, T. Daems, J. de Hoon, A. Van Hecken, M. Depre, M.P. Bouche, P. Prinsen, G. Verreck, J. Peeters, M.E. Brewster, and G. Van den Mooter. Clinical study of solid dispersions of itraconazole prepared by hot-stage extrusion. Eur J Pharm Sci. 24:179-186 (2005).
52. C. Reppas and M. Vertzoni. Biorelevant in-vitro performance testing of orally administered dosage forms. J Pharm Pharmacol. 64:919-930 (2012).

53. E. Jantravid and M. Vertzoni. Dissolution testing to forecast *In vivo* performance of immediate-release formulations. In J.B. Dressman and C. Reppas (eds.), *Oral Drug Absorption: Prediction and Assessment*, Informa Healthcare, NY, 2010, pp. 224-243.
54. J.B. Dressman, G.L. Amidon, C. Reppas, and V.P. Shah. Dissolution testing as a prognostic tool for oral drug absorption: Immediate release dosage forms. *Pharm Res.* 15:11-22 (1998).
55. Y. Shono, E. Jantravid, N. Janssen, F. Kesisoglou, Y. Mao, M. Vertzoni, C. Reppas, and J.B. Dressman. Prediction of food effects on the absorption of celecoxib based on biorelevant dissolution testing coupled with physiologically based pharmacokinetic modeling. *Eur J Pharm Biopharm.* 73:107-114 (2009).
56. E. Nicolaidis, M. Symillides, J.B. Dressman, and C. Reppas. Biorelevant dissolution testing to predict the plasma profile of lipophilic drugs after oral administration. *Pharm Res.* 18:380-388 (2001).
57. E. Jantravid, N. Janssen, C. Reppas, and J.B. Dressman. Dissolution media simulating conditions in the proximal human gastrointestinal tract: An update. *Pharm Res.* 25:1663-1676 (2008).
58. A. Aburub, D.S. Risley, and D. Mishra. A critical evaluation of fasted state simulating gastric fluid (FaSSGF) that contains sodium lauryl sulfate and proposal of a modified recipe. *Int J Pharm.* 347:16-22 (2008).
59. E. Galia, J. Horton, and J.B. Dressman. Albendazole generics--a comparative *in vitro* study. *Pharm Res.* 16:1871-1875 (1999).
60. N. Fotaki and M. Vertzoni. Biorelevant dissolution testing and IVIVCs. *The Open Drug Delivery Journal.* 4:2-13 (2010).
61. J.L. Cohen, B.B. Hubert, L.J. Leeson, C.T. Rhodes, J.R. Robinson, T.J. Roseman, and E. Shefter. The development of USP dissolution and drug release standards. *Pharm Res.* 7:983-987 (1990).
62. E. Galia, E. Nicolaidis, D. Hörter, R. Löbenberg, C. Reppas, and J.B. Dressman. Evaluation of various dissolution media for predicting *In vivo* performance of class I and II drugs. *Pharm Res.* 15:698-705 (1998).
63. N. Fotaki, M. Symillides, and C. Reppas. Canine versus *in vitro* data for predicting input profiles of l-sulpiride after oral administration. *Eur J Pharm Sci.* 26:324-333 (2005).
64. J.B. Dressman. Dissolution testing of IR products and its application to forecasting *in vivo* performance. In J.B. Dressman and H. Lennernäs (eds.), *Oral Drug Absorption: Prediction and Assessment*, Marcel Dekker, NY, 2000, pp. 155-181.
65. P.E. Luner. Wetting properties of bile salt solutions and dissolution media. *J Pharm Sci.* 89:382-395 (2000).

66. S.C. Sweetman. Martindale : the complete drug reference [Internet database], Pharmaceutical Press.Electronic version, Greenwood Village, Colo: Thomson Micromedex. Updated periodically., London, 2010.
67. Merck Index. Cetyltrimethylammonium bromide Online version(2011).
68. K. Kleberg, J. Jacobsen, and A. Müllertz. Characterising the behaviour of poorly water soluble drugs in the intestine: application of biorelevant media for solubility, dissolution and transport studies. *J Pharm Pharmacol*:no-no (2010).
69. C.G. Wilson. The organization of the gut and the oral absorption of drugs: Anatomical, biological and physiological considerations in oral formulation development. In C.G. Wilson and P.J. Crowley (eds.), *Controlled Release in Oral Drug Delivery*, Springer US 2011, pp. 27-48.
70. S. Delgado-Aros, F. Cremonini, J.E. Castillo, H.J. Chial, D.D. Burton, I. Ferber, and M. Camilleri. Independent influences of body mass and gastric volumes on satiation in humans. *Gastroenterology*. 126:432-440 (2004).
71. W.S. Jellish, V. Kartha, E. Fluder, and S. Slogoff. Effect of metoclopramide on gastric fluid volumes in diabetic patients who have fasted before elective surgery. *Anesthesiology*. 102:904-909 (2005).
72. A. Lindahl, A.L. Ungell, L. Knutson, and H. Lennernas. Characterization of fluids from the stomach and proximal jejunum in men and women. *Pharm Res*. 14:497-502 (1997).
73. L. Kalantzi, K. Goumas, V. Kalioras, B. Abrahamsson, J.B. Dressman, and C. Reppas. Characterization of the human upper gastrointestinal contents under conditions simulating bioavailability/bioequivalence studies. *Pharm Res*. 23:165-176 (2006).
74. S. Mahe, J.F. Huneau, P. Marteau, F. Thuillier, and D. Tome. Gastroileal Nitrogen and Electrolyte Movements after Bovine-Milk Ingestion in Humans. *Am J Clin Nutr*. 56:410-416 (1992).
75. B.L. Pedersen, A. Mullertz, H. Brondsted, and H.G. Kristensen. A comparison of the solubility of danazol in human and simulated gastrointestinal fluids. *Pharm Res*. 17:891-894 (2000).
76. A. Müllertz. Biorelevant Dissolution Media. *Solvent Systems and Their Selection in Pharmaceutics and Biopharmaceutics* 2007, pp. 151-177.
77. T.T. Kararli. Comparison of the gastrointestinal anatomy, physiology, and biochemistry of humans and commonly used laboratory animals. *Biopharm Drug Dispos*. 16:351-380 (1995).
78. J.R. Malagelada, G.F. Longstreth, W.H. Summerskill, and V.L. Go. Measurement of gastric functions during digestion of ordinary solid meals in man. *Gastroenterology*. 70:203-210 (1976).

79. J.B. Dressman, R.R. Berardi, L.C. Dermentzoglou, T.L. Russell, S.P. Schmaltz, J.L. Barnett, and K.M. Jarvenpaa. Upper gastrointestinal (GI) pH in young, healthy men and women. *Pharm Res.* 7:756-761 (1990).
80. P.E. Macheras and C.I. Reppas. Studies on freeze-dried drug-milk formulations. II: Effect of regenerated fluid volume on nitrofurantoin bioavailability. *J Pharm Sci.* 75:1145-1150 (1986).
81. P. Macheras, M. Koupparis, and E. Apostolelli. Dissolution of 4 controlled-release theophylline formulations in milk. *Int J Pharm.* 36:73-79 (1987).
82. P.L.H. McSweeney and P.F. Fox. *Advanced Dairy Chemistry Volume 3: Lactose, water, salts and minor constituents*; pg 608. (2010).
83. D.M. Mudie, G.L. Amidon, and G.E. Amidon. Physiological parameters for oral delivery and *in vitro* testing. *Mol Pharm.* 7:1388-1405 (2010).
84. S. Klein, J. Butler, J.M. Hempenstall, C. Reppas, and J.B. Dressman. Media to simulate the postprandial stomach I. Matching the physicochemical characteristics of standard breakfasts. *J Pharm Pharmacol.* 56:605-610 (2004).
85. A. Diakidou, M. Vertzoni, B. Abrahamsson, J. Dressman, and C. Reppas. Simulation of gastric lipolysis and prediction of felodipine release from a matrix tablet in the fed stomach. *Eur J Pharm Sci.* 37:133-140 (2009).
86. E. Jantratid and J. Dressman. Dissolution media simulating conditions in the proximal human gastrointestinal tract: An update. *Dissolut Technol.* 16:21-25 (2009).
87. E. Jantratid, N. Janssen, H. Chokshi, K. Tang, and J.B. Dressman. Designing biorelevant dissolution tests for lipid formulations: Case example - Lipid suspension of RZ-50. *Eur J Pharm Biopharm.* 69:776-785 (2008).
88. J. Fallingborg, L.A. Christensen, M. Ingemannielsen, B.A. Jacobsen, K. Abildgaard, and H.H. Rasmussen. pH-profile and regional transit times of the normal gut measured by a radiotelemetry device. *Aliment Pharmacol Ther.* 3:605-613 (1989).
89. B.L. Pedersen, H. Brondsted, H. Lennernas, F.N. Christensen, A. Mullertz, and H.G. Kristensen. Dissolution of hydrocortisone in human and simulated intestinal fluids. *Pharm Res.* 17:183-189 (2000).
90. E.M. Persson, A.S. Gustafsson, A.S. Carlsson, R.G. Nilsson, L. Knutson, P. Forsell, G. Hanisch, H. Lennernas, and B. Abrahamsson. The effects of food on the dissolution of poorly soluble drugs in human and in model small intestinal fluids. *Pharm Res.* 22:2141-2151 (2005).
91. J. Brouwers, J. Tack, F. Lammert, and P. Augustijns. Intraluminal drug and formulation behavior and integration in *in vitro* permeability estimation: A case study with amprenavir. *J Pharm Sci.* 95:372-383 (2006).

92. D. Alvaro, M. Angelico, A. Cantafora, A. Dibiase, A. Desantis, F. Bracci, G. Minervini, S.G. Corradini, A.F. Attili, and L. Capocaccia. Biliary-secretion of phosphatidylcholine and its molecular-species in cholecystectomized T-Tube patients - effects of bile-acid hydrophilicity. *Biochem Med Metab Biol.* 36:125-135 (1986).
93. D.P. McNamara, K.M. Whitney, and S.L. Goss. Use of a physiologic bicarbonate buffer system for dissolution characterization of ionizable drugs. *Pharm Res.* 20:1641-1646 (2003).
94. M. Vertzoni, N. Fotaki, E. Kostewicz, E. Stippler, C. Leuner, E. Nicolaidis, J. Dressman, and C. Reppas. Dissolution media simulating the intraluminal composition of the small intestine: physiological issues and practical aspects. *J Pharm Pharmacol.* 56:453-462 (2004).
95. S. Ladas, P.E.T. Isaacs, Y. Qureshi, G. Murphy, and G. Sladen. Effect of long and medium chain triglyceride meals on human ileal flow-rate and luminal bile-acid concentrations. *Clin Sci.* 61:P39-P39 (1981).
96. A. Tangerman, A. Vanschaik, and E.W. Vanderhoek. Analysis of conjugated and unconjugated bile-acids in serum and jejunal fluid of normal subjects. *Clin Chim Acta.* 159:123-132 (1986).
97. M. Armand, P. Borel, B. Pasquier, C. Dubois, M. Senft, M. Andre, J. Peyrot, J. Salducci, and D. Lairon. Physicochemical characteristics of emulsions during fat digestion in human stomach and duodenum. *Am J Physiol.* 271:G172-183 (1996).
98. E.M. Persson, R.G. Nilsson, G.I. Hansson, L.J. Lofgren, F. Liback, L. Knutson, B. Abrahamsson, and H. Lennernas. A clinical single-pass perfusion investigation of the dynamic *in vivo* secretory response to a dietary meal in human proximal small intestine. *Pharm Res.* 23:742-751 (2006).
99. E. Nicolaidis, E. Galia, C. Efthymiopoulos, J.B. Dressman, and C. Reppas. Forecasting the *in vivo* performance of four low solubility drugs from their *in vitro* dissolution data. *Pharm Res.* 16:1876-1882 (1999).
100. R. Löbenberg, J. Krämer, V.P. Shah, G.L. Amidon, and J.B. Dressman. Dissolution testing as a prognostic tool for oral drug absorption: Dissolution behavior of glibenclamide. *Pharm Res.* 17:439-444 (2000).
101. T. Hamaguchi, D. Shinkuma, Y. Yamanaka, and N. Mizuno. Bioavailability of mefenamic-acid - influence of food and water-intake. *J Pharm Sci.* 75:891-893 (1986).
102. W.N. Charman, M.C. Rogge, A.W. Boddy, and B.M. Berger. Effect of food and a monoglyceride emulsion formulation on danazol bioavailability. *J Clin Pharmacol.* 33:381-386 (1993).



103. S. Clarysse, J. Tack, F. Lammert, G. Duchateau, C. Reppas, and P. Augustijns. Postprandial evolution in composition and characteristics of human duodenal fluids in different nutritional states. *J Pharm Sci.* 98:1177-1192 (2009).
104. J.E. Boni, R.S. Brickl, J.B. Dressman, and M.L. Pfefferle. Instant FaSSIF and FeSSIF—biorelevance meets practicality. *Dissolut Technol.* 16:41-45 (2009).
105. European Pharmacopoeia 7th ed., Council of Europe, European Directorate for the Quality of Medicines & Healthcare, Strasbourg, France, 2011.
106. European Medicines Agency. ICH Topic Q4B Annex 7 Dissolution Test General Chapter. Available online [http://www.ema.europa.eu/docs/en\\_GB/document\\_library/Scientific\\_guideline/2009/09/WC500002776.pdf](http://www.ema.europa.eu/docs/en_GB/document_library/Scientific_guideline/2009/09/WC500002776.pdf). (2008 ).
107. A.M. Healy, L.G. McCarthy, K.M. Gallagher, and O.I. Corrigan. Sensitivity of dissolution rate to location in the paddle dissolution apparatus. *J Pharm Pharmacol.* 54:441-444 (2002).
108. L.M. Bocanegra, G.J. Morris, J.T. Jurewicz, and J.W. Mauger. Fluid and particle laser Doppler velocity measurements and mass transfer predictions for the USP Paddle Method Dissolution apparatus. *Drug Dev Ind Pharm.* 16:1441-1464 (1990).
109. British Pharmacopoeia Commission., General Medical Council (Great Britain), Great Britain. Medicines Commission., Great Britain. Dept. of Health., Great Britain. Scottish Office., Great Britain. Welsh Office., and Great Britain. Dept. of Health and Social Services Northern Ireland. *British pharmacopoeia 2000*, Stationery Office, London, 2000.
110. W.L. Hulse, J. Gray, and R.T. Forbes. A discriminatory intrinsic dissolution study using UV area imaging analysis to gain additional insights into the dissolution behaviour of active pharmaceutical ingredients. *Int J Pharm.* 434:133-139 (2012).
111. J. Ostergaard, E. Meng-Lund, S.W. Larsen, C. Larsen, K. Petersson, J. Lenke, and H. Jensen. Real-time UV imaging of nicotine release from transdermal patch. *Pharm Res.* 27:2614-2623 (2010).
112. J.P. Boetker, M. Savolainen, V. Koradia, F. Tian, T. Rades, A. Mullertz, C. Cornett, J. Rantanen, and J. Ostergaard. Insights into the early dissolution events of amlodipine using UV imaging and Raman spectroscopy. *Mol Pharm.* 8:1372-1380 (2011).
113. J. Ostergaard, F.B. Ye, J. Rantanen, A. Yaghmur, S.W. Larsen, C. Larsen, and H. Jensen. Monitoring lidocaine single-crystal dissolution by ultraviolet imaging. *J Pharm Sci.* 100:3405-3410 (2011).

114. S. Gordon, K. Naelapaa, J. Rantanen, A. Selen, A. Mullertz, and J. Ostergaard. Real-time dissolution behavior of furosemide in biorelevant media as determined by UV imaging. *Pharm Dev Technol*(2012).
115. J.P. Boetker, J. Rantanen, T. Rades, A. Mullertz, J. Ostergaard, and H. Jensen. A new approach to dissolution testing by UV imaging and finite element simulations. *Pharm Res*(2013).
116. Paraytec Ltd. SDI 300 manual: Theory and operation. P/N 340-9004 Rev A, York, UK:1-32 (2010).
117. Paraytec Ltd. Actipix SDI300:Rapid dissolution measurement for API development (Technical report). (2011).
118. F.B. Ye, A. Yaghmur, H. Jensen, S.W. Larsen, C. Larsen, and J. Ostergaard. Real-time UV imaging of drug diffusion and release from Pluronic F127 hydrogels. *Eur J Pharm Sci.* 43:236-243 (2011).
119. J. Pajander, S. Baldursdottir, J. Rantanen, and J. Ostergaard. Behaviour of HPMC compacts investigated using UV-imaging. *Int J Pharm.* 427:345-353 (2012).
120. K. Box, Comer, J., Mole, J., Taylor, R., Karki, S., Price, R. and Fotaki, N. Small scale assays for studying dissolution and precipitation of pharmaceutical cocrystals. Accessed 12 Dec 2012. Available from <http://abstracts.aapspharmaceutica.com/Verify/AAPS2012/postersubmissions/T2040.pdf>. *AAPS J*(2012).
121. N. Qiao, K. Wang, W. Schlindwein, A. Davies, and M. Li. In situ monitoring of carbamazepine-nicotinamide cocrystal intrinsic dissolution behaviour. *Eur J Pharm Biopharm.* 83:415-426 (2013).
122. M. Thing, C. Larsen, J. Ostergaard, H. Jensen, and S.W. Larsen. *In vitro* release from oil injectables for intra-articular administration: Importance of interfacial area, diffusivity and partitioning. *Eur J Pharm Sci.* 45:351-357 (2012).
123. F. Ye, S.W. Larsen, A. Yaghmur, H. Jensen, C. Larsen, and J. Østergaard. Real-time UV imaging of piroxicam diffusion and distribution from oil solutions into gels mimicking the subcutaneous matrix. *Eur J Pharm Sci.* 46:72-78 (2012).
124. J. Lenke. Two dimensional orthogonal imaging of laminar fluid flow across API surface: insight into dosage concentration inside GI lumen and permeability. Accessed 12 June 2012 from <http://www.sciforum.net/presentation/523>, 1st Electron Conf Pharm Sci2011, pp. 1-18.
125. E. Soderlind and J.B. Dressman. Physiological factors affecting drug release and absorption in the gastrointestinal tract. In J.B. Dressman and C. Reppas (eds.), *Oral Drug Absorption: Prediction and Assessment*, Informa Healthcare, NY, 2010, pp. 1-20.

126. B. Agoram, W.S. Woltosz, and M.B. Bolger. Predicting the impact of physiological and biochemical processes on oral drug bioavailability. *Adv Drug Deliv Rev* 50:(2001).
127. N. Parrott and T. Lavé. Prediction of intestinal absorption: Comparative assessment of GASTROPLUS™ and IDEA™. *Eur J Pharm Sci.* 17:51-61 (2002).
128. H.W. Davenport. *Physiology of the digestive tract: an introductory text.* Year Book Medical Publishers, Inc. Chicago. pg. 41-2471982.
129. D.A. Norris, N. Puri, and P.J. Sinko. The effect of physical barriers and properties on the oral absorption of particulates. *Adv Drug Deliv Rev.* 34:135-154 (1998).
130. P. Artursson, K. Palm, and K. Luthman. Caco-2 monolayers in experimental and theoretical predictions of drug transport. *Adv Drug Deliv Rev.* 22:67-84 (1996).
131. M. Kobayashi, N. Sada, M. Sugawara, K. Iseki, and K. Miyazaki. Development of a new system for prediction of drug absorption that takes into account drug dissolution and pH change in the gastro-intestinal tract. *Int J Pharm.* 221:87-94 (2001).
132. S. Hurst, C.-M. Loi, J. Brodfuehrer, and A. El-Kattan. Impact of physiological, physicochemical and biopharmaceutical factors in absorption and metabolism mechanisms on the drug oral bioavailability of rats and humans. *Expert Opin Drug Metab Toxicol.* 3:469-489 (2007).
133. P. Macheras, V. Karalis, and G. Valsami. Keeping a critical eye on the science and the regulation of oral drug absorption: A review. *J Pharm Sci.* 102:3018-3036 (2013).
134. U. Fagerholm. Prediction of human pharmacokinetics - Renal metabolic and excretion clearance. *J Pharm Pharmacol.* 59:1463-1471 (2007).
135. M.N. Martinez and G.L. Amidon. A mechanistic approach to understanding the factors affecting drug absorption: a review of fundamentals. *J Clin Pharmacol.* 42:620-643 (2002).
136. B.S. Abuasal, M.B. Bolger, D.K. Walker, and A. Kaddoumi. In silico modeling for the non-linear absorption kinetics of UK-343,664: a P-gp and CYP3A4 substrate. *Mol Pharm*(2012).
137. E.J. Wang, K. Lew, C.N. Casciano, R.P. Clement, and W.W. Johnson. Interaction of common azole antifungals with P glycoprotein. *Antimicrob Agents Chemother.* 46:160-165 (2002).
138. M.V.S. Varma, K. Sateesh, and R. Panchagnula. Functional role of P-glycoprotein in limiting intestinal absorption of drugs: Contribution of passive

- permeability to P-glycoprotein mediated efflux transport. *Mol Pharm.* 2:12-21 (2005).
139. R.K. Mittapalli, S. Vaidhyanathan, R. Sane, and W.F. Elmquist. Impact of P-glycoprotein (ABCB1) and breast cancer resistance protein (ABCG2) on the brain distribution of a novel BRAF inhibitor: vemurafenib (PLX4032). *J Pharmacol Exp Ther.* 342:33-40 (2012).
  140. M.F. Paine, M. Khalighi, J.M. Fisher, D.D. Shen, K.L. Kunze, C.L. Marsh, J.D. Perkins, and K.E. Thummel. Characterization of interintestinal and intrainestinal variations in human CYP3A-dependent metabolism. *J Pharmacol Exp Ther.* 283:1552-1562 (1997).
  141. A. Kaneko, M. Kato, C. Endo, K. Nakano, M. Ishigai, and K. Takeda. Prediction of clinical CYP3A4 induction using cryopreserved human hepatocytes. *Xenobiotica.* 40:791-799 (2010).
  142. H. Zhou. Pharmacokinetic strategies in deciphering atypical drug absorption profiles. *J Clin Pharmacol.* 43:211-227 (2003).
  143. M.F. Paine, C.L. Davis, D.D. Shen, C.L. Marsh, V.A. Raisys, and K.E. Thummel. Can oral midazolam predict oral cyclosporine disposition? *Eur J Pharm Sci.* 12:51-62 (2000).
  144. C. Versantvoort, C. Rompelberg, and A. Sips. Methodologies to study human intestinal absorption. A review. (2000).
  145. L.Z. Benet. The drug transporter-metabolism alliance: uncovering and defining the interplay. *Mol Pharm.* 6:1631-1643 (2009).
  146. A.S. Darwich, S. Neuhoff, M. Jamei, and A. Rostami-Hodjegan. Interplay of metabolism and transport in determining oral drug absorption and gut wall metabolism: a simulation assessment using the "Advanced Dissolution, Absorption, Metabolism (ADAM)" model. *Curr Drug Metab.* 11:716-729 (2010).
  147. L.Z. Benet, C.L. Cummins, and C.Y. Wu. Transporter-enzyme interactions: implications for predicting drug-drug interactions from *in vitro* data. *Curr Drug Metab.* 4:393-398 (2003).
  148. L.Z. Benet, C.L. Cummins, and C.Y. Wu. Unmasking the dynamic interplay between efflux transporters and metabolic enzymes. *Int J Pharm.* 277:3-9 (2004).
  149. L.Z. Benet. Predicting drug disposition via application of a Biopharmaceutics Drug Disposition Classification System. *Basic Clin Pharmacol Toxicol.* 106:162-167 (2009).
  150. R. Bouer, L. Barthe, C. Philibert, C. Tournaire, J. Woodley, and G. Houin. The roles of P-glycoprotein and intracellular metabolism in the intestinal absorption of methadone: *in vitro* studies using the rat everted intestinal sac. *Fundam Clin Pharmacol.* 13:494-500 (1999).

151. G.L. Amidon, P.J. Sinko, and D. Fleisher. Estimating human oral fraction dose absorbed - a correlation using rat intestinal-membrane permeability for passive and carrier-mediated compounds. *Pharm Res.* 5:651-654 (1988).
152. A. Dokoumetzidis, G. Valsami, and P. Macheras. Modelling and simulation in drug absorption processes. *Xenobiotica.* 37:1052-1065 (2007).
153. Y. Qiu, Q. Yihong, C. Yisheng, G.Z.Z. Geoff, L. Lirong, and R.P. William. Rational design of oral modified-release drug delivery systems. *Developing Solid Oral Dosage Forms*, Academic Press, San Diego, 2009, pp. 469-499.
154. S. Stegemann, F. Leveiller, D. Franchi, H. de Jong, and H. Lindaln. When poor solubility becomes an issue: From early stage to proof of concept. *Eur J Pharm Sci.* 31:249-261 (2007).
155. L.X. Yu, J.R. Crison, and G.L. Amidon. Compartmental transit and dispersion model analysis of small intestinal transit flow in humans. *Int J Pharm.* 140:111-118 (1996).
156. L.X. Yu, E. Lipka, J.R. Crison, and G.L. Amidon. Transport approaches to the biopharmaceutical design of oral drug delivery systems: Prediction of intestinal absorption. *Adv Drug Deliv Rev.* 19:359-376 (1996).
157. L.X. Yu and G.L. Amidon. A compartmental absorption and transit model for estimating oral drug absorption. *Int J Pharm.* 186:119-125 (1999).
158. M. Jamei, G.L. Dickinson, and A. Rostami-Hodjegan. A framework for assessing inter-individual variability in pharmacokinetics using virtual human populations and integrating general knowledge of physical chemistry, biology, anatomy, physiology and genetics: A tale of 'bottom-up' vs 'top-down' recognition of covariates. *Drug Metab Pharmacokinet.* 24:53-75 (2009).
159. M.G. Grass, Sinko, P J. Physiologically-based pharmacokinetic simulation modeling. *Adv Drug Deliv Rev.* 54:433-451 (2002).
160. N. Fotaki. Pros and cons of methods used for the prediction of oral drug absorption. *Expert Review Clin Pharmacol.* 2:195-208 (2009).
161. S.-M. Huang, D.R. Abernethy, Y. Wang, P. Zhao, and I. Zineh. The utility of modeling and simulation in drug development and regulatory review. *J Pharm Sci.* 102:2912-2923 (2013).
162. N. Parrott and T. Lave. Applications of physiologically based absorption models in drug discovery and development. *Mol Pharm.* 5:760-775 (2008).
163. Simulation Plus Inc. *GastroPlus™ 8 User Manual*. Lancaster, California. (2012).
164. S.S. De Buck, V.K. Sinha, L.A. Fenu, M.J. Nijssen, C.E. Mackie, and R.A.H.J. Gilissen. Prediction of human pharmacokinetics using physiologically based modeling: A retrospective analysis of 26 clinically tested drugs. *Drug Metab Dispos.* 35:1766-1780 (2007).

165. H.M. Jones, I.B. Gardner, W.T. Collard, P.J. Stanley, P. Oxley, N.A. Hosea, D. Plowchalk, S. Gernhardt, J. Lin, M. Dickins, S.R. Rahavendran, B.C. Jones, K.J. Watson, H. Pertinez, V. Kumar, and S. Cole. Simulation of human intravenous and oral pharmacokinetics of 21 diverse compounds using physiologically based pharmacokinetic modelling. *Clin Pharmacokinet.* 50:331-347 (2011).
166. Q. Wang, N. Fotaki, and Y. Mao. Biorelevant dissolution: methodology and application in drug development. *Dissolut Technol.* 16:6-12 (2009).
167. Food and Drug Administration (FDA) and Center for Drug Evaluation and Research (CDER). Guidance for Industry. Immediate Release Solid Oral Dosage Forms Scale-Up and Postapproval Changes: Chemistry, Manufacturing, and Controls, *In vitro* Dissolution Testing, and *In vivo* Bioequivalence Documentation (SUPAC-IR). Available from: <http://www.fda.gov/downloads/Drugs/GuidanceComplianceRegulatoryInformation/Guidances/ucm070636.pdf>. Accessed Date: September 11, 2010 1995.
168. P.A. Dickinson, W.W. Lee, P.W. Stott, A.I. Townsend, J.P. Smart, P. Ghahramani, T. Hammett, L. Billett, S. Behn, R.C. Gibb, and B. Abrahamsson. Clinical relevance of dissolution testing in quality by design. *AAPS J.* 10:380-390 (2008).
169. P.G. Welling. *In vitro* method to determine bioavailability: *In vitro-in vivo* correlations. In P.G. Welling, F.L.S. Tsee, and S.V. Dighe (eds.), *Pharmaceutical Bioequivalence*, Marcel Dekker, NY, 1991, pp. 223-231.
170. F.D.A. US Department of Health and Human Services, Center for Drug Evaluation and Research. Extended release oral dosage forms: Development, evaluation, and application of *in vitro/in vivo* correlations: Guidance for industry, US Government Printing Office, Rockville, MD, 1997.
171. Committee for Proprietary Medicinal Products (CPMP). Note for guidance on the investigation of bioavailability and bioequivalence CPMP/EWP/QWP/1401/98 Available from: [http://www.ema.europa.eu/docs/en\\_GB/document\\_library/Scientific\\_guideline/2009/09/WC500003519.pdf](http://www.ema.europa.eu/docs/en_GB/document_library/Scientific_guideline/2009/09/WC500003519.pdf). Accessed Date: September 11, 2010, European Medicines Evaluation Agency (EMA) 2001.
172. E. Gupta, D.M. Barends, E. Yamashita, K.A. Lentz, A.M. Harmsze, V.P. Shah, J.B. Dressman, and R.A. Lipper. Review of global regulations concerning biowaivers for immediate release solid oral dosage forms. *Eur J Pharm Sci.* 29:315-324 (2006).
173. Y. Qiu. Design and applications of *in vitro* tests for *in vitro-in vivo* correlations of oral extended-release dosage forms. *Am Pharm Review.* 9:94-99 (2006).

174. S. Souliman, S. Blanquet, E. Beyssac, and J.M. Cardot. A level a *in vitro/in vivo* correlation in fasted and fed states using different methods: Applied to solid immediate release oral dosage form. *Eur J Pharm Sci.* 27:72-79 (2006).
175. R.C. Rossi, C.L. Dias, E.M. Donato, L.A. Martins, A.M. Bergold, and P.E. Froehlich. Development and validation of dissolution test for ritonavir soft gelatin capsules based on *in vivo* data. *Int J Pharm.* 338:119-124 (2007).
176. R. Morita, R. Honda, and Y. Takahashi. Development of a new dissolution test method for an oral controlled release preparation, the PVA swelling controlled release system (SCRS). *J Control Release.* 90:109-117 (2003).
177. Y. Qiu, J. Garren, E. Samara, G. Cao, C. Abraham, H.S. Cheskin, and K.R. Engh. Once-a-day controlled-release dosage form of divalproex sodium II: Development of a predictive *in vitro* drug release method. *J Pharm Sci.* 92:2317-2325 (2003).
178. S. Dutta, Y.H. Qiu, E. Samara, G.L. Cao, and G.R. Granneman. Once-a-day extended-release dosage form of divalproex sodium III: Development and validation of a level a *in vitro-in vivo* correlation (IVIVC). *J Pharm Sci.* 94:1949-1956 (2005).
179. N. Sirisuth, L.L. Augsburger, and N.D. Eddington. Development and validation of a non-linear IVIVC model for a diltiazem extended release Formulation. *Biopharm Drug Dispos.* 23:1-8 (2002).
180. J.E. Polli. IVIVR versus IVIVC. *Dissolut Technol.* 7:6-9 (2000).
181. J.B. Dressman and C. Reppas. *In vitro-in vivo* correlations for lipophilic, poorly water-soluble drugs. *Eur J Pharm Sci.* 11:(2000).
182. Y. Qiu, Q. Yihong, C. Yisheng, G.Z.Z. Geoff, L. Lirong, and R.P. William. *In vitro-in vivo* correlations: Fundamentals, development considerations, and applications. *Developing Solid Oral Dosage Forms*, Academic Press, San Diego, 2009, pp. 379-406.
183. T. Shepard, C. Farrell, and M. Rochdi. Study design considerations for IVIVC studies. In J. Dressman (ed.), *Pharmaceutical dissolution testing*, Taylor and Francis 2005.
184. L.X. Yu, G.L. Amidon, J.E. Polli, H. Zhao, M.U. Mehta, D.P. Conner, V.P. Shah, L.J. Lesko, M.L. Chen, V.H.L. Lee, and A.S. Hussain. Biopharmaceutics classification system: The scientific basis for biowaiver extensions. *Pharm Res.* 19:921-925 (2002).
185. E. Rinaki, A. Dokoumetzidis, G. Valsami, and P. Macheras. Identification of biowaivers among class II drugs: Theoretical justification and practical examples. *Pharm Res.* 21:1567-1572 (2004).
186. M. Siewert. Perspectives of *in vitro* dissolution tests in establishing *in vivo/in vitro* correlations. *Eur J Drug Metab Pharmacokinet.* 18:7-18 (1993).

187. A.-L. Ungell and B. Abrahamsson. Biopharmaceutical support in formulation development In M. Gibson (ed.), *Pharmaceutical Preformulation and Formulation: A Practical Guide from Candidate Drug Selection to Commercial Dosage Form*, Interpharm/CRC, Boca Raton, 2004, pp. 97-156.
188. W.R. Gillespie. *PCDCON: Deconvolution for pharmacokinetic applications*. University of Texas, Austin, TX (1992).
189. A. Frick, H. Muller, and E. Wirbitzki. Biopharmaceutical characterization of oral controlled/modified-release drug products. *In vitro/in vivo* correlation of roxatidine. *Eur J Pharm Biopharm.* 46:313-319 (1998).
190. H. Mahayni, G.S. Rekhi, R.S. Uppoor, P. Marroum, A.S. Hussain, L.L. Augsburger, and N.D. Eddington. Evaluation of "external" predictability of an *in vitro-in vivo* correlation for an extended-release formulation containing metoprolol tartrate. *J Pharm Sci.* 89:1354-1361 (2000).
191. S. Li, A. Royce, and A. Serajuddin. *In vitro–in vivo* correlation in dosage form development: Case studies. *Biopharmaceutics Applications in Drug Development 2008*, pp. 359-382.
192. V.H. Sunesen, B.L. Pedersen, H.G. Kristensen, and A. Mullertz. *In vivo in vitro* correlations for a poorly soluble drug, danazol, using the flow-through dissolution method with biorelevant dissolution media. *Eur J Pharm Sci.* 24:305-313 (2005).
193. N. Tanaka, K. Imai, K. Okimoto, S. Ueda, Y. Tokunaga, R. Ibuki, K. Higaki, and T. Kimura. Development of novel sustained-release system, disintegration-controlled matrix tablet (DCMT) with solid dispersion granules of nilvadipine (II): *In vivo* evaluation. *J Controlled Release.* 112:51-56 (2006).
194. D. Law, E.A. Schmitt, K.C. Marsh, E.A. Everitt, W.L. Wang, J.J. Fort, S.L. Krill, and Y.H. Qiu. Ritonavir-PEG 8000 amorphous solid dispersions: *In vitro* and *in vivo* evaluations. *J Pharm Sci.* 93:563-570 (2004).
195. D.M. Ryan, C. O'Callaghan, and P.W. Muggleton. Cefuroxime, a new cephalosporin antibiotic: activity *in vivo*. *Antimicrob Agents Chemother.* 9:520-525 (1976).
196. C.H. O'Callaghan, R.B. Sykes, A. Griffiths, and J.E. Thornton. Cefuroxime, a new cephalosporin antibiotic: activity *in vitro*. *Antimicrob Agents Chemother.* 9:511-519 (1976).
197. R.D. Foord. Cefuroxime: human pharmacokinetics. *Antimicrob Agents Chemother.* 9:741-747 (1976).
198. A.M. Emmerson. Cefuroxime axetil. *J Antimicrob Chemother.* 22:101-104 (1988).
199. K. Stoeckel, W.L. Hayton, and D.J. Edwards. Clinical pharmacokinetics of oral cephalosporins. *Antibiot Chemother.* 47:34-71 (1995).



200. S.M. Harding, P.E. Williams, and J. Ayrton. Pharmacology of cefuroxime as the 1-acetoxyethyl ester in volunteers. *Antimicrob Agents Chemother.* 25:78-82 (1984).
201. S.W. Jun, M.S. Kim, G.H. Jo, S. Lee, J.S. Woo, J.S. Park, and S.J. Hwang. Cefuroxime axetil solid dispersions prepared using solution enhanced dispersion by supercritical fluids. *J Pharm Pharmacol.* 57:1529-1537 (2005).
202. M.E. Klepser, M.N. Marangos, K.B. Patel, D.P. Nicolau, R. Quintiliani, and C.H. Nightingale. Clinical pharmacokinetics of newer cephalosporins. *Clinical Pharmacokinetics.* 28:361-384 (1995).
203. Y.H. Zhao, J. Le, M.H. Abraham, A. Hersey, P.J. Eddershaw, C.N. Luscombe, D. Boutina, G. Beck, B. Sherborne, I. Cooper, and J.A. Platts. Evaluation of human intestinal absorption data and subsequent derivation of a quantitative structure-activity relationship (QSAR) with the Abraham descriptors. *J Pharm Sci.* 90:749-784 (2001).
204. W.F. Richter, Y.H. Chong, and V.J. Stella. On the mechanism of isomerization of cephalosporin esters. *J Pharm Sci.* 79:185-186 (1990).
205. F. Kees, U. Lukassek, K.G. Naber, and H. Grobecker. Comparative Investigations on the Bioavailability of Cefuroxime Axetil. *Arzneimittelforschung.* 41-2:843-846 (1991).
206. N.A.T. Nguyen. The relationship of diastereomer hydrolysis kinetics to shelf-life predictions for cefuroxime axetil. *Pharm Res.* 8:893-898 (1991).
207. C.M. Perry and R.N. Brogden. Cefuroxime axetil: A review of its antibacterial activity, pharmacokinetic properties and therapeutic efficacy. *Drugs.* 52:125-158 (1996).
208. D.E. Nix, W.T. Symonds, and J.M. Hyatt. Comparative pharmacokinetics of oral ceftibuten, cefixime, cefaclor, and cefuroxime axetil in healthy volunteers. *Pharmacother.* 17:121-125 (1997).
209. A. Finn, A. Straughn, M. Meyer, and J. Chubb. Effect of dose and food on the bioavailability of cefuroxime axetil. *Biopharm Drug Dispos.* 8:519-526 (1987).
210. I. Ivana, Z. Ljiljana, and Z. Mira. A stability indicating assay method for cefuroxime axetil and its application to analysis of tablets exposed to accelerated stability test conditions. *J Chromatogr A.* 1119:209-215 (2006).
211. N. Ruiz-Balaguer, A. Nacher, V.G. Casabo, and M. Merino. Nonlinear intestinal absorption kinetics of cefuroxime axetil in rats. *Antimicrob Agents Chemother.* 41:445-448 (1997).
212. N. Ruiz-Balaguer, A. Nacher, V.G. Casabo, and M. Merino Sanjuan. Intestinal transport of cefuroxime axetil in rats: absorption and hydrolysis processes. *Int J Pharm.* 234:101-111 (2002).

213. P. Ruiz-Carretero, M. Merino-Sanjuan, A. Nacher, and V.G. Casabo. Pharmacokinetic models for the saturable absorption of cefuroxime axetil and saturable elimination of cefuroxime. *Eur J Pharm Sci.* 21:217-223 (2004).
214. Itraconazole (DB01167). Available from: <http://www.drugbank.ca/drugs/DB01167>. Accessed Date: Nov 12,2010. DrugBank.2010.
215. Janssen-Cilag Ltd. Sporanox<sup>®</sup> (itraconazole) capsule product info.Available from: [http://www.janssen.com.au/files/Products/Sporanox\\_Capsules\\_PI.pdf](http://www.janssen.com.au/files/Products/Sporanox_Capsules_PI.pdf). Accessed 10 March 20132013.
216. J. Peeters, P. Neeskens, J.P. Tollenaere, P. Van Remoortere, and M.E. Brewster. Characterization of the interaction of 2-hydroxypropyl- $\beta$ -cyclodextrin with itraconazole at pH 2, 4, and 7. *J Pharm Sci.* 91:1414-1422 (2002).
217. K. De Beule and J. Van Gestel. Pharmacology of itraconazole. *Drugs.* 61 Suppl 1:27-37 (2001).
218. M.J. O'Neil. The Merck index [electronic resource] : an encyclopedia of chemicals, drugs, and biologicals. Available from: <http://www.medicinescomplete.com/mc/merck/current/>. Accessed Date: September 11, 2010, Whitehouse Station, N.J. : Merck2010.
219. H.S. Ghazal, A.M. Dyas, J.L. Ford, and G.A. Hutcheon. *In vitro* evaluation of the dissolution behaviour of itraconazole in biorelevant media. *Int J Pharm.* 366:117-123 (2009).
220. J.M. Poirier and G. Cheymol. Optimisation of itraconazole therapy using target drug concentrations. *Clinical Pharmacokinetics.* 35:461-473 (1998).
221. G. Arredondo, R. Martinezjorda, R. Calvo, C. Aguirre, and E. Suarez. Protein-binding of itraconazole and fluconazole in patients with chronic-renal-failure. *Int J Clin Pharmacol Ther.* 32:361-364 (1994).
222. S.M. Grant and S.P. Clissold. Itraconazole. A review of its pharmacodynamic and pharmacokinetic properties, and therapeutic use in superficial and systemic mycoses. *Drugs.* 37:310-344 (1989).
223. D.W. Warnock. Itraconazole and fluconazole: new drugs for deep fungal infection. *J Antimicrob Chemother.* 24:275-277 (1989).
224. J.A. Barone, J.G. Koh, R.H. Bierman, J.L. Colaizzi, K.A. Swanson, M.C. Gaffar, B.L. Moskovitz, W. Mechlinski, and V. Van de Velde. Food interaction and steady-state pharmacokinetics of itraconazole capsules in healthy male volunteers. *Antimicrob Agents Chemother.* 37:778-784 (1993).
225. T.C. Hardin, J.R. Graybill, R. Fetchick, R. Woestenborghs, M.G. Rinaldi, and J.G. Kuhn. Pharmacokinetics of itraconazole following oral administration to normal volunteers. *Antimicrob Agents Chemother.* 32:1310-1313 (1988).

226. N. Isoherranen, K.L. Kunze, K.E. Allen, W.L. Nelson, and K.E. Thummel. Role of itraconazole metabolites in CYP3A4 inhibition. *Drug Metab Dispos.* 32:1121-1131 (2004).
227. S. Rendic. Summary of information on human CYP enzymes: Human P450 metabolism data. *Drug Metab Rev.* 34:83-448 (2002).
228. H.Y. Yun, M.S. Baek, I.S. Park, B.K. Choi, and K.I. Kwon. Comparative analysis of the effects of rice and bread meals on bioavailability of itraconazole using NONMEM in healthy volunteers. *Eur J Clin Pharmacol.* 62:1033-1039 (2006).
229. T. Zimmermann, R.A. Yeates, M. Albrecht, H. Laufen, and A. Wildfeuer. Influence of concomitant food-intake on the gastrointestinal absorption of fluconazole and itraconazole in Japanese subjects. *Int J Clin Pharmacol Res.* 14:87-93 (1994).
230. T. Zimmermann, R.A. Yeates, H. Laufen, G. Pfaff, and A. Wildfeuer. Influence of concomitant food-intake on the oral absorption of 2 triazole antifungal agents, itraconazole and fluconazole. *Eur J Clin Pharmacol.* 46:147-150 (1994).
231. J. Bevernage, B. Hens, J. Brouwers, J. Tack, P. Annaert, and P. Augustijns. Supersaturation in human gastric fluids. *Eur J Pharm Biopharm.* 81:184-189 (2012).
232. Hoffmann-La Roche Inc. Product Information: Zelboraf™ oral tablet, vemurafenib oral tablet. Nutley, NJ. (2011).
233. Center for Drug Evaluation and Research. Clinical pharmacology and biopharmaceutics review: Vemurafenib Available online [http://www.accessdata.fda.gov/drugsatfda\\_docs/nda/2011/202429Orig1s000ClinPharmRpdf](http://www.accessdata.fda.gov/drugsatfda_docs/nda/2011/202429Orig1s000ClinPharmRpdf) Accessed 12 Feb 2012(2011).
234. A. Chatterji, Z. Dong, H.K. Sandhu, and N.H. Shah. Patent WO 2008/138755 A2. Pharmaceutical compositions for poorly soluble drugs F Hoffmann-La Roche AG (2008).
235. D. Desai, R. Diodone, Z. Go, P.N. Ibrahim, R. Iyer, H.-j. Mair, H.K. Sandhu, N.H. Shah, G. Visor, N. Wyttenbach, S. Lauper, J. Pudewell, and F. Wierschem. Compositions and Uses Thereof (US Patent 20100310659). In United States Patent Agency (ed.), United States 2010.
236. A. Ribas, W. Zhang, I. Chang, K. Shirai, M.S. Ernstoff, A. Daud, C.L. Cowey, G. Daniels, E. Seja, E. O'Laco, J.A. Glaspy, B. Chmielowski, T. Hill, A.K. Joe, and J.F. Grippo. The effects of a high-fat meal on single-dose vemurafenib pharmacokinetics. *J Clin Pharmacol*:Early online view.doi: 10.1002/jcph.1255 (2014).
237. H.A. Crisp, J.C. Clayton, L.G. Elliott, and E.M. Wilson. PCT appl. DE3327449: Amorphous cefuroxime axetil for improved bioavailability from the gastrointestinal tract. (1984).

238. H.A. Crisp, H. Weald, and J.C. Clayton. Amorphous form of cefuroxime ester. US Patent No 4,562,181(1985).
239. R.R. Namburi and J.E. Kerr. Oral itraconazole formulations and methods of making the same. United States Patent 6663897. In U.P. Office (ed.)2003.
240. M.B. James and L.G. Elliott. United States Patent No. 4865851 "Pharmaceutical composition comprising cefuroxime axetil", Glaxo Group Ltd.1989.
241. D.S. Deutsch and A. Jamshed. United States Patent No. 4865851 "Pharmaceutical Composition"1990.
242. B.C. Sherman. European Patent Office Patent No. EP0996449 B1 "Pharmaceutical compositions comprising cefuroxime axetil", European Patent Specification1998.
243. Joint Formulary Committee. British National Formulary 59, Pharmaceutical Press, London, 2010.
244. P. Gilis, V. De Conde, and R. Vandecruys. Beads having a core coated with an antifungal and a polymer. US Patent 5,633,0151997.
245. R. Vandecruys, V. De Conde, P. Gilis, and J. Peeters. Pellets having a core coated with an antifungal and a polymer. WO 98423181998.
246. M.E. Brewster, R. Vandecruys, J. Peeters, P. Neeskens, G. Verreck, and T. Loftsson. Comparative interaction of 2-hydroxypropyl-beta-cyclodextrin and sulfobutylether-beta-cyclodextrin with itraconazole: Phase-solubility behavior and stabilization of supersaturated drug solutions. Eur J Pharm Sci. 34:94-103 (2008).
247. A. Albano, Shah, N., Sandhu, H., Phuapradit, W., Iyer, R., Desai, D. Solid complexes with ionic polymers. Innovations in Pharma Science. Pharm Tech. 32:46-47 (2008).
248. Y. Heakal, M. Kester, and S. Savage. Vemurafenib (PLX4032): an orally available inhibitor of mutated BRAF for the treatment of metastatic melanoma. Ann Pharmacother. 45:1399-1405 (2011).
249. N. Shah, R.M. Iyer, H.J. Mair, D.S. Choi, H. Tian, R. Diodone, K. Fahrnich, A. Pabst-Ravot, K. Tang, E. Scheubel, J.F. Grippo, S.A. Moreira, Z. Go, J. Mouskountakis, T. Louie, P.N. Ibrahim, H. Sandhu, L. Rubia, H. Chokshi, D. Singhal, and W. Malick. Improved human bioavailability of vemurafenib, a practically insoluble drug, using an amorphous polymer-stabilized solid dispersion prepared by a solvent-controlled coprecipitation process. J Pharm Sci. 102:967-981 (2013).
250. N. Shah, H. Sandhu, W. Phuapradit, R. Pinal, R. Iyer, A. Albano, A. Chatterji, S. Anand, D.S. Choi, K. Tang, H. Tian, H. Chokshi, D. Singhal, and W. Malick. Development of novel microprecipitated bulk powder (MBP) technology for

- manufacturing stable amorphous formulations of poorly soluble drugs. *Int J Pharm.* 438:53-60 (2012).
251. D.T. Friesen, R. Shanker, M. Crew, D.T. Smithey, W.J. Curatolo, and J.A.S. Nightingale. Hydroxypropyl methylcellulose acetate succinate-based spray-dried dispersions: an overview. *Mol Pharm.* 5:1003-1019 (2008).
  252. Roche Pharmaceuticals. Compound X interim company report, Hoffmann-La Roche Inc., Nutley, New Jersey, USA. (2009).
  253. M.V. Vertzoni, C. Reppas, and H.A. Archontaki. Optimization and validation of a high-performance liquid chromatographic method with UV detection for the determination of ketoconazole in canine plasma. *J Chromatogr B Analyt Technol Biomed Life Sci.* 839:62-67 (2006).
  254. N.O. Can, G. Altıokka, and H.Y. Aboul-Enein. Determination of cefuroxime axetil in tablets and biological fluids using liquid chromatography and flow injection analysis. *Analytica Chimica Acta.* 576:246-252 (2006).
  255. H.S. Ghazal. The impact of biorelevant media on the in-vitro dissolution of azole antifungal drugs School of Pharmacy and Biomolecular Sciences, Vol. PhD, Liverpool John Moores University, Liverpool, 2009, p. 197.
  256. J.B. Dressman, M. Vertzoni, K. Goumas, and C. Reppas. Estimating drug solubility in the gastrointestinal tract. *Adv Drug Deliv Rev.* 59:591-602 (2007).
  257. P. Finholt and S. Solvang. Dissolution kinetics of drugs in human gastric juice--the role of surface tension. *J Pharm Sci.* 57:1322-1326 (1968).
  258. I. Tomaszewska and N. Fotaki. Phosphate and maleate buffer: Surface tension and buffer capacity measurement (unpublished data). PhD project, University of Bath (2010).
  259. D. Qiang, J.A. Gunn, L. Schultz, and Z.J. Li. Evaluation of the impact of sodium lauryl sulfate source variability on solid oral dosage form development. *Drug Dev Ind Pharm.* 36:1486-1496 (2010).
  260. J.R. Crison, N.D. Weiner, and G.L. Amidon. Dissolution media for *in vitro* testing of water-insoluble drugs: Effect of surfactant purity and electrolyte on *in vitro* dissolution of carbamazepine in aqueous solutions of sodium lauryl sulfate. *J Pharm Sci.* 86:384-388 (1997).
  261. W. Sun, C.K. Larive, and M.Z. Southard. A mechanistic study of danazol dissolution in ionic surfactant solutions. *J Pharm Sci.* 92:424-435 (2003).
  262. E.S. Stippler. Biorelevant dissolution test methods to assess bioequivalence of drug products, PhD thesis, Johann Wolfgang Goethe-Universität, Frankfurt/Main, Germany. Available from Shaker Verlag, Aachen. 2004.
  263. D.B. Lakings, C. Lizarraga, W.J. Haggerty, and M.J. Williamson. High-performance liquid chromatographic microdetermination of indoprofen in human milk. *J Pharm Sci.* 68:1113-1116 (1979).

264. K. Stoeckel, W. Hofheinz, J.P. Laneury, P. Duchene, S. Shedlofsky, and R.A. Blouin. Stability of cephalosporin prodrug esters in human intestinal juice: Implications for oral bioavailability. *Antimicrob Agents Chemother.* 42:2602-2606 (1998).
265. N. Fotaki, M. Symillides, and C. Reppas. *In vitro* versus canine data for predicting input profiles of isosorbide-5-mononitrate from oral extended release products on a confidence interval basis. *Eur J Pharm Sci.* 24:115-122 (2005).
266. M. Vertzoni, M. Symillides, A. Iliadis, E. Nicolaidis, and C. Reppas. Comparison of simulated cumulative drug versus time data sets with indices. *Eur J Pharm Biopharm.* 56:421-428 (2003).
267. F.O. Costa, J.J.S. Sousa, A.A.C.C. Pais, and S.J. Formosinho. Comparison of dissolution profiles of Ibuprofen pellets. *J Control Release.* 89:199-212 (2003).
268. J.G. Wagner. Interpretation of percent dissolved-time plots derived from *in vitro* testing of conventional tablets and capsules. *J Pharm Sci.* 58:1253-1257 (1969).
269. R.W. Korsmeyer, R. Gurny, E. Doelker, P. Buri, and N.A. Peppas. Mechanisms of solute release from porous hydrophilic polymers. *Int J Pharm.* 15:25-35 (1983).
270. V. Pillay and R. Fassihi. *In vitro* release modulation from crosslinked pellets for site-specific drug delivery to the gastrointestinal tract: I. Comparison of pH-responsive drug release and associated kinetics. *J Control Release.* 59:229-242 (1999).
271. P. Costa and J.M.S. Lobo. Evaluation of mathematical models describing drug release from estradiol transdermal systems. *Drug Dev Ind Pharm.* 29:89-97 (2003).
272. P. Costa and J.M. Sousa Lobo. Modeling and comparison of dissolution profiles. *Eur J Pharm Sci.* 13:123-133 (2001).
273. P.L. Ritger and N.A. Peppas. A simple equation for description of solute release II. Fickian and anomalous release from swellable devices. *J Control Release.* 5:37-42 (1987).
274. N.A. Peppas. Analysis of fickian and non-fickian drug release from polymers. *Pharm Acta Helv.* 60:110-111 (1985).
275. J. Siepmann and N.A. Peppas. Modeling of drug release from delivery systems based on hydroxypropyl methylcellulose (HPMC). *Adv Drug Deliv Rev.* 48:139-157 (2001).
276. N. Fotaki and C. Reppas. The flow through cell methodology in the evaluation of intraluminal drug release characteristics. *Dissolut Technol.* 12:17-21 (2005).

277. K.J. Watson, J. Davis, and H.M. Jones. Application of physiologically based pharmacokinetic modeling to understanding the clinical pharmacokinetics of UK-369,003. *Drug Metab Dispos.* 39:1203-1213 (2011).
278. M. Tubic, D. Wagner, H. Spahn-Langguth, M.B. Bolger, and P. Langguth. In silico modeling of non-linear drug absorption for the P-gp substrate talinolol and of consequences for the resulting pharmacodynamic effect. *Pharm Res.* 23:1712-1720 (2006).
279. M. Kuentz, S. Nick, N. Parrott, and D. Röthlisberger. A strategy for preclinical formulation development using GastroPlus™ as pharmacokinetic simulation tool and a statistical screening design applied to a dog study. *Eur J Pharm Sci.* 27:91-99 (2006).
280. H.M. Jones, N. Parrott, G. Ohlenbusch, and T. Lave. Predicting pharmacokinetic food effects using biorelevant solubility media and physiologically based modelling. *Clinical Pharmacokinetics.* 45:1213-1226 (2006).
281. N. Parrott, N. Paquereau, P. Coassolo, and T. Lave. An evaluation of the utility of physiologically based models of pharmacokinetics in early drug discovery. *J Pharm Sci.* 94:2327-2343 (2005).
282. C.L. Stoner, A. Cleton, K. Johnson, D.M. Oh, H. Hallak, J. Brodfuehrer, N. Surendran, and H.K. Han. Integrated oral bioavailability projection using *in vitro* screening data as a selection tool in drug discovery. *Int J Pharm.* 269:241-249 (2004).
283. A.T.K. Lu, M.E. Frisella, and K.C. Johnson. Dissolution modeling: Factors affecting the dissolution rates of polydisperse powders. *Pharm Res.* 10:1308-1314 (1993).
284. J. Wang, Flanagan, D. R. General solution for diffusion-controlled dissolution of spherical particles. 1. Theory. *J Pharm Sci.* 88:731-738 (1999).
285. W. Hayduk and H. Laudie. Prediction of diffusion coefficients for nonelectrolytes in dilute aqueous solutions. *Aiche J.* 20:611-615 (1974).
286. Merck Index (online version). Cefuroxime axetil Merck: Whitehouse Station, NJ 2012.
287. N. Rojanasthien, C. Boonchaliew, B. Kumsorn, and C. Sangdee. A bioequivalence study of the cefuroxime axetil in healthy volunteers. *J Med Assoc Thai.* 86:1063-1072 (2003).
288. K.H. Donn, N.C. James, and J.R. Powell. Bioavailability of cefuroxime axetil formulations. *J Pharm Sci.* 83:842-844 (1994).
289. Scifinder (online version). Itraconazole, Chemical Abstracts Service: Columbus, OH2012.

290. N.A.R.A. Ghazal. Influence of excipients on stabilization of amorphous cefuroxime axetil under process conditions of compression and coating, Dept of Pharmacy and Pharmacology, Vol. Ph.D, University of Bath, Bath, 2005, p. 276.
291. J. Heykants, A. Vanpeer, V. Vandeveld, P. Vanrooy, W. Meuldermans, K. Lavrijsen, R. Woestenborghs, J. Vancutsem, and G. Cauwenbergh. The clinical pharmacokinetics of itraconazole - an overview. *Mycoses*. 32:67-87 (1989).
292. S. Clarysse, J. Brouwers, J. Tack, P. Annaert, and P. Augustijns. Intestinal drug solubility estimation based on simulated intestinal fluids: comparison with solubility in human intestinal fluids. *Eur J Pharm Sci*. 43:260-269 (2011).
293. J.W. Polli, S.A. Wring, J.E. Humphreys, L. Huang, J.B. Morgan, L.O. Webster, and C.S. Serabjit-Singh. Rational use of *in vitro* P-glycoprotein assays in drug discovery. *J Pharmacol Exp Ther*. 299:620-628 (2001).
294. I. Oszczapowicz, E. Malafiej, M. Szelachowska, A. Horoszewicz-Malafiej, C. Kuklewicz, E. Sieranska, A. Denys, and J. Niedworok. Esters of cephalosporins. Part II. Differences in the properties of various forms of the 1-acetoxyethyl ester of cefuroxime. *Acta Pol Pharm*. 52:397-401 (1995).
295. M.A. Barrett, M.J. Lawrence, A.J. Hutt, and A.B. Lansley. Stereoselective absorption and hydrolysis of cefuroxime axetil diastereomers using the Caco-2 cell monolayer model. *Eur J Drug Metab Pharmacokinet*. 22:409-413 (1997).
296. U. Fagerholm, M. Johansson, and H. Lennernas. Comparison between permeability coefficients in rat and human jejunum. *Pharm Res*. 13:1336-1342 (1996).
297. K.M. Mahar Doan, J.E. Humphreys, L.O. Webster, S.A. Wring, L.J. Shampine, C.J. Serabjit-Singh, K.K. Adkison, and J.W. Polli. Passive permeability and P-glycoprotein-mediated efflux differentiate central nervous system (CNS) and non-CNS marketed drugs. *J Pharmacol Exp Ther*. 303:1029-1037 (2002).
298. K. Stoeckel, M. Harell, and M. Dan. Penetration of cefetamet pivoxil and cefuroxime axetil into the maxillary sinus mucosa at steady state. *Antimicrob Agents Chemother*. 40:780-783 (1996).
299. R.A. Yeates, T. Zimmermann, H. Laufen, M. Albrecht, and A. Wildfeuer. Comparative pharmacokinetics of fuconazole and of itraconazole in Japanese and in German subjects. *Int J Clin Pharmacol Ther*. 33:131-135 (1995).
300. V.K. Sinha, J. Snoeys, N.V. Osselaer, A.V. Peer, C. Mackie, and D. Heald. From preclinical to human--prediction of oral absorption and drug-drug interaction potential using physiologically based pharmacokinetic (PBPK) modeling approach in an industrial setting: a workflow by using case example. *Biopharm Drug Dispos*. 33:111-121 (2012).
301. S. Mouly and M.F. Paine. P-glycoprotein increases from proximal to distal regions of human small intestine. *Pharm Res*. 20:1595-1599 (2003).



302. G. Englund, F. Rorsman, A. Ronnblom, U. Karlbom, L. Lazorova, J. Grasjo, A. Kindmark, and P. Artursson. Regional levels of drug transporters along the human intestinal tract: co-expression of ABC and SLC transporters and comparison with Caco-2 cells. *Eur J Pharm Sci.* 29:269-277 (2006).
303. E.M. del Amo, A.T. Heikkinen, and J. Mönkkönen. *In vitro-in vivo* correlation in p-glycoprotein mediated transport in intestinal absorption. *Eur J Pharm Sci.* 36:200-211 (2009).
304. J. Heykants, M. Michiels, W. Meuldermans, J. Monbaliu, K. Lasvrijsen, A. Van Peer, J.C. Levron, R. Woestenborghs, and G. Cauwenbergh. The pharmacokinetics of itraconazole in animals and man: an overview. In R.A. Fromtling (ed.), *Recent trends in the discovery, development and evaluation of antifungal agents*, Prous Science Publishers, Barcelona, 1987, pp. 223-249.
305. A. Van Peer, R. Woestenborghs, J. Heykants, R. Gasparini, and G. Gauwenbergh. The effects of food and dose on the oral systemic availability of itraconazole in healthy subjects. *Eur J Clin Pharmacol.* 36:423-426 (1989).
306. M. Schaferkorting. Pharmacokinetic optimization of oral antifungal therapy. *Clinical Pharmacokinetics.* 25:329-341 (1993).
307. D.A. Stevens. Itraconazole in cyclodextrin solution. *Pharmacother.* 19:603-611 (1999).
308. H. Komura and M. Iwaki. *In vitro* and *in vivo* small intestinal metabolism of CYP3A and UGT substrates in preclinical animals species and humans: species differences. *Drug Metab Rev.* 43:476-498 (2011).
309. Y. Adachi, H. Suzuki, and Y. Sugiyama. Comparative studies on *in vitro* methods for evaluating *in vivo* function of MDR1 P-glycoprotein. *Pharm Res.* 18:1660-1668 (2001).
310. K.S. Lown, J.C. Kolars, K.E. Thummel, J.L. Barnett, K.L. Kunze, S.A. Wrighton, and P.B. Watkins. Interpatient heterogeneity in expression of CYP3A4 and CYP3A5 in small bowel. Lack of prediction by the erythromycin breath test. *Drug Metab Dispos.* 22:947-955 (1994).
311. S. Haller, F. Schuler, S.E. Lazic, D. Bachir-Cherif, S.D. Kramer, N.J. Parrott, G. Steiner, and S. Belli. Expression profiles of metabolic enzymes and drug transporters in the liver and along the intestine of beagle dogs. *Drug Metab Dispos.* 40:1603-1610 (2012).
312. GlaxoSmithKline. Ceftin/Zinnat prescribing information. Accessed 18 Dec 2011; [http://www.accessdata.fda.gov/drugsatfda\\_docs/label/2007/050605s042lbl.pdf](http://www.accessdata.fda.gov/drugsatfda_docs/label/2007/050605s042lbl.pdf). (2007).
313. G.L. Mosher, J. McBee, and D.B. Shaw. Esterase activity toward the diastereomers of cefuroxime axetil in the rat and dog. *Pharm Res.* 9:687-689 (1992).

314. A.N. Saab, L.W. Dittert, and A.A. Hussain. Isomerization of cephalosporin esters: implications for the prodrug ester approach to enhancing the oral bioavailabilities of cephalosporins. *J Pharm Sci.* 77:906-907 (1988).
315. C.J. Campbell, L.J. Chantrell, and R. Eastmond. Purification and partial characterization of rat intestinal cefuroxime axetil esterase. *Biochem Pharmacol.* 36:2317-2324 (1987).
316. A. Mullertz. Food effects on drug absorption and dosage form performance. In: Dressman JB, Reppas C, editors. *Oral Drug Absorption: Prediction and Assessment.* 2nd ed. NY: Informa Healthcare; 2010. p. 90-107. 2010.
317. J.G. Wagner. Absorption analysis and bioavailability. *Pharmacokinetics for the Pharmaceutical Scientist*, Technomic Pub. Co. Inc . Lancaster, PA, 1993, pp. 159 - 206.
318. P. Macheras, C. Reppas, and S. Antimisiaris. Binding of drugs in milk: the role of casein in milk protein binding--comments on the paper by Stebler and Guentert. *Pharm Res.* 8:550 (1991).
319. T. Zoeller and S. Klein. Simplified biorelevant media for screening dissolution performance of poorly soluble drugs. *Dissolut Technol.* 14:8-13 (2007).
320. V.P. Shah, A. Noory, C. Noory, B. Mccullough, S. Clarke, R. Everett, H. Naviasky, B.N. Srinivasan, D. Fortman, and J.P. Skelly. In-vitro dissolution of sparingly water-soluble drug-dosage forms. *Int J Pharm.* 125:99-106 (1995).
321. A.T. Florence and D. Attwood. Chapter 6: Surfactant. *Physicochemical Principles of Pharmacy*, 4th ed. London. Pharmaceutical Press. 2006, pp. 177-228.
322. C.Y. Poon. Tonicity, osmoticity, osmolality and osmolarity. In D.B. Troy (ed.), *Remington : the science and practice of pharmacy*, Lippincott Williams & Wilkins, Philadelphia, Pa., 2006, p. 264.
323. H. Allaboun, K.A. Alkhamis, and N.D. Al Jbour. Effect of surfactant on dissolution of spherical particles in micellar systems. *Eur J Pharm Biopharm.* 65:188-197 (2007).
324. D. Zhou, W.R. Porter, and G.G.Z. Zhang. Drug stability and degradation studies. *Developing Solid Oral Dosage Forms*, Academic Press, San Diego, 2009, pp. 87-124.
325. C. Pan, F. Liu, and M. Motto. Identification of pharmaceutical impurities in formulated dosage forms. *J Pharm Sci*(2010).
326. H.J. Robson, D.Q.M. Craig, and D. Deutsch. An investigation into the release of cefuroxime axetil from taste-masked stearic acid microspheres - Part 1: The influence of the dissolution medium on the drug release profile and the physical integrity of the microspheres. *Int J Pharm.* 190:183-192 (1999).

327. B.R. Rohrs, T.J. Thamann, P. Gao, D.J. Stelzer, M.S. Bergren, and R.S. Chao. Tablet dissolution affected by a moisture mediated solid-state interaction between drug and disintegrant. *Pharm Res.* 16:1850-1856 (1999).
328. Y. Choi, S.E. Jin, M.K. Lee, and C.K. Kim. *In vitro* dissolution and *in vivo* bioequivalence evaluation of two brands of cefuroxime axetil tablets. *Arzneimittelforschung.* 59:42-48 (2009).
329. L.J. Naylor, V. Bakatselou, and J.B. Dressman. Comparison of the mechanism of dissolution of hydrocortisone in simple and mixed micelle systems. *Pharm Res.* 10:865-870 (1993).
330. T.S. Wiedmann and L. Kamel. Examination of the solubilization of drugs by bile salt micelles. *J Pharm Sci.* 91:1743-1764 (2002).
331. M.E. Matteucci, J.C. Paguio, M.A. Miller, R.O. Williams, and K.P. Johnston. Highly supersaturated solutions from dissolution of amorphous itraconazole microparticles at pH 6.8. *Mol Pharm.* 6:375-385 (2009).
332. S.B. Murdande, M.J. Pikal, R.M. Shanker, and R.H. Bogner. Aqueous solubility of crystalline and amorphous drugs: Challenges in measurement. *Pharm Dev Technol*(2010).
333. D. Engers, J. Teng, J. Jimenez-Novoa, P. Gent, S. Hossack, C. Campbell, J. Thomson, I. Ivanisevic, A. Templeton, S. Byrn, and A. Newman. A solid-state approach to enable early development compounds: selection and animal bioavailability studies of an itraconazole amorphous solid dispersion. *J Pharm Sci.* 99:3901-3922 (2010).
334. P. Lehto, H. Kortejarvi, A. Liimatainen, K. Ojala, H. Kangas, J. Hirvonen, V.P. Tanninen, and L. Peltonen. Use of conventional surfactant media as surrogates for FaSSIF in simulating *in vivo* dissolution of BCS class II drugs. *Eur J Pharm Biopharm.* 78:531-538 (2011).
335. S. Anwar, J.T. Fell, and P.A. Dickinson. An investigation of the disintegration of tablets in biorelevant media. *Int J Pharm.* 290:121-127 (2005).
336. S. Janssens, H.N. de Armas, W. D'Autry, A. Van Schepdael, and G. Van den Mooter. Characterization of ternary solid dispersions of Itraconazole in polyethylene glycol 6000/polyvidone-vinylacetate 64 blends. *Eur J Pharm Biopharm.* 69:1114-1120 (2008).
337. S. Diebold. Physiological parameters relevant to dissolution testing: Hydrodynamic considerations. *Pharmaceutical Dissolution Testing*:127-191 (2005).
338. D.A. Miller, J.C. DiNunzio, W. Yang, J.W. McGinity, and R.O. Williams. Enhanced *in vivo* absorption of itraconazole via stabilization of supersaturation following acidic-to-neutral pH transition. *Drug Dev Ind Pharm.* 34:890-902 (2008).

339. J.C. DiNunzio, D.A. Miller, W. Yang, J.W. McGinity, and R.O. Williams, 3rd. Amorphous compositions using concentration enhancing polymers for improved bioavailability of itraconazole. *Mol Pharm.* 5:968-980 (2008).
340. S.B. Murdande, M.J. Pikal, R.M. Shanker, and R.H. Bogner. Solubility advantage of amorphous pharmaceuticals, part 3: Is maximum solubility advantage experimentally attainable and sustainable? *J Pharm Sci*(2011).
341. M. Van Speybroeck, R. Mols, R. Mellaerts, T.D. Thi, J.A. Martens, J. Van Humbeeck, P. Annaert, G. Van den Mooter, and P. Augustijns. Combined use of ordered mesoporous silica and precipitation inhibitors for improved oral absorption of the poorly soluble weak base itraconazole. *Eur J Pharm Biopharm.* 75:354-365 (2010).
342. T. Imai, Y. Saito, H. Matsumoto, T. Satoh, and M. Otagiri. Influence of Egg-Albumin on Dissolution of Several Drugs. *Int J Pharm.* 53:7-12 (1989).
343. C.M. Buchanan, N.L. Buchanan, K.J. Edgar, S. Klein, J.L. Little, M.G. Ramsey, K.M. Ruble, V.J. Wachter, and M.F. Wempe. Pharmacokinetics of itraconazole after intravenous and oral dosing of itraconazole-cyclodextrin formulations. *J Pharm Sci.* 96:3100-3116 (2007).
344. J.A. Hughes, A.M. persky, X. Guo, and T.K. Ghosh. Solubility. In T.K. Ghosh and B.R. Jasti (eds.), *Theory and Practice of Contemporary Pharmaceutics*, CRC Press, Boca Raton, FL, 2004, pp. 55-81.
345. J.L. Ford. Thermal analysis of hydroxypropylmethylcellulose and methylcellulose: powders, gels and matrix tablets. *Int J Pharm.* 179:209-228 (1999).
346. A. Streubel, J. Siepmann, and R. Bodmeier. Gastroretentive drug delivery systems. *Expert Opin Drug Deliv.* 3:217-233 (2006).
347. D. Psachoulas, M. Vertzoni, K. Goumas, V. Kalioras, S. Beato, J. Butler, and C. Reppas. Precipitation in and supersaturation of contents of the upper small Intestine after administration of two weak bases to fasted adults. *Pharm Res*(2011).
348. J.M. Lynch, D.M. Barbano, and J.R. Fleming. Indirect and direct determination of the casein content of milk by Kjeldahl nitrogen analysis: collaborative study. *J AOAC Int.* 81:763-774 (1998).
349. W.C. Duane. The intermicellar bile salt concentration in equilibrium with the mixed-micelles of human bile. *Biochim Biophys Acta.* 398:275-286 (1975).
350. J.P. Lakshman, Y. Cao, J. Kowalski, and A.T.M. Serajuddin. Application of melt extrusion in the development of a physically and chemically stable high-energy amorphous solid dispersion of a poorly water-soluble drug. *Mol Pharm.* 5:994-1002 (2008).

351. J. Montet, M. Reynier, A. Montet, and A. Gerolami. Distinct effects of three bile salts on cholesterol solubilization by oleate-monoolein-bile salt micelles. *Biochim Biophys Acta*. 575:289-294 (1979).
352. G.A. Kossena, B.J. Boyd, C.J.H. Porter, and W.N. Charman. Separation and characterization of the colloidal phases produced on digestion of common formulation lipids and assessment of their impact on the apparent solubility of selected poorly water-soluble drugs. *J Pharm Sci*. 92:634-648 (2003).
353. J.J. Sheng, P.J. Sirois, J.B. Dressman, and G.L. Amidon. Particle diffusional layer thickness in a USP dissolution apparatus II: A combined function of particle size and paddle speed. *J Pharm Sci*. 97:4815-4829 (2008).
354. G.Z. Papageorgiou, D. Bikiaris, E. Karavas, S. Politis, A. Docoslis, Y. Park, A. Stergiou, and E. Georgarakis. Effect of physical state and particle size distribution on dissolution enhancement of nimodipine/PEG solid dispersions prepared by melt mixing and solvent evaporation. *AAPS J*. 8:(2006).
355. M. Bisratand C. Nyström. Physicochemical aspects of drug release. VIII. The relation between particle size and surface specific dissolution rate in agitated suspensions. *Int J Pharm*. 47:223-231 (1988).
356. L. Prandtl. *Essentials of fluid dynamics: With applications to hydraulics aeronautics, meteorology, and other subjects*. Hafner Pub. Co1952.
357. K.G. Nelson and A.C. Shah. Convective diffusion model for a transport - controlled dissolution rate process. *J Pharm Sci*. 64:610-614 (1975).
358. J. Nunthanid, K. Huanbutta, P. Sriamornsak, S. Limmatvapirat, M. Luangtananan, Y. Yoshihashi, E. Yonemochi, and K. Terada. Swelling kinetics of spray-dried chitosan acetate assessed by magnetic resonance imaging and their relation to drug release kinetics of chitosan matrix tablets. *Eur J Pharm Biopharm*. 77:320-326 (2011).
359. C.W. Pouton. Lipid formulations for oral administration of drugs: non-emulsifying, self-emulsifying and 'self-microemulsifying' drug delivery systems. *Eur J Pharm Sci*. 11:S93-S98 (2000).
360. W. Yang, J. Tam, D.A. Miller, J. Zhou, J.T. McConville, K.P. Johnston, and R.O. Williams. High bioavailability from nebulized itraconazole nanoparticle dispersions with biocompatible stabilizers. *Int J Pharm*. 361:177-188 (2008).
361. R.-M. Dannenfelser, H. He, Y. Joshi, S. Bateman, and A.T.M. Serajuddin. Development of clinical dosage forms for a poorly water soluble drug I: Application of polyethylene glycol-polysorbate 80 solid dispersion carrier system. *J Pharm Sci*. 93:1165-1175 (2004).
362. O. Keinke and H.J. Ehrlein. Effect of oleic acid on canine gastroduodenal motility, pyloric diameter and gastric emptying. *Q J Exp Physiol*. 68:675-686 (1983).

363. J.B. Dressman. Comparison of canine and human gastrointestinal physiology. *Pharm Res.* 3:123-131 (1986).
364. A. Scholz, E. Kostewicz, B. Abrahamsson, and J.B. Dressman. Can the USP paddle method be used to represent in-vivo hydrodynamics? *J Pharm Pharmacol.* 55:443-451 (2003).
365. M. Arndt, H. Chokshi, K. Tang, N.J. Parrott, C. Reppas, and J.B. Dressman. Dissolution media simulating the proximal canine gastrointestinal tract in the fasted state. *Eur J Pharm Biopharm*(2013).
366. F. Johansson and R. Paterson. Physiologically based in silico models for the prediction of oral drug absorption. In C. Ehrhardt and K.-J. Kim (eds.), *Drug Absorption Studies*, Vol. VII, Springer US 2008, pp. 486-509.
367. A.J. Humberstone, C.J.H. Porter, and W.N. Charman. A physicochemical basis for the effect of food on the absolute oral bioavailability of halofantrine. *J Pharm Sci.* 85:525-529 (1996).
368. G. Levy. Levy G, Hayes B, "Physicochemical basis of the buffered acetylsalicylic acid controversy. *New Engl. J. Med.* 262:1053-1058 (1960)"--the backstory. *AAPS J.* 13:320-322 (2011).
369. M. Armand, B. Pasquier, M. André, P. Borel, M. Senft, J. Peyrot, J. Salducci, H. Portugal, V. Jaussan, and D. Lairon. Digestion and absorption of 2 fat emulsions with different droplet sizes in the human digestive tract. *Am J Clin Nutr.* 70:1096-1106 (1999).

## Appendix 1

Typical chromatograms of CA, ITR and CX are presented in Figure A1, A2 and A3.

### CA

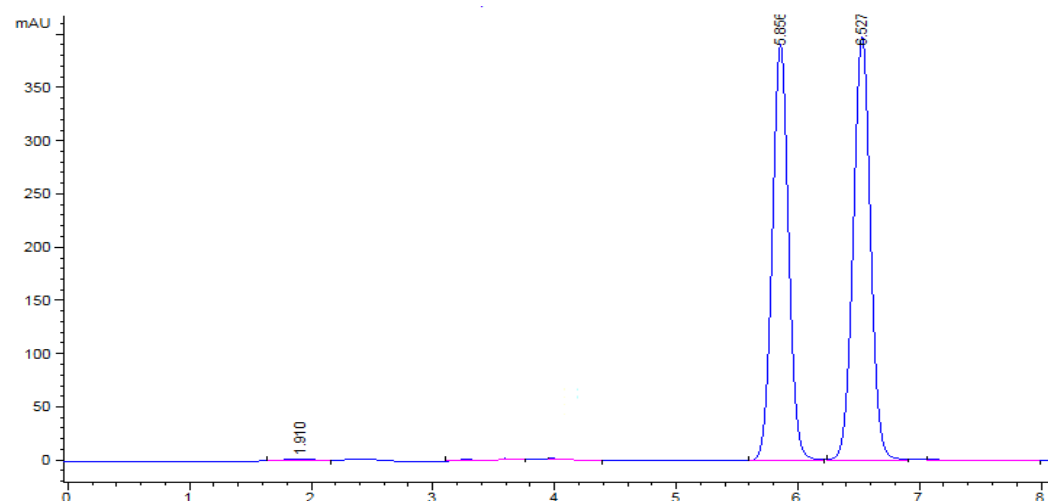


Figure A1: Chromatogram of a sample from a 240  $\mu\text{g/mL}$  solution of CA in SG. Retention time: diastereomer A:5.8 and diastereomer B:6.5 min).

Note: CA is a 50:50 mixture of diastereomers A and B. The HPLC assay for CA involves summing the A and B isomers in the mixture (206).

### ITR

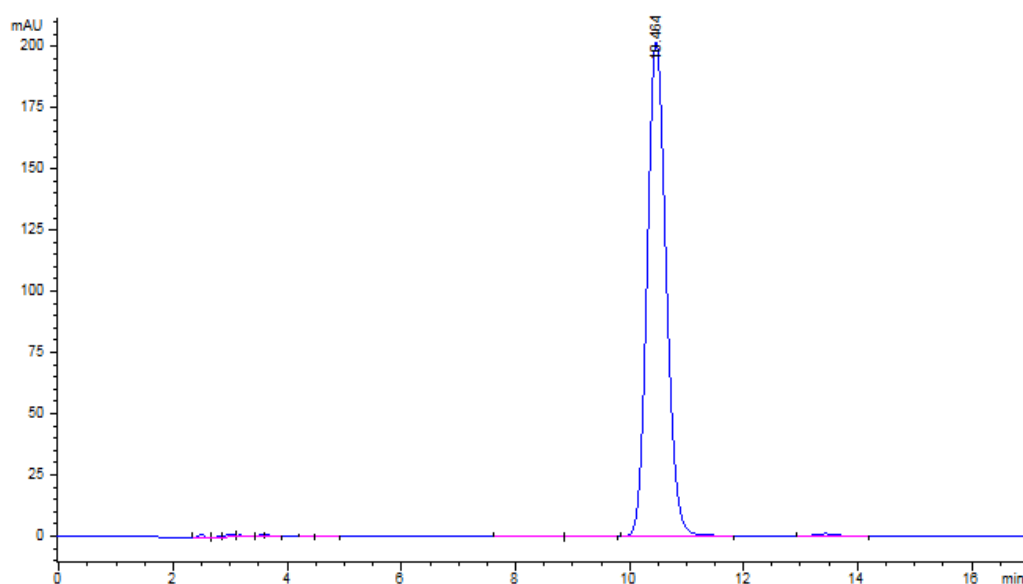


Figure A2. Chromatogram of a sample from a 100 $\mu\text{g/mL}$  solution of ITR in SGF. Retention time: 10.5 min.

**CX**

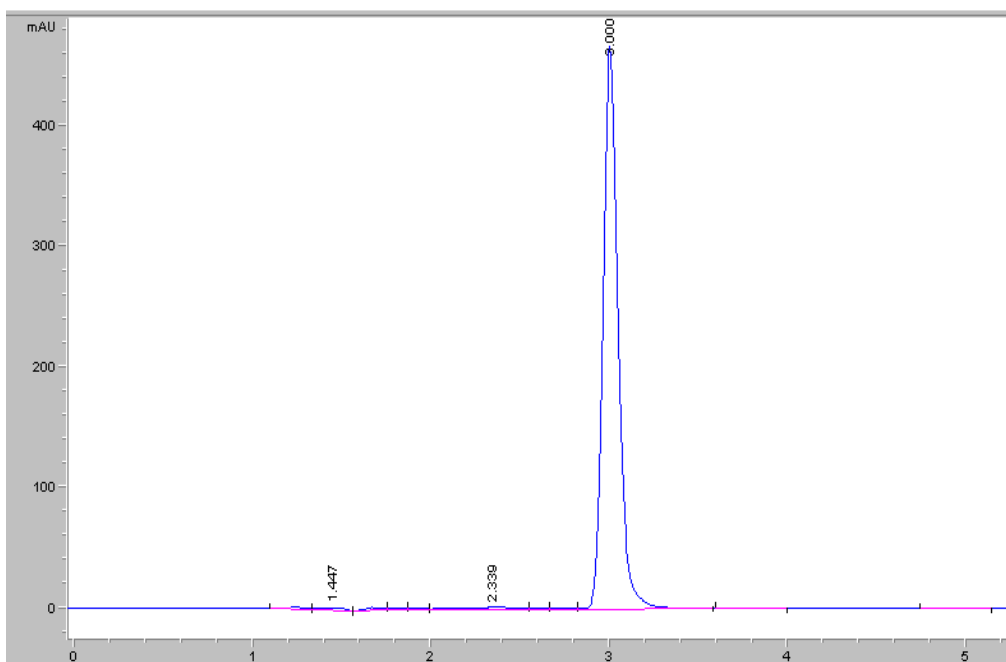


Figure A3: Chromatogram of a sample from a 40  $\mu\text{g/mL}$  solution of Compound X in SGF. Retention time: 3 min.



## Appendix 2

Calculation of extinction coefficient using Beer's law (Equation A1)(116)

$$A = \epsilon bc \quad \text{Equation A1}$$

where  $A$  is absorbance,  $\epsilon$  is the extinction coefficient (units:  $M^{-1}cm^{-1}$ ),  $b$  is the path length that the light has travelled (units: cm) and  $c$  is concentration (units: M).

Absorbance of the standard solution at various known concentrations need to be measured and then a graph of absorbance versus concentration need to be plotted. The graph is interpreted with linear function ( $y = mx$ ) where  $y =$  Absorbance,  $x =$  concentration,  $m$  (slope) =  $\epsilon b$ . The length of the ActiPix™ quartz cell (path length is 0.4 cm) therefore  $\epsilon$  could be calculated from the slope of the linear curve.

### Appendix 3

Scaling of FaSSIF-V1 and FeSSIF-V1 solubility of ITR and CX was performed using measured humans HIF values (fasted and fed state) data presented in literature (103, 292). The reported solubility values of the model compounds in HIF, FaSSIF-V1 and FeSSIF-V1 were categorised according to the weak acid (CX) and weak base compounds and these values were plotted using log-log scale (Figure A4: fasted state and Figure A5: fed state conditions).

#### Fasted state conditions

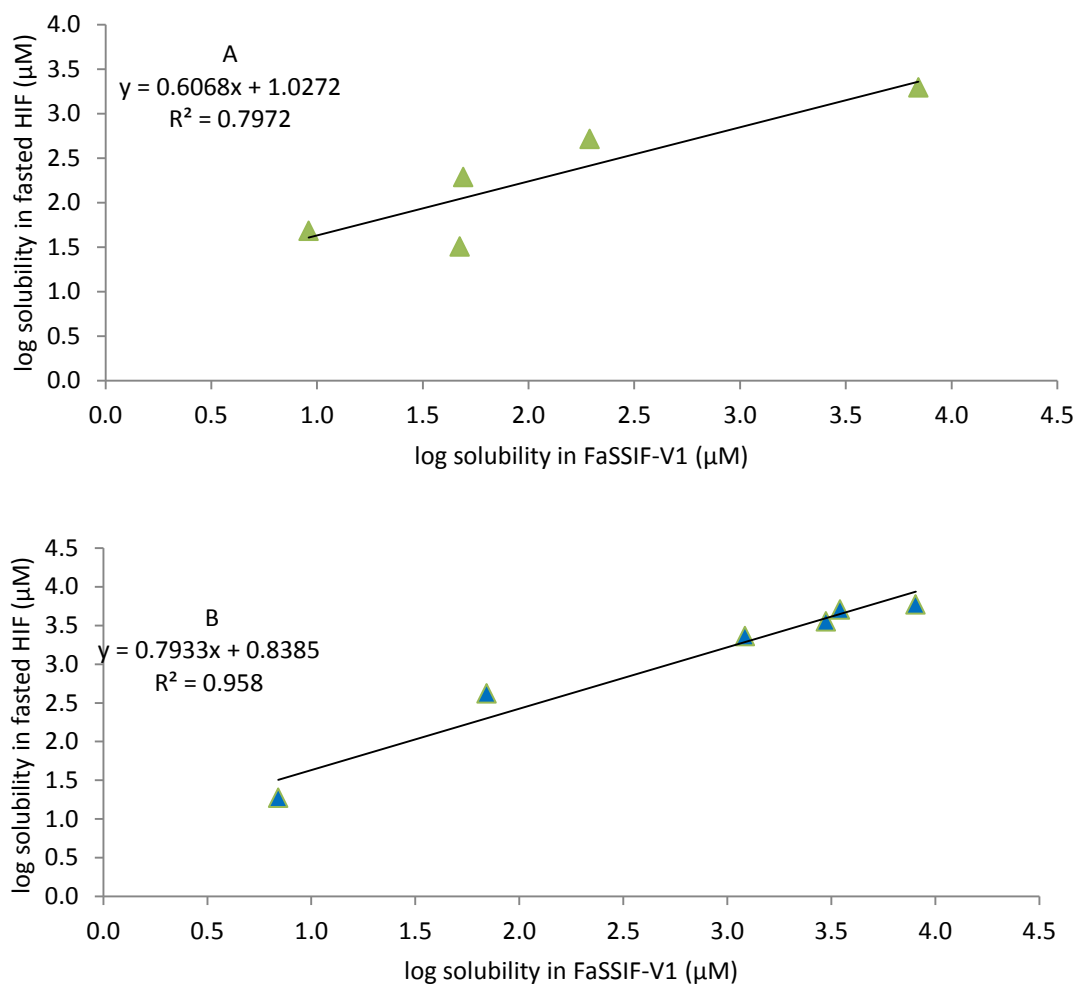


Figure A4. Mean solubility in fasted HIF as a function of mean solubility in FaSSIF-V1, the weak base (A, for ITR) and weak acid (B, for CX) model drugs. The correlation line and correlation function between both parameters are indicated.

## Fed state conditions

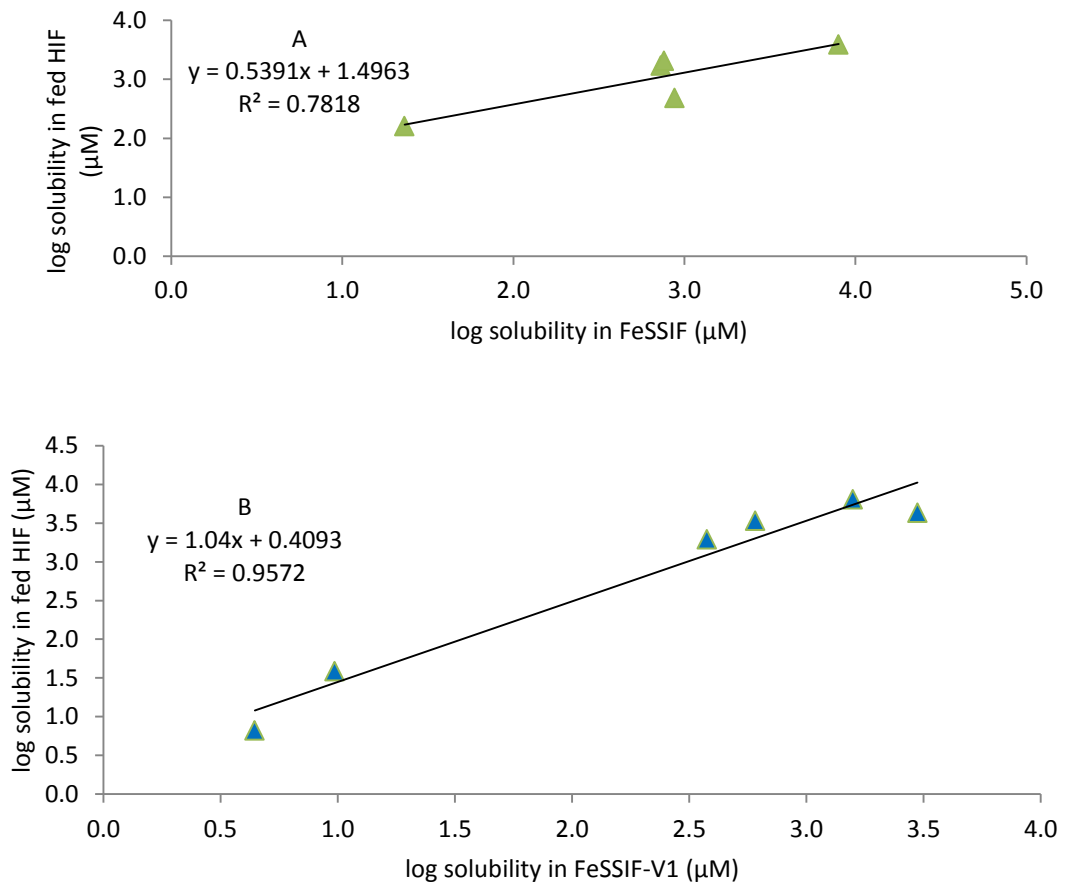


Figure A5. Mean solubility in fed HIF as a function of mean solubility in FeSSIF-V1 the weak base (A, for ITR) and weak acid (B, for CX) model drugs. The correlation line and correlation function between both parameters are indicated.

The regression functions were used to scale the solubility value of ITR and CX based on their solubility values in FaSSIF-V1 and FeSSIF-V1 for the fasted and fed state conditions respectively.

## Appendix 4

The Caco-2 value used in GastroPlus™ Caco-2 converter (163) is presented in Table A1.

Table A1: Caco-2 value used in GastroPlus™ Caco-2 converter

	Apparent permeability coefficient	(X10 <sup>-4</sup> cm/s)		Apparent permeability coefficient	(X10 <sup>-4</sup> cm/s)
1	Amoxicillin	0.08	8	Hydrochlorothiazide	0.051
2	Antipyrine	2.82	9	Terbutaline	0.038
3	Atenolol	0.02	10	Ranitidine	0.049
4	Cephalexin	0.05	11	Cimetidine	0.074
5	Metoprolol	2.37	12	Desipramine	2.16
6	Naproxen	3.95	13	Ranitidine	0.049
7	Piroxicam	3.56	14	Propranolol	4.19
8	Frusemide	0.012			

## Appendix 5

Plasma concentration profile after IV administration of CA, ITR and CX (Figure A6).

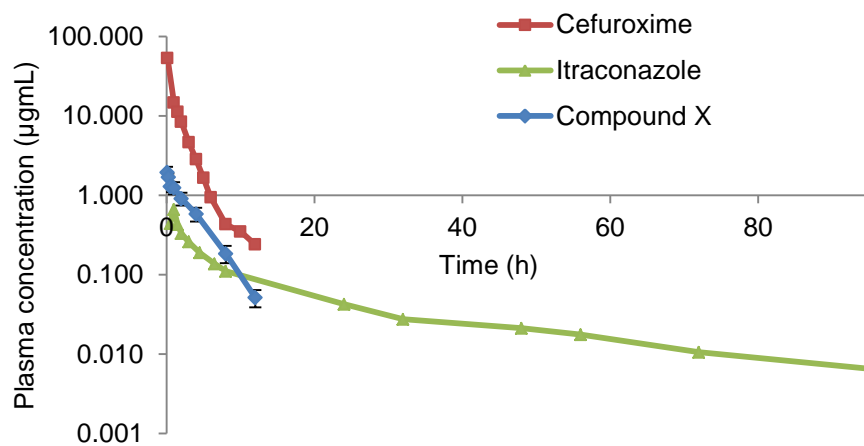


Figure A6: Mean plasma concentration vs time profiles of cefuroxime (humans), itraconazole (humans) and Compound X (dogs). Redrawn from published data (209, 252, 291).

## Appendix 6

Composition and ionic strength of SGF-M1 and fasted state human gastric fluid are presented in Table A2.

Table A2. Composition and ionic strength of SGF-M1 and human gastric fluid.

Component	SGF-M1	Fasted state human gastric fluid
NaCl (mM)	34.2	-
KH <sub>2</sub> PO <sub>4</sub> (mM)	-	-
NaOH (mM)	-	-
SLS (mM)	0.346	-
HCl (mM)	70	-
pH	1.2	-
Na <sup>+</sup> (mM)	34.2+0.346=34.55	68*
K <sup>+</sup> (mM)	-	13*
PO <sub>4</sub> <sup>3-</sup> (mM)	-	-
HCO <sub>3</sub> <sup>-</sup> (mM)	-	-
Cl <sup>-</sup> (mM)	34.2+70=104.2	102*
H <sup>+</sup> (mM)	63.096+70=133.096	-
OH <sup>-</sup> (mM)	-	-
Calculation	$\frac{1}{2}(34.55 \times 1^2 + 104.2 \times 1^2 + 133.096 \times 1^2)$	$\frac{1}{2}(68 \times 1^2 + 13 \times 1^2 + 102 \times 1^2)$
Ionic strength (M)	0.136	~0.1

\*Reported in literature (72)

Ionic strength is defined by the Equation A2 (72):

$$I = \frac{1}{2} \sum z_i^2 m_i \quad \text{Equation A2}$$

where  $m_i$  is the concentration of the  $i$ -th ion concentration,  $z$  is the valence factor. The summation,  $\sum$ , is taken over all the possible ions in the solution.

## Appendix 7

### Prediction of CA *in vivo* performance based on PBPK models

#### Solubility-based model

The plasma concentration-time of simulated (solubility-based model) and the observed (humans) profiles after an oral administration of Zinnat<sup>®</sup> tablet in fasted state is presented in Figure A7, A8 and A9.

#### Single solubility value model

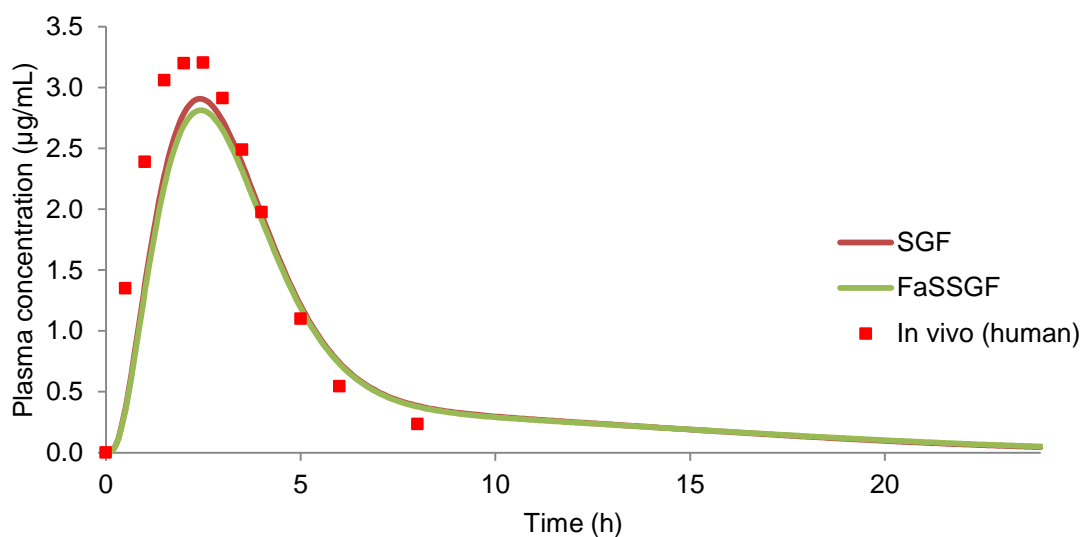


Figure A7. Simulation (line) of oral Zinnat<sup>®</sup> profiles in humans using solubility measured in SGF and FaSSGF compared to the observed *in vivo* profile (human, fasted; ■)(287).

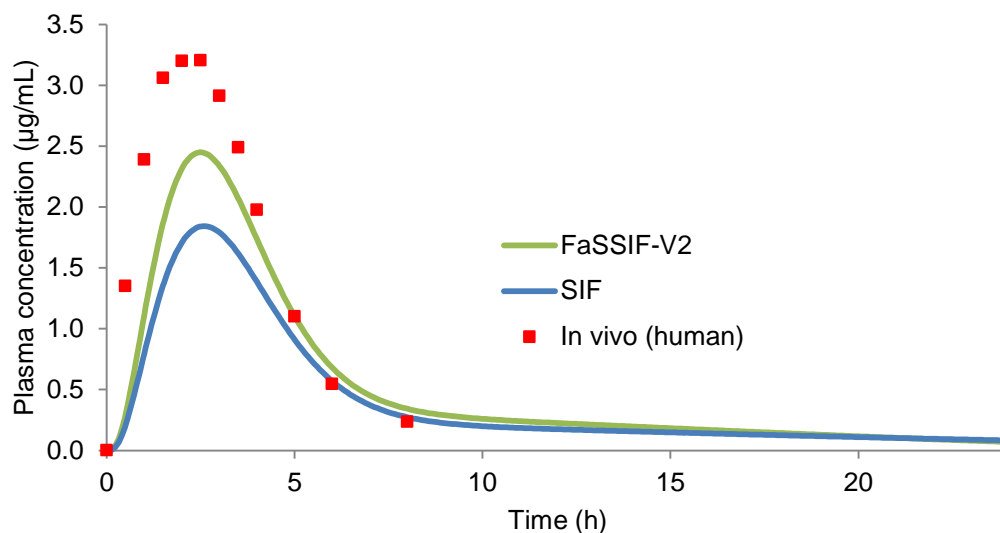


Figure A8. Simulation (line) of oral Zinnat<sup>®</sup> profiles in humans using solubility measured in SIF and FaSSIF-V2 compared to the observed *in vivo* profile (human, fasted; ■)(287).

The simulation using solubility value of CA in SGF and FaSSGF is comparable to the *in vivo* profiles ( $f_1$  SGF: 18.99,  $f_1$  FaSSGF: 21.18) mainly because both media have similar solubility. In contrast, the solubility values of SIF and FaSSIF-V2 are different ( $f_1$  SIF: 45.10,  $f_1$  FaSSIF-V2: 29.56). It must be noted the profile for SIF was simulated using SIF dissolution profile that has lower dissolution due to high degradation rate of CA in SIF.

### pH solubility range model

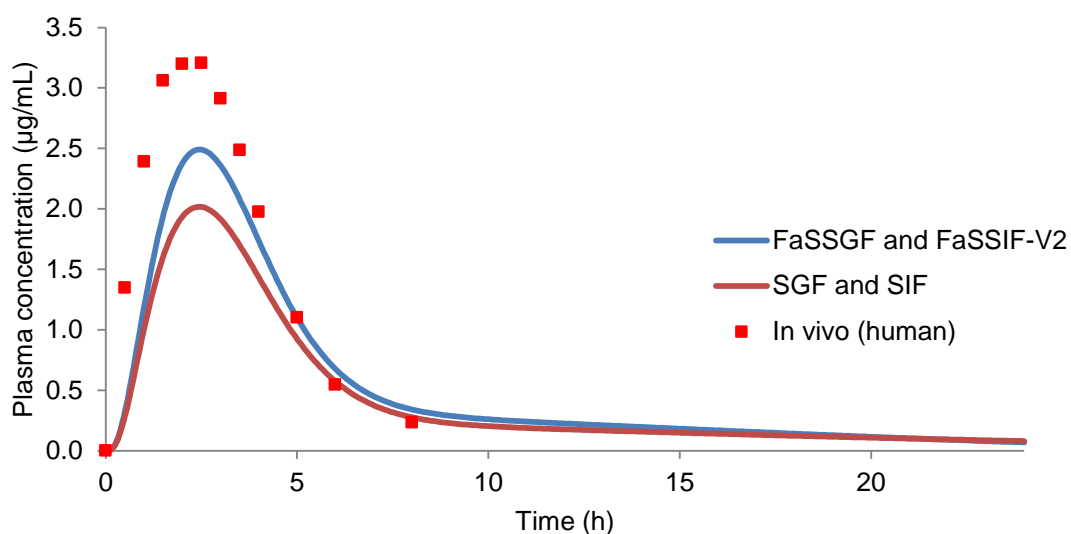


Figure A9. Simulation (line) of oral Zinnat<sup>®</sup> profiles in humans using solubility-pH in biorelevant and compendial media compared to the observed *in vivo* profile (human, fasted; ■)(287).



As seen in Figure A9 (solubility-pH range based), the simulations are less predictive compared to individual solubility with compendial media (SGF and SIF) leading to underestimation of the observed profile while the solubility with biorelevant media (FaSSGF and FaSSIF-V2) shows a much closer simulation ( $f_1$  SGF and SIF: 39.82;  $f_1$  FaSSGF and FaSSIF-V2: 28.21).

The plasma concentration-time of simulated (solubility-based model) and the observed (humans) profiles after an oral administration of Zinnat<sup>®</sup> tablet in fed state is presented in Figure A10.

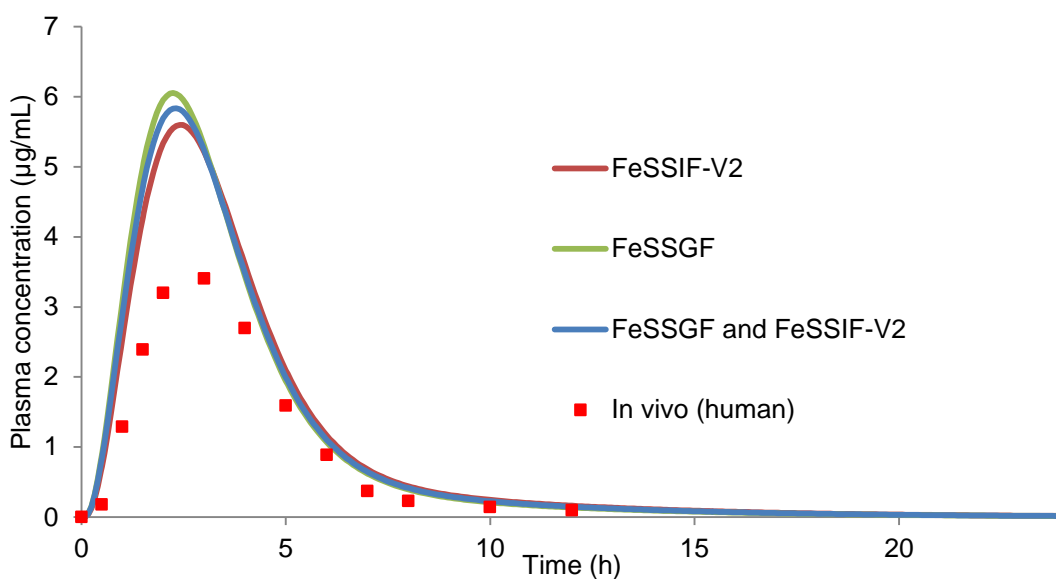


Figure A10. Simulation (line) of oral Zinnat<sup>®</sup> profiles in humans using reference solubility-pH in FeSSIF-V2, FeSSGF and solubility-pH range (FeSSGF and FeSSIF-V2) compared to the observed *in vivo* profile (human, fed; ■)(288).

The simulation using solubility value of CA in FeSSIF-V2 (0.372 mg/mL) and FeSSGF (0.535 mg/mL) and combination of FeSSGF and FeSSIF-V2 all overestimated the *in vivo* profiles ( $f_1$  FeSSIF-V2: 60.6,  $f_1$  FeSSGF: 70.6,  $f_1$  FeSSGF and FeSSIF-V2: 66.4).

## Appendix 8

### Prediction of ITR *in vivo* performance based on PBPK models

#### Solubility-based model

The plasma concentration–time of simulated (solubility based model) and observed (human) profiles after oral administration of one Sporanox<sup>®</sup> capsule in fasted state is presented in Figure A11 and A12.

#### Single solubility value model

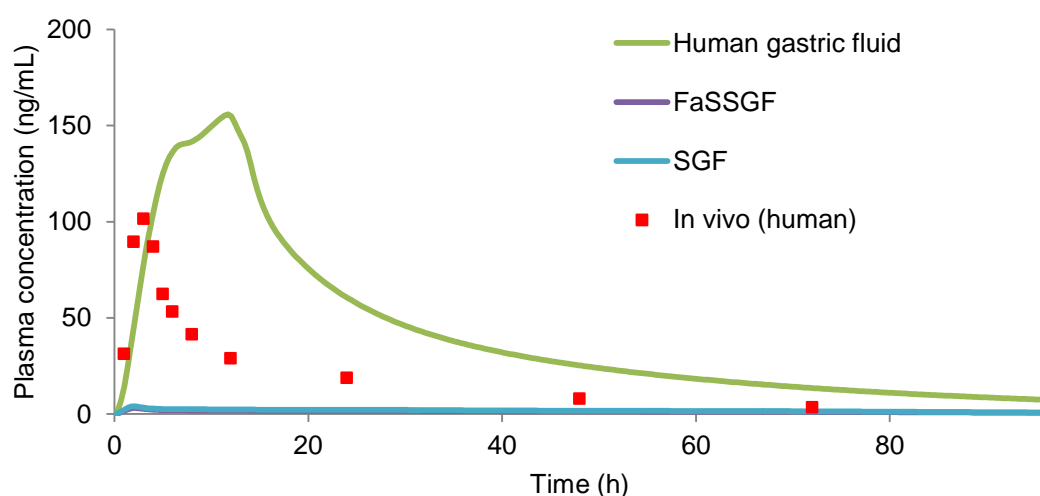


Figure A11. Simulation (line) of oral Sporanox<sup>®</sup> profiles in humans using solubility measured in SGF and FaSSGF compared to the observed *in vivo* profile (human, fasted; ■)(299).

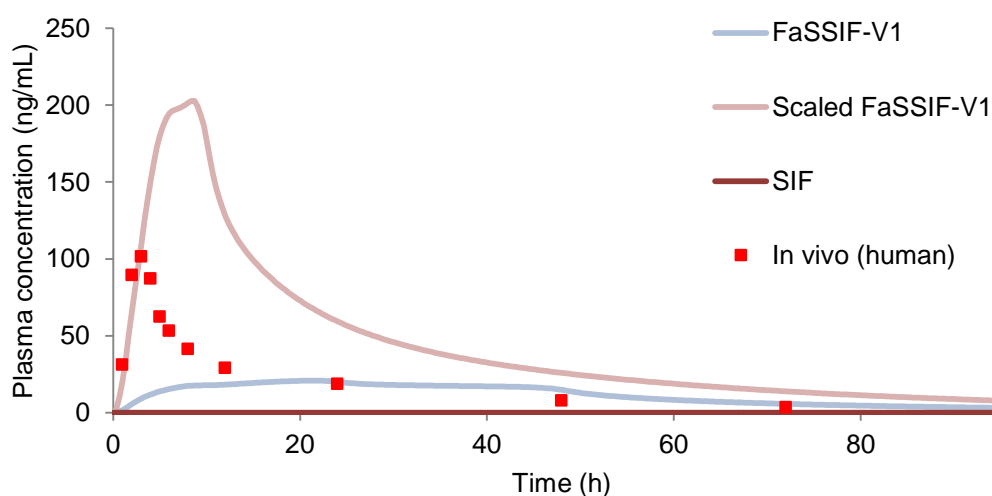


Figure A12. Simulation (line) of oral Sporanox<sup>®</sup> profiles in humans using solubility measured in HIF, SIF, FaSSIF-V1 and FaSSIF-V1 (Scaled solubility) compared to the observed *in vivo* profile (human, fasted; ■)(299).

The solubility of ITR in human gastric fluids and FaSSGF is 3.19 and 2.08  $\mu\text{g/mL}$  respectively (30). Interestingly, an approximately 50% increase in the ITR solubility in the FaSSGF could lead to a huge difference in the simulated profiles (Figure A11). According to Figure A11, the simulated profile using ITR solubility in SGF and FaSSGF underestimated the *in vivo* profile ( $f_1$  SGF: 94.77;  $f_1$  FaSSGF: 95.92).

Similarly, the same trend is observed from simulated profiles using solubility measured in SIF, FaSSIF-V1 and scaled FaSSIF-V1 (ITR solubility, according to the sequence 6.21, 0.003, 0.34, 4.81  $\mu\text{g/mL}$ ) (30). It is apparent that the *in vivo* solubility of ITR with the presence of bile salts and lipids in the intestinal fluids changed significantly the solubility compared to that in compendial medium. According to Figure A12, the simulated profile using ITR solubility in humans intestinal fluid overestimated the observed *in vivo* profile ( $f_1$  scaled FaSSIF-V1: 131.97) whereas underestimation occurred for SIF and FaSSIF-V1 ( $f_1$  SIF: 100.00;  $f_1$  FaSSIF-V1: 78.47).

### pH solubility range model

The plasma concentration–time of simulated (solubility-pH based model) and observed (humans) profiles after oral administration of one Sporanox<sup>®</sup> capsule in fasted state is presented in Figure A13.

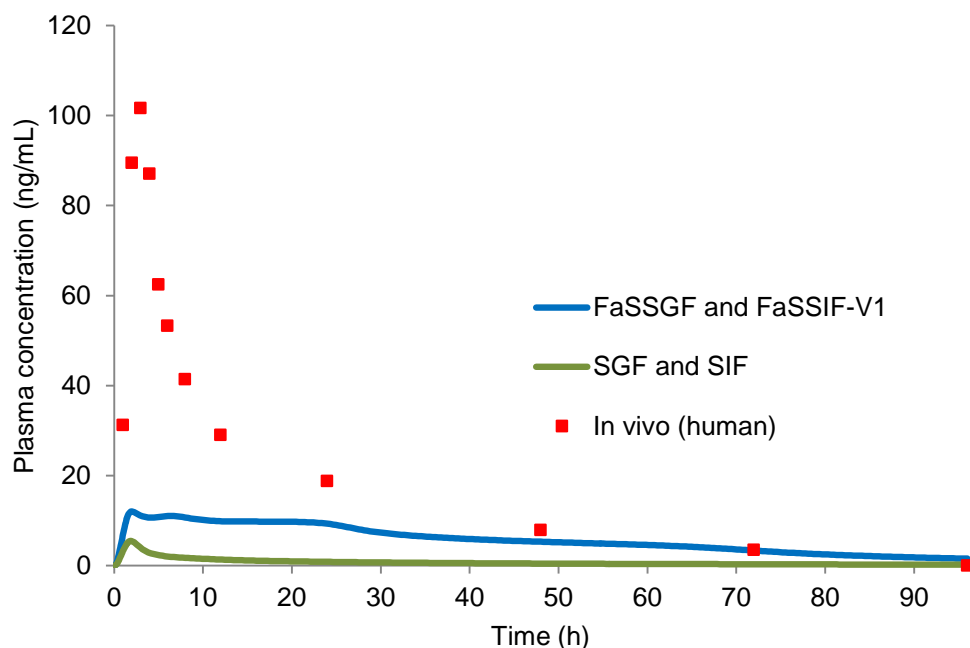


Figure A13. Simulation (line) of oral Sporanox<sup>®</sup> profiles in humans using solubility-pH range measured in SGF-SIF and FaSSGF-FaSSIF-V1 compared to the observed *in vivo* profile (human, fasted; ■)(299).

According to Figure A13, pH-solubility range using FaSSGF and FaSSIF-V1 simulated better the observed *in vivo* profile compared to SGF and SIF ( $f_1$  FaSSGF and FaSSIF-V1:80.8;  $f_1$  SGF and SIF:95.3). Even though both simulated profiles underestimated the observed *in vivo* profile, the results show more accurate prediction compared to the single solubility based model (as presented previously in Figure A11 and A12).

The plasma concentration-time of simulated (solubility based model) and observed (humans) profiles after an oral administration of Sporanox<sup>®</sup> capsule in fed state is presented in Figure A14.

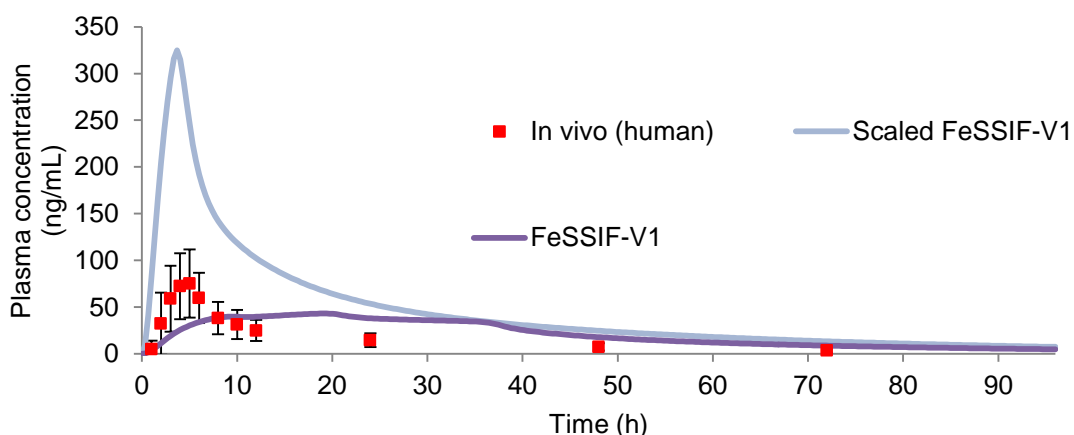


Figure A14. Simulation (line) of oral Sporanox<sup>®</sup> profiles in humans using reference with single solubility measured in FeSSIF-V1, humans intestinal fluid (fed) and scaled FeSSIF-V1 (using HIF fed) compared to observed *in vivo* (human, fed; ■)(228).

The reported ITR solubility in scaled FeSSIF-V1 are 12.35  $\mu\text{g/mL}$  and 22.50  $\mu\text{g/mL}$  (30) which are approximately 17 and 31 times higher than the solubility in FeSSIF-V1 (0.73  $\mu\text{g/mL}$ ), respectively. According to Figure A14, the simulated profile using ITR solubility in scaled FeSSIF-V1 overestimated the observed *in vivo* profile ( $f_1$  scaled FeSSIF-V1: 99.68). On the other hand, the simulated profile using ITR solubility in FeSSIF-V1 greatly underestimated the observed *in vivo* profile ( $f_1$  FeSSIF-V1:99.95).

ITR solubility value is a critical factor for an accurate prediction because the closest solubility value to the *in vivo* value will estimate for the true amount of ITR absorbed as solubility is the limiting parameter as a BCS Class 2 compound.